789

THE BEHAVIOUR OF A PROTOTYPE FORM-REINFORCED BRIDGE DECK SLAB UNDER STATIC AND REPEATED LOADING

A thesis submitted for the Degree of
Doctor of Philosophy in the
Faculty of Engineering of
The University of London

by

Peter Kenneth Gorf, B.Sc.(Hons), A.C.G.I.

Imperial College of Science and Technology
London

September, 1978

To my parents

ABSTRACT

This thesis describes an investigation into the application of cold-formed corrugated steel decking as both formwork and reinforcement in the construction of concrete bridge decks. The 'form-reinforced' slab concept is used extensively in the floors of buildings, particularly in North America, and a review is given of the types of formwork available and the advantages and disadvantages of the method of construction. A brief review of research in the related field of composite beams is also presented.

The majority of the thesis is concerned with an experimental assessment of the performance of a full-scale prototype permanent composite steel form which was manufactured specifically for this research project. The steel form consisted of galvanised steel sheet, cold formed into regular trapezoidal corrugations and designed to span transversely between longitudinal girders of a bridge, in a one-way mode. Embossments pressed into the webs and top flanges of the corrugations such that they projected into the concrete, provided shear connection between the steel and concrete.

The main experimental programme consisted of static loading tests on the bare formwork to simulate construction conditions and both static and repeated loading tests on the composite form-reinforced slab. Fatigue failure of the steel formwork unit was encountered in two of the composite specimens subjected to repeated loading. These failures were due to cracks originating from embossments in the webs of the unit and small scale fatigue tests on sections of the web were therefore carried out to check the possibility of fatigue failure

occurring in the formwork units during service. In addition, a limited number of push-out tests were conducted to investigate the behaviour of the shear connection.

The results of the composite static tests are compared with the theoretical predictions of both complete and partial interaction analyses. The latter was performed by means of a computer program to include non-linear response of the concrete and the shear-connection, and strain hardening in the steel.

Problems which may arise in the manufacture and practical application of the prototype formwork units in an actual bridge deck are discussed in a qualitative manner. The conclusions and design recommendations which are presented indicate that this method of construction is suitable for bridge decks and that the prototype form tested will be adequate for the purpose.

ACKNOWLEDGEMENTS

The research work presented in this thesis was carried out in the Structures Section of the Civil Engineering Department of Imperial College, University of London.

The author wishes to record his gratitude to Dr. P.J. Dowling, Reader in Steel Structures, for providing invaluable supervision and guidance throughout the course of the work. The author also wishes to express his appreciation of the support given by Professor B.G. Neal, Head of Department.

The author gratefully acknowledges the Department of Transport for sponsoring the testing programme and CONSTRADO for supplying the prototype formwork units and additional financial support.

The author would like to thank Mr. H.V. Hill (formerly of CONSTRADO) and Mr. N. Makins (of CONSTRADO) for their help and suggestions during the project and Mr. H.V. Norton of the Cwmfelin Pressworks (B.S.C.), Swansea, where the formwork units were manufactured.

Special thanks are due to the members of the Structures Laboratory Staff, particularly Mr. J. Williams, and Mr. J. Finn for their excellent technical work under the direction of Mr. J. Neale. Thanks are also due to Miss J. Gurr for preparing the photographs.

The author wishes to thank his friends and colleagues for their help during the experimental work.

Finally the author wishes to express his deepest gratitude to his wife, Karen, for typing the manuscript and for supplying constant encouragement throughout the course of the work.

CONTENTS

		Page
	ABSTRACT	3
	ACKNOWLEDGEMENTS	5
1.	INTRODUCTION	13
	1.1 GENERAL INTRODUCTION	13
	1.2 DEVELOPMENT OF THE FORM-REINFORCED SLAB CONCEPT	14
	1.3 ADVANTAGES AND DISADVANTAGES OF STEEL DECK SYSTEMS	21
	1.4 A BRIEF REVIEW OF RESEARCH ON COMPOSITE BEAMS	24
	1.5 SCOPE AND LAYOUT OF THIS THESIS	34
2.	DEVELOPMENT OF THE PROTOTYPE FORMWORK UNIT	37
	2.1 DESIGN CONSIDERATIONS	37
	2.2 DESCRIPTION OF PROTOTYPE UNIT	40
	2.3 MANUFACTURE OF UNITS	42
	2.4 DIMENSIONAL TOLERANCES	43
3.	STATIC TESTS	46
	3.1 GENERAL	46
	3.2 PUSH-OUT TESTS	46
	3.2.1 Objective of Push-Out Tests	46
	3.2.2 Details of Test Specimens	48
	3.2.2.1 *General*	48
	3.2.2.2 *Test Series 1*	49
	3.2.2.3 *Test Series 2*	49
	3.2.2.4 *Test Series 3*	49

CONTENTS (Continued) Page

3.2.2.5 *Test Series 4* 49

3.2.2.6 *Test Series 5* 50

3.2.2.7 *Durbar Specimen* 50

3.2.3 Test Procedure 50

3.2.4 Results of Push-Out Tests 51

3.2.5 Discussion of Results 52

3.3 CONSTRUCTION LOADING TEST (TEST 1) 55

3.3.1 Objective of Test 55

3.3.2 Derivation of Applied Loads 55

3.3.2.1 *Wet Concrete Load* 55

3.3.2.2 *Wet Concrete plus Additional Construction Load* 56

3.3.2.3 *Ultimate Load Test* 56

3.3.2.4 *Loading System Employed* 56

3.3.3 Description of Test Rig 57

3.3.4 Instrumentation 57

3.3.5 Test Procedure 58

3.3.6 Results 58

3.3.6.1 *Construction Loading Tests* 58

3.3.6.2 *Ultimate Load Test* 59

3.3.7 Discussion of Results 60

3.3.7.1 *Construction Loading* 60

3.3.7.2 *Ultimate Load Test* 61

3.4 COMPOSITE STATIC TESTS 62

3.4.1 Objective of Tests 62

3.4.2 Description and Preparation of Specimens 63

3.4.2.1 *Design of Specimens* 63

3.4.2.2 *Casting* 64

3.4.2.3 *Instrumentation* 65

3.4.2.4 *Geometric Properties of Specimens* 66

3.4.3 Description of Test Rig 66

CONTENTS (Continued)

			Page
3.4.4	Test Procedures		67
3.4.5	Results		68
	3.4.5.1	*Composite Slab in Sagging Bending - Test 2*	68
	3.4.5.2	*Composite Slab in Hogging Bending - Test 3*	69
	3.4.5.3	*Auxiliary Tests*	70
3.4.6	Discussion of Results		71
	3.4.6.1	*Composite Slab in Sagging Bending - Test 2*	71
	3.4.6.2	*Composite Slab in Hogging Bending - Test 3*	72
4.	REPEATED LOADING TESTS		74
4.1	OBJECTIVES OF DYNAMIC TEST PROGRAMME		74
4.1.1	General		74
4.1.2	Design Loading Spectra		76
4.1.3	Outline of Testing Programme		78
4.2	TEST SPECIMENS		79
4.2.1	Design of Specimens		79
4.2.2	Casting		79
4.2.3	Instrumentation		79
	4.2.3.1	*Strain Gauges*	79
	4.2.3.2	*Slip and Separation Measurement*	80
	4.2.3.3	*Deflection Gauges*	80
	4.2.3.4	*Curvature Gauge*	80
4.2.4	Geometric Properties of Specimens		81
4.3	TEST PROCEDURES		81
4.3.1	General		81
4.3.2	Description of Test Rig		82
4.3.3	Static Elastic Tests (Stages I & II)		82

CONTENTS (Continued) Page

4.3.4 Dynamic Testing (Stage III) 83
4.3.4.1 *General* 83
4.3.4.2 *Test 4* 83
4.3.4.3 *Constant Amplitude Tests* 84
4.3.5 Static Ultimate Tests (Stage IV) 85
4.3.6 Auxiliary Tests 85
4.4 RESULTS OF TESTS 85
4.4.1 Presentation of Results 85
4.4.2 Initial Elastic Tests 86
4.4.3 Dynamic Tests 87
4.4.3.1 *Test 4* 87
4.4.3.2 *Test 5* 87
4.4.3.3 *Test 6* 88
4.4.3.4 *Test 7* 89
4.4.3.5 *Test 8* 89
4.4.3.6 *Test 9* 89
4.4.4 Static Ultimate Tests 90
4.4.5 Auxiliary Tests 90
4.5 DISCUSSION OF RESULTS 91
4.5.1 Initial Static Elastic Tests 91
4.5.2 Dynamic Tests 92
4.5.2.1 *General Response* 92
4.5.2.2 *Fatigue of Steel Formwork* 93
4.5.3 Static Ultimate Tests 97

5. 'IN-AIR' FATIGUE TESTS OF EMBOSSMENT DETAIL 100

5.1 OBJECTIVE OF TESTS 100
5.2 DESCRIPTION OF SPECIMENS 102
5.3 STRESS DISTRIBUTION IN THE VIBROPHORE SPECIMEN 103
5.4 TEST PROCEDURE 106
5.5 RESULTS 107

CONTENTS (Continued) Page

5.6 ANALYSIS OF RESULTS 107

5.7 DESIGN IMPLICATIONS 111

6. SIMPLE BENDING ANALYSIS OF THE BARE FORMWORK SECTION 112

6.1 GENERAL 112

6.2 ELASTIC SECTION PROPERTIES 113

6.2.1 Assumptions 113

6.2.2 Fully Effective Section 114

6.2.3 Reduced Section due to Embossments 115

6.3 CONSTRUCTION STAGE DEFLECTIONS AND STRESSES 116

6.3.1 General 116

6.3.2 Ponding Effect and Deflections 117

6.3.3 Maximum Stress in the Section 120

6.4 ULTIMATE CAPACITY OF SECTION 121

7. THEORETICAL ANALYSIS - COMPOSITE STAGE 123

7.1 PURPOSE OF ANALYSIS 123

7.2 PARTIAL INTERACTION ANALYSIS 124

7.2.1 General 124

7.2.2 Assumptions 125

7.2.3 Derivation of Equations 127

7.2.4 Shear Connection Characteristics 131

7.2.5 Material Stress-Strain Relations 132

7.2.5.1 *Steel* 132

7.2.5.2 *Concrete* 132

7.2.6 Method of Solution 133

7.2.6.1 *General* 133

7.2.6.2 *Predictor-Corrector Equations* 134

CONTENTS (Continued) Page

7.2.6.3 *Calculation of Starting Values* 137

7.2.6.4 *Section Analysis* 138

7.2.6.5 *Construction Load Stresses and Deflections* 140

7.2.6.6 *Upper and Lower Bound Criteria* 141

7.3 COMPLETE INTERACTION ANALYSIS 142

7.4 CORRELATION WITH TEST RESULTS 143

7.4.1 General 143

7.4.2 Static Test Correlation - Test 2 145

7.4.3 Dynamic Test Correlation - Tests 4 and 5 147

7.4.4 Prediction of Ultimate Loads 149

7.4.5 General Assessment of the Partial Interaction Theory 152

7.5 EFFECT OF THE END OVERHANG 153

7.6 EFFECT OF EMBOSSMENT SPACING 154

8. PRACTICAL ASPECTS 156

8.1 GENERAL 156

8.2 METHOD OF MANUFACTURE 156

8.3 DIMENSIONAL TOLERANCES 158

8.3.1 General 158

8.3.2 Transverse Out-of-Flatness 158

8.3.3 Longitudinal Out-of-Flatness 159

8.3.4 Width Variation 159

8.3.5 Embossment Geometry 160

8.4 END CONNECTION 160

8.5 LONGITUDINAL CONNECTION 161

8.6 ADDITIONAL REINFORCEMENT 162

8.7 SEALING 162

8.8 COMPOSITE ACTION WITH MAIN BEAMS 163

8.9 CORROSION AND DURABILITY 164

CONTENTS (Continued) Page

9. CONCLUSIONS AND RECOMMENDATIONS FOR DESIGN 167

9.1 GENERAL CONCLUSIONS 167
9.1.1 Push-Out Tests 167
9.1.2 Bare Formwork Response 168
9.1.2.1 *Deflections* 168
9.1.2.2 *Stresses* 169
9.1.2.3 *Ultimate Capacity* 170
9.1.3 Composite Static Tests 171
9.1.4 Repeated Loading Tests 172
9.1.5 Vibrophore Tests 173
9.1.6 Theoretical Analysis 174
9.1.7 Manufacturing Tolerances 176
9.2 RECOMMENDATIONS FOR DESIGN 177
9.2.1 General 177
9.2.2 Manufacturing Tolerances 178
9.2.3 Construction Stage 178
9.2.4 Composite Stage 180
9.2.4.1 *Static Response* 180
9.2.4.2 *Fatigue Response* 180
9.3 FUTURE RESEARCH 181

APPENDICES 184 - 188

REFERENCES 189 - 198

NOTATION 199 - 204

TABLES 205 - 217

LIST OF FIGURES 218 - 220

FIGURES 221 - 325

PLATES

CHAPTER 1

INTRODUCTION

1.1 GENERAL INTRODUCTION

The use of corrugated steel decking as both formwork and reinforcement for concrete slabs is well established in the construction of building floors, particularly in North America where the majority of development has taken place. There are three ways in which corrugated steel decking may be combined with a concrete slab. Firstly, the steel deck may be designed to carry all dead and live loads in which case a non-structural lightweight concrete topping provides a level surface. Conversely, the concrete slab may be designed to carry all live and superimposed dead loads, while the steel deck acts solely as structurally non-participating permanent formwork. The third possibility is a composite design in which the permanent formwork participates structurally in resisting superimposed dead and live loads once the concrete has hardened.

Almost all steel deck formwork systems now in use in building floor slab construction are provided with means by which composite action between the deck and the in-situ concrete may be ensured, resulting in what is best described as a 'form-reinforced slab'. There are several methods by which composite action may be attained as illustrated in Figure 1. Due to the relatively low loading intensity to which building floors are subjected, together with the fact that normally no fatigue problem exists, the use of

light gauge steel sections has been very successful.

Although permanent steel formwork is employed in the construction of bridge decks, at the present time a system in which the formwork is designed to act compositely with the slab in the final structure, is not available. This appears to be due primarily to the lack of information regarding the response of form-reinforced slabs to repeated loading.

This thesis describes an investigation into the structural feasibility of a one-way form-reinforced slab system for bridge deck construction and is based essentially on tests carried out on a full size prototype steel deck form which was manufactured specifically for this project. The experimental work consisted of static loading tests on the bare formwork unit to simulate construction conditions, and both static and repeated loading tests on the composite slab to investigate the possibility of fatigue failure. The results of these tests are presented and design implications are discussed.

The behaviour of the composite slab under static loading is compared with theoretical analyses for both complete and partial interaction conditions. The partial interaction analysis was performed using a computer program incorporating non linear behaviour of the shear connection and concrete and strain hardening in the steel formwork.

1.2 DEVELOPMENT OF THE FORM-REINFORCED SLAB CONCEPT

Cold formed corrugated steel decking was first used in the construction of building floors during the early 1930's in the

United States and an interesting account of development is given by Dallaire [1], who also discusses the reasons why it is now so popular in the design of high rise steel framed structures in North America.

Originally this method of construction was devised to provide a lightweight flooring system with the aim of reducing labour costs, erection time and overall structural weight. This was achieved by designing the steel decking as the sole structural element of the floor and providing a level surface by means of a lightweight concrete topping, the strength of which was ignored. By the late 1930's engineers were beginning to use the corrugations of the decking as a natural ducting for electrical services. However, growth in usage of this early type of floor was slow due to the need for expensive ceilings to attain the necessary fire rating. The arrival of 'spray-on' fire proofing in the early 1950's led to a more rapid development in this field.

The first floor designed to combine the structural properties of the steel decking and the overlying concrete and provide composite action became available in the United States in 1950. The composite action was achieved by welding a grid of wires to the tops of the decking corrugations in a transverse direction. Horizontal shear and vertical separation forces were thereby transferred by dowel action of the wires from the concrete via the welds to the steel deck. The performance of this type of form-reinforced slab compared very favourably with that of a normal reinforced concrete slab, in tests described by Friberg [2].

The early 1960's saw the introduction of a system which provides shear connection by means of embossments pressed into the webs of the steel deck and by 1967 several types of steel deck formwork were available in North America.

Ekberg[3] and Schuster[3,4] have described the various types of decking and these may be divided into three distinct groups depending upon the type of shear connection employed. These are :

Type I : In this type of deck, steel mesh or bars are welded to the tops of the corrugations. Longitudinal shear and transverse separation forces are transmitted to the steel deck via the welds.

Type II : The provision of 'embossments' ('dimples' or 'nibs') in the webs and flanges of the steel deck can provide excellent composite action and many manufacturers supply this type of decking. There are many ways in which the embossments may be arranged to resist shear and separation, one popular method being to slope the embossments in different directions on adjacent webs.

Type III : The third basic type of composite deck is that which relies entirely upon natural bond between the steel and concrete to resist longitudinal shear forces while the corrugations are shaped to provide resistance to separation in a dovetail action. The corrugation shape used is often referred to as 're-entrant'.

The three types of formwork are shown schematically in Figure 1.

Natural or chemical bond between the steel and concrete components enhances the strength of the connection and in the majority of cases is included in the design of Types I and II, but an adequate factor of safety is necessary at working loads to prevent bond failure.

McDermott [5] has reported on a composite floor system which is not included in the above categories. This system utilized cold formed channel shaped pans between which flat sheets of steel were arched to produce a voided slab, as shown in Figure 1(d). Holes punched in the webs of the pans ensured a connection between the steel and the in-situ concrete.

Development of form-reinforced slab systems also began in Europe in the late 1960's. Bryl [6] reported tests on several types and identified three distinct phases of composite action :

(i) For positive bending, with the formwork in tension and with natural bond intact, the section may be analysed as uncracked, with full interaction.

(ii) When natural bond is destroyed, sudden failure occurs in the absence of mechanical shear transfer devices, and

(iii) mechanical shear transfer devices provide a great increase in strength after natural bond failure and if the shear connection strength is sufficient, the fully plastic moment may be attained.

Wethmar [7] has reported tests on a system of Type II, which has been employed in Holland. In this deck shear connection is provided by circular embossments at the top and bottom of the webs of the steel deck and the longitudinal spacing of these embossments was one of the parameters investigated.

Several publications [8,9,10] in this country in the early 1970's brought the concept of the form-reinforced slab to the attention of engineers and in 1975 the European Convention for Constructional Steelwork published recommendations [11] for the design of composite floors with profiled steel sheet.

Due to the proprietary nature of permanent composite steel formwork, the majority of research and development has been carried out by individual steel companies to provide safe load tables for their own products. Recent research at Iowa State University has attempted to bring some uniformity into design methods by carrying out tests on various types of decking to investigate the possible modes of failure. This extensive programme, which has now been reported [12], consisted mainly of two-point static loading tests on specimens of form-reinforced slabs spanning in one direction between simple supports.

Three possible modes of failure have been defined by Porter and Ekberg [13]. These are, (i) flexure of an under-reinforced section; (ii) flexure of an over-reinforced section; and (iii) shear bond. The latter is characterized by a diagonal tension crack at or near one loading point, resulting in loss of natural bond and slip in the shear span. This causes a reduction in the degree of interaction, dependent upon the reserve strength

in any mechanical shear connectors which are present. The research at Iowa State University has been mainly concerned with the shear-bond failure mode, for which three design equations have been compared with test results using a semi-empirical approach. One of the design equations was derived by Schuster [14]. The need for a semi-empirical approach is a reflection of the difficulty which has been experienced in defining the behaviour of the shear connection and the effect of slip between the steel and concrete components on the stress and strain distribution within the materials.

The behaviour of form-reinforced slabs acting in a two-way mode has been studied by Porter and Ekberg [15] who tested specimens of Types I and II under four point loading to represent a vehicle load and in some cases ten loading cycles were applied. As in the case of one-way acting form-reinforced slabs, the shear-bond mode of failure was found to be critical.

Due to the relatively static nature of the loading to which building floors are subjected, there has been very little research into the behaviour of form-reinforced slabs under repeated loading. However, the application of the concept to floors in warehouses, where stock is frequently stored and removed, has raised the question of fatigue failure. Sayed, Temple and Madugula [16] have reported on a series of tests on one-way, simply supported specimens of a form-reinforced slab of Type II, under a central point load. The design of the composite slab used, relied mainly on natural bond, which was found to govern the failure of the slab in static load tests. The main conclusion drawn from the investigation was

that specimens subjected to dynamic loads of less than 60% of the static bond failure load, for two million cycles, did not show any reduction in shear-bond failure load when tested statically and since, in practice, working loads would be less than this 60% value, no allowance need be made for the effect of repeated loading. However, two million was the maximum number of cycles applied to any one specimen and the response of such composite slabs to a greater number of loading cycles is open to question.

The feasibility of the use of form-reinforced slab systems in bridge deck construction was investigated by Climenhaga and Johnson [17], who carried out repeated loading tests on scaled down slab specimens employing three types of steel decking. The shear connection in one type was provided by embossments pressed into the webs of the corrugations at an angle of 60^{o} to the longitudinal axis of the deck unit. The embossments were arranged to slope in opposite directions on adjacent webs to provide resistance to separation and no allowance was made for natural bond, which was prevented during casting of the specimens. The second type of deck provided composite action by means of steel bars welded to the tops of the corrugations and again natural bond was prevented. The third group of specimens tested utilized the American 'Inryco' building floor deck which relied on a combination of embossments in the webs and natural bond to achieve composite action. All tests were carried out on the assumption that the H.B. loading spectrum, which consists of a relatively small number of loading cycles (1.1 million) producing fairly large stresses, would be

most detrimental to the shear connection strength. On this basis, it was concluded that the first two groups of decking appeared to have adequate strength under repeated loading for bridge deck construction, but the performance of the 'Inryco' form, which relied on natural bond, was poor.

The investigation which forms the basis of this thesis was essentially a continuation of the work carried out by Climenhaga and Johnson.

There are many other types of composite and non-composite permanent formwork available for the construction of reinforced concrete slabs and precast concrete units may be cited as an example. Here again the product is of a proprietary nature and systems are manufactured for use in both buildings and bridges. Dowling et al [18,19] investigated the behaviour of a precast concrete system designed for the deck of a composite bridge, under static and repeated loading. This system consisted of individual concrete planks reinforced with a steel lattice of reinforcing bars which extended above the top surface of the concrete to provide a mechanical shear connection with the in-situ concrete. The system was shown to be suitable for application to composite bridge construction and recommendations were given for design.

1.3 ADVANTAGES AND DISADVANTAGES OF STEEL DECK SYSTEMS

There are many inherent advantages in the use of steel decking systems in floor construction, but there are also several disadvantages and the decision to employ the technique in preference to a conventional reinforced concrete slab with timber formwork may often depend on local labour costs and material

availability. However, disregarding local conditions, the advantages of steel decking systems, relating to building floors, may be set out as follows :

(i) The steel deck acts as permanent formwork for the in-situ concrete slab and depending upon the strength of the steel section employed and the spans involved, temporary shoring may be minimised or completely eliminated. The costly procedures of timber formwork construction and removal thus become unnecessary. Indeed, the removal of timber formwork can be a very dangerous operation.

(ii) If an adequate means of shear connection is provided, composite action may be achieved between the concrete and the steel deck, which then acts as reinforcement for the slab. Additional reinforcement is then necessary only for shrinkage and temperature control and in the regions of negative (hogging) bending.

(iii) Deck systems employed in building floors are manufactured from light gauge steel sheet, a thickness of 1.0 to 1.5 mm being typical and the units are normally ready cut to length before delivery to the site. Construction time can be greatly reduced as the formwork units are easily handled and fixed into place, frequently with the now common "through the deck" stud welding technique, which can also ensure composite action between the slab and supporting steel beams.

(iv) When fixed in place the decking provides a natural working surface for following trades, although in some cases it may present

a surface which is difficult to walk on.

(v) The use of steel decking often leads to reduced slab weight which can result in significant savings in supporting beams, columns and foundations.

(vi) The corrugations of the decking provide natural ducting for services. This has been particularly advantageous with the increasing volume of electrical wiring required for telephones, computers and other office equipment in modern buildings.

(vii) Finally, cost comparisons may show that form-reinforced slab construction is cheaper than conventional timber formed reinforced concrete.

This impressive list explains why form-reinforced slab construction is now very popular in high rise steel framed buildings. The prestigious Sears Tower [20] in Chicago may be cited as an example of its application.

As in most structural systems, there are disadvantages which must be considered in the choice of a form-reinforced slab system in preference to normal reinforced concrete construction. The most important disadvantages are :

(i) To ensure composite action, care must be taken to compact the concrete around the mechanical shear connection devices, particularly in the case of embossments in the webs of corrugations. The surface of the decking must be cleaned to remove all traces of grease and dust to promote good natural bond when the latter features in the design for composite action.

(ii) The steel formwork is exposed to the atmosphere and requires protection against corrosion. This is normally achieved by

galvanising the steel deck and in adverse conditions regular maintenance and painting may be required.

(iii) A specific fire rating is necessary. This may be achieved by the provision of a suspended ceiling or through the use of spray-on fire proofing, but the need for fire-rating tests will lead to increased development costs.

As regards the application of the form-reinforced slab to bridge decks, many of the advantages given above will be equally applicable and with the increasing trends in labour and timber formwork costs it may be a preferable alternative to conventional construction. However, there are disadvantages and in the case of bridge decks, the corrosion problem is probably most important. In the final analysis, however, it must be the economic appraisal of any possible system which governs and in particular the cost of individual steel deck units and any long term maintenance costs.

1.4 A BRIEF REVIEW OF RESEARCH ON COMPOSITE BEAMS

Composite construction in steel and concrete is a very diverse field covering many types of structural element within the broad classifications of composite beams, columns and plates. During the past twenty years the knowledge in this field has increased rapidly due to extensive research programmes to the point where composite construction is used extensively throughout the world.

A report [21] published in 1974 has provided an excellent review of the present State-of-the-Art, together with an extensive

bibliography covering every aspect of composite construction. Porter and Ekberg [22], in response to this report indicated the extent to which research was being conducted into form-reinforced slab construction at Iowa State University at that time.

In the context of this brief review a composite beam is defined as a steel I-beam which acts compositely with a concrete slab through the provision of shear connectors which are welded to the top flange of the beam. To avoid any possible confusion with a form-reinforced slab, a composite plate is defined as a structural element consisting of a flat steel plate which acts compositely with a concrete slab by means of welded shear connectors.

In terms of structural action a form-reinforced slab is closer to a composite beam than a composite plate due to the inherently greater bending stiffness of a corrugated steel plate in the direction of the corrugations, compared with the transverse direction. The transverse load distribution characteristics may be improved by providing the concrete slab with transverse tension reinforcement, but the interaction between the resulting reinforced concrete slab and the steel decking remains, essentially, a one-way mode.

Ideal composite action between steel and concrete will exist if two criteria relating to the interface between the two materials and the adjacent fibres, are satisfied. The first criterion is that there should be no strain discontinuity at the interface; that is, there should be no relative movement or slip between the two materials in the direction parallel to the interface. The

second is that there should be no separation, implying that deflections of both elements normal to the interface should be equal. If these two conditions are satisfied, 'complete interaction' is said to exist. Theoretically this can occur only when the natural bond (or chemical cohesion) between the concrete and steel is intact everywhere. Natural bond is of a highly variable nature and cannot be relied upon in design, as bond strength between a perfectly flat steel plate and concrete is very low. Further, one overload is sufficient to destroy natural bond, thereby reducing the shear connection strength to zero in the absence of additional shear transfer devices. The existence of natural bond is therefore normally ignored, except in the case of steel members completely encased in concrete, where shrinkage of the concrete increases bond strength, as for steel reinforcing bars in reinforced concrete construction or concrete encased columns. An additional exception, as mentioned earlier, is the case of form-reinforced slabs in building floors, where natural bond plays a significant role in the shear connection.

To develop the full potential strength of a composite section it is necessary to provide a secondary means by which the two criteria of zero slip and separation may be satisfied, to attain complete interaction. This is achieved by the use of shear connectors welded to the steel element to transfer shear and separation forces across the interface. Several devices have been used for this purpose, including channel sections, bars or tees acting with hoops and spirals, but the most common type of shear connector is the headed stud.

However, most shear connectors have some degree of flexibility, which, together with local compressive strains in the adjacent concrete, allows small amounts of slip and separation, which increase with applied load, until failure occurs. This behaviour can be seen in a push-out test, which is the standard method of establishing the strength and response of a shear connector.

If the two conditions of zero slip and separation at the interface are not fulfilled, 'partial interaction' is said to exist. In the extreme case of there being no shear connection and no friction at the interface, the condition is one of 'zero-interaction'.

Normally the role of the shear connector is to reduce the slip and separation to small values, so that the composite action may approximate to complete interaction in so far as design is concerned.

A review of early research on composite beams, which commenced in both Europe and the United States in the 1920's has been given by Viest [23]. In 1964, Chapman [24] presented a discussion of the behaviour of the simple composite beam and indicated the type of behaviour to be expected of more complicated composite sections, the number of which is potentially large, for both beams and plates. Research in the field of composite beams was very active during the 1960's and experimental investigations were carried out to provide design rules for both buildings and bridges. A review of research in Great Britain between 1960 and 1970 has been presented by Johnson [25].

This work was mainly concerned with the determination of shear connector strength and the required number and spacing along the beam to ensure that the behaviour of the beam approximated to complete interaction at working loads and enabled the section to attain its full flexural capacity prior to shear connector failure. Chapman and Balakrishnan [26] carried out an extensive testing programme from which they concluded that shear connectors may be loaded to 80% of their ultimate capacity at the calculated flexural failure load of the beam and that the effect of interface slip and separation in the elastic range was small, even when the shear connection was designed to fail at the flexural failure load. Slutter and Driscoll [27] carried out similar research in the United States and reached essentially the same conclusions.

A study of the effects of repeated loading and fatigue of shear connectors was made by Teraskiewicz [28], who, together with Chapman [29] presented a review of research on composite construction carried out during the 1960's at Imperial College. Mainstone [30,31] and Menzies [31,32] have reported on a great number of push-out tests designed to study the behaviour of various types of shear connector under both static and fatigue loading comparing the results with the strengths of shear connectors specified in C.P. 117 [33,34].

Barnard and Johnson [35,36] investigated the application of simple plastic design to simply supported and continuous beams on the assumption that complete interaction was applicable and concluded that this was possible, providing that secondary failures (e.g. interface shear failure) were prevented. However, they noted

that, with the plastic neutral axis within the concrete slab, the assumption of full plasticity in the steel beam could lead to an overestimation of the ultimate moment by 5% - 11%.

The behaviour of shear connectors in concrete which is cracked in tension, which can occur in the hogging moment regions of continuous composite beams, has been studied by Johnson et al [37], by means of push-out tests. On the basis of this study it was recommended that the maximum design load of a stud in cracked concrete should be taken as 64% of the ultimate capacity as determined by the standard push-out test.

Several theoretical investigations have been carried out to determine the effects of partial interaction on the behaviour of composite beams. The classic theory developed by Newmark [38] for partial interaction in the elastic region was based on the assumptions of zero separation, linear load-slip behaviour of the shear connection and linear material response. The essence of Newmark's theory was to assume that shear transfer between the steel and concrete occurred in a continuous nature along the interface, rather than at discreet points determined by the position of the shear connectors. This theory was used by Goodman and Popov [39] in an application to multilayered timber beams, incorporating non-linear shear connection behaviour in a step-wise application of a linear load slip relationship.

The effect of separation, in the absence of slip, was studied by Balakrishnan [40], using as a basis a theory developed by Chapman [41] for the analysis of the interaction between the hull and superstructure of a ship. Balakrishnan found that

significant tensile stresses were developed in shear connectors and emphasized the need to ensure that the concrete slab was adequately 'tied down' to the steel beam.

A numerical method of analysis of composite beams to include non-linear behaviour of both concrete and the shear connection was developed by Yam [42] and was used to study the ultimate load behaviour of simply supported and continuous beams. The results of this investigation have been reported by Yam and Chapman [43,44] and were found to agree very well with the test results obtained by Balakrishnan [40] and Teraskiewicz [28]. For the purpose of the analysis, Yam assumed that no separation between the steel and concrete occurred and that the interface shear is transferred in a continuous nature, as in Newmark's theory.

Dai et al [45] have used a finite difference approach to investigate ultimate load behaviour by assuming the interface shear force to be transferred at the positions of the shear connectors and equating the shear force at each connector position with the change in longitudinal force in the concrete slab. The compatibility condition which exists between slip and strain difference, in the absence of separation, was then used, together with a multilinear load-slip curve for the shear connection, to establish a set of simultaneous equations, which were then solved. This finite difference method was originally used by Stussi [46] for composite beam analysis with a linear shear connection load-slip response.

The partial interaction analysis of composite beams is

far too complicated for use in normal design procedures and composite beams are therefore usually provided with the necessary shear connection strength to approximate to complete interaction. There are occasions, however, where partial interaction design may be economically beneficial. For example, if the size of a steel beam and the concrete slab thickness have been predetermined to be greater than necessary, due to architectural considerations, a complete interaction design will result in a beam which is far stronger and therefore more expensive, than necessary. Stark [47] has proposed that a partial interaction design, in which fewer shear connectors are employed, will be more economical and, if designed correctly, of sufficient strength. Johnson and May [48] studied this problem and on the basis of a parametric computer study concluded that the maximum span to depth ratios applicable to beams with partial interaction may have to be reduced relative to those for complete interaction design, to counteract the greater in-service deflections expected for the partial interaction beam. However, Frodin, Taylor and Stark [49] have recently reported an investigation of the deflections in partial interaction beams in comparison with the full interaction case under service load conditions, using a linear analysis, but also making an allowance for the non-linear behaviour of shear connectors under working loads. As a result of this investigation, it was concluded that the deflections of a composite beam with partial shear connection under its service load, will not be greater than the in-service deflections of the corresponding complete interaction beam, since

the service load for the latter will be greater than for the partial interaction design.

The popularity of form-reinforced slab construction for building floors in recent years has led to an additional area of research in the field of composite beams to determine the degree of interaction which may be achieved between the concrete slab and the supporting steel beams. When the steel decking is orientated such that the corrugations are parallel to the main supporting beams composite action between the concrete slab and the steel beam is essentially as for a haunched slab and the interaction is not directly affected by the presence of the formwork. In this case normal design methods may be applied, as, for example, in Ref. (11). When the corrugations run in a direction perpendicular to the steel beam, the formwork is very often designed to be continuous and stud shear connectors are welded straight through the lower flanges of the decking into the top flange of the beam. In this case the composite action between the slab and the steel beam may be significantly reduced by the presence of the steel deck as this presents a more flexible region in the critical interface zone.

Robinson [50] studied this problem in a series of tests on composite beams with steel decking acting as non-composite formwork to the concrete slab and concluded that the geometry of the corrugations, or more precisely the ratio of the height to the width of the concrete ribs is the governing criterion in the degree of interaction achieved. In a further publication [51], Robinson applied elastic partial interaction theory to the problem and by the

use of an interaction coefficient, expressed the performance of the composite beam in terms of complete interaction modified by an efficiency factor. This work has also been reported by Clark [52].

In 1970, Fisher [53] proposed that for composite beams with corrugated steel decking, when the overall depth of the latter does not exceed 75 mm, the shear strength of a stud in a concrete rib of the slab is proportional to the product of the shear strength of the stud in a solid slab and the ratio of the rib width to height. A proportionality factor was derived empirically from test data to complete a design equation.

An extensive programme of tests on composite beams incorporating various steel decking systems without embossments has been carried out at Lehigh University [54]. This programme utilised steel decks of 38 mm, 51 mm and 75 mm in depth to study the effect of the height of the studs, the stud spacing and the number of studs per concrete rib. On the basis of the test results it has been proposed to include the effect of these parameters on the shear strength of the studs in a modification to the equation proposed by Fisher [53].

In relation to this work on composite beams with steel decking, it is interesting to note that these investigations have again been concerned with the application to building floors, in which the thickness of the steel decking employed is normally between 1.0 and 1.5 mm. The effect of decking in which the steel thickness is greater than 1.5 mm has not been considered, although the depth of the decking has been included in the empirical design equations mentioned.

1.5 SCOPE AND LAYOUT OF THIS THESIS

The main objective of this thesis is to assess the feasibility of the use of a form-reinforced slab in bridge deck construction by investigating the performance of the system under static and repeated loading, and to provide guidance for design. A major part of the thesis is therefore concerned with a description of the objectives, procedures and results of the static and repeated loading test programmes. A theoretical study has also been carried out to examine the correlation between the test results and complete and partial interaction theory.

The design considerations and development of the full size prototype formwork unit for the test programme are outlined in Chapter 2, together with the method of manufacture.

The next three chapters describe the experimental studies. Chapter 3 deals with the static testing programme which commenced with a preliminary investigation of the shear connection characteristics by means of push-out tests. An examination of the construction loading conditions and details of tests on a bare formwork unit are presented. The final section of this chapter describes static tests on the composite slab unit under both sagging moment (with the formwork in tension) and hogging moment (formwork in compression) conditions.

Chapter 4 deals with the repeated loading, or dynamic, tests. Design loading spectra and the possibilities of fatigue failure are examined and the preparation of test specimens, test procedures and results are described in detail. An extension of the

studies of Chapter 4 is presented in Chapter 5, describing tests to determine the fatigue characteristics of the embossments by means of 'in-air' tests on sections of the steel formwork in tension.

The behaviour of the bare formwork unit under construction loading conditions and up to ultimate load, is examined in Chapter 6, by comparison with simple bending theory.

The main theoretical study relating to the behaviour of the composite slab in a simply supported sagging moment mode is presented in Chapter 7. A method of partial interaction analysis which is an extension of the numerical solution developed by Yam [42] is described. A computer program written to perform the analysis includes non-linear behaviour of the concrete and shear connection and strain hardening in the steel. The analysis assumes that there is no separation between the concrete and the formwork. The experimental results are compared with the partial interaction analysis and an additional complete interaction analysis which was performed by a modified version of the computer program, incorporating non-linear behaviour of the concrete, strain hardening in the steel formwork and the effects of dead load construction stresses in the steel formwork. This dead load effect is also included in the partial interaction analysis.

A general qualitative discussion relating to potential problems in the manufacture of the formwork and the practical application of form-reinforced slab systems in bridge decks, has been included in Chapter 8. Unfortunately, an economic appraisal

cannot be presented as this depends essentially on the cost of producing the steel deck formwork, which, as yet, is not generally available.

The final chapter consists of an examination of the results of the experimental and theoretical studies, in relation to possible design recommendations. Although the conclusions drawn are applicable primarily to the prototype formwork unit employed in the testing programme, there are several aspects of behaviour which are applicable generally to form-reinforced slab construction.

CHAPTER 2

DEVELOPMENT OF THE PROTOTYPE FORMWORK UNIT

2.1 DESIGN CONSIDERATIONS

Due to the relatively high loading intensities and the fatigue aspects for which bridges must be designed, a permanent composite formwork system for use in bridge deck construction will require a more robust section, in terms of a thicker steel sheet, a deeper section and a potentially stronger shear connection than building floor formwork employs.

As mentioned in section 1.2, the majority of building floor systems incorporate the strength of the natural bond between the steel formwork and the concrete in the design and the role of the embossments in the webs and flanges is to augment the shear connection strength, thereby increasing the potential natural bond strength. In the event of bond failure, although significant slip may occur, causing increased deflections and stresses, the presence of the embossments often provide sufficient reserve shear strength to prevent total collapse. This partial dependence upon natural bond is acceptable in the relatively static loading conditions of buildings. In view of the large number of loading cycles which constitute the design loading spectra for most bridges, although the majority of these cycles are at relatively low loading intensities, there is no foundation for an allowance for natural bond in the design of a form-reinforced slab system for bridge decks. This claim is supported by the work of Climenhaga and Johnson [17].

It is therefore considered that resistance to shear and separation forces between the form and the concrete must be achieved entirely by mechanical means. In practice the presence of natural bond will provide additional strength to the shear connection, thereby increasing the stiffness of the slab, but in the event of bond failure during service, or the prevention of natural bond due to, for example, an oil film on the deck prior to casting, the shear connection will depend solely upon the mechanical shear transfer devices present.

Two of the three groups of formwork tested by Climenhaga and Johnson [17] correspond to the Types I and II depicted in Figure 1. The third group, which did not have a re-entrant corrugation shape, but relied upon embossments pressed into the webs to augment natural bond strength, utilised the American 'Inryco' floor decking as a half scale bridge deck specimen. This deck consisted of 1.6 mm galvanised steel sheet, cold formed into a corrugated section of 38 mm overall depth. The ratio of the height of the embossments to the sheet thickness of 0.66 was inadequate to provide the necessary shear connection strength after bond failure. The bond strength was found to be relatively low and was further reduced by repeated loading.

The two other types of decking tested by Climenhaga and Johnson were fabricated from 1.6 mm steel sheet into a 50 mm deep trapezoidal corrugation shape to represent two-thirds scale bridge deck specimens. One group of specimens utilised bars welded to the deck to provide shear connection (Type I) while the other was

provided with embossments in the webs of the corrugations, inclined at 60^{o} to the longitudinal axis of the unit and in opposite directions on adjacent webs (Type II). Both types of formwork performed well in the absence of natural bond and were considered to be suitable for bridge decks.

The fatigue behaviour of the Type I formwork was dependent upon the welds between the bar connectors and the deck, as all four specimens tested failed at this weld. However, it was suggested that a reduction in the size of the connector bars and welds may improve fatigue behaviour. Presumably, an increase in the number of bars and welds would therefore be necessary, thereby making the decking less attractive economically.

In the Type II formwork the ratio of the embossment projection above the deck surface to the steel sheet thickness was 2.5, as compared to 0.66 for the 'Inryco' deck. Thus the actual height of the embossments was almost four times the height for the 'Inryco' deck. The test results indicated that the shear connection was adequate to attain the fully plastic moment of the section in sagging bending and it was therefore suggested that a successful design would have a ratio of embossment height to sheet thickness (H/t) of at least 2.0.

The shear connection design was based upon the bearing stress of the concrete on the area of the embossments projected into the plane at right angles to the longitudinal axis of the decking. This bearing stress, σ_d, was taken as 0.6 of the design cube strength for the concrete, under the maximum design shear for

H.B. loading. As a result of the investigation it was recommended that the bearing stress should not exceed 0.6 of the design cube strength of the concrete.

The prototype formwork unit was required to comply with criteria relating to construction loading conditions in addition to those for the composite working stage. As a permanent formwork system the decking must be able to support its own weight plus that of the wet concrete, without the need for temporary shoring, with a specified limitation on the maximum deflection. The use of the formwork as a working platform during construction implies that additional loads, due to concrete plant, personnel, etc., must be supported without distress. An allowance must also be made for the possibility of loads in excess of the weight of the concrete alone, due to concrete pumping, impact forces, or heaping of the concrete, during casting.

The performance of the prototype unit under the various construction loading conditions is investigated experimentally in Chapter 3.

In unpropped construction, with long spans, the deflection of the formwork under the wet concrete load may cause a significant increase in the dead load which the formwork is required to support. The implications of this ponding effect also require investigation.

2.2 DESCRIPTION OF PROTOTYPE UNIT

The prototype formwork unit was based essentially on the Type II unit tested by Climenhaga and Johnson [17] and was designed

for use in a typical motorway bridge of composite construction, consisting of longitudinal steel girders at 3.5 metres centres, supporting and acting compositely with a reinforced concrete deck of 250 mm overall depth. The formwork units would therefore span transversely between the main girders, being supported by the top flanges. Considerations of the details in the region of the top flanges of the supporting girders indicated that the clear span of the formwork units would be of the order of 3.33 metres.

A preliminary specification [55] for construction loading, together with design calculations for the composite stage assuming that complete interaction existed between the formwork and the concrete indicated that the section shown in Figure 2 would satisfy the criteria.

The steel sheet thickness of 3 mm and the overall corrugated depth of 75 mm ensured that the construction loading conditions would be satisfied, on the basis of simple bending theory, over a span of 3.33 m. The width of the formwork unit (720 mm) was fixed by the width of standard flat steel sheet from which it would be manufactured and the consideration that the individual formwork unit should be easily handled.

The shear connection was designed on the basis of the local concrete bearing stress not exceeding 0.6 of the design cube strength of the concrete and that the ratio H/t should be 2.0. The height of the embossments was therefore fixed at 6 mm. The embossments on the webs are inclined at 60° to the longitudinal axis of the unit and in opposite directions on adjacent webs to provide resistance to

separation forces. The shear connection pattern was modified to include embossments on the top flanges in addition to the webs, in an attempt to reduce the possibility of fatigue failure.

The length of the embossments was originally specified as 50 mm overall, but it was found that the actual effective length projecting into the concrete should be taken as 40 mm due to the radius of curvature required for pressing.

The spacing of embossments on both webs and top flanges was specified as 45 mm between centres. This pattern in fact ensured a factor of safety of 1.6 on the average local concrete bearing stress σ_d, with respect to the factor of 0.6 applied to the design cube strength of the concrete, which was taken as Grade 30. Thus the average concrete bearing stress on the embossments under the conditions producing maximum horizontal shear force at the interface would be 11 N/mm^2, compared with the proposed allowable maximum of 18 N/mm^2 for a Grade 30 concrete.

For the purpose of the testing programme, the length of the formwork units was specified as 3.6 metres to permit testing with a simply supported span of 3.33 metres.

2.3 MANUFACTURE OF UNITS

The production of a limited number of formwork units was undertaken by the British Steel Corporation for the purpose of this investigation.

The steel decking systems used in building floor construction utilise a steel sheet which is usually between 1.0 and 1.5 mm in thickness and the sections are manufactured by the process of cold

rolling. For the production of the limited number of specimens required for the testing programme described in this thesis a method of pressing and press-brake forming was used. An interesting description of these methods of cold forming of steel sheet may be found in Ref. 56.

The manufacture of the formwork units consisted of two operations. The first was the pressing of the embossment pattern into the flat sheet. This was achieved using a punch and die to press the required number of nine embossments across the width of the sheet in individual lines, the sheet being advanced in the longitudinal direction after each pressing to give the necessary spacing of 45 mm. The second operation consisted of press-brake forming the sheet, with embossments, into the required corrugated shape.

A number of difficulties were experienced in the manufacture of the units. The punch and die for the first operation was specially machined so that the position of each embossment relative to the junctions, or bend-lines of the webs and flanges could be adjusted individually, so that after the section had been formed into the corrugated shape, the embossments were located centrally in the webs and flanges. The press-brake forming operation required a complicated sequence to achieve the necessary section, as the equipment used was not designed specifically for the task.

A total of eleven formwork units were manufactured.

2.4 DIMENSIONAL TOLERANCES

A detailed dimensional investigation of each formwork unit was carried out and direct measurements of the cross-sections are given in

Table 1. Measurements were taken at two or three cross-sections and averaged to give the values shown. Figure 3 provides a schematic representation of the notation used in the table.

Measurements of the sheet thickness, excluding galvanising, indicated very little deviation from the specified value and a constant thickness of 3 mm was assumed to apply to all units.

Many of the dimensional aspects covered by Table 1 are fairly critical in relation to the practical application of the formwork in an actual bridge deck and will be discussed more fully in Chapter 8.

The height, or projection of the embossments above the surface of the plate was investigated fairly extensively. Measurements were taken from five of the prototype units. It was found that the height of the embossments on any one flange or web was constant to within 0.05 mm, which is understandable, as all embossments on any one flange or web were pressed using the same punch and die. There was a more significant variation in height between the embossments on different webs and flanges. The smallest value of H on any one web or flange was 5.48 mm, while the greatest value was 5.74 mm. The overall average height measured on any one unit was 5.6 mm. This is 7% less than the specified height of 6 mm and it has a significant affect on the average local concrete bearing stress, σ_d, which under the maximum design shear force is increased from 11 N/mm^2 to 11.8 N/mm^2, while the factor of safety on the value of 0.6 of the design cube strength is reduced from 1.6 to 1.5.

A less detailed investigation of the thickness of the steel at the corners of the embossments revealed that, on average, the steel

thickness in these regions was reduced to approximately 2.0 mm. This reduction in thickness is shown in Figure 4, which shows the longitudinal and transverse cross-section profile of the embossment shape.

An examination of the longitudinal profile of the units indicated significant deviations from the two planes in which the top and bottom flanges would lie, for an ideal, perfectly flat unit. The magnitude of these deviations is indicated in Figure 5, which shows the profile of the top and bottom flanges of one unit measured relative to a straight line taken between the ends of the flange in question.

CHAPTER 3

STATIC TESTS

3.1 GENERAL

The aim of this first phase of the testing programme was to establish the response of the formwork unit in the various conditions of construction loading and in the composite mode where it acts as reinforcement for the slab. In addition, a number of simple push-out tests were carried out in order to increase the understanding of the shear connection and to establish the expected load-slip response.

3.2 PUSH-OUT TESTS

3.2.1 Objective of Push-Out Tests

The degree of interaction between the steel deck and the concrete in the composite slab depends entirely on the strength and stiffness of the shear connection. The manner in which the embossments in the webs and flanges transfer shear and separation forces across the interface between the two materials is very complex. Although the basic mode of operation of the shear connection is well established through the successful application to floor construction, it appears that the details of the concrete bearing stress distribution on the embossments, the means by which separation is resisted and the effects of embossment height and angle of inclination to the longitudinal axis are not fully understood.

A limited number of simple push-out tests were carried out to

investigate the action of the shear connection and the load-slip response which may be operative in the composite slab.

Among the variables upon which the strength of the connection will depend are the embossment shape and dimensions, in terms of height, length, spacing and angle of inclination of the webs. The effect of the concrete strength and aggregate size must also be considered. Furthermore, the strength will be dependent to some extent upon the cross sectional shape of the formwork unit, particularly the angle between the webs and the flanges (θ). When this angle is greater than 90^{o} for example, considerable resistance to separation will be developed by a 'dovetail' action.

It was assumed that the thickness of the steel sheet and the stiffness of the embossments were sufficiently large to prevent local deformations in the embossment profile and that the shear connectors may be classed as 'rigid'. Throughout the testing programme, no evidence was discovered to indicate that this assumption was not valid.

An extensive test programme would be necessary to determine, in terms of all possible variables, the optimum geometry for maximum shear and separation resistance. Since the geometry of the cross section and embossments of the prototype formwork unit had been previously determined it was decided to conduct a limited number of push-out tests to investigate the effects of varying the embossment height (H) and the angle of inclination to the longitudinal axis on the webs (α). Variations in the cross sectional geometry were not considered and in many of the push-out specimens the prototype

embossment geometry was modelled to provide information regarding the load-slip response which may exist in the composite slab.

3.2.2 Details of Test Specimens

3.2.2.1 *General*

The push-out specimens consisted essentially of two sections of a single corrugation tack welded together along the edges AA' as shown in Figure 6, with the void between the troughs filled with concrete. When these tests were devised the prototype formwork units were in the early stages of development and the decision to add embossments to the top flanges had not been made. The push-out test specimens therefore employ one embossment on each web only (except for Test Series 5) and initially the embossments were simulated using steel rods, split in half and welded to the 3 mm steel plate from which the specimens were prepared. Later, when samples of pressings became available, embossments were cut from the sample sheets and welded into the steel plate to represent the geometry more accurately. This particular design for the push-out test was chosen to provide a specimen which was cheap and very simple to prepare.

All push-out tests utilised a concrete mix as specified in Appendix A. This mix was designed as a Grade 30 concrete with a maximum aggregate size of 20 mm. All specimens were cast in an inverted position to the depth shown in Figure 6 and a thin coating of grease was used to prevent natural bond.

Tests were carried out in five series, each of which consisted of four individual specimens. Each set of specimens was cast from a single batch of concrete, together with six 100 mm concrete cubes.

In addition, a single specimen was fabricated from a non-slip flooring plate.

3.2.2.2 *Test Series 1*

This first series was devised to study the variation in the angle of inclination of the web embossments to the longitudinal axis (α). The embossment profile was simulated using steel rods split in half and welded to the plate to give a height, H, of 6 mm. The angle α was varied as shown in Table 2 and to keep the projected area resisting the applied load constant, the length of the steel rods was varied. All specimens were laterally restrained by welding along the edges AA'. (See Figure 6).

3.2.2.3 *Test Series 2*

The effect of altering the embossment height was studied in this series of tests using a 4 mm embossment height, which was again simulated using steel rods split in half. The other parameters were exactly as for Series 1. All specimens were laterally restrained by welding.

3.2.2.4 *Test Series 3*

The lateral restraint provided by welding the two sections of the corrugations together was removed in this series of tests and all four specimens were tested in a completely unrestrained mode so that only the locking action of the embossments prevented separation. Two of the specimens were given an embossment height of 6 mm and the other two a height of 4 mm, again using steel rods. In all tests the embossment length, l, was 50 mm and the value of α, 60^{o}.

3.2.2.5 *Test Series 4*

On receiving a flat sheet of sample pressings, push-out tests

were carried out incorporating the pressed embossments. In this series of tests, four specimens with exactly the same geometry were tested, two in a laterally restrained mode and two in an unrestrained mode. It was found that these first sample pressings achieved heights of approximately 5 mm, 1 mm short of the specified height.

3.2.2.6 *Test Series 5*

In this final series, it was decided to check the effect of incorporating two embossments at 45 mm spacing on each web. All other parameters were as for Series 4.

3.2.2.7 *Durbar Specimen*

A single specimen fabricated from 'Durbar' flooring plate was tested in an attempt to determine the effect of a drastic reduction in the value of H. 'Durbar' is a non-slip flooring plate in which projections of 1.5 mm are rolled into one surface. The thickness of the 'Durbar' plate used in this specimen was 5 mm. The specimen was tested in a laterally restrained mode.

3.2.3 Test Procedure

All specimens were tested in an Amsler 35 ton testing machine at an age of between 28 and 30 days. Load was applied to the concrete via a 25 mm thick steel platen. A 0.0001" dial gauge was used to measure slip, which was taken as the relative movement between the platens of the testing machine. In addition, four 0.0001" dial gauges were used to measure the separation between the steel and the concrete in the positions shown in Figure 6.

Load was applied in increments of approximately one-tenth of the calculated ultimate load, Q_c, given in Table 2. The concrete cubes were tested on the same day as the corresponding push-out specimens.

3.2.4 Results of Push-Out Tests

The values of the cube strength, f_{cu}, obtained from the cube tests for each push-out test series, are shown in Table 2 together with the calculated load Q_c, which represents the load required for uniaxial crushing of the concrete on the projected area of the embossments in the plane normal to the longitudinal axis of the specimen. The values of Q_u, the ultimate load for each specimen and η_u, the ratio of Q_u to Q_c are also shown in the table. The value of η_u represents the average concrete bearing stress on the embossments at failure, as a proportion of the concrete cube strength, f_{cu}.

The load-slip curves for the Series 1 to 5 are shown in Figures 7 - 11 respectively, as plots of the slip against η, the ratio of the applied load Q to the calculated load Q_c.

In all tests, as the ultimate load was approached a significant creep effect was evident and it was necessary to control the test in terms of recorded slip rather than load. At the ultimate load the slip increased rapidly and the load decreased slightly as the concrete pushed through the steel casing.

The load-separation curves for the five series were very similar and as separation between the steel and concrete is a secondary effect, the results for Series 4 only are presented in Figure 12.

The pattern of concrete crushing around the embossments subsequent to failure is shown in Plates 1 and 2 which show the specimens of push-out tests 4.2 and 4.4, with the steel casing removed.

The separation effect is shown in Plate 3, which shows the top view of specimens 1.3 and 4.3.

3.2.5 Discussion of Results

It may be seen from Figures 7 to 11 that the load-slip curves for the specimens within a given series are very similar and the most interesting aspect of the results is the difference between the laterally restrained tests, for which the values of η_u range from 1.45 to 1.8 and the laterally unrestrained tests, for which η_u lies between 0.52 and 0.83.

The results of the first two series of tests indicated that values of α of either 45^o or 60^o were preferable to the value of 30^o. There was little difference between the load-slip curves or the ultimate loads achieved for α values of 45^o and 60^o and since the latter value had already been prescribed for the prototype units it seemed pointless to pursue the determination of the optimum value.

The similarity between the values of η_u obtained from Series 1 and 2 indicated that the reduction of H from 6 mm to 4 mm did not affect the performance of the connectors, apart from the pro rata reduction in ultimate load, Q_u. This result prompted the question of the effect of a much reduced value of H. The performance of the 'Durbar' specimen, in which the value of H was 1.5 mm, was inferior to previous specimens and η_u at failure was 0.55. Inspection of the specimen indicated that the resistance to slip was afforded only by the fairly weak concrete paste, unlike the larger values of H which also provided interlock with the aggregates. It appears that between the values of 1.5 mm and 4 mm there exists a critical value of H, which is insufficient to ensure aggregate interlock with the particular concrete used. It seems reasonable to suggest that this critical value of H will depend upon the aggregate sizes. The

unrestrained tests of Series 3 also indicated a direct proportionality between ultimate load and embossment height. The results of Series 4, in which the sample pressings were incorporated were very similar to the previous tests.

The values of Q_c given in Table 2 for Series 5 were calculated on the basis of two embossments in each web and it can be seen from the values of η_u that the ultimate load is not directly proportional to the number of embossments present. This is because the direct compressive load applied to a push-out test specimen can result in an unequal distribution of forces on the connectors when multiple connectors in the direction of application of the load are employed, particularly in this case, where the embossments may be classed as rigid connectors. For this reason the results of Series 5 are excluded from the following discussion.

The most interesting result of the push-out tests lies in the effective bounding of the value of η_u which may be attained in an actual slab. The restraint at the extremities of each corrugation in an actual bridge deck is difficult to assess, but it is considered that the push-out specimens tested in a fully restrained mode represent the absolute upper limit of restraint which may exist. The average value of η_u for these tests, for $\alpha = 60^\circ$, is approximately 1.6 and represents an upper bound on the shear connection strength. The average value has been taken because the small number of tests carried out does not warrant a statistical analysis. The results obtained from the unrestrained tests, again for $\alpha = 60^\circ$, provide an average lower bound on η_u of 0.6. It is of interest here to note that this figure corresponds exactly to the value suggested by

Climenhaga and Johnson[17], as the limiting design value of the ratio of concrete bearing stress to the concrete cube strength. The value of η_u which may be expected in an actual composite slab has therefore been bounded from above and below and the difference between the upper and lower bounds is a measure of the difficulty of defining the shear connection strength.

The load-separation curves of Figure 12 indicate a significant twisting effect of the corrugations about the axis of the applied load and this can be seen in Plate 3. This effect is due to the fact that the embossments slope in opposite directions on adjacent webs. It should be noted here that all push-out specimens were designed to be symmetrical about the line AA, (see Figure 6), so that this separation effect could be measured using the pairs of opposing dial gauges which are marked Δ_1 and Δ_2 in the figure.

For the pair of webs on which the embossments slope away from the bottom flange of the corrugation with respect to the direction of the applied load (to which Δ_2 applies), the concrete bearing stress distribution on the embossments is such as to subject these webs to a separation force which is greater than that acting on the other pair of webs. In fact, it may be seen from Figure 12, that for the laterally restrained tests this smaller force causes negative separation (Δ_1) for small values of η.

The greater separation on one pair of webs must be detrimental to the load-slip stiffness of the specimens and it is possible that the strength of the shear connection may be increased by arranging the embossments to slope alternately in opposite directions on the same web in the actual formwork unit. This may be an interesting

point to pursue in future work.

The maximum separations recorded for the laterally unrestrained tests on the two sides of the bottom flanges were 0.5 mm and 1.0 mm. For the laterally restrained tests the corresponding values were 0.25 mm and 0.8 mm. These figures demonstrate that even for the unrestrained tests, resistance to separation is fairly substantial.

3.3 CONSTRUCTION LOADING TEST (TEST 1)

3.3.1 Objective of Test

If temporary shoring is to be avoided during construction, the formwork unit must be capable of supporting its own weight and the weight of the wet concrete without excessive deflection when the in-situ slab is cast, since this deflection will be permanent. In addition, the formwork will be used during construction as a working platform and must therefore be designed to support loads due to, for example, contractors equipment and personnel.

This test, which is designated as Test 1, was devised to observe the response of the formwork unit to proof loads designed to simulate the above conditions and then to load the unit to failure to check the ultimate capacity of the section.

3.3.2 Derivation of Applied Loads

3.3.2.1 *Wet Concrete Load*

The load applied to the unit to simulate the wet concrete load was calculated on the basis of a concrete slab thickness of 250 mm, which is a typical value for a bridge deck and corresponds to the design depth for the subsequent composite tests. Assuming

this load to be uniformly distributed over the formwork unit, its value may be calculated to be 3.49 kN per metre length of the unit. For a simply supported span of 3.33 m this load induces a maximum bending moment, M_{max}, of 4.84 kNm and a maximum shear, V_{max}, of 5.81 kN.

3.3.2.2 *Wet Concrete plus Additional Construction Load*

The additional construction load for which the formwork must be designed is represented by a load of 9 kN uniformly distributed over a circle of 1.2 m diameter[55] . When the 720 mm width of a single formwork unit is considered, this is equivalent to a uniformly distributed load of 6.0 kN over a one metre length of the unit. The maximum bending moment which may be induced due to the wet concrete load plus the additional construction load is 9.34 kNm with a corresponding maximum shear of 9.0 kN. The absolute maximum shear induced, when the additional construction load is adjacent to a support is 11.2 kN.

3.3.2.3 *Ultimate Load Test*

The ultimate load test was carried out using four point loads (relative to the span) of equal magnitude. The ultimate fully plastic moment calculated on the basis of a fully effective, rigid cross section (as shown in Figure 2) is 25.8 kNm, using a yield stress of 295 N/mm^2 which was obtained from tensile tests on specimens taken from samples of the steel sheet from which the units were manufactured. Six tensile specimens were tested and the average ultimate stress obtained was 420 N/mm^2.

3.3.2.4 *Loading System Employed*

To simulate the loading conditions outlined above it was

decided that a four point loading system, at one fifth span points relative to the longitudinal axis of the formwork unit would provide a good approximation to the conditions existing in practice, when the position of the additional construction load is considered.

The loads required in this four point loading system to simulate the loading conditions are shown in Table 3.

3.3.3 Description of Test Rig

The arrangement of the test rig for the construction loading tests is shown in Plate 4, in which the condition of the formwork unit after failure is depicted.

To obtain á uniform distribution of the loads across the width of the shutter it was decided to use five tension jacks at each of the loading positions attached to the floor of the laboratory via a steel base plate. Steel rods attached to the jack rams passed through 5 mm diameter holes in each flange and the load was transferred to the top surfaces of the flanges via 90 mm square loading pads. The jacks employed had a capacity of five tons which was far greater than necessary but the relatively long stroke of the jacks was required to accommodate the large deflections which were expected to occur during the ultimate load test.

The unit was tested on a simply supported span of 3.33 m. At the supports the formwork unit was bolted to 25 mm thick steel plates to provide transverse restraint against spreading of the unit.

3.3.4 Instrumentation

To obtain a clear picture of the stress distribution in the section, a complete band of strain gauges was used to record both

longitudinal and transverse strains at one section as shown in Figure 13. The strain gauges were connected to automatic strain gauge data logging equipment.

Lateral (out of plane) deflections of the unit were measured at midspan using 0.001" dial gauges at the seven points shown in Figure 13, which also shows the positions of two 0.0001" dial gauges used to measure any transverse spreading tendency at midspan.

3.3.5 Test Procedure

Each of the construction loading tests, as defined in Table 3 by 1.1, 1.2(a) and 1.2(b) were carried out three times and average values of the three sets of readings of deflections and strains were taken.

Having completed the construction loading tests, the jack hydraulic system was adjusted slightly so that the four point loads were of equal magnitude and utilised the three jacks which applied load through the top flanges only. Using this system the unit was loaded to ultimate with load increments of 0.05 of the calculated ultimate load, shown in 1.3 of Table 3. The test was terminated when deflections became excessive.

3.3.6 Results

3.3.6.1 *Construction Loading Tests*

The deflections at midspan produced by applying the various construction loading conditions are shown in Table 4(a) in which the readings taken in the three runs have been averaged. The positions of the dial gauges are shown in Figure 13. In Table 4(b) these results are presented as an overall average for lateral deflections

and a transverse expansion of the unit in the plane of the flanges.

Also shown in Table 4(b) are the deflections calculated using simple bending theory under test loading conditions, the percentage error between test and calculated values and for comparison, the calculated deflections for the fully effective design section under the uniformly distributed loads assumed to exist in practice. All deflections refer to the midspan section.

The recorded strain gauge data has provided valuable information concerning the distribution of stress within the section. For the case of the wet concrete load alone (Load Case 1.1) the longitudinal mid-plane stress distribution is shown in Figure 14. The application of the wet concrete load plus the additional construction load (Load Case 1.2) produced a very similar distribution (Figure 15). The stress discontinuities indicated in Figures 14 and 15 will not exist in practice. This representation has been used to show the differences in stress in the 'flat' and 'embossed' sections of the webs and flanges.

3.3.6.2 *Ultimate Load Test*

The formwork unit behaved in a very stable manner during the ultimate load test. Failure was of a flexural nature, aided by the tendency of the unit to spread transversely, so that the section was almost entirely yielded at failure.

There was no premature buckling of the webs, although a slight rippling of the top compression flanges between embossments was visible in the late stages of the test.

The response of the unit in terms of deflection is shown in

Figure 16 where the midspan deflection is plotted against the load W applied at each of the four lines of jacks as indicated in Case 1.3, Table 3. At values of W greater than 10.3 kN the deflections began to creep significantly due to the spreading of the cross-section, which is also indicated in Figure 16, in terms of transverse expansion at midspan.

The unit failed at a load of 11.7 kN per loading point. This load was supported by the unit until the test was terminated due to excessive deflection. Attempts to increase the load simply resulted in an increase in the rate of change of deflection. On removal of the load, the midspan residual deflection was recorded as 234 mm.

Figure 17 shows the longitudinal strains in the mid-plane section of the top and bottom flanges plotted with respect to the applied load W.

3.3.7 Discussion of Results

3.3.7.1 *Construction Loading*

The average deflection at midspan under the wet concrete load only was 10.17 mm (see Table 4). Assuming a fully effective rigid cross section, the deflection calculated on the basis of simple bending theory due to the loading conditions applied in the test is 9.75 mm.

The deflection limit which has been suggested as a design criterion is L/300 where L is the span. For the test span of 3.33 m, this results in a limit of 11.1 mm and the value obtained in the test is 9% within the limit.

The simulation of the wet concrete load and the additional construction load acting together to produce maximum bending moment

resulted in a midspan deflection of 20.6 mm, but it is the stress distribution which is of greatest significance here.

The presence of the embossments reduces the effective area of the section by virtue of the fact that the axial stiffness of the plate is reduced within the embossed width. This results in a maximum longitudinal mid-plane stress in the flat portions of the top flanges which is significantly greater than the value calculated assuming a fully effective section. The actual stress distribution is shown in Figure 15 from which it can be seen that the average maximum stress in the top flanges is of the order of 160 N/mm^2. The maximum stress calculated from simple bending theory, with a fully effective section is 120 N/mm^2. The actual maximum stress is therefore 33% greater than that predicted by simple theory.

The maximum vertical shear force due to the wet concrete plus the additional construction load occurs when the latter is adjacent to a support. This condition was simulated in order to ensure that there is no possibility of local web crippling due to the maximum shear force envisaged during construction. The response of the section under shear was very stable and there was no sign of web buckling under this loading condition or during the ultimate load test.

3.3.7.2 *Ultimate Load Test*

The ultimate load test produced a response which was linear until yield occurred in the flat portions of the top flanges at a load of approximately 8.5 kN per loading point, which corresponded to 0.65 of the calculated ultimate load, assuming a fully effective rigid section. However, in practice the cross-section geometry is dependent upon the applied load due to the tendency of the unit to spread trans-

versely. The unit cannot, therefore, attain the fully plastic moment predicted by simple theory unless the edges of the unit are restrained against in-plane translation. The failure load of 11.7 kN per loading point corresponded to 0.9 of the calculated ultimate load neglecting distortion of the cross-section.

The transverse expansion of the section, which, at the maximum attainable load, was in excess of 20 mm, caused a decrease in the overall section depth, and therefore increased stresses and deflections, which in turn, tended to increase the transverse expansion. Thus, at loads in excess of 90% of the maximum attainable load, the rate of creep was excessive.

In practice, the load carrying capacity of the bare formwork may be increased by the restraint provided by adjacent units, depending upon the longitudinal edge connection which is employed.

3.4 COMPOSITE STATIC TESTS

3.4.1 Objective of Tests

The two composite static tests were devised to determine the response of the composite form-reinforced slab under working and ultimate loads, in the two cases of sagging bending, with the formwork in tension (Test 2) and in hogging bending (Test 3). Interest was centred upon the section response and the performance of the shear connection with regard to slip and separation and the degree of interaction which exists.

The mode of action of the composite slab is essentially one-way, as far as interaction between the concrete and the formwork is

concerned, although transverse reinforcement within the concrete will assist load distribution in the transverse direction, thereby providing a two-way action. Since this investigation is concerned with the interaction between the steel formwork and the concrete it was considered that slab specimens of a width determined by one formwork unit should be tested in a one-way mode, that is, essentially as a beam element, using a loading arrangement such that the loads were uniformly distributed, as nearly as possible across the width of the specimen.

3.4.2 Description and Preparation of Specimens

3.4.2.1 *Design of Specimens*

The design of the basic section was based on the H.A. and H.B. static design loads for a simply supported one-way slab, spanning 3.33 metres between longitudinal girders. The resulting design bending moments and shear forces are given in Appendix B.

For the case of positive (sagging) bending, the section is shown in Figure 18. No allowance was made for additional tensile reinforcement and nominal compression and transverse reinforcement was included in the form of 8 mm diameter GK 60 deformed bars. In an actual bridge deck significant transverse tensile reinforcement would be required, but as the specimens were designed to act in a one-way mode, this was omitted. The overall slab depth of 250 mm is representative of a typical motorway bridge deck, for which a Grade 30 concrete is often specified.

The cross-section of the specimen designed for the negative (hogging) moment test is shown in Figure 19. A bending moment

equal in magnitude to the design positive moment was used as a basis. The tension reinforcement consisted of six 20 mm diameter GK 60 deformed bars, while nominal transverse reinforcement was again provided in the form of 8 mm diameter bars.

3.4.2.2 *Casting*

It is assumed that in the construction of an actual bridge deck, there will be some means of connection between the steel formwork and the main supporting girders. The degree of rotational restraint afforded by this connection to the ends of the formwork unit during casting naturally depends upon the type of connection employed. The condition of zero restraint (simply supported) has been covered in the construction loading test. In the casting of the composite specimens, it was decided to simulate the degree of restraint which may exist in practice. For casting, the ends of the units were bolted to short lengths of I-beam, which in turn were bolted to the floor of the laboratory.

It was initially intended to use the concrete mix as specified for the push-out tests, but due to limitations in the quantity of concrete which could be mixed in the laboratory (a total of 1.3 cubic metres was required for the two specimens), it was decided to use a concrete supplied by Ready Mixed Concrete Ltd. The concrete was supplied to the specification of a Grade 30 mix, with a maximum aggregate size of 20 mm. The two slabs were cast from the same batch of concrete, together with a total of twelve 100 mm cubes and six 150 mm by 300 mm cylinders.

Natural bond between the steel formwork and the concrete

was prevented by a thin layer of oil.

The concrete was cured under wet sacking covered with polythene for a period of seven days, after which both slabs and concrete control specimens were air dried.

3.4.2.3 *Instrumentation*

Strain Gauges: Longitudinal strain gauges were attached to the two specimens on the underside of the steel formwork and the top surface of the concrete at midspan, in the positions shown in Figure 20. All strain gauges were connected to automatic strain gauge data-logging equipment.

Slip and Separation: To facilitate measurement of slip and separation at the interface, brackets were fabricated to carry two 0.0001" dial gauges. The brackets were bolted to studs which were cast into the concrete in the positions shown in Figure 21. The provision of a corresponding gauge point on the steel deck, in the form of a small steel plate welded to the unit, enabled relative slip and separation between the concrete and steel to be recorded.

Deflection Gauges: Several 0.001" dial gauges were used to record the deflection at midspan. The positions of these gauges are shown in Figure 20 for the positive moment test (Test 2). In the negative moment test, one dial gauge was positioned on the longitudinal centre line with two further gauges close to the sides of the slab.

Curvature Gauge: A curvature gauge with a gauge length of 150 mm was used in both composite tests to measure the curvature at midspan.

3.4.2.4 *Geometric Properties of Specimens*

There was significant deviation from the nominal design dimensions, mainly in respect of overall slab depth, which was due partly to deflections under the wet concrete load. The main cause, however, was a significant out-of-flatness of the shutter units relative to the ideal situation of the bottom flanges lying in one plane. This problem is discussed more fully in Chapter 4.

3.4.3 Description of Test Rig

The composite specimens were tested in a rig constructed for a simply supported span of 3.33 m with two point loading applied symmetrically. The length of the shear span was chosen to be 750 mm from considerations of the interface concrete bearing stress on the embossments and the flexural strength of the specimens. The loading was applied through two 50 ton capacity Amsler hydraulic jacks which were supported by an arrangement of columns and cross-beams. The general arrangement of the rig may be seen in Plate 5, which shows the specimen for Test 2, in position and ready for testing.

The loads were uniformly distributed across the width of the specimens by a spreader beam system and four 90 mm square loading pads at each loading point. This system was designed to accommodate the case of Test 3, in which the specimen was tested in an inverted position to simulate hogging bending.

The support conditions were arranged to reflect continuity of the formwork units in the transverse direction and the existence of some type of connection between the formwork and the main supporting

girders. Steel plates were tack welded to the bottom flanges of the units to provide transverse restraint to the corrugations. In the positive moment test (Test 2) this plate also served to present a continuous bearing for the full width rollers which were employed at the supports to maintain one-way action of the specimen. In all specimens, for both static and dynamic tests, it was necessary to provide packing between the support plates and the formwork unit to establish bearing over the full width of the bottom flanges. The amount of packing required was usually of the order of 2 - 4 mm, for one or two of the bottom flanges.

3.4.4 Test Procedures

Both composite static tests were carried out in the three stages outlined below:

Stage I:

On first loading the specimen, the load was increased in increments from zero to a value in excess of the working load with regard to the bending moment at midspan. The maximum load applied was 100 kN per jack to ensure that the response remained as linear as the concrete permitted. The load was then gradually reduced to zero. During this first load stage the section was transformed from an uncracked to a cracked concrete section.

Stage II:

The Stage I loading sequence was then repeated on the cracked section so that design stresses and deflections could be checked.

Stage III:

The final loading stage consisted of incremental loading

of the specimen to collapse. The load increments were reduced as the ultimate load was approached. A significant degree of creep set in during the later stages and it was necessary to control the test by means of deflections, but this proved difficult as the rate of creep became excessive.

3.4.5 Results

3.4.5.1 *Composite Slab in Sagging Bending - Test 2*

On first loading the specimen the response was non-linear and at a load of approximately 40 kN per jack, distinct cracking sounds were heard, indicating that the concrete was cracking in tension. Above 60 kN the cracking sounds diminished and the response of the specimen became almost linear, showing that the section had attained the fully cracked state. The Stage II loading sequence produced a much more linear response. Figure 22 shows a correlation between experimental and simple bending theoretical strain distributions at the midspan section at a load of 100 kN per jack, during Stage II.

The ultimate load test response was almost exactly as for Stage II up to the 100 kN maximum which was used for the first two stages. At loads greater than this limit the response departed gradually from the initial linearity until, at a load of 180 kN per jack, when first yield occurred in the bottom flanges of the shutter unit, a marked non-linearity set in. At a load of 200 kN, yield had spread throughout the bottom flanges and the formwork unit continued to yield as the load was increased until failure occurred at a load of 254 kN per jack.

Failure occurred by crushing of the concrete in the mid-span section adjacent to the loading pads at the north end of the slab. Shear cracks appeared in the shear spans adjacent to the loading points at a load of 140 kN and the width of the cracks increased with the load. The crushing failure, together with the considerable width of the shear crack may be seen in Plate 6.

It was found that the recorded midspan deflections differed by no more than 5% in the transverse direction. Figure 23 therefore shows the average midspan deflection plotted against the load, while Figure 24 shows the curvature at midspan with respect to load. Figures 25 and 26 show the slip and separation distributions measured during the ultimate load test.

3.4.5.2 *Composite Slab in Hogging Bending - Test 3*

The response of the composite unit in hogging bending in the first stage of loading was non-linear up to a load of 60 kN per jack while flexural cracking spread through the concrete tension zone. The response was linear thereafter up to the maximum load of 100 kN.

The response of the cracked concrete section was much more linear throughout the loading range. At this stage the extent of flexural cracking indicated a neutral axis depth of between 90 and 100 mm.

The ultimate load test produced an almost linear response up to a load of 210 kN at which point the tensile reinforcement bars yielded. Increasing the load beyond this value resulted in increases in deflection and curvature of a magnitude which suggested

that the ultimate load, to all intents and purposes, had been attained and that failure was imminent. At a load of 220 kN failure occurred as the north shear-span suddenly developed a shear crack from the support to the loading point. The failure may be seen in Plate 7.

The midspan deflection and curvature recorded during the test are shown in Figures 27 and 28, while Figures 29 and 30 show the slip and separation distributions recorded during the ultimate test.

3.4.5.3 *Auxiliary Tests*

The results of cube tests carried out prior to both Test 2 and Test 3 are shown in Table 5. The results are consistent and the average value of the cube strength, f_{cu}, was 66 N/mm^2 for both tests. The results of tests on the cylinders for Young's Modulus and the tensile strength of the concrete are also given in Table 5.

The compressive strength of concrete predicted by cube tests is invariably greater than the actual strength in a test specimen such as a beam or column, due to variability in the concrete strength and the fact that during test, cubes are subjected to frictional forces by the platens of the testing machine. It is common practice to employ a reduction factor of 0.85 together with a variability factor of 0.8 to provide an overall reduction factor, on the cube strength, ν, of approximately 0.67. The validity of this procedure has been demonstrated, for example, by Virdi and Dowling [57] in a series of tests on biaxially restrained columns, where a reduction factor ν, of 0.6415 gave very good correlation between theoretical

and experimental ultimate loads. In all calculations relating to the flexural strength of the composite specimens, the compressive strength of the concrete is therefore taken to be 0.67 f_{cu}.

The results of tensile tests on samples of the steel from which the formwork units were manufactured are also shown in Table 5, together with tensile test results for the reinforcing bars employed in the two specimens.

3.4.6 Discussion of Results

3.4.6.1 *Composite Slab in Sagging Bending - Test 2*

The elastic tests performed on this first composite specimen show that the section response is very similar to that predicted by simple elastic theory assuming a fully effective section for the steel formwork. This may be seen with reference to Figure 22 which shows experimental and theoretical strain distributions at the midspan section for a load of 100 kN. The differences between the experimental and theoretical distributions may be due to a slight variation in concrete properties between the slab and cylinders, but a more important error may arise from considerations of the effective steel section.

The presence of the embossments in the webs and top flanges not only reduces the effective area of the unit, but also lowers the effective centroid. The reduction in effective area will lead to increased stresses while the lowering of the centroid tends to decrease the stresses, due to the increased moment lever arm. The difference between the experimental and theoretical curvatures in Figure 22 is only 4% and the only significant errors arise in the

estimation of stresses, but these errors appear to be on the safe side.

The ultimate load for flexural failure of this specimen was calculated to be 240 kN, using simple rectangular stress block theory, assuming full yield in the formwork and 0.8 of the reduced crushing strength obtained from cube tests, for the concrete. The ultimate load of 254 kN is 6% greater than the calculated value.

The longitudinal slip distributions shown in Figure 25 indicate that there was very little distress of the shear connection up to the ultimate load. The maximum slip measured at a load of 244 kN may be seen to be approximately 0.5 mm. This value may be compared with the slip at failure in the push-out test curves, which show that the shear connection attains ultimate load at a slip in excess of 3 mm. The maximum concrete bearing stress on the embossments was calculated to be 28.4 N/mm^2 at failure. If this figure is compared with the cube strength of the concrete, f_{cu}, the resulting value of η is 0.43.

3.4.6.2 *Composite Slab in Hogging Bending - Test 3*

The results of this test show once again that elastic bending theory may be used to predict the response of the section with reasonable accuracy, until the tensile reinforcement yields, which was calculated to be at a load of 219 kN. In fact tensile yield occurred at 210 kN, an error in the calculated value of 4%. Up to this stage the formwork unit had been in overall compression and had remained elastic. Yielding of the tension reinforcement resulted in a redistribution of stress throughout the section such

that the bottom (non-embossed) flanges remained in compression, while the stress in the top flanges became tensile. Thus the response of the section was almost entirely dependent upon the steel in the section, with most of the concrete depth being cracked in tension.

At a load of 215 kN per jack the bottom flanges of the unit began to yield in compression and at this stage it was noted that the rate of increase of the midspan deflection was becoming excessive. Yield had spread throughout the bottom flanges at a load of 219 kN and increasing the load to 220 kN resulted in the shear failure in the north shear span.

In reverse bending the compressive force in the section is distributed between the concrete and the formwork. Changes in this compressive force over a short distance will therefore result in a smaller change in that portion taken by the formwork than would be the case in sagging bending, with the unit in tension. The result of this is a very small interface shear force, which is therefore not a critical factor in the case of hogging bending. At failure the maximum value of the concrete bearing stress, σ_d, on the embossments was calculated to be 6 N/mm^2.

CHAPTER 4

REPEATED LOADING TESTS

4.1 OBJECTIVES OF DYNAMIC TEST PROGRAMME

4.1.1 General

The transient nature of bridge deck loading can give rise to the phenomenon of fatigue failure and it is therefore essential to understand the response of the structural components of bridges to repeated loading. In any structure there exist minor defects or local geometrical changes which give rise to stress concentrations. Such stress concentrations can initiate the propagation of the very defects which cause them and can reduce structural strength dramatically. Fatigue cracks lead to increases in stresses and deflections and may impair the serviceability of a structure. Repair may rectify the problem, but if left unattended, fatigue cracks may propagate and cause collapse at loads significantly below the static design loads.

The objective of the dynamic test programme was to establish the effects of repeated loading on the form-reinforced slab as a whole and to define any changes in structural response which may be caused by the loading spectra to which the bridge would be subjected during its life.

The form-reinforced slab consists of three basic structural components, namely (1) the concrete slab, (2) the steel formwork and (3) the shear connection. The possibility of fatigue failure of each is considered below.

(1) Concrete Slab. The fatigue failure of plain and reinforced

concrete is not normally a problem in most structures. It is generally agreed that, for a life of 10^7 cycles, concrete in compression, flexure or tension has a fatigue strength of between 50 and 55% of the static strength. In normal design stresses are limited to well below this value and the possibility of fatigue failure is very remote. Nordby [58] has reviewed research on the fatigue of concrete up to 1958, while examples of more recent research may be found in References 59 and 60.

(2) *Steel Formwork.* Steel is much more susceptible to fatigue failure, especially in the vicinity of welds and a great deal of research has been carried out in recent years on this subject (see for example, References 61 and 62). This research has provided means by which steel structures may be designed against fatigue and the new draft bridge code B116.Pt.10 [63] deals with the fatigue design of steel details in bridges. The presence of the embossments pressed into the webs and top flanges of the formwork presents a local variation in geometry which may, when subjected to longitudinal bending stresses, cause stress concentrations sufficient to initiate fatigue failure.

(3) *Shear Connection.* There is no data available regarding the fatigue characteristics of this type of shear connection, but there are two possibilities which must be considered. These are the fatigue of the embossment detail and the local fatigue of the concrete which transmits the horizontal shear forces from the steel to the concrete slab. The results of the static

tests have shown that the bearing stress, σ_d, in the region of hogging bending is very low. The possibility of fatigue failure of the shear connection is therefore greater in regions of sagging bending where the bearing stress is greater. All dynamic tests were carried out under sagging moment conditions, i.e. with the steel deck in tension.

4.1.2 Design Loading Spectra

The loading spectra for which highway bridges must be designed are set out in the new unified bridge code Bl16.Pt.2 [64] and define the frequency of occurrence of various proportions of the H.A. and H.B. static design loads. In general, the H.A. spectrum consists of a very high number of loading cycles which produce relatively low stresses, while the H.B. spectrum consists of a relatively small number of cycles producing much higher stresses. The above document also defines the projected annual frequency of H.A. and H.B. loading cycles, thus enabling the designer to determine the total number of cycles of any loading intensity to which a bridge will be subjected during its life.

Separate spectra are defined for longitudinal and transverse members and as the form-reinforced slab has been designed to span between longitudinal girders, the transverse loading spectra will be applicable. The relevant data for the two spectra, together with the projected annual frequencies are given in Appendix C.

The components of a bridge in general must be capable of withstanding the combined effects of both the H.A. and H.B. spectra. As stated previously, the tests carried out by Climenhaga and Johnson [17] were based on the assumption that the H.B. spectrum

would be the more critical as regards the shear connection. This may well be the case, but the effects of the H.A. spectrum must also be considered, particularly in view of the fact that in general, where weld details are concerned, it is often this spectrum which causes most damage. This immediately poses a problem concerning the number of cycles which need to be considered in the testing programme. The expected annual frequency of occurrence of all proportions of H.B. loading intensity is 0.009 million cycles, which over a design life of 120 years amounts to 1.08 million cycles. This presents no problem and the H.B. spectrum can be simulated in the laboratory in a relatively short time. However, for the H.A. spectrum, for bridges having four or more lanes, the corresponding figures are 4.8 million cycles per annum, with a total of 576 million cycles. For bridges having two or three lanes, the figures for the H.A. spectrum may be halved.

As can be seen from Appendix C the majority of occurrences of both loading spectra are at low intensities and since the stresses produced by the H.A. loads are relatively small it is probable that a great number of the total H.A. cycles may be non-damaging. The question then arises as to what is the stress range below which it may be safely assumed that no damage occurs. This question can be answered only by testing at a constant stress range until fatigue failure occurs or until the number of applied loading cycles is so great as to suggest an infinite life.

A plot of stress range against the number of cycles to failure provides what is generally known as an S-N curve and once this has been established for a particular detail the cumulative

effects of numbers of cycles at different stress levels may be ascertained by using Miner's cumulative damage rule [65], which is outlined in Appendix D.

4.1.3 Outline of Testing Programme

To cover the effects of both the H.A. and H.B. loading spectra it was considered that the dynamic testing programme should consist of subjecting any one specimen to a constant amplitude loading. However, in view of the relative ease with which the H.B. spectrum may be simulated, it was decided to subject one specimen to this spectrum as a starting point to the investigation. The remaining five specimens were subjected to cyclic loading of constant amplitude until fatigue failure of a particular nature was encountered or until a very large number of cycles had been applied. The definition of 'very large number' is governed by the running speed of the equipment used. This was an Amsler pulsator unit which applied cyclic loading via hydraulic jacks at a rate of 250 cycles per minute. At this speed it was found that approximately 1.5 million cycles could be applied to a specimen in one week. This gives an indication as to the time consuming aspect of fatigue testing.

Prior to dynamic testing, all specimens were subjected to static elastic loading, which provided a datum against which to measure specimen response subsequent to the application of repeated loading. Those specimens which did not fail in fatigue were finally tested statically to collapse.

4.2 TEST SPECIMENS

4.2.1 Design of Specimens

All specimens were designed as simply supported one-way slab elements with a span of 3.33 m and were essentially the same as the specimen tested statically in sagging bending. (See Chapter 3, Section 3.4.2). The nominal design section is shown in Figure 18.

4.2.2 Casting

The casting procedure adopted was also as for the previous static test specimens. Concrete was supplied by Ready Mixed Concrete Ltd., to a specification of a Grade 30 mix, a maximum aggregate size of 20 mm and a 28 day target cube strength of 30 N/mm^2.

The specimens were prepared and cast in pairs, together with twenty 100 mm concrete cubes and six 150 mm by 300 mm cylinders. Natural bond was again prevented in all specimens by a thin coat of oil applied to the steel formwork before casting.

4.2.3 Instrumentation

4.2.3.1 *Strain Gauges*

Longitudinal strain gauges were attached to all specimens at midspan in the positions shown in Figure 20. In addition for the specimens used in Tests 6-9 inclusive, strain gauges were attached to the steel shutter in one shear span as shown in Figure 31. The position of the strain gauges relative to the supports and loading points is depicted in Figure 32. The additional strain gauges in the shear span were attached to both surfaces of the steel flanges with the aim of providing a clearer picture of the stress distribution in the vicinity of the embossments. The gauges on the top surface of

the formwork were protected as far as possible by using a waterproof covering. However, due to either the effects of casting or the abrasive action of the concrete on connecting wires during testing it was found that only about 50% of these strain gauges were operational. All strain gauges were connected to automatic strain gauge data logging equipment.

4.2.3.2 *Slip and Separation Measurement*

To facilitate measurement of slip and separation at the interface, brackets carrying two 0.0001" dial gauges were bolted to studs which were cast into the concrete in the positions shown in Figure 21, as for the previous static tests. Corresponding gauge points were provided on the formwork in the form of small aluminium plates fixed to the steel with Araldite. In the previous static tests the gauge points consisted of steel plates welded to the formwork unit, but the possibility of fatigue failure due to the weld called for a different method of connection. The Araldite connection was tested in a high speed Vibrophore under the maximum stress range which would be encountered in the dynamic tests and was found to be satisfactory.

4.2.3.3 *Deflection Gauges*

Several 0.001" dial gauges were used for the measurement of deflection at midspan. The positions of the gauges are shown in Figure 20. In addition, 0.0001" dial gauges were positioned directly beneath the loading points on the longitudinal centre line of the specimen.

4.2.3.4 *Curvature Gauge*

A curvature gauge with a gauge length of 150 mm was used in all tests to measure the curvature at midspan.

4.2.4 Geometric Properties of Specimens

In all specimens there were deviations from the nominal design section. The measured geometrical properties of the individual formwork units are presented in Table 1.

The most important deviation from design cross-section geometry was in respect of overall slab depth. Prior to casting, with the ends of the units bolted down, measurements revealed two aspects of the out-of-flatness of the formwork units which can only be attributed to residual stresses induced during manufacture. These measurements showed a significant sag relative to the ends, together with a less significant twisting about the longitudinal axis. Table 6 shows the elevations of the outer bottom flanges relative to the ends of the units at 300 mm intervals along the length, prior to casting for three of the specimens. Also shown are the measurements of the overall depth of the composite slab at the same positions after the concrete had cured. In general, casting of the concrete increased the sag of the shutter units and caused increased non-uniformity of overall depth over the length of the unit.

4.3 TEST PROCEDURES

4.3.1 General

The testing procedure consisted of four stages which were :

Stage I :- Static elastic test on uncracked specimen.

Stage II :- Static elastic test on cracked specimen.

Stage III :- Dynamic testing.

Stage IV :- Static ultimate test.

4.3.2 Description of Test Rig

The test rig was basically as for the previous composite static tests. The rig was constructed for a simply supported span of 3.33 m with two point loading applied symmetrically with a shear span length of 750 mm. The loading was applied through two Amsler hydraulic jacks of 50 tons static/25 tons dynamic capacity, supported by an arrangement of columns and cross beams. The loads were uniformly distributed across the width of the specimen via four 90 mm square loading pads by a spreader beam system.

For the dynamic testing the two jacks were connected to an Amsler Pulsator unit, which was also used for the preliminary elastic tests. For ultimate load tests it was necessary to use a conventional Amsler static loading cabinet. The arrangement of the test rig is shown in Plate 8, which depicts the condition of the specimen of Test 4, after failure.

4.3.3 Static Elastic Tests (Stages I and II)

Preliminary static elastic tests were necessary to provide a datum against which to gauge the structural response of specimens during and subsequent to, dynamic testing. Two separate elastic tests were required, the first (designated Stage I) to transform the uncracked section to a cracked section and the second (Stage II) to provide data on the initial elastic response.

These tests, to which all specimens were subjected, consisted of increasing the load from zero to a maximum in equal increments. After each increment readings of strain, slip and separation, deflection and curvature were taken. This process was repeated as the load was reduced gradually to zero. The maximum load applied was

equal to or slightly greater than the maximum load to be used in dynamic testing (see Table 7).

The static response of the specimens also provided data from which small adjustments to the dynamic loads could be calculated to allow for inertia effects.

4.3.4 Dynamic Testing (Stage III)

4.3.4.1 *General*

Dynamic testing consisted of repeatedly applying a predetermined load amplitude at a constant rate of 250 cycles per minute, thus subjecting the specimens to a forced vibration at this frequency. This cyclic loading was superimposed on a static minimum load which was maintained at 12.5 kN per jack for all tests. This minimum load subjected the slab to a state of stress roughly equivalent to that which would be caused by a surface finish.

The specimens were tested continuously during the week and allowed to rest at weekends. At convenient stages the dynamic testing was halted for a short time while specimen response to static loading was monitored by data measurement at zero, minimum and maximum loads.

Six specimens were subjected to dynamic loading, the values of which are outlined below. The tests are designated by numbers 4 to 9, following on from the three tests carried out in the static testing programme. The specimens are designated by the corresponding test number.

4.3.4.2 *Test 4*

In the preliminary test it was decided to subject the first specimen to the full H.B. loading spectrum.

The H.A. and H.B. static design bending moments and shear forces for which the slab was designed are outlined in Appendix B. The test load amplitude corresponding to maximum load in the H.B. spectrum was taken as the maximum design live load shear due to 45 units of H.B. load. With a shear span of 0.75 m the corresponding maximum bending moment in the specimen was approximately 1.5 times the maximum live load bending moment. It was considered that this would provide an adequate test of both the shear connection in the shear spans and the embossment detail in the midspan section. Also, the full H.B. spectrum shown in Figure 33 was used as a basis, instead of the reduced spectrum which actually applies to transverse members (see Appendix C).

A spectrum in excess of the full H.B. spectrum was applied to the specimen (see Figure 33) starting with the higher loads and a total number of 1.185 million cycles was covered.

4.3.4.3 *Constant Amplitude Tests*

The remaining five tests were carried out using constant amplitude loading, the details of which are given in Table 7. The number of cycles applied to each specimen are given in Table 9. The load amplitudes used ranged from 78% to 55.6% of the maximum H.B. load used in Test 4.

The specimens in Tests 7 and 8 were each subjected to five million cycles at loads of 55.6% and 61% of the maximum H.B. load with no sign of fatigue failure. It was apparent that testing at loads below 55.6% to provide a more realistic state of stress with respect to the H.A. spectrum would not result in any useful information within a reasonable time scale.

In Tests 6 and 9 indications of the nature of the critical detail for fatigue design appeared in the form of fatigue cracks in the formwork units in the midspan constant moment region, apparently originating from the bottom of an embossment in the web. These specimens were subjected to further cyclic loading after detailed inspection, as it was considered of more value to investigate the rate of propagation of the cracks than to carry out ultimate load tests, which would have resulted in tearing of the formwork units.

4.3.5 Static Ultimate Tests (Stage IV)

The specimens which survived dynamic testing with no signs of fatigue failure were subsequently tested to collapse under static loading. The procedure consisted of increasing the load slowly in increments from zero to the maximum attainable load, using smaller increments as the maximum was approached, until failure occurred.

4.3.6 Auxiliary Tests

Nine concrete cubes and three cylinders were used to determine the strength of the concrete in each specimen. The cubes were tested in groups of three, before, during and immediately after dynamic testing. The cylinders were used to determine the elastic modulus and the tensile strength of the concrete.

Sections of the formwork bottom flange taken from the vicinity of the supports were used to determine the static yield and ultimate stress of the steel in each specimen.

4.4 RESULTS OF TESTS

4.4.1 Presentation of Results

The results of the tests are presented in graphical form in

Figures 34-76 inclusive. A list of figures is given for ease of reference.

Deflections, midspan curvature and strains are presented with respect to applied load. Slip between the steel and concrete is presented as a distribution plotted at a given load, except in a few instances where a plot of slip with respect to load is given. The sign convention used is such that positive slip represents movement of the concrete relative to the steel formwork, away from midspan.

Slip was measured on both sides of the specimen and the results show the average of corresponding pairs. The values recorded on the two sides of the specimen were often substantially different, due to the embossment shear connectors sloping in opposite directions on adjacent webs. This leads to greater slip on the side of the specimen where the embossments slope in an upward direction away from midspan, but this is an edge effect which would be eliminated in practice.

The results of individual tests are described below and a discussion concerning the various aspects of structural behaviour is presented in Section 4.5.

4.4.2 Initial Elastic Tests

The behaviour of all specimens under initial elastic loading was very similar. On first loading (up to about 30 kN/jack) the response was non-linear as flexural cracking occurred in the tensile zone of the concrete. Above 30 kN per jack the response became more linear and remained so up to the maximum load. On unloading it was found that the specimens retained a residual midspan deflection,

which, on average was of the order of 1.5 mm (Figure 34). This residual effect was reflected in the midspan curvature (Figure 35) and in the longitudinal slip distribution (Figure 36). These figures show the results of Test 4. The specimens in the remaining tests responded in a very similar manner and presentation of all the results would be repetitive.

The Stage II static loading produced a much more linear response from all specimens. Figures 34, 35 and 36 show the midspan deflection and curvature and the maximum slip distribution for Test 4. Similar results were obtained for the other specimens and for comparison are presented with the dynamic test results. The maximum strains at midspan in the steel and concrete for Stages I and II are shown in Figures 37 and 38.

4.4.3 Dynamic Tests

4.4.3.1 *Test 4*

The specimen was subjected to spectrum loading in excess of the full H.B. loading, as shown in Figure 33. Static load runs were made after each set of cycles forming the spectrum, before reducing the load for the next set. The data recorded for midspan deflection is presented in Figure 34. The results show an increase in the permanent deflection at midspan, but the elastic stiffness of the specimen remained unchanged. After 1.185 million cycles of loading there was no sign of fatigue failure.

4.4.3.2 *Test 5*

This was the first test using a constant amplitude load and as such was exploratory. The load amplitude of 87.5 kN per jack represented 78% of the maximum H.B. live load used in Test 4. A

total of 1.263 million cycles were applied to the specimen, during which several static load checks were carried out. The results plotted in Figures 39-41 again show a slow increase in permanent set with the number of cycles, but very little, if any, change in the elastic response under static load. The total increase in permanent deflection at midspan after the completion of the test was of the order of 1 mm. Figure 42 shows the slip distribution before and after the dynamic testing while Figures 43 and 44 show the strains in the steel bottom flange and concrete surface at midspan, recorded during static runs.

4.4.3.3 *Test 6*

A constant load amplitude of 66.7% of the maximum H.B. load was applied for 1.7 million cycles, when a crack appeared in the formwork, 383 mm from midspan, apparently originating from the bottom of a web embossment. Data recorded during static load checks is plotted in Figures 45-49 inclusive and indicate a trend similar to that in Test 5, with an increase in permanent midspan deflection of about 1.2 mm. There are indications that the rate of increase of the permanent set was decreasing towards the latter stages.

When first noticed, the crack extended across one bottom flange and into two embossments on the adjacent webs and is thought to have originated at the lower end of one embossment and propagated very rapidly across the bottom flange. Plate 9 shows the initial extent of the crack. The dynamic testing was continued to investigate the rate of propagation of the crack. A further 160,000 cycles, at the same load, were applied, by which time the crack extended over almost two-thirds of the shutter width. However, the specimen

continued to support the load although the stiffness had reduced considerably. The initial extent of the crack and the rate of propagation are indicated in Figure 50.

4.4.3.4 *Test 7*

The load was reduced to 55.6% of the maximum H.B. load for this test, for which the results are shown in Figures 51-55. The results show the same trend of increasing permanent deflection, which appeared to be stabilizing towards the end of the test. After five million cycles there was no sign of fatigue failure and it was therefore decided to stop the dynamic loading and carry out a static ultimate test.

4.4.3.5 *Test 8*

The negative result of Test 7 as regards fatigue failure suggested that a higher load was required to produce a fatigue failure in a reasonable time. The load amplitude for Test 8 was therefore increased to 61% of the maximum H.B. load, but again there was no sign of failure after five million cycles. The results for Test 8 are shown in Figures 56-59.

4.4.3.6 *Test 9*

At this stage, the occurrence of one fatigue failure from five tests suggested that the crack obtained in Test 6 may have been due to a particularly bad detail. The load amplitude for this final test was therefore set midway between the values used in Tests 5 and 6. After the application of 1.22 million cycles a fatigue crack was discovered in the steel formwork in the midspan section, 128 mm from the north loading point. The pattern of the crack was exactly as for that in Test 6. The static response results obtained during dynamic

testing are presented in Figures 60-62. The test was again continued to investigate the rate of propagation of the crack, which is depicted in Figure 63. After an additional 226,800 cycles the crack had propagated to one edge of the unit and the test was then terminated. The final extent of the fatigue crack is shown in Plate 10.

4.4.4 Static Ultimate Tests

Static ultimate tests were carried out on the specimens in Tests 4, 5, 7 and 8. The ultimate loads attained in each test are given in Table 7. All specimens failed in a mode which is defined as shear-bond-compression. It must be emphasized that the word 'bond' is used here to describe the mechanical shear connection between the steel and concrete and not the chemical bond, which was destroyed in all specimens. The mode of failure was characterized by slip in the shear span which was greatest just outside the loading points. This slip increased with the load and was associated with the appearance of a diagonal shear crack. The maximum load in all cases was attained immediately prior to crushing of the top surface of the concrete in the vicinity of one of the loading points, after which the load began to decrease and deflections increased rapidly.

This behaviour is depicted in Figures 64-76, which show some of the results for deflections, midspan curvature, midspan strains and slip distributions for Tests 4, 5, 7 and 8, plotted with respect to the load. The mode of failure is shown in Plates 8 and 11, while Plate 12 shows the final condition of specimen 7.

4.4.5 Auxiliary Tests

The results of cube and cylinder tests for the concrete in

each specimen are given in Table 8. The strength of the concrete in the slab was estimated by applying a reduction factor of 0.67 to the cube strength, as for the static tests.

Also shown are the results of tensile tests on the steel from each shutter in terms of static yield stress and ultimate stress.

4.5 . DISCUSSION OF RESULTS

4.5.1 Initial Static Elastic Tests

The behaviour of all specimens under preliminary elastic loading was very similar. In terms of deflections, midspan curvature and strains in both steel and concrete this behaviour was approximately linear once the section had attained the cracked state. Slip between the steel and concrete was very small and again approximately linear with respect to load.

A comparison between the experimental results and complete interaction linear elastic theory has been made using measured geometrical and material properties of the specimens and assuming a uniform depth equal to the average depth over the length of the specimen. The stiffness predicted by linear elastic theory is represented in the relevant figures and it can be seen that agreement is excellent. The elastic section properties were calculated using a fully effective steel section, ignoring any reduction in effective area due to the embossments, which were found to have a significant effect on the stresses in the shutter under construction loading conditions. Elastic calculations carried out with a reduced shutter cross-section to allow for this effect produced a slightly less stiff

section, giving poor correlation with experimental results.

4.5.2 Dynamic Tests

4.5.2.1 *General Response*

The general structural behaviour of all specimens under repeated loading showed a similar trend, which is best indicated by the deflections at midspan.

The non-recoverable or residual deflections remaining after removal of the load increased with the number of cycles and the maximum increase recorded was of the order of 1.2 mm. For the special case of Test 4, almost all the residual deflection was due to the first 33,000 cycles at the maximum H.B. load. In the remaining tests most of the residual deflection occurred during the first few hundred thousand cycles.

There appear to be two possible causes of this increasing residual deflection effect. The high frequency used in the tests, relative to that which would occur in practice may have caused a fatigue effect in the concrete compression zone very similar to creep. The interrelation of fatigue effects and creep of concrete has been noted by Nordby [58]. The second and more likely cause may be explained by the shear connection response. The shear forces transferred by the shear connection will cause a non-uniform local stress distribution in the concrete surrounding the embossments and in some areas this local stress may be much greater than the fatigue limit and possibly the cube strength. This will cause local failure of some areas of concrete resulting in slip and a stress redistribution which will continue until the 'hard points' have been removed and the local bearing stresses have become more uniform. The slip necessary to

mobilise the shear connection strength after this local crushing of the concrete will be non-recoverable and will cause increased residual deflection of the slab, until the situation has stabilized. This effect may be clearly seen in Figures 41, 47 and 52 where the maximum slip is plotted with respect to load and in Plate 13, which shows two views of the south shear span of specimen 6, after the formwork had been very carefully cut away. Plate 14 shows a similar view for specimen 7, for comparison,after static failure.

The static checks carried out on the specimens during the dynamic testing showed little, if any, change in the elastic response. A significant reduction in the elastic stiffness of the specimens in Tests 6 and 9 was apparent after the occurrence of the fatigue cracks in the steel formwork.

4.5.2.2 *Fatigue of Steel Formwork*

The occurrence of fatigue cracks in the steel shutter in Tests 6 and 9 indicates that the embossment detail will be the most likely cause of fatigue failure in this type of form-reinforced slab. Both cracks occurred in the midspan section of the specimens where the vertical and horizontal shear forces in the slab are zero, assuming that the jack loads are exactly equal. Any difference between the two jack loads would subject the shear connection in the midspan region to small shear forces, but the resulting stresses in the steel shutter will be negligible compared with the longitudinal bending stresses. This also applies to any interface shear due to the non-uniform depth. It is therefore concluded that the fatigue cracks were due entirely to the longitudinal tensile stresses in the steel formwork, caused by overall bending.

The implications of the cracks are best discussed in relation to the fatigue of steel details as set out in Bll6.Pt.lO [63]. This document defines several classes of structural steel detail, ranging from plain steel (Class B), to weld metal (Class W), which is the class most susceptible to fatigue failure. For each class an S-N relationship is specified, thereby defining the number of cycles to failure for a given constant stress range.

The procedure for fatigue design consists of classifying the detail concerned and using the known loading spectra and S-N relationship in a Miner's Rule calculation to determine the annual accumulation of fatigue damage. To avoid the possibility of failure, the fatigue damage accumulation during the design life of the structure must not exceed unity.

The S-N relationships are specified in such a way as to limit the probability of fatigue failure to specific values, which, for the limit state design criteria of strength and serviceability are 2½% and 16% respectively. The higher probability of failure for the serviceability criterion is justified only if inspection and maintenance procedures ensure that the repair of a structure may be achieved, should fatigue cracks occur.

It is difficult to classify the shear connector detail from the results of the dynamic tests as the stresses in the steel formwork at the points of failure can only be estimated from the strain gauge readings at midspan. The stress distribution in the steel is complicated by two factors, the first of which is the non-uniform overall depth of the slab. The second is that in the region of the loading points there is likely to be a localised increase in strain in

both the steel and concrete due to some loss of interaction. This is a local phenomenon and is negligible as far as overall elastic response is concerned, but may increase the stresses to which the embossment detail is subjected. This is particularly important in the case of Test 9, in which the crack occurred only 120 mm from the north loading point. However, since the slab depth at midspan is a maximum and a reduction in depth leads to increased stresses, an attempted classification on the basis of midspan strains, although not accurate, will be conservative.

Another problem is the determination of the stress range to be used in the classification. When the cracks were discovered they extended across one bottom flange and up into the embossments on the adjacent webs. It is fairly certain that the cracks originated from the lower end of an embossment in the web, but the fact that no reduction in stiffness occurred until the crack had traversed the bottom flange indicates that the stress range in the bottom flange is more relevant. The stress ranges at midspan in the bottom flange and the lower sections of the webs in the five constant amplitude tests are given in Table 9, which also shows the number of cycles applied to the specimens. A comparison between these results and the standard detail S-N relationships specified by Bll6.Pt.10 is shown in Figure 77. For the purpose of this comparison the probability of failure for the standard details has been taken as 50%, that is, the mean line.

The smaller stress ranges of Tests 7 and 8, in which no fatigue cracks occurred, indicate a slightly higher class of detail than the other tests and this may be significant when considering the actual stress ranges to which the formwork would be subjected in

practice.

There is another aspect of the results which is worth noting in respect of statistics. As far as the embossment detail is concerned, the dynamic tests consisted of testing a large number of similar details at the same time, there being 240 web embossments within the constant moment region. Tests 6 and 9 resulted in only one fatigue crack in each unit, even after continued dynamic testing, so the results obtained indicate a lower bound. It may therefore be tentatively suggested that the mean line (50% probability of failure) lies significantly above the test results shown in Figure 77.

On the basis of the available data, the embossment detail (or bottom flange) appears to be classed in the D-E region. The S-N curves for these two details are relatively close together and an accurate classification cannot be made on the basis of five tests alone, but a tentative estimate of the design life may be obtained.

The H.A. and H.B. live load datum stresses in the bottom flange and the lower section of the web of the formwork assuming a nominal design section are given in Appendix B. Corresponding values are also given for a section with an overall depth of 260 mm which includes a 10 mm increase to allow for the deflection of the formwork under the wet concrete load at midspan.

The fatigue life for the eight detail classes B to W may easily be calculated, given the design datum stresses, using the procedures specified in Bll6.Pt.10. The estimation of fatigue life is based on the strength criterion S-N relations (2½% probability of failure) since the repair of fatigue cracks in the formwork will be difficult, if not impossible. Figure 78 shows the calculated fatigue

life for the H.A. spectrum alone, for details C-F inclusive in transverse members for datum stress ranges of the same order of magnitude as those expected in design. Figure 79 shows a similar representation for the H.B. spectrum alone. It can be seen from these two figures that the H.A. spectrum is the more severe of the two, although both spectra must be considered in design.

For a simply supported span and using the datum stresses specified in Appendix B, the design life for a slab of depth 250 mm is 68 years for a Class D detail, or 43 years for a Class E detail. For a slab of depth 260 mm the corresponding figures are 76 years and 46 years. It is apparent that the class specified for the detail is most important, while the slab depth is a contributory factor in the calculation of fatigue life. The fatigue life has been calculated assuming four or more traffic lanes. For bridges with only two or three lanes, the figures for fatigue life may be doubled.

4.5.3 Static Ultimate Tests

The ultimate loads achieved by the specimens in Tests 4, 5, 7 and 8 are shown in Table 7, together with the calculated ultimate loads for flexural failure based on plastic stress block theory. The stresses used in this calculation were the yield stress for the steel and 0.8 of the compressive strength (0.67 of the cube strength) for the concrete. In calculating the flexural strength, the critical section was that of minimum depth in the midspan section and was invariably at one of the loading points.

All four specimens failed at loads marginally less than the calculated ultimate load. Expressed as percentages of the theoretical

ultimate loads the experimental values for Tests 4, 5, 7 and 8 are 99%, 98%, 98% and 97% respectively. These results may be compared with the result of the previous static Test 2 for which the corresponding figure was 106%.

At first glance it seems that this reduction in ultimate load capacity is due to the repeated loading. However, the monitoring of the elastic response during dynamic testing revealed no decrease in stiffness of any specimen prior to fatigue failure (in Tests 6 and 9) and it is therefore difficult to envisage that the dynamic testing should have any effect on the ultimate load.

The cause of this reduction in capacity may lie in the concrete strength. The cube strengths and estimated concrete strength in the specimens are given in Table 8. The concrete strength does not affect the theoretical capacity of the section (for full interaction) significantly, but it does have a great effect on the interface shear connection load-slip relationship. This is particularly important as the shear-bond-compression mode of failure is partly due to interface slip.

A great deal of research [4,12,13] has been carried out on the static ultimate strength of form-reinforced slabs in building floors in the United States. This research has been mainly concerned with the shear-bond mode of failure, which may or may not be accompanied by concrete crushing. If the shear connection is sufficiently weak shear bond failure will result, causing large slips and tensile cracking in the concrete. This approaches the zero-interaction case as the shear connection strength is reduced. At the other end of the scale is the complete interaction case, in which there is zero

slip and failure occurs by crushing of concrete in the compression zone. Between these two extremes lies the partial interaction case in which the mode of failure is a combination of slip and concrete crushing. This failure mode must cover the majority of form-reinforced slabs since the objective of the shear connection is to approximate to the full interaction case, although this can never be achieved in practice.

Table 7 shows the calculated concrete bearing stress on the projected area of the embossments at failure, in the shear span for the ultimate load tests, together with the ratio of this bearing stress to the concrete cube strength. There appears to be some correlation between this ratio and the ultimate load expressed as a percentage of the calculated value, but it is not possible to establish whether this is the case on the basis of the limited data available.

The effect of partial interaction can also be seen in the comparison between the experimental results and the response predicted by complete interaction linear elastic theory. Although the agreement is excellent in the region of design loads, there is some deviation from the linear response just prior to the complete interaction elastic limit, resulting in increased deflection, which can be seen in Figures 64, 67, 70 and 72. This may be partly due to the onset of non-linearity in the stress-strain relation of the concrete in the compression zone, but partial interaction is considered to be the main cause.

CHAPTER 5

'IN-AIR' FATIGUE TESTS OF EMBOSSMENT DETAIL

5.1 OBJECTIVE OF TESTS

The dynamic testing programme described in the previous chapter demonstrated the general structural behaviour of the form-reinforced slab under repeated loading and indicated the possibility of fatigue failure occurring in the formwork unit. Thus the critical factor in fatigue design appears to be the failure of the steel deck caused by tensile stresses associated with overall longitudinal bending and initiated by a crack originating from the lower end of an embossment pressed into the web.

However, the composite slab dynamic tests provided a limited amount of data regarding the fatigue characteristics of the embossment detail. On the basis of this data, the fatigue life estimated for a four lane bridge is approximately 75 years (assuming that the embossment detail is Class D), but this is conservative for several reasons. The stress ranges which caused the two fatigue failures may be significantly higher than those at midspan, which were used for a preliminary classification, due to the non-uniform depth of the slab and the local effects of partial interaction in the region of the loading points. Also, the results of tests 7 and 8 indicated a slightly higher fatigue life and this may be significant with regard to the H.A. loading spectrum, which is more damaging in this respect than the H.B. spectrum (see Figures 78 and 79). Furthermore, only one crack occurred in the specimens of Tests 6 and 9, even after continued dynamic testing although there were

240 web embossments in the midspan section of the specimen. This indicates that the mean line (50% probability of failure) lies significantly above the test results shown in Figure 77.

The natural scatter of fatigue test results and the design life of 120 years normally specified for highway bridges requires a more accurate assessment of the S-N relationship for the detail in question. The tests described in this chapter were devised to attain this objective.

One conclusion of the previous chapter was that the initiation and propagation of the fatigue cracks, which occurred in the midspan sections of specimens 6 and 9, were due to the longitudinal tensile stresses in the steel formwork under bending and that these cracks emanated from the lower end of embossments in the web. This is based on the reasonable assumption that any interface shear forces which might exist in the midspan section will produce stresses of a negligible magnitude in the vicinity of the embossments compared with the tensile bending stresses.

It was therefore concluded that the conditions under which fatigue cracks occurred in the full scale slab specimens could be reproduced approximately in simple tensile fatigue tests on samples of the steel formwork webs. Although the stress and strain gradients which exist in the webs of the composite slab will not be reproduced in a direct tension test, it is unlikely that this stress gradient will significantly increase the stress concentration in the vicinity of the lower end of the embossment.

For the purpose of these tests, specimens of the webs were extracted from the last remaining formwork unit for testing in a

high speed Amsler Vibrophore machine. A complete description of the Vibrophore and the principles by which it functions will not be given here. It will suffice to say that the machine provides a means of fatigue testing, in tension or compression, small samples of material at frequencies up to 300 Hertz, under loads of $\pm$ 10 tons.

To obtain a more accurate assessment of the S-N relationship for the embossment detail it was decided to carry out a number of direct tension fatigue tests on web specimens at each of five values of stress range.

5.2 DESCRIPTION OF SPECIMENS

The Vibrophore machine dictated the maximum length of the specimens and a length of 315 mm was chosen such that each specimen consisted of a length of web containing seven embossments. The specimens were carefully machined to a width of 70 mm which was the maximum width attainable after removal of the bend radius of the web to flange junctions, to provide as uniform and symmetrical a cross-section as possible.

To provide a design suitable for the specimen grips, it was necessary to machine off the projections of the two embossments at the ends of the plate. The resulting holes in the plate were filled with 'Araldite', which was also used to locate two small steel plates at each end of the specimen to complete the gripping arrangement.

This specimen is in fact non-symmetrical, due to the presence of the embossments and under longitudinal tensile load, the strain distribution within the specimen indicated a significant degree

of out-of-plane bending, together with a reduction in the overall effective area of the specimen, a phenomenon which was first noted in the bare formwork construction loading tests. The final design consisted of a double specimen in an attempt to remove the bending effect and this resulted in a significant reduction in the local bending stresses. However, some local bending of the plate is due to the variation of the section along the length of the specimen and is caused by the presence of the embossments. The effect cannot therefore be completely eliminated.

The final design of the Vibrophore specimen is shown in Figure 80.

5.3 STRESS DISTRIBUTION IN THE VIBROPHORE SPECIMEN

Two of the Vibrophore specimens were provided with strain gauge instrumentation to investigate the distribution of stress in the section and the effect of the embossments. The position of the strain gauges is shown in Figure 80.

The stress distributions obtained from these strain gauges is shown in Figure 81, for loads (W_v) of 20 kN and 40 kN. It is the presence of the embossments in the centre of the plate which produces this non-uniform stress distribution.

Figure 80 shows three longitudinal sections of the web plate ranging from the flat plate AA to the fully embossed section CC, via a transition section BB. The longitudinal in plane stiffness of the flat plate AA is considerably greater than the section CC, which tends to flatten out under axial load. The stiffness within the transition width varies between the flat plate and the fully embossed section.

Thus the flat outer edges of the plate transmit the majority of the longitudinal tensile load, while the contribution of the embossed width is relatively small.

In the elastic range, for which the stress distribution is shown in Figure 81, the relationship between applied load W_v, for the double specimen and the maximum recorded mid-plate tensile stress $(\sigma_v)_{max}$, is shown in Figure 82. The effective area of a single web plate may be calculated from:

$$A_{eff} = W_v/2(\sigma_v)_{max} \tag{5.1}$$

The average stress $(\sigma_v)_{ave}$, calculated assuming a fully effective section of area A_w is given by:

$$(\sigma_v)_{ave} = W_v/2A_w \tag{5.2}$$

The effective area will be defined as the product of an effective width, w_{eff} and the plate thickness t, thus;

$$A_{eff} = w_{eff}t \tag{5.3}$$

and similarly the gross area is the product of the actual width and the plate thickness,

$$A_w = w_a t \tag{5.4}$$

If the effective width is the sum of the flat plate width and the embossed plate width modified by an effective width factor k_w, then

$$W_{eff} = w_a - (\ell \sin\alpha)(1-k_w) \tag{5.5}$$

where ℓ is the embossment length and α is the angle of inclination of the embossments to the longitudinal axis. It will be assumed here that the effect of the transition width may be allowed for by the inclusion of the embossment effective length, ℓ, used for the calculation of the interface concrete bearing stress, rather than the

overall embossment length, which is 50 mm.

From equation (5.5)

$$k_w = 1-(w_a-w_{eff})/(\ell \sin\alpha) \qquad (5.6)$$

Using values of 40 mm, 70 mm and 60° for ℓ, w_a and α respectively and w_{eff} calculated from equations (5.1) and (5.3) for the relationship shown in Figure 82, the value of k_w, from equation (5.6), is 0.3.

A relationship between $(\sigma_v)_{max}$ and $(\sigma_v)_{ave}$ may be derived from equations (5.1) to (5.6) such that

$$(\sigma_v)_{ave} = (\sigma_v)_{max}\{1-\ell \sin\alpha(1-k_w)/w_a\} \qquad (5.7)$$

and using the numerical values as above, we have,

$$(\sigma_v)_{ave} = 0.654(\sigma_v)_{max} \qquad (5.7a)$$

Thus the maximum longitudinal mid-plane stress in the Vibrophore specimen is approximately 1.53 times the average stress calculated on the gross area. This effect was also found to exist within the bare formwork section in the construction loading tests, which produced a considerably higher stress in the flat portions of the top flanges than the value predicted using a fully effective section.

While this phenomenon is of interest as regards the maximum stress in the bare formwork section, for the purpose of fatigue design it was decided to base the Vibrophore tests on stress ranges defined by the values of $(\sigma_v)_{ave}$. Thus the proposed in-air fatigue testing programme consisted of performing five tests, at each of five stress ranges (for $(\sigma_v)_{ave}$) from 40 N/mm^2 to 120 N/mm^2 in intervals of 20 N/mm^2.

5.4 TEST PROCEDURE

The calibration of the Vibrophore machine was checked using a proving ring before testing the web specimens and was found to be accurate to within 2%.

All tests were carried out using a minimum value of stress $(\sigma_v)_{ave}$ of 20 N/mm^2. This is representative of the stress in the flat sections of the webs adjacent to the bottom flanges in the composite dynamic test specimens. The maximum, minimum and mean values of $(\sigma_v)_{ave}$ and the resulting stress ranges are shown in Table 10 for the five groups of specimens, which are designated VS1-VS5, in ascending order of stress range.

Testing was commenced with specimens of VS2, for which the stress range was 60 N/mm^2 and as no fatigue failures were encountered, specimens VS1 were not tested.

Each specimen in groups VS2-VS5 was tested at a constant stress range at a frequency of 150 cycles per second until failure occurred, or until the number of cycles applied became so large as to suggest an infinite life. Failure was defined by the appearance of a crack emanating from the end of an embossment. Several specimens were subjected to continued testing at the same load levels subsequent to the first appearance of a crack and in all cases, the rate of propagation of the crack towards the edge of the specimen was very rapid, reaching the edge within a further 5000 cycles. This demonstrates that the first appearance of a crack is acceptable as a failure criterion. The number of cycles at which a test was discontinued in the event of survival was always greater than 45 million and for any given stress

range was greater than the endurance cycles for a Class C detail as defined by B116 Pt.10[63].

A specimen under test in the Vibrophore is shown in Plate 15, while Plate 16 shows a typical failure on first appearance of the crack.

5.5 RESULTS

The results of the Vibrophore tests are presented in Table 11 and are plotted in Figure 83, where a logarithmic base is used for both stress range and number of cycles to failure. The results of run-outs (specimens which did not fail) are plotted together with the failures. Twelve of the twenty specimens resulted in failures, while the remaining eight were classed as run-outs. All five specimens of the group VS2 were subjected to at least 70 million cycles at a stress range of 60 N/mm^2, but no failures were encountered. Three of the five specimens of group VS3 survived, while the remaining two specimens, together with all specimens in groups VS4 and VS5 produced failures.

These results immediately indicate the existence of an endurance limit at a stress range of between 60 and 70 N/mm^2.

The results of the composite repeated loading tests are also shown in Figure 83, for comparison with the Vibrophore tests.

5.6 ANALYSIS OF RESULTS

The results of the tests have been analysed on the assumption that a relationship of the form

$$N_p = K_m/(\sigma_r)^{m'} \qquad (5.8)$$

exists between the number of cycles to failure, N_p, for a probability

of failure, p and the stress range σ_r. The parameter K_m is a constant relating to the mean-line, i.e. 50% probability of failure, while the exponent, m', is also a constant. Equation (5.8) may be expressed as

$$\log N_p = \log K_m - m' \log(\sigma_r) \tag{5.9}$$

or

$$Y = \bar{A} + \bar{B}X \tag{5.10}$$

Thus the relationship is assumed to be a straight line on the logarithmic base of Figure 83, where

$$Y = \log N_p \tag{5.11}$$

and

$$X = \log(\sigma_r) \tag{5.12}$$

If the calculated values of σ_r for each test are assumed to be exact, a linear regression analysis on the results of the individual tests provides the values of $\bar{A}$ and $\bar{B}$ in equation (5.10) such that the sum of the squares of the deviations of values of logN for the tests from those predicted by the straight line, is a minimum. The values of $\bar{A}$ and $\bar{B}$ are given by,

$$\bar{A} = \frac{\Sigma(x_i)^2 \, \Sigma y_i - \Sigma x_i \, \Sigma(x_i y_i)}{n \, \Sigma(x_i)^2 - (\Sigma x_i)^2} \tag{5.13}$$

and

$$\bar{B} = \frac{n \, \Sigma(x_i y_i) - \Sigma x_i \, \Sigma y_i}{n \, \Sigma(x_i)^2 - (\Sigma x_i)^2} \tag{5.14}$$

where x_i are the values of $\log(\sigma_r)$ and y_i are the values of logN for the test results, for i = 1 to n.

For the purpose of this linear regression analysis, the run-outs have been included, thereby providing a conservative estimate of the relationship at low stress range values. The application of equations (5.13) and (5.14) to the twenty test results gives values of $\bar{A}$ and $\bar{B}$ of 22.3 and -8.0 respectively. Thus the equation (5.9)

becomes

$$\log N_p = 22.3-(8.0)\log(\sigma_r) \qquad (5.15)$$

and is shown in Figure 83, as the mean line. This is the best estimate of the S-N relationship for the embossment detail on the basis of the results available.

The mean values of the test results in the four groups VS2 - VS5 are shown in Table 11 in terms of y_i values, together with estimates of the standard deviation within the individual groups. The mean values are plotted in Figure 83 for comparison with the derived linear relationship. Although these mean values agree reasonably well with the mean line, the standard deviations of Table 11 are inconsistent.

The British Standard for methods of fatigue testing, B.S. 3518 [66], recommends that five is the minimum number of specimens which should be employed in any group of fatigue tests under the same stress levels to predict mean, or 50% probability of failure, values. To provide information regarding the distribution of actual failures about the mean value at any stress range, it would be necessary to increase the number of specimens tested. The statistical distribution of the number of cycles at failure for any stress level is particularly important in the context of the design philosophy of B116 Pt.10 [63] in terms of the limit states of strength and serviceability, for which the S-N curves for welded details are specified so as to limit the probability of failure to 2½% and 16% respectively. To accommodate the specification of a probability of failure other than 50%, which is given by the mean line, the equation of (5.8) is modified to,

$$N_p = K_m \Delta^{d'}/(\sigma_r)^{m'} \qquad (5.16)$$

where $\log\Delta^{-1}$ is the standard deviation of logN and d'is the number of standard deviations below the mean line for a probability of failure p (<50%).

The standard deviations of logN and the corresponding values of Δ for the four groups of test specimens are given in Table 11. The value of d'for a given probability of failure p depends upon the statistical distribution of logN, which is unknown for the detail in question. It is therefore necessary to assume the form of this distribution and it is found that fatigue test results are predicted very closely by the Normal (or Gaussian) Distribution. For this distribution function, the mean line minus two standard deviations gives a probability of failure p = 2½%, while the mean minus one standard deviation gives a value of p = 16%, approximately. This is in fact the basis of the fatigue design criteria specified in Ref. 63.

Assuming that this distribution function may be applied to predict the fatigue failure of the embossment detail, the equation of (5.16) may be expressed in a logarithmic base to define the strength criterion S-N relationship (2½% probability of failure) as,

$$\log N_p = \log K_m - 2(\log\Delta^{-1}) - m'\log\sigma_r \qquad (5.17)$$

A conservative approach will be adopted by taking the minimum value of Δ in Table 11, i.e. $\Delta = 0.258$. The previously determined values of $\overline{A}$ and $\overline{B}$ inserted into equation (5.17) give (for p = 2½%),

$$\log N_p = 21.12 - 8\log\sigma_r \qquad (5.18)$$

or

$$N_p = 1.33\times10^{21}/(\sigma_r)^8 \qquad (5.19)$$

Equation (5.18) is shown in Figure 83, designated as mean minus two standard deviations. This will be adopted as the strength criterion S-N relationship and in the following section a re-estimate

of the fatigue life is obtained.

5.7 DESIGN IMPLICATIONS

The results of the Vibrophore tests show that the embossment detail cannot be specified as one of the standard classes of BS116 Pt.10 [63] and thus the estimation of design life based on a fatigue detail of Class D, given in Chapter 4 is incorrect.

Using equation (5.19) as the strength criterion S-N relationship for the embossment detail, the expected design life may be calculated from Miner's Rule (Appendix D) and the loading spectra specified in Appendix C. Figure 84 shows the calculated design life for the H.A. and H.B. spectra acting separately, for various datum stresses. If values of 70 N/mm^2 and 120 N/mm^2 are taken for the H.A. and H.B. datum stresses respectively, the design life for the two spectra acting together may be calculated as 214 years, which is quite adequate for normal bridge construction. The greater design life indicated by the results of Tests 7 and 8 has thus been verified.

CHAPTER 6

SIMPLE BENDING ANALYSIS OF THE BARE FORMWORK SECTION

6.1 GENERAL

The main purpose of this chapter is to investigate the application of simple bending theory to the analysis of the bare formwork section under construction loading conditions. The results of the tests on the bare formwork unit described in Chapter 3 have demonstrated that the main point of concern during construction, apart from the maximum deflection sustained by the formwork due to the weight of the in-situ concrete, is the effect of additional construction loads and the maximum stress induced in the top flanges.

The stress distribution in the section is affected by the presence of the embossments, which appear to reduce the effective area of the steel. This effect was demonstrated in Chapter 5 in relation to the 'in-air' fatigue tests on samples of the webs.

Throughout this chapter it is assumed that the bare formwork section remains rigid and that there is no transverse spreading or distortion of the cross-section under load. Although this assumption is not strictly valid, it may be seen from Figure 16, which shows the midspan deflection and transverse expansion of the section during the ultimate load test, that for loads less than 75% of the maximum attainable load the transverse expansion was less than 5 mm. The error resulting from the assumption of a rigid section will therefore be fairly small. As the ultimate load is approached, the transverse

expansion increases rapidly, but in practice this may be controlled by adjacent units, depending upon the longitudinal connection employed.

This chapter is divided into three sections, the first of which is concerned with the basic cross-section properties of the formwork unit. The next section deals with the construction loading conditions and in particular, the effect of the apparent reduction in effective area of the steel and the increases in deflection and stresses which may be expected due to the 'ponding effect' of the concrete during casting. In the final section the experimental response in the ultimate load test is compared with linear elastic theory and the calculated fully plastic moment of the section.

6.2 ELASTIC SECTION PROPERTIES

6.2.1 Assumptions

In calculating the cross-section properties of the formwork unit, the effect of the corner radii at the web to flange junctions are ignored and the section is assumed to consist of rectangular elements, the length of which are defined by a for the bottom flange, b for the top flange and c for the webs. The thickness of the elements is defined by the steel sheet thickness, t. The section geometry is completely defined by the five parameters d, t, ϕ, λ and β, where d is the overall depth of the section and ϕ, λ and β are the ratios of a, b and c, to d, respectively. A schematic definition of these parameters is given in Figure 3.

For the purpose of analysis, a single module of width B, between the longitudinal centre lines of two adjacent bottom flanges

is considered and the bare formwork unit, as tested is assumed to consist of three of these modules acting in parallel. Using this approach, the effects of the edges of the unit, i.e. the hook and lip details, are also ignored.

6.2.2 Fully Effective Section

The cross-section will be defined as fully effective if the presence of the embossments in the webs and top flanges is ignored. The effect of the embossments will be considered later.

An examination of the top compression flange for which the slenderness ratio b/t is of the order of 30, using the criteria given in the A.I.S.I. Design Manual [67] for cold formed steel members (see also Ref. 11), shows that the full width of the flange may be considered to be effective and that the resulting stress distribution within the flange is uniform.

In terms of the five parameters defined in the previous section, the cross-sectional area, A_s, of the fully effective section module is given by:

$$A_s = dt(\phi+\lambda+2\beta) \qquad (6.1)$$

The height of the centroid above the soffit is

$$y_s = d(\lambda+\beta)/(\phi+\lambda+2\beta) \qquad (6.2)$$

and the second moment of area of the section about the x-x axis (see Figure 3) is,

$$I_s = td^3\{\lambda+2\beta/3-(\lambda+\beta)^2/(\phi+\lambda+2\beta)\} \qquad (6.3)$$

The prototype formwork section is a special case in that $\lambda=\phi$ and the above three equations reduce to,

$$A_s = 2dt(\lambda+\beta) \qquad (6.1.a)$$

$$y_s = d/2 \qquad (6.2.a)$$

and

$$I_s = td^3(\lambda/2+\beta/6) \qquad (6.3.a)$$

6.2.3 Reduced Section Due to Embossments

To determine the effect of the embossments on the section, the value of k_w determined for the Vibrophore test specimens in Chapter 5 will be used to derive the reduced cross-section properties. The value of $k_w = 0.3$ was obtained from strain gauge readings on sections of the web in tension and the validity of applying the same value to the compression flange embossments, which are perpendicular to the longitudinal axis, is doubtful. However, the use of this figure for both web and flange embossments will enable a comparison between theoretical and experimental stress distributions and the resulting differences may be taken as an estimate of the error involved.

The effective width of the top compression flange may be taken as the sum of the width of the flat portions plus the product of the embossed width (ℓ) and k_w. The effective thickness of the embossed portions of the web may be taken as $k_w t$. The resulting section will be referred to as the effective section, as opposed to the fully effective section, to which equations (6.1) to (6.3) apply.

The cross-sectional area, A_{se}, of the effective section, is given by,

$$A_{se} = dt(\phi+\lambda+2\beta)-\ell t(1-k_w)(1+2\sin\alpha) \qquad (6.4)$$

where α is the angle of inclination of the web embossments to the longitudinal axis of the unit and ℓ is the effective length of the embossments.

The centroid of the effective section is lowered relative to the fully effective section and the height of the centroid above the soffit, y_{se}, is given by,

$$y_{se} = \{td^2(\lambda+\beta)-d\ell t(1-k_w)(1+\sin\alpha)\}/A_{se} \qquad (6.5)$$

The second moment of area of the section is also reduced and the resulting expression is,

$$I_{se} = td^3\{(1-\kappa)^2\lambda+\phi\kappa^2+\beta(2\kappa^2-2\kappa+2/3)\}$$
$$-\ell td^2(1-k_w)\{\ell^2\sin^3\alpha/6\beta^2d^2+(1-\kappa)^2+(2\kappa-1)^2\sin\alpha/2\} \qquad (6.6)$$

where $\kappa = y_{se}/d$.

It may also be interesting for design purposes, in view of the more complicated expression for I_{se}, to consider the possibility of ignoring the embossed width of the compression flange completely and assuming the webs to be fully effective, since the stresses in the central portion of the web will be small. For this case, the cross-section properties may be calculated using equations (6.1) to (6.3), in which the value of λ is replaced by λ', where

$$\lambda' = (b-\ell)/d \qquad (6.7)$$

This cross-section will be referred to as the approximate effective section. The three cross-sections are shown schematically in Figure 85.

6.3 CONSTRUCTION STAGE DEFLECTIONS AND STRESSES

6.3.1 General

The performance of the steel decking as formwork may be measured by the maximum deflection induced during casting of the concrete slab. For the present purpose it will be assumed that there is no overall out of flatness of the formwork unit and that the design

of the composite slab specifies a composite slab depth, D, at the supports.

In unpropped construction, non-uniform slab depth is inevitable under the wet concrete load and the increase in slab depth over the nominal design depth, D, may be calculated approximately assuming a uniform load over the span. This value will be less than the actual deflection, as a result of the increase in volume and hence weight of concrete necessary due to the formwork deflection. This 'ponding effect' will be investigated in the following section.

In the event of the formwork units exhibiting a longitudinal sag relative to the ends, as in the prototype units, it may be necessary to include the effects of initial non-uniform slab depth in the calculation of wet concrete load and deflections, but for the present purpose this consideration will be omitted on the understanding that production units will show a significantly improved quality.

6.3.2 Ponding Effect and Deflections

With reference to Figure 86 and again considering a single formwork module width, B, the load per unit length of the unit, for a uniform slab depth D, is

$$w = A_c \gamma g \qquad (6.8)$$

where γ is the concrete density, g is acceleration due to gravity and A_c, the area of concrete in the section is given by

$$A_c = DB - (\lambda + \sqrt{\beta^2 - 1})\, d^2 \qquad (6.9)$$

For the symmetrical section $\phi = \lambda$ and since

$$B = (\lambda + \phi + 2\sqrt{\beta^2 - 1})\, d \qquad (6.10)$$

the concrete area A_c may be redefined as

$$A_c = (D-d/2)B \tag{6.11}$$

The deflection of the formwork due to a uniform load w per unit length, assuming a simply supported span, L, is given by

$$v = \frac{wL^4}{24E_sI_s}\{u+u^4-2u^3\} \tag{6.12}$$

where $u = x/L$ and x is measured from one support.

The maximum value of v is

$$v_{max} = \frac{5wL^4}{384E_sI_s} \tag{6.13}$$

Equations (6.12) and (6.13) are easily derived assuming simple elastic bending theory, from the bending moment-curvature relationship

$$M_x = -E_sI_s\frac{d^2v}{dx^2} = \frac{wLx}{2}-\frac{wx^2}{2} \tag{6.14}$$

The deflection v leads to increased concrete depth and a non-uniform increase in the wet concrete load, which is now given by

$$w' = w+\delta w \tag{6.15}$$

where

$$\delta w = vB\gamma g\delta x \tag{6.16}$$

Under this loading intensity, the new bending moment distribution may be calculated as

$$M'_x = -E_sI_s\frac{d^2v'}{dx^2} = M_x+\Phi L^6\{u-5u^3/3+u^5-u^6/3\} \tag{6.17}$$

where $\Phi = B\gamma gw/240E_sI_s$ (6.18)

By integrating equation (6.17) twice and applying the boundary conditions at the support and at midspan, the new deflection may be written as

$$v' = v + \frac{\Phi L^8}{E_sI_s}\left\{\frac{41u}{336} - \frac{u^3}{6} - \frac{5u^5}{60} + \frac{u^7}{42} - \frac{u^8}{168}\right\} \tag{6.19}$$

and the maximum value of v', which occurs at midspan, is

$$v'_{max} = v_{max} + \frac{0.04\Phi L^8}{E_s I_s} \qquad (6.20)$$

The additional deflection (v'-v) also causes an increase in concrete load and the process continues. However, the successive increases in deflection will rapidly approach zero in a practical situation and it is unlikely that a more accurate assessment than equation (6.20) will be necessary. For a design slab depth of D=250 mm and a fully effective formwork section, the increase in the midspan deflection calculated from equation (6.20) is approximately 4.5% of the deflection given by equation (6.13).

All of the above equations apply to a simply supported span. If a similar approach is used for encastré ends, the resulting increase in midspan deflection is 0.45% of the maximum value calculated for a uniform concrete slab depth. The latter deflection is one fifth of the maximum for a simply supported span and thus the effect of ponding may be neglected for encastré ends, in this particular case.

Table 12 shows the calculated values of maximum deflections and bending moments at midspan for the three sections depicted in Figure 85, for a simply supported span of 3.33 m and a nominal slab depth of 250 mm. The deflections may be compared with the values in Table 4 for Load Case 1.1, obtained from the bare formwork test, in which the load due to the nominal concrete depth only was considered, with no allowance for the ponding effects. The experimental deflection of 10.17 mm is most accurately predicted by the fully effective section. The deflections for the effective and approximate effective sections are greater than the test value and on the basis of this one test it appears that for calculation of deflections, the section may be considered to be fully effective.

6.3.3 Maximum Stress in the Section

The bare formwork test demonstrated that the maximum stress in the top, compression flange is significantly greater than that predicted by simple bending theory and the fully effective section. It was also seen that the load-deflection response (Figure 16) becomes non-linear subsequent to first yield, which will then lead to undesirable non-recoverable deflections. A reduced section must therefore be used to provide an estimate of this maximum stress and to ensure that the yield stress of the steel is not exceeded, particularly in the case of the additional construction loads.

The maximum bending moments (for a 3B width) for the loading conditions employed in the bare formwork test are given in Table 3, while the stress distributions obtained from strain gauge readings are shown in Figures 14 and 15, for the load cases 1.1. and 1.2.(a) respectively. The stresses in the mid-plane of the flanges at mid-span, predicted by simple bending theory for the above two loading cases, are given in Table 12 for the fully effective, effective and approximate effective sections of Figure 85. For easy comparison, the values in Table 12 are indicated in Figures 14 and 15, from which it may be seen that the effective section and the approximate effective section provide fairly good estimates in the top flanges.

This comparison between experimental and theoretical stress distribution has shown that the value of k_w ($\simeq 0.3$) determined from the Vibrophore specimens provides a sufficiently accurate means by which it may be ensured that the yield stress is not exceeded.

6.4 ULTIMATE CAPACITY OF SECTION

The response of the formwork section during the ultimate load test is depicted in Figure 17, which shows the mid-plane longitudinal strains in the bottom flange and in the flat and embossed widths of the top flange, plotted against midspan bending moment.

Also shown in Figure 17 are the relationships between bending moment and top flange mid-plane strain for the three sections depicted in Figure 85. The fully effective section is symmetrical and thus the top and bottom flange strains are equal in magnitude. It may be seen from Table 12 that the bottom flange strain in the effective and the approximate effective sections differs from that of the fully effective section by only 4% and to a first approximation, the line OA in Figure 17 provides the bending moment-strain relationship for the bottom flange in all three sections.

The maximum stress in the section occurs in the flat portions of the top flange and is predicted fairly well by the effective and approximate effective sections, until the onset of yield.

Subsequent to first yield, it may be seen that load is shed into the embossed width, where the strain and stress increase rapidly and in fact full yield is attained throughout the top and bottom flanges. This indicates that the fully effective section may be employed in the calculation of the fully plastic moment of the section and calculated values for the three different sections (for a yield stress of 295 N/mm^2) are shown in Figure 17, for comparison with the maximum attainable midspan bending moment in the test.

It may be seen from Figure 16 that the transverse expansion of the section increases rapidly after first yield and the ultimate load is thus reduced by virtue of the resulting reduction in depth. If it is assumed that this transverse expansion will be prevented in practice, it may be concluded that the bare formwork section will attain the fully plastic moment as calculated using the fully effective section.

CHAPTER 7

THEORETICAL ANALYSIS - COMPOSITE STAGE

7.1 PURPOSE OF ANALYSIS

The response of the composite slab to both working and ultimate loads depends to a great extent upon the strength of the interface shear connection. It was noted in Chapter 1 that only when both the slip and separation between the steel and concrete elements are zero, can the condition of complete interaction apply, thereby permitting a theoretical analysis based on a continuous linear strain distribution throughout the depth of the slab. The test results clearly show that these conditions are not satisfied, although the magnitudes of slip and separation were small in the working load range.

The results of the push-out tests described in Chapter 3 provided some indication of the stiffness of the shear connection and upper and lower bounds on the strength which may exist in the composite slab were obtained. The margin between these upper and lower bounds is considerable and therefore the actual stiffness of the interface shear connection is still open to question.

A measure of the performance of the composite specimens may be obtained by comparison of the test results with the response predicted by complete interaction theory and it has been shown that complete interaction linear elastic theory predicts the behaviour well for small loads.

However, it would be advantageous to compare the test results with a partial interaction analysis, to obtain a more accurate assessment of the shear connection strength, particularly as regards ultimate

load behaviour. If the results of such an analysis prove to be in reasonable agreement with the test results, it would be possible to investigate, for example, the effects of various loading conditions and variation of embossment spacing without the need to resort to expensive and time consuming testing programmes.

With this objective, this chapter describes a method of partial interaction analysis for the simply supported form-reinforced slab under static loading conditions, incorporating the non-linear behaviour of the shear connection and material response. The results of this analysis are presented and compared with the test results and a complete interaction analysis, which is also briefly described.

The analyses for partial and complete interaction were performed by means of computer programs, which were written in FORTRAN for use on a CDC 6500 machine. Both programs may include non-uniform slab depth and dead load effects, if required.

Throughout this chapter it is assumed that the composite slab acts in a one-way mode and the composite test specimens are considered to consist of three beams of width B acting in parallel, as for the bare formwork unit. The basic section employed in both the partial and complete interaction analyses is as shown in Figure 3.

7.2 PARTIAL INTERACTION ANALYSIS

7.2.1 General

It is clear that the behaviour of the shear connection employed in the form-reinforced slab is more complex than that provided by, for example, stud shear connectors in a composite beam. It is also clear, in the light of the theoretical research which has been undertaken in

the field of composite beams, that a complete analysis to take account of the slip, separation and twisting effects which were demonstrated in the push-out tests, if indeed it is possible to do so, would require a large amount of time and effort.

It has therefore been necessary, at the outset, to make the basic assumption that the separation between the steel and concrete in the form-reinforced slab is sufficiently small as to have a negligible effect on the response.

The equations which govern the partial interaction analysis of a composite beam are easily derived for the case of zero separation, but an explicit solution of these equations is possible only for the case of linear load-slip behaviour of the shear connection and linear elastic stress-strain response of the steel and concrete. To incorporate non-linear behaviour it is necessary to formulate a numerical solution and the method employed here is based upon that developed by Yam [42] for composite beams.

7.2.2 Assumptions

The assumptions upon which the analysis is based are as follows :

1. The strain distributions within the steel and concrete elements are linear and continuous within the individual materials.
2. Separation between the steel and concrete is sufficiently small to be neglected.
3. The transfer of shear force between the concrete and steel at the interface occurs in a continuous nature, rather than at discrete points defined by the position of the embossments.

4. The distribution of interface shear over the surface of the formwork does not affect the stress distribution due to bending in the steel section.
5. The load-slip characteristics of the shear connection are similar to those obtained from the push-out tests.
6. Concrete is assumed to have no tensile strength.
7. No distortion of the formwork section occurs under load and the section is assumed to be fully effective.

Separation between the concrete and steel was measured during the tests and was found to be small (less than 0.1 mm) in the working load range, although as the load approached ultimate, values of up to 1 mm were recorded in the shear spans. However, separation was measured only along the sides of the specimens and it appears that the larger values occurring in the latter stages of the tests were due to local bending of the edges of the formwork due to the interface shear forces acting on the embossments in the webs adjacent to the edges. Subsequent to failure, a close examination of the underside of the concrete slab of all specimens, after careful removal of the formwork, revealed no evidence to suggest that separation of any significant magnitude had occurred (See Plates 13 and 14). These observations suggest that the assumption of zero separation is valid. The local bending of the edges of the formwork implied by the larger values of separation recorded in the shear spans, is an edge effect which will not seriously affect the assumption of a rigid steel section. In a practical situation, transverse continuity of the bridge deck will tend to reduce this effect. A direct implication of the assumption of zero separation is that the curvature in the steel and concrete sections are equal.

The relatively close spacing of the embossments in the formwork compared with shear connectors in a composite beam implies a continuous interface shear transfer. This also implies a continuous slip distribution along the span, although local flexural cracking of the concrete, which is not predicted in the analysis, may affect the correlation between experimental and theoretical slip distributions.

A prior knowledge of the shear connection load-slip characteristics is essential to enable a partial interaction analysis to be performed. It is therefore necessary to assume that the load-slip behaviour is similar to that observed in the push-out tests.

7.2.3 Derivation of Equations

The sign convention adopted requires clarification at this point. Tensile stresses and strains are defined as positive and compression as negative. As regards slip between the steel and concrete, positive slip is defined as movement of the concrete relative to the steel in the negative direction of x, which is measured from one free end as shown in Figure 87.

The equations which govern the partial interaction of a composite beam may be derived by considering compatibility between strain and slip along the length of the beam and the equilibrium of forces within the section.

A relationship between slip and the longitudinal strains in the two materials may be derived, with reference to Figure 87, by considering the increase in slip from s to $s+\left(\frac{ds}{dx}\right)\delta x$ over a small length δx, which is sufficiently small to ignore changes in longitudinal strain.

Clearly, compatibility requires that

$$s + \delta x(1+\varepsilon_s) = s + \frac{ds}{dx}\delta x + \delta x(1+\varepsilon_c)$$

$$\text{or} \qquad \frac{ds}{dx} = \varepsilon_s - \varepsilon_c \qquad (7.1)$$

where ε_s and ε_c are the strains in the steel and concrete at a given level z below the top surface of the slab. Thus the rate of change of slip with respect to x is equal to the strain difference within the section and is often referred to as slip strain.

The existence of the strain difference and the assumption that both materials are subjected to the same curvature, ρ, implies that the neutral axes of the steel and concrete sections do not coincide. If the depth of the neutral axes, at any section, below the top surface of the concrete are denoted by n_s and n_c, the strain in the steel (ε_s) and concrete (ε_c) are given by,

$$\left.\begin{aligned} \varepsilon_s &= \rho(z-n_s) \\ \text{and} \qquad \varepsilon_c &= \rho(z-n_c) \end{aligned}\right\} \quad (7.2)$$

Substitution of (7.2) into (7.1) leads to the expression,

$$\frac{ds}{dx} = \rho(n_c - n_s) \qquad (7.3)$$

The three parameters ρ, n_c and n_s are variables with respect to x.

The stress distributions which accompany the strain distributions of (7.2) are defined by the stress-strain relations of the materials thus;

$$\left.\begin{aligned} \sigma_s &= \sigma_s(\varepsilon_s) \\ \text{and} \qquad \sigma_c &= \sigma_c(\varepsilon_c) \end{aligned}\right\} \quad (7.4)$$

and are uniquely determined by the strains ε_s and ε_c.

These stress distributions give rise to internal moments and forces which may be determined as follows. The force in the concrete in the x-direction, P_c, may be found by integrating the stresses over the area of concrete in compression, thus

$$P_c = \int_{A_c} \sigma_c dA_c \tag{7.5}$$

while a similar expression gives the force in the steel section as

$$P_s = \int_{A_s} \sigma_s dA_s \tag{7.6}$$

Similarly, the internal moments may be expressed as

$$M_c = \int_{A_c} \sigma_c z dA_c \tag{7.7}$$

and

$$M_s = \int_{A_s} \sigma_s z dA_s \tag{7.8}$$

Equilibrium of the section under bending, caused by forces acting in the direction of z only, requires that the resultant force in the x-direction is zero. Hence

$$\left.\begin{aligned} P_c + P_s &= 0 \\ \text{or} \quad P_s &= -P_c = P \end{aligned}\right\} \tag{7.9}$$

where P is defined as the section force.

A summation of the internal moments must be equilibrated by the externally applied bending moment, M, which is a function of x, dependent upon the loading conditions. Therefore, at any section,

$$M_c + M_s = M \tag{7.10}$$

A relationship between the section force P and the slip may be derived by considering the change in the internal force in the steel section, from P to $P+\frac{dP}{dx}\delta x$, again over the very small length δx,

together with the assumption that the load Q in a push-out test may be equated to the product of the interface shear force per unit length, q, and the spacing of the embossments, C, in the beam. Equilibrium of forces in the x-direction for the steel section alone then leads to the expression

$$q = \frac{Q}{C} = \frac{dP}{dx} \qquad (7.11)$$

The stiffness of the shear connection obtained from push-out tests, provides the expression required to complete the basic equations, such that Q is a function of the slip, s. Equation (7.11) then becomes,

$$\frac{dP}{dx} = \frac{1}{C} Q(s) \qquad (7.12)$$

If the values of the three parameters ρ, n_s and n_c are specified at any section, x, the equations (7.2) define the strain distribution in the section and the stress distribution is given by equations (7.4). The internal forces P_s and P_c, which may then be calculated from (7.5) and (7.6), must be of equal magnitude, from equation (7.9). Therefore it is necessary to define values for only two of the three parameters ρ, n_s and n_c to enable the section force P, the internal moments M_s and M_c and thus the external moment M, to be calculated. It follows that if the values of P and M and specified, the values of ρ, n_s and n_c are uniquely determined. From equation (7.3) the slip strain may therefore be expressed as a function of P and M, or

$$\frac{ds}{dx} = f(M,P) \qquad (7.13)$$

The two equations (7.12) and (7.13) are the differential equations which govern the distribution of s and P with respect to x. The boundary conditions for these equations are that the value of the

section force, P, should be zero at the ends of the beam. The ease with which a solution to these equations may be obtained depends upon the specification of the three functions $Q(s)$, $\sigma_s(\varepsilon_s)$ and $\sigma_c(\varepsilon_c)$, that is, the load-slip relationship and the material stress-strain characteristics.

7.2.4 Shear Connection Characteristics

The load-slip curves of the push-out test specimens for which the value of α is 60^o are shown in Figure 88 in the form

$$\psi = \psi(s) \qquad (7.14)$$

where ψ is the ratio of applied load to ultimate load. Also shown in this figure is a plot of the function

$$\psi = 1-e^{-As} = Q/Q_u \qquad (7.15)$$

where e is the base of naperian logarithms and A is a constant. It may be seen that this function, which was also used by Yam[42], provides a close approximation to the shape of the load-slip curve, when A = 0.8. The ultimate load Q_u in the push-out tests was expressed as a proportion of the calculated load, Q_c, to give uniaxial crushing, at the cube strength, of the concrete on the projected area of the embossments in a plane perpendicular to the longitudinal axis of the formwork, thus,

$$Q_u = \eta_u Q_c \qquad (7.16)$$

Using the function defined in (7.15) for ψ, then

$$Q = \eta_u Q_c (1-e^{-As}) \qquad (7.17)$$

The value of A defines the shape of the load-slip curve, while η_u defines the maximum attainable load (as $s \to \infty$), as a proportion of Q_c. The values of η_u obtained from the push-out tests were 1.6 for the laterally restrained specimens and 0.6 for the laterally unrestrained specimens. Substituting equation (7.17) in equation (7.12), gives

$$\frac{dP}{dx} = \frac{\eta_u Q_c}{C}(1-e^{-As}) \qquad (7.18)$$

where, for this particular embossment configuration, A = 0.8 and $0.6 < \eta_u < 1.6$.

7.2.5 Material Stress-Strain Relations

7.2.5.1 *Steel*

The stress-strain relation for steel has been idealised as a bilinear curve of the form,

$$\left.\begin{aligned} \sigma_s &= E_s\varepsilon_s \qquad 0 < \sigma_s < \sigma_{ys} \\ \text{and} \quad \sigma_s &= \sigma_{ys}+\mu(E_s\varepsilon_s-\sigma_{ys}) \qquad \sigma_s > \sigma_{ys} \end{aligned}\right\} \qquad (7.19)$$

to cover the two cases of elastic-perfectly plastic behaviour, (μ=0) and elastic-strain hardening (μ>0). The response is assumed to be the same in tension and compression.

A typical stress-strain curve from tensile tests on samples of the steel formwork is shown in Figure 89, together with the idealised form. The value of the strain hardening parameter μ, has been taken as 0.015 as representative of the observed behaviour in tensile tests.

7.2.5.2 *Concrete*

Several functions have been used in research work to model the stress-strain behaviour of concrete. A polynomial representation proposed by Basu[68] and based upon tests conducted at Cambridge University by Barnard and Johnson[35], is used here. The expression is

$$\frac{\sigma_c}{\sigma_u} = C_1\varepsilon_r + C_2\varepsilon_r^2 + C_3\varepsilon_r^3 + C_4\varepsilon_r^4 \qquad (7.20)$$

where $\varepsilon_r = \varepsilon_c/\varepsilon_u$

σ_u = maximum concrete stress

and ε_u = concrete strain corresponding to σ_u.

The coefficients C_1 to C_4 are obtained by fitting stress-strain data from uniaxial compression tests of concrete cubes and cylinders. The results of the tests carried out at Cambridge using a stiff constant strain rate testing machine[69,70] gave the following values for the coefficients:

$$C_1 = 2.41 \qquad C_2 = -1.865$$

$$C_3 = 0.50 \qquad C_4 = -0.045$$

The form of the curve is shown in Figure 90. The value of ε_u is generally taken as 0.0025 and the crushing strain of concrete as 0.0035.

This representation has been used in recent research on composite columns[71,72].

7.2.6 Method of Solution

7.2.6.1 *General*

The method which has been employed to solve the differential equations (7.12) and (7.13) may be described as a step by step solution, achieved by the use of a predictor-corrector set of equations which are derived from the approximation of $\frac{ds}{dx}$ and $\frac{dP}{dx}$ as polynomial functions with respect to x. For clarity, a slight change in notation is introduced here, such that s' and P' represent the first derivatives of s and P, respectively, with respect to x.

In general, the two boundary conditions for the equations are that the value of P is zero at the free ends of the beam. For a beam where both the geometry and the loading are symmetrical about midspan, the boundary condition of zero slip at midspan may be specified and a solution obtained for one half of the beam only.

The step-by-step method requires the knowledge of the initial boundary values, at x=0, of s and P, which are designated as s_I and P_I. When the position x=0 corresponds to a free end of the beam, P_I=0, but the value of s_I is unknown and must be assumed. Solution of the equations (7.12) and (7.13) will then lead to a final boundary value for P (designated P_F) at the other end of the beam or s at midspan (designated s_F), for a symmetrical beam. The solution will be correct when the final boundary value, P_F or s_F, is equal to zero. In practice, a solution is acceptable when the magnitude of P_F (or s_F) is less than a predetermined small value.

An iterative procedure is therefore necessary to obtain the value of s_I (s_I*) which results in the final boundary value being satisfied. The success of the method depends upon determining whether a given value of s_I is an upper bound ($s_I > s_I$*) or a lower bound ($s_I < s_I$*) on the value of s_I*, to ensure that convergence may be attained.

The various aspects of the method of solution are considered in detail in the following sections.

7.2.6.2 *Predictor-Corrector Equations*

If the value of a function f(x) is known at (n+1) points (x_0,y_0), (x_1,y_1) .... (x_n,y_n), then the function may be replaced by a polynomial F(x) of degree n, such that

$$F(x) = y = a_0 + a_1 x + ... + a_n x^n$$

Substituting the known values (x_k,y_k) for k = 0 to n, in this equation the desired polynomial may be expressed as

$$F(x) = y = \sum_{k=0}^{n} L_k(x) y_k$$

where

$$L_k(x) = \frac{(x-x_0)(x-x_1)\ldots\ldots(x-x_{k-1})(x-x_{k+1})\ldots\ldots(x-x_n)}{(x_k-x_0)(x_k-x_1)\ldots(x_k-x_{k-1})(x_k-x_{k+1})\ldots(x_k-x_n)} \qquad (7.21)$$

Further, if the values of the function are known at equidistant points such that $x_k = x_0 + kh$, then putting $x = x_0 + mh$, whence $dx = hdm$, equation (7.21) may be expressed as,

$$F(x) = \sum_{k=0}^{n} L_k y_k$$

where

$$L_k = \frac{m(m-1)\ldots(m-k+1)(m-k-1)\ldots(m-n)}{k(k-1)\ldots\ldots(1)(-1)\ldots\ldots(k-n)} \qquad (7.22)$$

The equation (7.22) may be integrated to obtain

$$\int_{x_0}^{x_n} F(x)dx = (x_n - x_0) \sum_{k=0}^{n} C_k^n y_k$$

where

$$C_k^n = \frac{1}{n} \int_0^n L_k dm \qquad (7.23)$$

The numbers C_k^n are called Cote's numbers (see Ref.73) and they satisfy the relations $C_k^n = C_{n-k}^n$ and $\sum_{k=0}^{n} C_k^n = 1$.

A prediction of the value of $\int F(x)dx$ at x_{n+1} may be obtained by integrating over the range x_0 to x_{n+1}, such that

$$\int_{x_0}^{x_{n+1}} F(x)dx = h \sum_{k=0}^{n} y_k \int_0^{n+1} L_k dm \qquad (7.24)$$

If the function s' is expressed in the form of equation (7.22), assuming that the values s_k' (k=0 to n) are known, such that

$$s' = \sum_{k=0}^{n} L_k s_k' \qquad (7.25)$$

a prediction of the value of s_{n+1} (at x_{n+1}) may be obtained from

equation (7.24), thus

$$s_{n+1} = s_0 + h \sum_{k=0}^{n} s'_k \int_0^{n+1} L_k dm \qquad (7.26)$$

while s_n is given by

$$s_n = s_0 + h \sum_{k=0}^{n} s'_k \int_0^{n} L_k dm \qquad (7.27)$$

A similar expression may be obtained for P_n (at x_n), as

$$P_n = P_0 + h \sum_{k=0}^{n} P'_k \int_0^{n} L_k dm \qquad (7.28)$$

The predictor-corrector equations used in this analysis are based on a value of n = 7. It is assumed that the values of s, s', P and P' are known at eight sections x_0 to x_7. The value of s_8 may then be predicted from equation (7.26), which for n = 7 becomes,

$$s_8 = s_0 + \frac{8h}{945}\{460(s'_1+s'_7)-954(s'_2+s'_6)+2196(s'_3+s'_5)-2459s'_4\} \qquad (7.29)$$

The value of P'_8 may then be calculated from equation (7.18) and a closed integration over the range x_1 to x_8, using equation (7.28), but with the curve fit advanced by one interval along the beam, yields the value of P_8, thus

$$P_8 = P_1 + \frac{7h}{17280}\{751(P'_1+P'_8)+3577(P'_2+P'_7)+1323(P'_3+P'_6)+2989(P'_4+P'_5)\} \qquad (7.30)$$

Using the values of P_8 and the value of the bending moment at this section, M_8, the value of s'_8 may be found from equation (7.13). The method of evaluation of the function f(M,P) is outlined in section (7.2.6.4).

The value of s_8 calculated from (7.29) may now be corrected by a closed integration, to include the value of s'_8.

The expression is

$$s_8 = s_1 + \frac{7h}{17280}\{751(s'_1+s'_8)+3577(s'_2+s'_7)+1323(s'_3+s'_6)+2989(s'_4+s'_5)\} \qquad (7.31)$$

A comparison of the resulting value of s_8 with that previously calculated from equation (7.29) will show if the required accuracy, which must be predefined, has been achieved.

The above procedure is continued, advancing the position of the points over which the curve fitting exercise is performed, by one interval at a time, until the other end of the beam is reached. An investigation of the final boundary condition, i.e. the value of P_F or S_F will then indicate the adjustment necessary to the value of s_I and the process is continued until the value of P_F or S_F is sufficiently small.

To initiate the predictor-corrector solution it is necessary to calculate the values of s, s', P and P' at the eight 'starting' sections x_0 to x_7 and the method employed for this purpose is outlined in the following section.

The predictor-corrector equations as outlined above require that the function d^2s/dx^2 is continuous with respect to x. Discontinuities will exist however, at the positions of point loads and supports for example, and it is therefore necessary to interrupt the predictor-corrector solution at these points. To continue the solution along the beam the values of s and P at the discontinuity calculated from the predictor-corrector solution are used to set up eight starting sections in the following region of continuity, thus allowing the procedure to continue.

7.2.6.3 *Calculation of Starting Values*

The method of calculation employed by Yam[42] to establish the required number of starting values was found to give rise to a discontinuous solution in regions of constant moment due to an accumulation of the errors introduced during the calculation of the initial values.

For the present study it was therefore necessary to use a more accurate method and for this purpose recourse was made to a Runge-Kutta approach (see Ref. 73), which was found to eliminate the discontinuous solution in regions of constant moment.

Since for any given load on a simply supported beam, the bending moment is a function of x, the equations (7.13) and (7.12) may be expressed as

$$\left.\begin{aligned} s' &= f_1(x,P) \\ \text{and} \quad P' &= f_2(s) \end{aligned}\right\} \quad (7.32)$$

Given the values of s_n and P_n, the values of s_{n+1} and P_{n+1} may be calculated from

$$\left.\begin{aligned} s_{n+1} &= s_n + \frac{1}{6}(\zeta_1+2\zeta_2+2\zeta_3+\zeta_4) \\ \text{and} \quad P_{n+1} &= P_n + \frac{1}{6}(\chi_1+2\chi_2+2\chi_3+\chi_4) \end{aligned}\right\} \quad (7.33)$$

where

$$\begin{aligned} \zeta_1 &= hf_1(x_n,P_n) \\ \chi_1 &= hf_2(s_n) \\ \zeta_2 &= hf_1(x_n+\tfrac{1}{2}h,P_n+\tfrac{1}{2}\chi_1) \\ \chi_2 &= hf_2(s_n+\tfrac{1}{2}\zeta_1) \\ \zeta_3 &= hf_1(x_n+\tfrac{1}{2}h,P_n+\tfrac{1}{2}\chi_2) \\ \chi_3 &= hf_2(s_n+\tfrac{1}{2}\zeta_2) \\ \zeta_4 &= hf_1(x_n+h,P_n+\chi_3) \\ \chi_4 &= hf_2(s_n+\zeta_3) \end{aligned}$$

where h is the solution interval.

7.2.6.4 *Section Analysis*

The determination of the function f(M,P) is performed using a Newton-Raphson iterative procedure. It was seen in section 7.2.3 that if the values of the curvature, ρ and the depth of the neutral

axes n_s and n_c are specified, then the internal forces and moments in the section may be determined from equations (7.5) to (7.8). The integrations specified in these equations may be carried out explicitly knowing the material stress-strain relations and the geometry of the section. The resulting expressions are complicated, but may be expressed as general functions dependent upon the variables ρ, n_s and n_c, thus

$$\left.\begin{aligned} P_s &= P_s(\rho, n_s) && \text{(a)} \\ P_c &= P_c(\rho, n_c) && \text{(b)} \\ M_s &= M_s(\rho, n_s) && \text{(c)} \\ \text{and} \quad M_c &= M_c(\rho, n_c) && \text{(d)} \end{aligned}\right\} \quad (7.34)$$

It is required to calculate the values ρ^*, and n_s^* and n_c^* corresponding to specified values P^* and M^*. If the values ρ, n_s and n_c are known to give an approximate solution, the corrections $\Delta\rho$, Δn_s and Δn_c required to achieve an improved solution may be calculated by expanding equations (7.34) in Taylor series form and truncating after the first-order terms. Hence,

$$\left.\begin{aligned} P_s + \Delta\rho \frac{\partial P_s}{\partial \rho} + \Delta n_s \frac{\partial P_s}{\partial n_s} &= P_s^* \\ P_c + \Delta\rho \frac{\partial P_c}{\partial \rho} + \Delta n_c \frac{\partial P_c}{\partial n_c} &= P_c^* \\ M_s + \Delta\rho \frac{\partial M_s}{\partial \rho} + \Delta n_s \frac{\partial M_s}{\partial n_s} &= M_s^* \\ \text{and} \quad M_c + \Delta\rho \frac{\partial M_c}{\partial \rho} + \Delta n_c \frac{\partial M_c}{\partial n_c} &= M_c^* \end{aligned}\right\} \quad (7.35)$$

The derivatives may be calculated from the explicit functions of (7.34) and using equations (7.9) and (7.10) such that

$$P_s^* = -P_c^* = P^*$$

and $$M_c^* + M_s^* = M^*,$$

the values of $\Delta\rho$, Δn_s and Δn_c may be determined from equations (7.35). The iteration may be continued to any desired accuracy. It was found that by taking the values of ρ, n_s and n_c from the previous section two or three iterations only were required. For the section at $x = 0$, since P and M are both zero, s' is also zero and for the section at $x = h$, the initial trial values were furnished by values calculated assuming complete interaction.

7.2.6.5 *Construction Load Stresses and Deflections*

The non-uniform depth of the concrete section, caused by the wet concrete load, may be easily included in the method of solution employed. For comparison with the test results the actual depth of the test specimens measured at intervals along the span were used to provide an approximate profile. For other general cases, the depth may be calculated, to include ponding effects if required, from equations given in Chapter 6.

The dead load stresses induced in the steel formwork during construction, being tensile in the bottom flanges, will cause first yield in the formwork to occur slightly earlier than will be the case if this 'prestress' effect is ignored. The effect may be included in the analysis by modifying the values of the neutral axis depth and curvature for the steel section alone while calculating the values of P_s, M_s and their derivatives with respect to n_s and ρ.

If the dead load curvature ρ_d for the bare steel is calculated at the section being considered, the actual curvature for the steel in the composite section analysis is given by

$$\rho' = \rho+\rho_d \tag{7.36}$$

and if the depth of the bare formwork centroid below the top of the concrete slab is defined as d_s, the steel section neutral axis depth is modified to

$$n_s' = (\rho n_s+\rho_d d_s)/\rho' \tag{7.37}$$

The effect of the dead load will be shown to be fairly small, but it must be included in the calculation of design stresses. In the majority of cases studied using the computer programs, the dead load stresses were calculated assuming a simply supported span.

7.2.6.6 *Upper and Lower Bound Criteria*

The iterative procedure by which s_I^* is calculated depends upon whether a given value of s_I is an upper or lower bound on s_I^*. It has been shown by Yam[42], that if the shear connection load-slip curve, Q(s), the steel stress-strain curve, $\sigma_s(\varepsilon_s)$ and the concrete stress-strain curve $\sigma_c(\varepsilon_c)$ are such that the slope of these curves are nowhere negative, then if $P_F>0$ (or $s_F>0$) then $s_I>s_I^*$ and conversely if $P_F<0$ (or $s_F<0$) then $s_I<s_I^*$.

The proofs of the above criteria depend essentially upon whether the internal forces and moments in the section increase or decrease for given changes in ρ, n_s and n_c.

The functions Q(s) and $\sigma_s(\varepsilon_s)$ adopted in the present investigation are such that the slopes of the curves are positive everywhere, but the Basu polynomial curve employed for $\sigma_c(\varepsilon_c)$ has a negative slope for $(\varepsilon_c/\varepsilon_u) > 1$ and requires some investigation on this point.

For a simply supported span, with the top of the slab in compression, the negative slope zone of the concrete stress-strain curve will be entered only when the concrete is close to failure. The neutral

axis for the concrete will then be above the top of the steel formwork, i.e. $n_c<(D-d)$. The concrete compression zone will therefore be a rectangle and the concrete force P_c and its derivatives with respect to ρ and n_c may be derived in an explicit form with relative ease. In this way it may be shown that

$$\frac{\partial P_c}{\partial n_c} < 0 \quad \text{for} \quad 0 < r < 2.0$$

and

$$\frac{\partial P_c}{\partial \rho} < 0 \quad \text{for} \quad 0 < r < 1.7$$

where $r = -\rho n_c/\varepsilon_u$.

Thus, as both n_c and ρ are increased the concrete force P_c decreases (note, P_c is negative) as long as r is less than 1.7. At values of $r > 1.7$, $\frac{\partial P_c}{\partial \rho}$ becomes positive. The critical point $r = 1.7$ corresponds to a surface strain (at $z = 0$) of $-\rho n_c$ which is given by,

$$\varepsilon_c(z=0) = -\rho n_c = r\varepsilon_u$$

Using the value of ε_u of -0.0025 and r of 1.7, it may be seen that the critical point occurs when the concrete surface strain is -0.00425, which is greater (in magnitude) than the assumed crushing strain, -0.0035. Thus, provided that it is ensured that the magnitude of the concrete surface strain does not exceed 0.00425, the upper and lower bound criteria as stated above, hold for the Basu concrete curve.

A more complete discussion of the proof of the upper and lower bound criteria has been given by Yam[42].

7.3 COMPLETE INTERACTION ANALYSIS

A complete interaction analysis of the composite slab was performed to provide a measure of the actual strength and stiffness

of the test specimens and that predicted by the partial interaction analysis, relative to ideal fully composite action.

For complete interaction it is assumed that both slip and separation are zero at all points. Thus the slip strain is also zero everywhere and the strain distribution in the section is linear and continuous throughout the overall depth of the slab. The conditions of stress and strain in the section are then completely determined by the value of the externally applied bending moment, M only and the determination of the response of a simply supported beam under any loading condition is very simple. However, to provide a direct comparison with the partial interaction analysis throughout the loading range, a computer program was also written to perform the complete interaction analysis.

The steel and concrete stress-strain relations employed were as defined in section 7.2.5 and the effects of non-uniform slab depth and dead load stresses were incorporated. The section analysis for a given value of M was carried out by a simplified version of that employed for partial interaction, as there are only two variables ρ and n' (where $n'=n=n_s=n_c$) for complete interaction.

The results of the complete and partial interaction analyses are compared with the test results in the following section.

7.4 CORRELATION WITH TEST RESULTS

7.4.1 General

The load-slip curve utilised in the partial interaction analysis of the composite slab is assumed to be of a similar form to that obtained from the push-out tests and it was shown that the

function defined in equation (7.15) provides a close approximation to the shape of this curve. All cases of the partial interaction analysis were carried out using a value for the parameter A, of 0.8, which provided, on average, the best fit for the specified function to the shape of the actual push-out test curves.

The value of η_u for the shear connection in the composite slab is unknown, but is assumed to lie between the upper and lower bounds obtained from the push-out tests, i.e. $0.6 < \eta_u < 1.6$. It was therefore necessary to vary the value of η_u to provide the best correlation between the theoretical analysis and the test results to give an estimate of the actual value of η_u which is operative in the composite slab.

The effect of repeated loading on the shear connection load-slip curve is also undefined, as the push-out tests were carried out under static loading, with no loading cycles having been previously applied to the specimens. Therefore the validity of using the assumed load-slip curves to determine the response of the slab specimens which were subjected to dynamic loading is questionable, but a measure of the effect of repeated loading may be obtained by a comparison with the partial interaction analysis for the static load-slip curves.

The correlation between the predictions of the theoretical analyses for the specimens of Tests 2, 4 and 5, and the corresponding test results is examined below. In both theoretical analyses, the test specimens have been assumed to be symmetrical about midspan in respect of both loading and geometry. This is not exactly correct where overall depth is concerned, but it is considered to be an

assumption which will cause insignificant errors, in view of the small differences between overall depths measured at points equidistant from midspan.

7.4.2 Static Test Correlation - Test 2

The midspan deflection with respect to load for the specimen of Test 2 is shown in Figure 91, together with the predicted complete interaction response, incorporating strain hardening in the steel and the two cases of zero and maximum dead load conditions, which correspond to ignoring dead load effects and assuming simple supports during casting, respectively. A comparison of these curves with the actual response in the test shows that in the working (elastic) range, the response is predicted almost exactly by complete interaction theory, but as the load increases and approaches ultimate, a significant deviation does occur, although it is still close to complete interaction. This indicates that the value of η_u will be at or near the top of the range obtained from the push-out tests and indeed for the response as predicted by partial interaction theory for $\eta_u = 1.6$ shown in the figure the agreement is good. However, it was found to be very difficult to follow the response to ultimate and the reason for this will be discussed later. For the moment, the correlation between the test results and the partial interaction results which are available will be considered.

The predicted and the experimental slip distributions at three load levels are depicted in Figures 92-94, for comparison. The experimental distributions shown in these figures are those recorded during the ultimate stage (Stage III) and are shown relative to the Stage III zero and the absolute zero corresponding to the start of

Stage I. There is a reasonable agreement between the absolute slip and the theory, although the slip near the supports is over-estimated. This is probably due to a reaction effect at the supports, where there will be considerable forces tending to prevent separation, thus increasing the shear resistance and preventing slip in this region. The distribution at the higher load (Figure 94) gives an improved correlation in the support region, but tends to under-estimate the maximum slip in the shear spans. At this very high load (97.6% of the failure load in the test) the separation effect along the edges of the slab may reduce the shear connection in this region, thus increasing the slip.

The predicted slip in the midspan region is very small and may be considered to be zero. The distribution recorded in this region in the test is affected by the presence of flexural cracking in the concrete. The presence of the shear cracks just outside the loading points is a factor which will also affect the magnitude of the slip and may be the main cause of under-estimation of the maximum slip by the partial interaction theory at high loads.

The longitudinal maximum strain distribution in the concrete and steel predicted by partial interaction theory, are shown in Figure 95 for a load of 220 kN/jack. The maximum strain and stress in both the steel and concrete occur at the loading point and are clearly greater than the values predicted by complete interaction theory. The peaking effect in the strain distribution is due to the very high slip strain (ds/dx) which occurs at the loading points (see Figures 92-94). This severe peaking effect was obtained by assuming an ideal point load. It will be shown in the next section

that if the load is assumed to be uniformly distributed over a length of 90 mm, which is more representative of the test conditions, then the peak strains are greatly reduced. It is unfortunate that strain gauges were not positioned at the loading points, since the data provided by these gauges would have proved invaluable in correlation between the test and theoretical results. Strain gauges were positioned only at midspan, where, due to the dead load effect, first yield was expected to occur.

The strains recorded at midspan in the bottom flanges of the steel formwork and the top surface of the concrete during the test are shown in Figure 95. The average of the recorded values agree well with the complete and partial interaction predictions, although there was a great deal of scatter in the values for the steel, probably due to non-uniform depth in the transverse direction.

7.4.3 Dynamic Test Correlation - Tests 4 and 5

The midspan deflections for the specimens of Tests 4 and 5 are shown in Figures 96 and 97 in which the experimental results are again compared with the complete and partial interaction predictions. It is immediately apparent that the repeated loading causes a significant reduction in the stiffness of the shear connection, leading to increased deflections at high loads and a reduction in the ultimate loads attained. This observation was also made for the specimens of Tests 7 and 8. Thus the value of $\eta_u = 1.6$ seems inappropriate subsequent to repeated loading, although the elastic response is again predicted well by complete interaction linear elastic theory. As the ultimate load is approached a significant loss of interaction is apparent.

The partial interaction response was therefore checked using values of η_u of 0.6 and 1.0 and the resulting curves are included in

the two figures. Clearly there is no direct correlation between the test results and the theoretical predictions and this must be due to a significant modification of the shape of the load-slip response of the shear connection as a result of the repeated loading. This will also account for the reduction relative to Test 2, in the ultimate loads attained by the four dynamic test specimens which were tested to collapse. It may be seen from Figures 96 and 97 that the partial interaction analysis for $\eta_u = 0.6$ provides a more realistic representation of the test response for loads greater than approximately 85% of the experimental ultimate load.

The predicted slip distributions corresponding to η_u values of 1.6, 1.0 and 0.6 are shown in Figure 98 for the specimen of Test 4 and are compared with the recorded values at a load of 180 kN per jack. Similar distributions are shown in Figure 99 for the specimen of Test 5, at a load of 190 kN per jack.

The longitudinal maximum strain distributions predicted for complete and partial interaction for Test 4 at a load of 180 kN are shown in Figure 100 and the experimentally obtained average values at midspan are also shown, for the same load. The peak effect at the assumed point load will not in fact occur in practice. This is demonstrated by a partial interaction analysis assuming the load to be uniformly distributed over a length of 90 mm, which is the actual condition in the tests. A significant reduction in the peak strains at the load point is apparent.

The validity of these strain distributions is in doubt as far as the actual test specimen is concerned, as it has been shown that there is little correlation between the behaviour of specimens

loaded statically subsequent to dynamic loading and static partial interaction theory. This theoretical pattern of longitudinal strain distribution has been noted to illustrate the following discussion concerning the estimation of the ultimate loads.

7.4.4 Prediction of Ultimate Loads

The peaking effect of the strains at the loading points indicated by the partial interaction analysis is in agreement with the mode of failure observed in the tests, in which spalling of the concrete occurred in the region of the loading points.

The prediction of the ultimate loads for the test specimens proved to be very difficult with the partial interaction program. This was due entirely to the degree of accuracy to which the initial boundary slip value s_I^* needs to be calculated. As a general indication to the very high accuracy required, it was necessary to calculate the value of s_I^* to six significant figures to obtain convergence (i.e. $s_F \simeq 0$ at midspan) over the majority of the load range. As the load approached ultimate, however, the required accuracy increased to nine significant figures and in many cases, convergence to the value of s_I^* was not achieved, even at this accuracy.

As mentioned previously, the Runge-Kutta method of calculation of the starting values for the predictor-corrector procedure proved effective in assisting convergence for the test loading conditions, but it appears that at very high loads, the method of solution is unsuitable for this particular loading arrangement.

The maximum loads attained, with convergence, for the partial interaction analysis were such as to cause maximum concrete strains at the loading points in excess of 3000 microstrain and for the case

of Test 5, a maximum value of 3450 μs was attained. The points at which non-convergence occurred are indicated for Tests 2, 4 and 5 in Figures 91, 96 and 97 respectively. In all cases it is evident that predicted failure occurs at a much smaller deflection than in the tests and this may be the result of containment of the concrete beneath the loading pads. Thus, if the concrete is prevented from crushing at the critical points, the deflections will increase until failure occurs by concrete crushing just inside the loading points, as observed in the tests.

Bearing in mind the above discussion, a comparison between predicted and experimental ultimate loads has been drawn up in Table 13. In this table the ultimate load for each specimen may be compared with (i) the ultimate load calculated by simple plastic stress block theory, ignoring dead load effects, (ii) the complete interaction theory ultimate load, with and without strain hardening, and for various dead load conditions, and (iii) the maximum attainable load for the partial interaction theory, with strain hardening and maximum dead load effect, for various values of η_u.

The experimental ultimate load for the static test (Test 2) is greater than that predicted by plastic stress block theory, due to strain hardening, but less than that calculated by complete interaction theory with strain hardening, as a result of partial interaction effects. The failure loads of all four dynamic specimens are marginally less (up to 3% less) than the loads calculated by plastic stress block theory and by comparison with Test 2, the strength of these specimens appears to have been reduced by the effects of repeated loading on the stiffness of the shear connection. The greater concrete strength of the specimen

in Test 2 is another factor which must be considered, but the fact that 98% of the plastic stress block ultimate load was achieved in Test 7, where the concrete strength was lowest, indicates that concrete strength has little influence on the reduction in strength due to repeated loading.

It appears that for the prototype formwork, for which the bearing stress, σ_d, was limited to 0.4 of the design cube strength (including the safety factor of 1.5 over and above the basic factor of 0.6) the ultimate capacity of the section may be predicted fairly accurately using the plastic stress block approach and assuming that complete interaction exists. If an allowance is made for the dead load moment, the effect of which is to slightly reduce the section capacity as may be seen for the complete interaction case in Table 13, it is considered that this will form a reasonable basis for design. The reduction in the ultimate capacity due to repeated loading in a practical situation, is unlikely to exceed that observed in the test specimens, which were subjected continuously to cycles of a relatively high loading intensity.

It may be seen that the maximum attainable loads in the partial interaction analysis may not be classed as failure loads on the basis of concrete crushing at a strain of 3500 microstrain, but the actual theoretical failure loads cannot be more than a few percent greater than the loads given in Table 13. A comparison between the experimental and partial interaction values does show that the latter are of the correct order of magnitude and that a reasonable correlation exists. The analysis indicates that a value of $\eta_u = 0.6$ is more appropriate for specimens which have been subjected to repeated loading, while a

value of 1.6 seems to apply in the purely static case. This tends to suggest that the basis for the shear connection design, i.e. that σ_d should not exceed 0.6 of the design cube strength, should be retained.

The values of the maximum slip at the maximum attainable loads for values of η_u of 1.6, 1.0 and 0.6 were of the order of 0.5 mm, 0.8 mm and 1.5 mm respectively. The load-slip curves of Figures 7-11 show that the maximum load for the push-out specimens occurred at a slip in excess of 3 mm. This demonstrates that the strength of the shear connection is adequate to prevent interface shear failure for the loading conditions employed in the test, although the existence of slip does reduce the ultimate load capacity.

7.4.5 General Assessment of the Partial Interaction Theory

The correlation between the partial interaction analysis and the test results for the one specimen which was tested statically, is fairly satisfactory where midspan deflections and slip distributions are concerned. However, for the specimens which were subjected to dynamic loading the correlation is much less satisfactory. As stated previously, this is believed to be the result of a considerable change in the load-slip response of the shear connection during the repeated loading.

It is possible that the utilisation of a different load-slip function or some other combination of values for the parameters A and η_u may result in improved theoretical predictions for the dynamic test specimens. The effect of repeated loading on the stiffness and strength of the shear connection could be studied by means of push-out tests.

Unfortunately, due to the time and financial limitations imposed upon the project, it was not possible to carry out a complete partial interaction parametric study. However, in view of the correlation obtained with the static test, it was decided to conduct a limited investigation into the effects of the end overhang condition and the longitudinal spacing of the embossments.

7.5 · EFFECT OF THE END OVERHANG

It has been shown that the partial interaction analysis tends to over-estimate the slip at the ends of the specimens due to the support reaction, which tends to increase the shear connection stiffness at the supports. In an actual bridge deck of composite construction, where the concrete slab is designed to act compositely with the main steel beams by means of stud shear connectors, for example, there will be a significant end anchorage between the steel formwork and the concrete slab via the stud shear connectors and the steel beam.

The effect of this end anchorage on the degree of interaction in the slab will be domonstrated by examining the result of increasing the end overhang in a partial interaction analysis, thereby increasing the strength of the shear connection beyond the support, assuming that the formwork is embossed throughout its length. Analyses for the specimen of Test 4 for end overhang lengths of zero, 120 mm, 240 mm and 360 mm, resulted in the slip distributions shown in Figure 101, for a load equivalent to 90 kN for the test slab width. It may be seen that the magnitude of the slip is reduced, with increasing end overhangs, over the majority of the shear span and the reduction at the support is substantial. However, the slope of the slip distribution at the

loading points remains essentially unchanged, implying that the peak strains also remain unchanged. In fact a reduction of approximately 5% in the peak strains was detected from the case of zero overhang to the value of 360 mm.

The slip distribution curve for the 360 mm overhang is similar to that recorded in the test specimens subsequent to repeated loading (see Figures 98 and 99). This fact suggests that during the application of repeated loading to the actual test specimens a greater reduction in shear connection stiffness occurred in the regions of maximum slip (i.e. just outside the loading points) than in the region of the supports. Thus, subsequent to repeated loading, the greater stiffness of the shear connection in the end overhangs, relative to that in the shear spans, will produce an effect similar to that caused by increasing the length of the end overhang. This may explain the considerable difference between the slip distributions before and after repeated loading.

7.6 EFFECT OF EMBOSSMENT SPACING

The effect of varying the embossment spacing was also studied to a limited extent. Clearly, a minimum number of embossments is desirable to reduce the possibility of fatigue failure, while maintaining a sufficient degree of interaction to limit the in-service deflections and stresses to acceptable values and to provide a reasonable factor of safety against collapse, in the event of overloading.

It is obvious that increasing the number of embossments, i.e. decreasing the spacing, will result in an increase in the shear connection strength and a higher degree of interaction, while increasing the spacing will reduce the degree of interaction, assuming that other geometric

properties of the embossments remain unchanged. This is another aspect which could be investigated by means of a parametric study.

To demonstrate quantitatively the change in the degree of interaction which may be expected by altering the embossment spacing, analyses were conducted for values of the spacing, C of 30 mm, 45 mm and 60 mm. The loading condition employed for this limited study consisted of a point load at midspan, while the end overhang of 120 mm employed in the test specimens was retained. The value of η_u was taken as 1.6 and strain hardening and maximum dead load effects were included.

The response in terms of midspan deflection with respect to load for the three cases is shown in Figure 102, together with the complete interaction case. There is a more significant deviation from the complete interaction case for this loading condition than for the symmetrical point loading system employed in the tests due to the fact that slip occurs over the full length of the span. The ultimate loads attained, are also shown in Figure 102. The reduction in ultimate load relative to the complete interaction case amounts to 3%, 4.5% and 7.5% for spacings of 30, 45 and 60 mm respectively.

The slip and strain distributions at a load of 60 kN are shown in Figures 103 and 104 respectively. The extreme peaking effect of the strains at the loading point is again evident and the use of a uniform load over a small length would result in a smoothing of the peak strains, as in the case of the test specimens.

CHAPTER 8

PRACTICAL ASPECTS

8.1 GENERAL

While the prime objective of this thesis is to assess the feasibility of a form-reinforced slab as a self-contained structural component it is considered that the investigation would be incomplete without a discussion of the possible problems which may arise in the manufacture of the formwork units and the practical application of the system to an actual bridge deck.

This chapter has therefore been included to identify, in a purely qualitative form, several aspects relating to the design, manufacture and practical application of the formwork units.

8.2 METHOD OF MANUFACTURE

In Chapter 1 it was noted that the decision to employ a form-reinforced slab in preference to conventional timber formed reinforced concrete for the construction of a bridge deck will depend almost entirely upon the relative costs of the two methods. The cost of the individual formwork units will be the most important aspect of an economic comparison.

The success of the form-reinforced slab in the application to building floors is partly due to the fact that the formwork sections are cold-roll formed in a continuous process and cut to lengths defined either by the manufacturers standard supply or by the individual customer requirements.

The method of manufacture employed for the limited number of formwork units tested during this investigation was one of pressing and press-brake forming and is described briefly in Chapter 2. This method of manufacture has two main disadvantages. Firstly, the range of lengths of the units would be fairly limited and secondly, the cost of manufacture for each individual unit will be higher, although the capital investment for tooling would be much lower than for cold-roll forming.

The choice of the method of manufacture will depend to a great extent upon the potential market for the formwork units and the capital cost of cold-roll forming equipment.

The majority of building floor decks are manufactured from steel sheet of 1.0 mm to 1.5 mm in thickness, which is relatively easily cold-roll formed. Cold-roll forming of the 3 mm thick steel plate required for the bridge deck formwork is understood to be possible although it is not known whether the embossments could be pressed in the same process. It is certain, however, that the capital investment necessary to manufacture the units by a cold-roll forming process will be substantial.

The potential market for the formwork units is open to question. In the present economic climate it is unlikely that the demand in this country alone will justify the capital cost of cold-roll forming equipment, but an investigation of export potential may indicate that a sufficiently large market does exist for such a venture.

An economic feasibility study is imperative to determine the potential of the form-reinforced slab concept in bridge deck construction.

8.3 DIMENSIONAL TOLERANCES

8.3.1 General

The prototype formwork units employed in this investigation were manufactured using equipment which, apart from the punch and die tooling necessary for the pressing of the embossments, was not designed specifically for the purpose. In view of this, it must be noted that the overall dimensional tolerances achieved in these units were quite adequate for the testing programme.

However, there are several dimensional aspects relating to overall out-of-flatness, variation in width and embossment geometry, which may lead to problems in the application of the formwork system to bridge deck construction. The question of minimum dimensional tolerances which may be achieved in the cold-forming of 3 mm steel sheet will require careful consideration in manufacture.

It is assumed that the geometrical quality of formwork units produced for the construction industry will show a significant improvement over the prototype samples. Some measure of the improvement necessary is demonstrated in the following discussion, which is based on the geometry of the prototype units.

8.3.2. Transverse Out-of-Flatness

A measure of the transverse out-of-flatness, Δ_{max}, which existed in the prototype units may be found in Table 1 and Figure 5. The minimum value of Δ_{max} was recorded to be 6 mm (see Figure 3), while in general, values were significantly greater than this, as can be seen in Figure 5 where the variation in the levels of the flanges along the length of one unit is plotted.

The tolerance required on the transverse out-of-flatness must be sufficiently small to enable the ends of the units to be fixed to the main supporting girders and so that transverse continuity may be achieved in the longitudinal joints between adjacent units. If the individual formwork units have similar geometrical properties to that depicted in Figure 5, it may be seen that transverse continuity will be impossible without excessive force being employed by means of an undesirable connection.

8.3.3 Longitudinal Out-of-Flatness

Each of the prototype formwork units exhibited a general sag in the longitudinal elevation of the flanges relative to the ends and this is depicted in Table 6 and Figure 5. This gives rise to non-uniform slab depth over the length of the unit even before the deflections due to the wet concrete are taken into account. The combination of these two effects in the composite units for the testing programme resulted in a slab depth which was greater than the nominal design depth in the midspan section and in some cases this increase was considerable (See Table 6).

The strength of the resulting composite section will be greater than that of the nominal design section and furthermore, the increase in strength will be greatest in the midspan region, where generally speaking, the maximum bending moment will occur. However, the longitudinal out-of-flatness will increase the wet concrete dead load, in addition to ponding effects, thereby increasing deflections and stresses in the formwork unit during the construction stage.

8.3.4. Width Variation

Table 1 shows that there was a considerable variation in width,

δ_e, over the length of a given unit, resulting from edge camber in the plane of the bottom flanges. The minimum value of δ_e recorded was 11 mm. This will also be a critical factor in the attainment of longitudinal connection and transverse continuity of the formwork units.

8.3.5. Embossment Geometry

The geometrical properties of the embossments are shown in Figure 4. The 50 mm overall length of the embossments specified in the original design in fact resulted in an effective length of 40 mm in terms of shear connection strength. The width of the embossments was fixed during manufacture by the radius of curvature necessary to attain the required height.

In the determination of the interface concrete bearing stress, the projected area of the embossments in the plane normal to the longitudinal axis depends primarily upon the embossment length and height. In Chapter 2 it was seen that the average height of the embossments of 5.6 mm, together with the actual effective length (40 mm) reduced the factor of safety on σ_d from 2.0 to 1.5 relative to the design guide of 0.6 f_{cu}.

The performance of the composite slab during test has shown that the factor of safety of 1.5 is adequate, but due care must be taken to ensure that the embossment geometry is consistent and accurate.

8.4 END CONNECTION

Steel decking formwork systems for floors are often fixed to the steel beams of the building frame using the "through-the-deck"

stud welding technique, in which a stud shear connector is welded through the steel deck and into the main beam using an automatic welding gun. This combines the two operations of steel deck fixing and the welding of stud shear connectors which then serve to provide composite action between the steel beams and the concrete slab. In addition, since the steel decking is then continuous over the main beams, precautions to close the ends of corrugations prior to concrete casting will become unnecessary.

At the present time, the maximum steel sheet thickness with which this welding technique may be employed is about 1.5 mm (see Ref. 11) and it will therefore not be possible with 3 mm sheet, but the possibility of punched holes in the deck to accommodate shear studs might be considered.

The need for a connection and the type of connection between the formwork and the main girders will depend primarily on the lengths of formwork available and the transverse out-of-flatness achieved.

Figure 105 shows possible connection details for steel main beams, assuming that continuity of the formwork over the main beams cannot be established.

8.5 LONGITUDINAL CONNECTION

The need for acceptable tolerances on both transverse out-of-flatness and uniform width of the formwork units to provide transverse continuity has been mentioned in section 8.2.

The longitudinal connection detail may require modification to ensure a two-way connection rather than the one-way connection which is provided by the 'hook and lip' arrangement of the prototype

unit. With the present detail, the hook edge is supported by the lip, but this support is not reciprocated. This gives rise to the possibility of non-uniform deflection of two adjacent units during casting, thereby causing leakage of concrete, which will not necessarily be automatically sealed when the two adjacent units are equally loaded, since aggregate may become trapped between the two units.

An alternative two-way longitudinal connection of the type shown in Figure 105 might be employed, although the problems in cold forming of 3 mm sheet into this shape are appreciated.

8.6 ADDITIONAL REINFORCEMENT

In regions of positive (sagging) bending the formwork acts as tension reinforcement and additional reinforcement is necessary only to control shrinkage and temperature effects. Reinforcement will be required in the top of the slab in regions of negative bending and transverse tensile reinforcement will be required as in a normal reinforced concrete deck.

The provision of tensile reinforcement within the slab over the main beams will also be necessary to allow for the possibility of the deflection of these main beams during service. If continuity of the steel decking units over the main beams is ensured, however, this tensile reinforcement would again be supplied by the formwork.

8.7 SEALING

Prior to casting it will be necessary to ensure that all longitudinal joints are adequately sealed against leakage of fines.

The end connections will require similar attention, but in addition, for formwork units which are not continuous over main beams, it will be necessary to close the corrugations. This may be achieved by welding plates to the ends of the corrugations.

This is possibly the greatest disadvantage in the application of this type of formwork system. Continuity of the steel decking over the main beams would solve this problem and seems an attractive proposition in this respect alone.

8.8 COMPOSITE ACTION WITH MAIN BEAMS

The degree of composite action which may be attained between a steel I-beam or girder and a form-reinforced slab, in the design of buildings has been the subject of several investigations in recent years and was discussed in the review of research on composite beams given in Chapter 1.

The bridge deck formwork system with which this thesis is concerned was designed to span transversely between longitudinal girders. If the formwork is orientated such that the corrugations are parallel to the longitudinal beams, the composite action between the latter and the concrete slab may be assessed on the basis of normal design procedures.

With the corrugations lying transversely to the longitudinal beams there are two conditions to be considered. When the formwork units are not continuous over the main beams, the presence of the formwork may be ignored and the design for composite action will be similar to that for a haunched slab, with due regard to the proximity of the slab voids to the stud shear connectors and the possibility of

lateral bursting of the concrete.

In the event of continuity of the formwork units being attained, due to, for example, punched holes in the decking to accommodate shear studs welded into the top flange of the main beams, the situation will require more detailed consideration. The presence of the corrugation voids within the slab between the concrete and the top flange of the beam can reduce the strength of shear studs embedded in the concrete ribs. This fact has been demonstrated in several research programmes [50,51,53,54]. The relevance of this research to the bridge deck form-reinforced slab is uncertain, due to the greater thickness (3 mm) of the steel sheet employed, compared to that in building floor formwork (1 - 1.5 mm). However, this greater thickness may increase the stiffness of the cellular zone between the beam and the solid portion of the slab, relative to that provided by building floor decks and the application of rules recommended for the latter may lead to conservative design.

8.9 CORROSION AND DURABILITY

Corrugated steel sheet has been used to a considerable extent in the construction of bridge decks solely as permanent formwork. The potential of the form-reinforced slab is evident and the technique should be a logical advance, but although the lack of knowledge of the effects of repeated loading on form-reinforced slabs has prevented this development, there appears to be another reason which is concerned with corrosion and durability of the concrete slab and formwork in the exposed conditions to which bridge decks are subjected.

A recent survey by the United States Transportation Research Board [74] describes the extent to which permanent non-composite steel formwork systems have been employed in bridge deck construction in the U.S.A. It appears that some state authorities do not allow the use of permanent steel forms due to the possibility of future maintenance problems while others feel that their advantages outweigh their disadvantages.

Concrete decks constructed with permanent steel formwork generally have higher moisture contents than conventional timber formed decks due to the prevention of evaporation from the lower surface. This, together with the possibility of moisture becoming entrapped between the formwork and the concrete, naturally leads to fears for the durability of both the formwork and the concrete, although the higher moisture content can assist in curing to increase the strength of the concrete.

The survey [74] mentioned above concluded that there is no evidence to suggest that the presence of the formwork does or does not contribute to concrete deck deterioration, while corrosion of the formwork itself is a quality control problem in respect of galvanising and maintenance painting. Certainly, corrosion of permanent formwork is likely to occur in the vicinity of expansion joints and deck drains unless care is exercised in the design of these details.

A case has been reported [75] where permanent non-composite formwork was re-used after seventeen years of service. On inspection it was found that less than 5% of the total surface area of the steel forms was affected by rust and this was mainly in the vicinity of

deck joints and drains.

The corrosion problem will be even more critical in the case of structurally participating permanent steel formwork, as corrosion will reduce the area of the decking and lead to increased stresses. In addition, any corrosion which may take place between the steel deck and the concrete, due to moisture being trapped, may reduce shear connection strength. In this context, the reduction in steel thickness due to the pressing of the embossments (see Figure 4) is particularly relevant.

However, assuming that adequate protection is afforded by means of galvanising and regular maintenance, there appears to be no reason why a form-reinforced slab deck should not have a life equal to that of a conventional reinforced concrete deck.

It is suggested that the possibility of galvanising after forming is considered as in several of the prototype units it was found that the pressing of the embossments had caused substantial flaking of the galvanising. The application of stainless steel or weathering steel may also be considered.

CHAPTER 9

CONCLUSIONS AND RECOMMENDATIONS FOR DESIGN

9.1 GENERAL CONCLUSIONS

9.1.1 Push-Out Tests

The results of the push-out tests have indicated upper and lower bounds of 1.6 and 0.6 respectively, with respect to the concrete cube strength, for the value of η_u which may be expected in the composite slab, given the values of the parameters H = 6 mm and $\alpha = 60^{\circ}$. These bounds were obtained for the two conditions of complete and zero lateral restraint applied to the longitudinal edges of one corrugation of the formwork and one embossment only in each web was employed in all push-out test specimens, except those of Test Series 5.

It was found that reducing the height of the embossments to 4 mm produced ultimate loads of approximately two-thirds of the values obtained using 6 mm embossments, in both the restrained and unrestrained conditions. This implies that the shear connection strength may be proportional to the height, H, providing the latter is sufficient to ensure embossment-aggregate interaction, as demonstrated by the result of the test on the Durbar specimen.

The resistance to separation was found to be substantial even in the case of unrestrained specimens, where separation is prevented solely by the locking action of the embossments. A significant proportion of this resistance must be attributed to the locking action on the ends of the embossments. This effect augments the resistance provided by sloping the embossments in opposite directions on adjacent webs. This

opposing orientation tends to cause a twisting effect in a push-out test, resulting in unequal degrees of separation on the two sides of a given corrugation.

The load-slip curves obtained from the tests have enabled an approximate representation to be established for application in the partial interaction theoretical analysis.

Although the limited number of push-out tests which were conducted have been very useful, further research is necessary to produce an optimum shear connection design in terms of all the possible variables. For example, the variation of the basic formwork cross-section has not been studied, but increasing the angle of inclination of the webs to the flanges will result in increased resistance to separation, which may then increase the load-slip stiffness. The possible benefits of such a change in the formwork cross-section must be measured against the increased cost per unit width of the steel deck.

9.1.2 Bare Formwork Response

9.1.2.1 *Deflections*

The behaviour of the bare formwork, as observed in Test 1, is adequate under the wet concrete load, for which the recorded average midspan deflection of 10.17 mm, for a simply supported span, is approximately 9% within the suggested design limit of span/300. It was shown in Chapter 6 that this deflection is most accurately predicted by the use of the fully effective formwork section.

An investigation of the ponding effect which will occur during concrete casting has shown that for a design slab depth of 250 mm, the increase in the midspan deflection in unpropped construction for a simply supported span of 3.33 m is approximately 4.5% of that calculated

assuming a constant slab depth. No allowance for ponding was made during the bare formwork test. The increase in deflection due to ponding for the case of encastré ends is of the order of 0.5% and may be ignored. It is recommended that the midspan deflection for unpropped, simply supported construction be calculated using equation (6.20), which results in a value for v'_{max} of 10.2 mm for a design slab depth of 250 mm.

9.1.2.2 *Stresses*

The bare formwork test demonstrated that the performance under the combined loading due to the wet concrete and the additional construction load was again adequate, but the maximum stress, which occurs in the flat portions of the embossed top flanges, must be restricted to a value which does not exceed the yield stress of the steel. The maximum stress in the test ($\sim$ -160 N/mm^2) was 33% greater, on average, than that predicted by simple theory ($\sim$ -120 N/mm^2), assuming a fully effective section. This is due to the presence of the embossments, which reduce the effective cross-sectional area of the unit and lower the effective centroid, both effects resulting in increased compressive stresses in the top flanges.

The use of an effective width factor, k_w, applied to the embossed width of the top flanges and to the plate thickness within the embossed sections of the webs, provides a means of calculating the maximum stress in the section. An alternative, approximate approach may be to ignore the embossed width in the top flanges completely and to consider the webs to be fully effective, since the stresses in the central portions of the webs are small. The former method, for a value of k_w = 0.3, resulted in a maximum stress in the top flange of -152 N/mm^2,

while for the approximate method this stress was -166 N/mm^2. The maximum tensile stresses in the bottom flange for the two approaches are 123 N/mm^2 and 125 N/mm^2, which are comparable with both the results of calculation assuming a fully effective section and the test. This is due to the lowering of the effective centroid. In view of the above figures, the adoption of the approximate effective section, which is slightly conservative, seems preferable to the use of the k_w factor, which tends to under-estimate the maximum stress, unless a smaller value of k_w is employed.

9.1.2.3 *Ultimate Capacity*

The behaviour of the bare formwork section during the ultimate load test was very stable and no buckling of the webs or flanges occurred, although a slight rippling between embossments on the top flanges was observed towards the end of the test. Failure was of a flexural nature, accompanied by a tendency of the unit to spread transversely under load. The maximum attainable load, which was maintained until the test was terminated due to excessive deflection, corresponded to 90% of the fully plastic moment calculated on the assumption of a fully effective, rigid cross-section. First yield occurred in the flat portions of the top flanges at 65% of the calculated ultimate load, after which load was shed into the embossed width of these flanges, where yield was also attained.

If the longitudinal edge connection is modified to provide a mutual restraint between adjacent units, thus preventing the spreading of the section, it is believed that the fully plastic moment will be attained. In the event of the existing edge details being retained, it is recommended that the capacity of the bare formwork section be taken

as 90% of the plastic moment calculated for a fully effective rigid cross-section.

9.1.3 Composite Static Tests

The results of the first composite test (Test 2) have shown that in the working load range the static behaviour of the composite section in sagging bending is adequately covered by complete interaction linear elastic theory, assuming a fully effective formwork section. The bending moment of 190.5 kNm at which flexural failure occurred in this test was 6% greater than the ultimate moment of resistance calculated using simple rectangular stress block theory.

The specimen failed in a mode which is defined as shear-bond-compression. It should be noted that the word 'bond' is used here to describe the mechanical shear connection and not natural bond, which was prevented during casting. This description of the mode of failure has been used to emphasise the effect of slip between the steel and concrete in the shear span, in reducing the load at which flexural failure of the concrete occurs.

The results of Test 3 show that simple elastic theory also predicts the static response of the composite unit in hogging bending where working loads are concerned. The ultimate behaviour in this case is such that the depth of cracked concrete renders the response dependent almost entirely on the steel in the section and the ultimate moment should be taken as that value required to produce yield in the tension reinforcement. The embossment bearing stress in the case of hogging bending is very low and the shear connection is more than adequate.

9.1.4 Repeated Loading Tests

The objectives of the dynamic test programme have been achieved by demonstrating the general structural behaviour of the composite slab under repeated loading and by indicating the critical aspect of fatigue failure of the steel formwork. In addition, the programme has supplied further information regarding the static response to both working and ultimate loads.

The behaviour of the composite slab under design loads is essentially linear once the section has attained the cracked state. It has been shown that complete interaction elastic theory, using a fully effective steel section provides excellent correlation with experimental results.

The elastic stiffness of the slab is unaffected by repeated loading prior to fatigue failure of the formwork. It is reasonable to assume that the relatively high loads used in the tests would be more detrimental in this respect than the lower loading intensities which would occur in practice.

In the working load range, the main effect of repeated loading on the overall behaviour is creep in the shear connection, leading to a gradual increase in residual slip and deflections with the number of cycles. This effect is most noticeable in the early stages of dynamic loading and the test results indicate that a stable condition would eventually be attained. The maximum increase in residual midspan deflection recorded during the dynamic tests was 1.5 mm and it is unlikely that this figure would be exceeded in practice under the H.A. spectrum. The 1.2 mm residual deflection caused by the H.B. spectrum in Test 4 indicates that the maximum residual deflection due to the

combined effects of H.A. and H.B. loading would be of the order of 2-3 mm.

The critical factor in fatigue design appears to be the possibility of failure of the steel formwork due to longitudinal bending stresses, initiated by a crack originating from the lower end of the embossments pressed into the web. The H.A. loading spectrum will be much more damaging in this respect than the H.B. spectrum. On the basis of the limited data available from the full scale beam tests, the fatigue life estimated for a four lane bridge is approximately 75 years, assuming an S-N relationship corresponding to a Class D detail.

The natural scatter of fatigue test results and the design life of 120 years normally specified for highway bridges required a more accurate assessment of the S-N relationship for the detail in question. This has been achieved by small scale fatigue tests on samples of the web subjected to constant stress ranges. (See 9.1.5).

The ultimate loads attained by the specimens which did not fail in fatigue were up to 3% less than the values predicted by simple rectangular stress block theory. All specimens failed in the mode which has been defined as shear-bond-compression. The reduced load capacity of specimens tested dynamically, relative to the previous static test (Test 2) appears to be a direct result of the repeated loading. The possibility of a greater reduction in the ultimate capacity due to the actual loading spectrum to which the slab would be subjected in practice is remote.

9.1.5 Vibrophore Tests

To provide a more accurate assessment of the S-N relationship for the embossment detail, tensile fatigue tests were conducted on

samples of the webs extracted from an unused formwork unit. From the results of these tests a mean S-N relationship, based on the stress range calculated assuming a fully effective section for the embossed plate, has been established for the embossment detail. The results of run-outs were included in the derivation of this relationship, which is therefore conservative at low stress ranges (less than $\sim$ 80 N/mm^2).

The number of tests carried out was insufficient to define the statistical distribution of the endurance and a Normal Distribution on a logarithmic base was assumed to determine a modified S-N function for the 2½% probability of failure corresponding to the strength criterion. Using this modified function (mean minus two standard deviations) the fatigue life of the formwork unit under the combined effects of the H.A. and H.B. spectra was calculated to be 214 years.

9.1.6 Theoretical Analysis

The response of all specimens tested in sagging bending is predicted satisfactorily by complete interaction linear elastic theory in the working load range, when the effect of slip is so small as to be negligible. A comparison between complete interaction theory, incorporating non-linear material behaviour and the results of the static test has shown that the response of this particular specimen was very close to complete interaction throughout the loading range, the ultimate load attained being approximately mid-way between the failure loads calculated by plastic stress block theory, and complete interaction with strain hardening and maximum dead load effects. It was found that the effect of the dead load was fairly small, causing first yield to occur slightly earlier and reducing the failure load by

an amount approximately equal to the maximum dead load moment induced in the bare formwork section.

However, the specimens which were tested to ultimate subsequent to repeated loading exhibited a behaviour which departed from the complete interaction prediction to a marked extent, although again, in the working load range, agreement was excellent. The creep effect in the shear connection and the resulting residual slip and deflection observed during the dynamic loading has no effect on the elastic stiffness of the specimens.

The predictions of the partial interaction analysis described in Chapter 7 were found to agree fairly well with the single static test when the value of η_u for the shear connection was assumed to be 1.6, but the correlation for specimens which had been subjected to repeated loading was poor in relation to slip and deflections. This is due to a substantial modification, during dynamic loading, to the static load-slip response which was assumed for the shear connection in the partial interaction analysis. The use of $\eta_u = 0.6$ resulted in predictions for the load-deflection response and slip distributions which were more representative of the observed behaviour for loads in excess of 85% of the experimental ultimate load.

A severe limitation of the partial interaction analysis was apparent in the estimation of failure loads for the loading conditions employed in the tests. Due to the very high accuracy with which it was necessary to calculate the value of the initial boundary slip, the rate of convergence of the predictor-corrector method was found to be very slow at high loads and therefore, failure loads for the criterion of concrete crushing at a strain of 0.0035 were not established. However,

the partial interaction theory failure loads cannot be more than a few percent greater than the maximum attainable loads, which resulted in maximum concrete strains in excess of 0.003, since in this zone of the concrete stress strain curve, the magnitude of the rate of increase of the maximum concrete strain with respect to the section moment and force, is very large.

The design of the prototype formwork shear connection was based on the recommendation of Climenhaga and Johnson[17], that the average concrete bearing stress on the embossments, σ_d, should not exceed 0.6 of the design cube strength of the concrete. The results of the experimental and theoretical investigations described in this thesis indicate that this recommendation for design should be retained. It is also recommended that for a section employing the prototype formwork unit, for which σ_d was limited to 0.4 of the design cube strength, the ultimate capacity of the section may be calculated on the basis of rectangular stress block theory, with an allowance for the dead load moment induced in the bare formwork during casting.

It was not possible to carry out a complete parametric study using the partial interaction analysis, but it has been shown that the theory does provide a means by which the behaviour of form-reinforced slabs may be studied.

9.1.7 Manufacturing Tolerances

The dimensional tolerances achieved in the manufacture of the prototype formwork units has been discussed in some detail and a considerable improvement is necessary to enable the system to be employed in bridge deck construction. A specification on tolerances is essential to ensure that individual units may be easily fixed in place and that

transverse continuity between adjacent units may be achieved. The three most important aspects of the geometry in this respect are (i) the longitudinal out-of-flatness, (ii) the transverse out-of-flatness, and (iii) the variation in width of an individual unit.

9.2 RECOMMENDATIONS FOR DESIGN

9.2.1 General

The type of permanent steel form employed in this investigation has been shown to be suitable for application in a form-reinforced slab for bridge deck construction. Under purely static loading conditions the behaviour of the composite slab is very close to the complete interaction condition. The effects of repeated loading, in the form of the H.A. and H.B. spectra is such as to cause a small, but significant reduction in the ultimate capacity of the section, but the elastic stiffness is unchanged. The possibility of fatigue failure of the steel deck has been demonstrated, but this will be unlikely to occur in a practical situation.

Recommendations to assist in the drafting of design specifications for this type of form-reinforced slab are set out below. Attention is drawn to the need for a suitable specification on dimensional tolerances during manufacture. Adequate inspection and maintenance procedures are necessary to prevent corrosion of the formwork. Evidence of peeling of the galvanising on the embossments was discovered in several of the prototype units and the possibility of galvanising subsequent to pressing should be considered.

The recommendations given apply essentially to the prototype formwork unit which has been tested.

9.2.2 Manufacturing Tolerances

1. The dimensional tolerances achieved in manufacture, in respect of longitudinal and transverse out-of-flatness and the width of the units, must be sufficiently small to ensure that the formwork units may be easily fixed in place on site and that transverse continuity between adjacent units may be achieved.

2. The longitudinal connection employed must be capable of preventing unequal deflections of adjacent units during casting of the concrete.

3. The geometry of the embossments must be maintained to within very close tolerances.

9.2.3 Construction Stage

1. Calculation of deflections and stresses induced in the bare formwork section due to self weight and the weight of the wet concrete alone must include the effects of ponding and variations from the nominal concrete slab depth due to longitudinal out-of-flatness of the decking must be considered in design.

2. The deflection v'_{max}, of the bare formwork unit under its own weight and that of the wet concrete, for a simply supported span L, may be calculated assuming a fully effective steel section from the equation

$$v'_{max} = \frac{5wL^4}{384E_sI_s} + \frac{0.04\Phi L^8}{E_sI_s}$$

where $\Phi = B\gamma gw/240E_sI_s$.

The second term in this equation is an allowance for ponding effects.

It is suggested that v'_{max} should not exceed L/300.

3. When the design of the formwork unit employs embossments in the top flange and webs only, the maximum stress induced in the section during the construction stage may be calculated by ignoring the embossed width of the top flanges and assuming that the webs are fully effective. Alternatively, the properties of the effective section may be calculated assuming a compression flange width equal to the sum of the flat, unembossed width plus the product of the embossed width and an effective width factor k_w, while the web thickness within the embossed length of the webs is taken as $k_w t$ where t is the steel plate thickness. For the prototype formwork section, the value of k_w is of the order of 0.3.

4. During construction, the maximum stress induced in the bare formwork section due to the wet concrete load plus an additional construction loading, must not exceed the yield stress of the steel.

   The additional construction load was simulated by a 9 kN load applied uniformly over a circular area of 1.0 m diameter.

5. It is recommended that where transverse restraint against lateral spreading of the section does not exist, the ultimate moment capacity of the bare formwork section is taken as 0.9 of the fully plastic moment calculated assuming a rigid cross-section. Where complete lateral restraint does exist, the ultimate moment capacity of the section may be taken as the fully plastic moment calculated assuming a rigid cross-section.

9.2.4 Composite Stage

9.2.4.1 *Static Response*

1. The concrete bearing stress, σ_d, on the projected area of the embossments in the plane normal to the longitudinal axis of the formwork unit due to the maximum design shear force should not exceed 0.6 of the design cube strength of the concrete. Due allowance shall be made for the embossment profile in calculating the projected area.

   For the prototype formwork unit which has been tested, the bearing stress σ_d was limited to 0.4 of the design cube strength.

2. The composite section may be analysed assuming that complete interaction exists between the steel formwork and the concrete for both sagging and hogging moments. The steel formwork section may be considered as fully effective.

3. The ultimate moment capacity of the composite section in sagging bending (with the formwork in tension) may be calculated on the basis of simple rectangular stress block theory, with due allowance for the dead load moment induced in the bare formwork section during the construction stage.

4. The ultimate moment capacity in hogging bending should be taken as that value which will produce yield in the tension reinforcement.

9.2.4.2 *Fatigue Response*

1. The fatigue life of the prototype formwork unit may be calculated for the strength criterion using the S-N relationship defined by

$$N_p = K_m \Delta^{d'} / (\sigma_r)^{m'}$$

where

N_p = Number of cycles to failure, for a probability of failure, p.

K_m = Constant relating to the mean line (50% probability of failure).

d' = Number of standard deviations below the mean line (d'= 2 for the strength criterion).

σ_r = Stress range.

m' = Constant.

$\log(1/\Delta)$ = Standard deviation of log N.

For the embossment detail in the web of the prototype formwork unit, the values of K_m, Δ and m' are;

$$K_m = 2.0 \times 10^{22}$$

$$m' = 8.0$$

$$\Delta = 0.258$$

The fatigue life of the prototype formwork unit under the combined effects of the H.A. and H.B. loading spectra for transverse members, has been calculated to be 214 years for H.A. and H.B. datum stresses of 70 N/mm^2 and 120 N/mm^2 respectively.

2. Any modifications in the embossment design or the method of manufacture may result in a change in the S-N response.

9.3 FUTURE RESEARCH

The determination of the optimum shear connection design for the type of steel formwork which employs embossments, requires further research on both the embossment pattern and the basic cross-section of the formwork itself. An arrangement in which the embossments are

orientated alternately in opposite directions on the same web may improve the resistance to separation and slip. Clearly there are many variations which may be explored.

There is also considerable scope for investigations into the application to bridge deck construction of other types of permanent steel formwork, for example, those of Types I and III, as shown in Figure 1.

The effect of repeated loading on the stiffness and strength of the shear connection and its relation to the ultimate capacity of the slab, requires further investigation. This might be achieved by subjecting push-out test specimens to repeated loading.

The method of partial interaction analysis has been shown to be applicable to form-reinforced slabs acting in a one-way mode and may be used to study the behaviour of form-reinforced slabs for bridges and for building floors in the absence of natural bond, given the load-slip characteristics of the shear connection.

While natural bond was deliberately destroyed for the purpose of the testing programme, its existence in practice may significantly affect the behaviour of the composite slab. Observation of the behaviour of an actual form-reinforced bridge deck slab may provide useful information in this respect.

If it proves feasible to manufacture steel decking in sufficient lengths to facilitate continuous construction over intermediate supporting girders, the effect of the presence of the corrugations on the degree of interaction attainable between the main girders and the concrete slab, will require investigation. As mentioned in Chapter 1, this is a field which has been studied recently in respect of building floor construction.

The increasing trends of labour and timber formwork costs ensure that form-reinforced slab construction, for both bridges and buildings, will become increasingly attractive and it is clear that there is great scope for further research and development in this field.

APPENDIX A

CONCRETE MIXES

(a) Mix Employed for Push-Out Tests

Mix Constituent	Mix Breakdown by Dry Weight
Cement (O.P.C.)	1.0
Sand	1.5
Aggregate (10 mm)	1.5
Aggregate (20 mm)	1.5

Water/Cement Ratio 0.6

(b) Mix Supplied by Ready Mixed Concrete Ltd

Mix Constituent	Mix Breakdown by Dry Weight
Cement (O.P.C.)	1.0
Sand	2.5
Aggregate (10 mm)	0.9
Aggregate (20 mm)	3.2

Water/Cement Ratio 0.6

APPENDIX B

H.A. AND H.B. STATIC DESIGN LIVE LOADS

All loads are specified for a slab width of 720 mm, i.e. the nominal width of a single formwork unit.

H.A. Live Load

Maximum Bending Moment: $M_{H.A.}$ = 33.0 kNm

Maximum Vertical Shear: $Q_{H.A.}$ = 25.2 kN

H.B. Live Load

Maximum Bending Moment: $M_{H.B.}$ = 54.0 kNm

Maximum Vertical Shear: $Q_{H.B.}$ = 112.5 kN

LIVE LOAD DATUM STRESSES

All stresses in N/mm^2.

H.A. Datum Stress:

	Slab Depth 250 mm	Slab Depth 260 mm
Maximum Concrete Stress	-5.3	-5.0
Maximum Steel Stress (Bottom Flange)	70	67
Lower Web Steel Stress	62	60

H.B. Datum Stress:

	Slab Depth 250 mm	Slab Depth 260 mm
Maximum Concrete Stress	-8.8	-8.3
Maximum Steel Stress (Bottom Flange)	120.0	115.0
Lower Web Steel Stress	106.0	103.0

APPENDIX C

H.A. and H.B. LOADING SPECTRA

H.A. Spectrum

The H.A. Loading Spectrum for transverse members is defined in the following table, which gives the values of γ_f corresponding to proportions of total frequency of Type H.A. Live Load.

Frequency Proportion Factor	Proportion of Load, γ_f
0.02	0.66
0.03	0.58
0.05	0.51
0.05	0.44
0.06	0.37
0.14	0.29
0.20	0.22
0.22	0.15
0.23	0.07

Annual Frequency of H.A. Loads

The total number of occurrences per annum of all proportions of H.A. Loading intensity is as follows:

For Transverse members:

Bridges with four or more lanes: 4.8×10^6 per annum

Bridges with three or two lanes: 2.4×10^6 per annum

H.B. Spectrum

The H.B. Loading Spectrum for transverse members is defined in the following table, which gives the values of γ_f to be applied to 45 units of Type H.B. Vehicle corresponding to proportions of total frequency of Type H.B. Live Load.

Frequency Proportion Factor	Proportion of Load, γ_f
0.03	0.71
0.03	0.67
0.04	0.62
0.07	0.57
0.08	0.52
0.09	0.48
0.12	0.43
0.19	0.38
0.35	0.33

Annual Frequency of H.B. Loads

The total number of occurrences of all proportions of H.B. Loading intensity for transverse members is 0.009×10^6 per annum, for any number of traffic lanes.

APPENDIX D

MINER'S SUMMATION

Constructional details may be designed against fatigue failure by ensuring that the cumulative damage summation

$$\frac{n_1}{N_1} + \frac{n_2}{N_2} + \frac{n_3}{N_3} + \text{---} + \frac{n_n}{N_n}$$

is not greater than 1.0.

Where n_1, n_2 --- n_n are the specified numbers of applied repetitions of the stress ranges in each part of the spectrum occurring in the design life of the structure, and

N_1, N_2 --- N_n are the numbers of repetitions to failure at the corresponding stress ranges, obtained from the S-N relationship.

If the values of n_i are specified as the number of occurrences per annum, the summation,

$$k' = \sum_{i=1}^{n} \frac{n_i}{N_i}$$

is equal to the inverse of the fatigue life.

REFERENCES

1. Dallaire, E.E., "Cellular Steel Floors Mature". Civil Engineering, A.S.C.E., Vol. 41, No. 7, July 1971, pp. 70 - 74.

2. Friberg, B.F., "Combined Form and Reinforcement for Concrete Floor Slabs". Journal A.C.I., Vol. 50, May 1954, pp. 697 - 716.

3. Ekberg, C.E., Jr., and Schuster, R.M., "Floor Systems with Composite Form-Reinforced Concrete Slabs". Final Report, International Association for Bridge and Structural Engineering, Eighth Congress, New York, September 1968, pp. 385 - 394.

4. Schuster, R.M., "Composite Steel-Deck Concrete Floor Systems". Proc. A.S.C.E., Vol. 102, No. ST5, May 1976, pp. 899 - 917.

5. McDermott, J.F., "Structural Tests of a Composite Floor System". Journal of the Structural Division, A.S.C.E., Vol. 93, No. ST1, February 1967, pp. 255 - 274.

6. Bryl, S., "The Composite Effect of Profiled Steel Plate and Concrete in Deck Slabs". Acier-Stahl-Steel, October 1967.

7. Wethmar, A., "Permanent Falsework". Paper Read to the XXth Congress of International Steel Information Centres, Salzburg, June 1971.

8. Hill, H.V., "Floors from Steel". Building with Steel, Volume 12, November 1972.

9. Iron and Steel Institute (London), "Sheet Steel in Building". Papers and Discussions for meeting organised by Iron and Steel Institute and R.I.B.A.

10. Johnson, R.P., "Composite Structures of Steel and Concrete. Volume 1 - Beams, Columns, Frames and Applications in Buildings". CONSTRADO Monographs, Crosby Lockwood Staples, 1975.

11. European Convention for Constructional Steelwork, "European Recommendations for the Design of Composite Floors with Profiled Steel Sheet". Committee II - Multi-Storey Buildings, 1975.

12. Porter, M.L., Ekberg, C.E., Jr., Greimann, L.F., and Elleby, H.A., "Shear Bond Analysis of Steel-Deck-Reinforced Slabs". Journal of the Structural Division, A.S.C.E., Vol. 102, No. ST12, December 1976.

13. Porter, M.L., and Ekberg, C.E., Jr., "Design Recommendations for Steel Deck Floor Slabs". Journal of the Structural Division, A.S.C.E., Vol. 102, No. ST11, November 1976.

14. Schuster, R.M., "Composite Steel-Deck-Reinforced Concrete Systems failing in Shear-Bond". Preliminary Report, International Association for Bridge and Structural Engineering, Ninth Congress, Amsterdam, May 1972, pp. 185 - 191.

15. Porter, M.L., and Ekberg, C.E., Jr., "Summary of Full-Scale Laboratory Tests of Composite Slabs Reinforced with Cold-Formed Steel Decking". Preliminary Report, International Association for Bridge and Structural Engineering, Ninth Congress, Amsterdam, May 1972, pp. 173 - 183.

16. Sayed, G.A., Temple, M.C., and Madugula, M.K.S., "Response of Composite Slabs to Dynamic Loads". Canadian Journal of Civil Engineering, Vol. 1, No. 1, 1974, pp. 62 - 70.

17. Climenhaga, J.J., and Johnson, R.P., "Use of Corrugated Metal Decking as Permanent Formwork for Composite Bridge Decks". Final Report on Research at Cambridge University, November 1971. Also published as, "Fatigue Strength of Form-Reinforced Composite Slabs for Bridge Decks". International Association for Bridge and Structural Engineering, Publications 35 - I, 1975, pp. 89 - 101.

18. Farrell, C., and Dowling, P.J., "The Behaviour of Lattice Type Precast Concrete Bridge Shutters". Draft Report of Engineering Structures Laboratories, Imperial College, 1971.

19. Dowling, P.J., and Labib, F., "Precast Concrete Bridge Shutters - Behaviour of Full Scale Bridge Model under Static and Dynamic Loading". CESLIC Report PS2, Engineering Structures Laboratories, Civil Engineering Department, Imperial College, April 1972.

20. Iyengar, S.H., and Zils, J.J., "Composite Floor System for Sears Tower". AISC Engineering Journal, American Institute of Steel Construction, Vol. 10, No. 3, 1973, pp. 74 - 81.

21. "Composite Steel - Concrete Construction". Report of the Subcommittee on the State-of-the-Art Survey of the Task Committee on Composite Construction of the Committee on Metals of the Structural Division. Journal of the Structural Division, A.S.C.E., Vol. 100, No. ST5, May 1974, pp. 1085 - 1139.

22. Discussion of the above paper by Porter, M.L., and Ekberg, C.E., Jr., Journal of the Structural Division A.S.C.E., Vol. 101, No. ST3, March 1975, pp. 615 - 616.

23. Viest, I.M., "Review of Research on Composite Steel - Concrete Beams". Journal of the Structural Division, A.S.C.E., Vol. 86, No. ST6, June 1960, pp. 1 - 21.

24. Chapman, J.C., "Composite Construction in Steel and Concrete - The Behaviour of Composite Beams". The Structural Engineer, Vol. 42, No. 4, April 1964, pp. 115 - 125.

25. Johnson, R.P., "Research on Steel - Concrete Composite Beams". Journal of the Structural Division, A.S.C.E., Vol. 96, No. ST3, March 1970, pp. 445 - 459.

26. Chapman, J.C., and Balakrishnan, S., "Experiments on Composite Beams". The Structural Engineer, Vol. 42, No. 11, November 1964, pp. 369 - 384.

27. Slutter, R.G., and Driscoll, G.C., "Flexural Strength of Steel - Concrete Composite Beams". Journal of the Structural Division, A.S.C.E., Vol. 91, No. ST2, April 1965, pp. 71 - 79.

28. Teraszkiewicz, J.S., "Static and Fatigue Behaviour of Simply Supported and Continuous Composite Beams of Steel and Concrete". Ph.D. Thesis, University of London (Imperial College), 1968.

29. Chapman, J.C., and Teraszkiewicz, J.S., "Research on Composite Construction at Imperial College". Proceedings of the Conference on Steel Bridges, London, 1968, British Constructional Steelwork Association, 1969, pp. 49 - 58.

30. Mainstone, R.J., "Shear Connectors in Steel - Concrete Composite Beams for Bridges and the New CP117:Part 2". Proceedings, The Institution of Civil Engineers, Vol. 38, September 1967, pp. 83 - 106.

31. Mainstone, R.J., and Menzies, J.B., "Shear Connectors in Steel - Concrete Composite Beams for Bridges, Part 1 : Static and Fatigue Tests on Push-Out Specimens". Concrete, London, Vol. 1, No. 9, September 1967, pp. 291 - 302.

32. Menzies, J.B., "CP117 and Shear Connectors in Steel - Concrete Composite Beams Made with Normal Density or Lightweight Concrete". The Structural Engineer, Vol. 49, No. 3, March 1971, pp. 137 - 154.

33. British Standard Code of Practice CP117:Part 1, "Composite Construction in Structural Steel and Concrete, Simply Supported Beams in Building". British Standards Institution, London, 1975.

34. British Standard Code of Practice CP117:Part 2, "Composite Construction in Structural Steel and Concrete, Beams for Bridges". British Standards Institution, London 1965.

35. Barnard, P.R., and Johnson,R.P., "Ultimate Strength of Composite Beams". Proceedings, The Institution of Civil Engineers, 32(Oct.), 1965, pp. 161 - 179.

36. Barnard, P.R., and Johnson, R.P., "Plastic Behaviour of Continuous Composite Beams". Proceedings, The Institution of Civil Engineers, 32(Oct.), 1965, pp 180 - 197.

37. Johnson, R.P., et al, "Stud Shear Connectors in Hogging Moment Regions of Composite Beams". The Structural Engineer, 1969, Vol. 47, No. 9, pp. 345 - 350.

38. Newmark, N.M., Siess, C.P., and Viest, I.M., "Tests and Analysis of Composite Beams with Incomplete Interaction". Proceedings of the Society for Experimental Stress Analysis, Vol. 9, No. 1, 1951, pp. 75 - 92.

39. Goodman, J.R., and Popov, E.P., "Layered Beam Systems with Interlayered Slip". Journal of the Structural Division, A.S.C.E., Vol. 94, No. ST11, November 1968.

40. Balakrishnan, S.M., "The Behaviour of Composite Steel and Concrete Beams with Welded Stud Shear Connectors". Ph.D. Thesis, University of London, (Imperial College), 1963.

41. Chapman, J.C., "The Interaction between a Ship's Hull and a Long Superstructure". Transactions of the Institution of Naval Architects, Vol. 99, October 1957.

42. Yam, L.C.P., "Ultimate Load Behaviour of Composite T-Beams having Inelastic Shear Connection". Ph.D. Thesis, University of London (Imperial College), 1967.

43. Yam, L.C.P., and Chapman, J.C., "The Inelastic Behaviour of Simply Supported Composite Beams of Steel and Concrete". Proceedings, The Institution of Civil Engineers, Vol. 41, (Dec.), 1968, pp. 651 - 684.

44. Yam, L.C.P., and Chapman, J.C., "The Inelastic Behaviour of Continuous Beams of Steel and Concrete". Proceedings, The Institution of Civil Engineers, Vol. 53, Part 2, Research and Theory, Dec. 1972, pp. 487 - 501.

45. Dai, P.K.H., Thiruvengadam, T.R., and Siess, C.P., "Inelastic Analysis of Composite Beams". Proceedings of American Society of Civil Engineers' Specialty Conference on Steel Structures, University of Missouri, 1970.

46. Stüssi, F., "Zusammengesetzte Vollwandträger". Publications, International Association for Bridge and Structural Engineering, Vol. VIII, 1947, pp. 249 - 269.

47. Stark, J.W.B., Papers presented to the Joint European Committee on Composite Construction. (Unpublished).

48. Johnson, R.P., and May, I.M., "Partial Interaction Design of Composite Beams". The Structural Engineer, London, Vol. 53, No. 8, Aug. 1975, pp. 305 - 311.

49. Frodin, J.G., Taylor, R., and Stark, J.W.B., "A Comparison of Deflections in Composite Beams having Full and Partial Shear Connection". Proceedings, The Institution of Civil Engineers, Vol. 65, Part 2, Research and Theory, June 1978, pp. 323 - 338.

50. Robinson, H., "Tests on Composite Beams with Cellular Steel Deck". Journal of the Structural Division, A.S.C.E., Vol. 93, No. ST4, Aug. 1967, pp. 139 - 164.

51. Robinson, H., "Composite Beam Incorporating Cellular Steel Decking". Journal of the Structural Division, A.S.C.E., Vol. 95, No. ST5, Mar. 1969, pp. 355 - 380.

52. Clark, J.C., "Composite Action of Beams with Cellular Steel Floors". Thin Walled Steel Structures; Their Design and Use in Building, International Symposium, University College of Swansea, 1967, Crosby Lockwood, 1969.

53. Fisher, J.W., "Design of Composite Beams with Formed Metal Deck". AISC Engineering Journal, American Institute of Civil Engineering, Vol. 7, No. 2, July 1970, pp. 88 - 96.

54. Grant, J.A. Jr., Fisher, J.W., and Slutter, R.G., "Composite Beams with Formed Metal Deck". AISC Engineering Journal, American Institute of Civil Engineering, Vol.14, 1977, pp. 24 - 43.

55. Department of the Environment Technical Memorandum (Bridges) No. BE 21/5/035, "Permanent Formwork for Composite Construction in Highway Bridges". Department of the Environment, 1973.

56. Building with Steel, No. 17, 1974. Theme: "Fabrication of Steel Sheet". British Steel Corporation, 1974.

57. Virdi, K.S., and Dowling, P.J., "The Ultimate Strength of Composite Columns in Biaxial Bending". Proceedings, The Institution of Civil Engineers, Vol. 55, Part 2, Research and Theory, March 1973, pp. 251 - 272.

58. Nordby, G.M., "Fatigue of Concrete - A review of Research". Journal of American Concrete Institute, Vol. 30, No. 2, August 1958.

59. Abeles Symposium, "Fatigue of Concrete", compiled from papers presented to the 1973 A.C.I. Spring Convention. A.C.I. Publication SP - 41, 1974.

60. A.C.I. Committee 215, "Considerations for Design of Concrete Structures Subject to Fatigue Loading". Journal of American Concrete Institute, Vol. 71, March 1974.

61. Wise, S., Gurney, T.R., and Maddox, S.J., "The Proposed New Code of Practice for the Design of Welded Structures Subject to Fatigue Loading". Paper presented to Conference - Improving Welded Product Design, London, Dec. 1971.

62. Gurney, T.R., and Maddox, S.J., "A Re-Analysis of Fatigue Data for Welded Joints in Steel". Welding Research International, Vol. 3, No. 4, 1973

63. Draft British Standard for the Design and Specification of Steel and Concrete Bridges, Bl16.Pt.10 - Fatigue. British Standards Institution, February, 1975.

64. Draft British Standard for the Design and Specification of Steel and Concrete Bridges, Bl16.Pt.2 - Loads. British Standards Institution, 1975.

65. Miner, M.A., "Cumulative Damage in Fatigue". Journal of Applied Mechanics, Vol. 12, No. 3, September 1945, pp. 159 - 164.

66. British Standard 3518, "Methods of Fatigue Testing", Part 5, "Guide to the Application of Statistics". British Standards Institution, 1966.

67. American Iron and Steel Institute, "Specification for the Design of Cold Formed Steel Structural Members". A.I.S.I., Washington, 1968.

68. Basu, A.K., "Computation of Failure Loads of Composite Columns". Proceedings, The Institution of Civil Engineers, Vol. 36, March 1967, pp. 557 - 578.

69. Barnard, P.R., "Researches into the complete stress - strain curve for Concrete". Magazine of Concrete Research, Vol. 16, No. 49, Dec. 1964, pp. 203 - 210.

70. Turner, P.W., and Barnard, P.R., "Stiff Constant Strain Rate Testing Machine". Engineer, London, July 1962, 214, pp. 146 - 148.

71. Virdi, K.S., "Inelastic column behaviour - its application to composite columns in biaxial bending and stiffened plates in compression". Ph.D. thesis, University of London, 1973.

72. May, I.M., and Johnson, R.P., "Inelastic Analysis of Biaxially Restrained Columns". Proceedings, The Institution of Civil Engineers, Vol. 65, Part 2, Research and Theory, June 1978, pp. 323 - 337.

73. Fröberg, C.E., "Introduction to Numerical Analysis". 2nd Edition, Addison-Wesley Publishing Company, 1970.

74. State-of-the-Art Report, "Permanent Bridge Deck Forms". Transport Research Board, Circular No. 181, September 1976.

75. "Steel Deck Forms Re-used After 17 years of Service". Acier-Stahl-Steel, No. 10, 1976.

NOTATION

a	width of bottom flange of steel formwork unit.
a_i	constant
A	constant for theoretical approximation for load-slip curve of shear connection.
$\overline{A}$	constant
A_c	area of concrete in section of width B.
A_{eff}	effective area of single web plate in Vibrophore specimen.
A_s	area of steel formwork in section of width B.
A_{se}	effective area of steel formwork in section of width B.
A_w	gross area of single web plate in Vibrophore specimen.
b	width of top flange of steel formwork unit.
B	width of single module of formwork unit.
$\overline{B}$	constant
B_T	total width of formwork unit; nominally $B_T = 3B$.
c	length of web of formwork unit, in the plane of the web.
C	spacing of embossments in the longitudinal direction.
C_i	constants in Basu polynomial stress-strain curve for concrete
C_k^n	Cote's numbers.
d	overall depth of steel formwork unit.
d'	number of standard deviations below mean line of S-N curve.
d_s	depth of the steel formwork section below the surface of the slab.
D	overall depth of the composite slab.
e	base of naperian logarithms.
E_c	Young's modulus for concrete.

E_s	Young's modulus for steel.
f, f_1, f_2	denote general functional relationship.
f_{cu}	cube strength of concrete
$F(x)$	polynomial curve fit to the function $y = f(x)$.
g	acceleration due to gravity.
h	solution interval for partial interaction analysis.
H	height of embossment
i	integer
I_s	second moment of area of bare formwork section about an axis parallel to the flanges, through the centroid.
I_{se}	second moment of area of bare formwork effective section about an axis parallel to the flanges, through the centroid.
k	integer
k_w	effective width factor for embossed regions of bare formwork section.
K_m	constant relating to the mean line (50% probability of failure) of S-N curve.
l	effective length of embossments.
L	span between simple supports.
$L_k(x)$	coefficients in the polynomial curve $F(x)$.
L_k	coefficients in the polynomial curve $F(x)$, for known values at equal intervals.
L_T	overall length of formwork unit.
m	transformation on the x-axis for derivation of L_k values.
m'	slope of S-N relationship on log-log basis.
M	externally applied bending moment.
M^*	given value of M for which it is required to calculate the values of ρ^*, n_s^* and n_c^*.
M_c	internal moment in concrete section.

M_i value of M at section $x = x_i$.

M_s internal moment in steel formwork section.

M_x bending moment induced in bare formwork under wet concrete load, for uniform slab depth.

M'_x bending moment induced in bare formwork under wet concrete load, including first order ponding effect.

M_{max} maximum bending moment in bare formwork section.

n integer

n_c depth of concrete neutral axis below surface of slab. (=n' for complete interaction).

n^*_c value of n_c corresponding to given values of M = M* and P = P*.

n_s depth of steel neutral axis below surface of slab. (=n' for complete interaction).

n^*_s value of n_s corresponding to given values of M = M* and P = P*.

n'_s modified value of neutral axis depth for steel to include dead load strain distribution.

N number of cycles to failure for Vibrophore test specimens.

N_p number of cycles to failure for a probability of failure, p.

p probability of failure.

P composite section force.

P' first derivative of P with respect to x.

P* given value of P for which it is required to calculate the values of ρ^*, n^*_s and n^*_c.

P_i value of P at section $x = x_i$.

P'_i value of P' at section $x = x_i$.

P_c internal force in concrete section.

P_F final boundary value of P (at a free end $P_F = 0$).

P_I initial boundary value of P (at a free end $P_I = 0$).

P_s	internal force in steel section.
q	interface shear force per unit length for slab of width B.
Q	applied load in push-out test.
Q_c	calculated push-out test load to give uniaxial crushing of the concrete on the area of the embossments projected into the plane normal to the applied load.
Q_u	ultimate load in push-out test.
r	ratio of the concrete surface strain to ε_u.
s	slip
s'	first derivative of s with respect to x, (slip strain).
s_i	value of s at section $x = x_i$.
s'_i	value of s' at section $x = x_i$.
s_F	final boundary value of s.
s_I	initial boundary value of s.
s^*_I	initial boundary value of s which results in a solution which satisfies the two boundary conditions.
t	thickness of formwork steel sheet.
u	transformation on the x-axis ($u = x/L$).
v, v_{max}	deflection of bare formwork under wet concrete load for uniform slab depth.
v', v'_{max}	deflection of bare formwork under wet concrete loading, including first order ponding effect.
V_{max}	maximum vertical shear force in the bare formwork section.
w	wet concrete load per unit length of formwork unit, for uniform slab depth.
w'	wet concrete load per unit length of formwork unit, including first order ponding effect.
w_a	actual width of Vibrophore specimen web plate.
w_{eff}	effective width of Vibrophore specimen web plate.

W, W_1, W_2	load
W_v	Vibrophore specimen load.
x	independent variable.
x_i	discreet values of an independent variable
X	$\log \sigma_r$
y	dependent variable
y_i	discreet values of the dependent variable.
y_s	height of centroid of bare formwork section above soffit.
y_{se}	height of centroid of bare formwork effective section above soffit.
Y	$\log N_p$
z	distance below slab surface
α	angle of inclination of web embossments to the longitudinal axis of the formwork unit.
β	ratio of c to d.
γ	density of concrete
δ_e	maximum variation in width of an individual formwork unit.
Δ_1, Δ_2	separation measured in push-out tests.
Δ_{max}	transverse out-of-flatness of the formwork unit.
Δn_c	correction of n_c.
Δn_s	correction of n_s.
$\Delta\rho$	correction of ρ
ε_c	concrete strain
ε_s	steel strain
ε_r	ratio of ε_c to ε_u.
ε_u	concrete strain corresponding to σ_u.
ϕ	ratio of a to d.

Φ = $B\gamma gw/240E_sI_s$

κ = y_{se}/d.

λ ratio of b to d.

λ' ratio of $(b-\ell)$ to d.

θ acute angle between web and flanges.

σ_c concrete stress

σ_d concrete bearing stress on area of embossments projected into the plane normal to the longitudinal axis of the formwork unit.

σ_r stress range

σ_s steel stress

σ_u maximum concrete stress.

σ_{ys} yield stress of steel

$(\sigma_v)_{ave}$ stress in Vibrophore specimen calculated assuming a fully effective section.

$(\sigma_v)_{max}$ maximum stress in Vibrophore specimen.

μ strain hardening factor for steel.

ρ curvature

ρ^* value of ρ corresponding to given values of $M = M^*$ and $P = P^*$.

ρ' modified value of curvature to include dead load strain distribution.

ρ_d dead load curvature in bare steel formwork

η_u ratio of Q_u to Q_c.

η ratio of Q to Q_c.

ψ ratio of applied load Q to ultimate load Q_u in push-out test

ν reduction factor applied to concrete cube strength to estimate specimen concrete strength.

$\log(1/\Delta)$ standard deviation of log N.

log represents logarithm to the base 10.

FORMWORK UNIT No.	TEST No.	Flange Width a (mm)	Web length c (mm)	Overall Depth d (mm)	Web-Flange Angle Θ (degrees)	Overall Width B_T=3B (mm)	Width Variation δ_e (mm)	Length L_T (mm)	Transverse Out-of-Flatness Δ_{max} (mm)
1		91.0	75.0	74.0	70	706	-39	3600	50
2	2	90.0	76.0	75.0	69	717	-12	3600	6
3	1	90.0	77.0	75.0	69	716	-16	3605	15
4	3	90.0	76.0	75.0	68	718	-16	3605	9
5	4	90.0	77.0	74.0	68	720	-15	3605	16
6	5	89.0	76.0	76.0	69	711	-14	3595	13
7	6	90.0	76.0	75.0	68	721	-13	3555	11
8	7	91.0	77.0	75.0	68	722	-11	3602	13
9	8	90.0	76.0	74.0	68	721	-11	3600	11
10	9	90.0	76.0	74.0	67	725	-14	3615	8
11		90.0	77.0	74.0	67	724	-16	3615	9

TABLE 1: GEOMETRICAL PROPERTIES OF FORMWORK UNITS

PUSH-OUT TEST SERIES	SPECIMEN No.	Number of Embossments per web	Form of Embossments	H (mm)	α (degrees)	l (mm)	Restraint*	Cube Strength f_{cu} (N/mm^2)	Q_c (kN)	Q_u (kN)	η_u
1	1	1	Solid	6	90	43.3	R	37.0	38.5	56.3	1.46
	2	1	"	6	60	50.0	R			59.8	1.55
	3	1	"	6	45	61.2	R			64.8	1.68
	4	1	"	6	30	86.6	R			57.3	1.49
2	1	1	Solid	4	90	43.3	R	38.6	26.8	38.9	1.45
	2	1	"	4	60	50.0	R			44.9	1.68
	3	1	"	4	45	61.2	R			44.2	1.65
	4	1	"	4	30	86.6	R			43.9	1.64
3	1	1	Solid	6	60	50.0	U/R	44.3	46.0	26.2	0.57
	2	1	"	6	60	50.0	U/R		46.0	23.9	0.52
	3	1	"	4	60	50.0	U/R		30.7	16.8	0.55
	4	1	"	4	60	50.0	U/R		30.7	19.9	0.65
4	1	1	Pressed	4.80	60	40.0	R	44.0	29.3	42.0	1.45
	2	1	"	5.07	60	40.0	R		30.5	44.3	1.48
	3	1	"	4.84	60	40.0	U/R		29.3	20.0	0.68
	4	1	"	5.00	60	40.0	U/R		30.5	17.1	0.57
5	1	2	Pressed	5.00	60	40.0	R	44.5	61.6	62.5	1.01
	2	2	"	5.20	60	40.0	R		64.2	64.8	1.01
	3	2	"	5.20	60	40.0	U/R		64.2	21.2	0.33
	4	2	"	5.20	60	40.0	U/R		64.2	25.2	0.39
Durbar	1	-	Solid	1.50	45	25.0	R	43.5	150.0	83.0	0.55

* R - laterally restrained by welding (see Figure 6)
U/R - laterally unrestrained

TABLE 2: DETAILS OF PUSH-OUT SPECIMENS

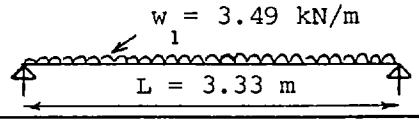
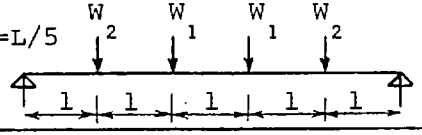
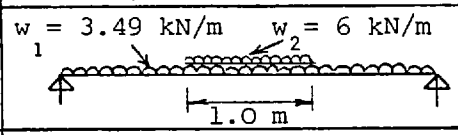
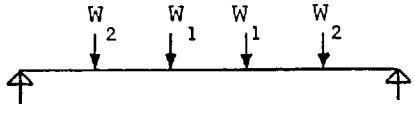
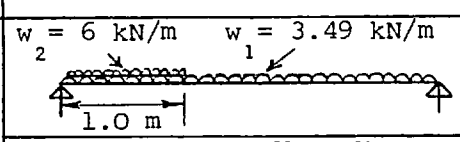
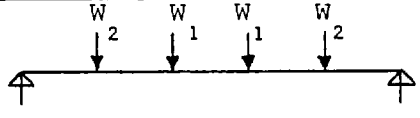
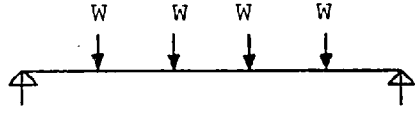
TEST 1 LOAD CASE	Loading Arrangements	Notes	M_{max} (kNm)	V_{max} (kNm)	W_1 (kN)	W_2 (kN)
1.1 Wet Concrete Load Only		Conditions in practice	4.84	5.81	-	-
		(1) Simulate maximum bending moment and shear force.	4.84	5.81	1.46	4.35
		(2) Simulate bending moment diagram as closely as possible	4.84	4.88	2.39	2.49
1.2.(a) Wet Concrete plus Additional Construction Load (Flexure)		Conditions in practice	9.34	9.04	-	-
		(1) Simulate maximum bending moment and shear force	9.34	9.04	4.99	4.05
		(2) Simulate bending moment diagram as closely as possible	9.34	7.96	6.07	1.89
1.2.(b) Wet Concrete plus Additional Construction Load (Shear)		Conditions in practice	6.5	11.21	-	-
		(1) W_1 = 0, W_2 = 11.21	7.47	11.21	0	11.21
		(2) Increase W_2 over 1.2.(a)(1)	10.8	11.21	4.99	6.22
1.3 Calculated Maximum Load		Ultimate Load Test	25.8	25.8	W	W

TABLE 3: SUMMARY OF CONSTRUCTION LOADING TEST CONDITIONS

LOAD CASE	GAUGE NUMBER								
	T1 WEST EDGE	1	2	3	4	5	6	7	T2 EAST EDGE
1.1.(1)	0.69	10.00	10.61	10.80	10.80	10.75	10.48	10.14	0.23
1.1.(2)	0.68	9.63	10.22	10.44	10.46	10.42	10.16	9.85	0.22
1.2.(a)(1)	1.51	19.62	20.93	21.44	21.51	21.40	20.96	20.13	0.55
1.2.(a)(2)	1.50	19.37	20.68	21.06	21.23	21.13	20.69	19.97	0.52
1.2.(b)(1)	1.57	19.09	20.41	20.97	21.11	21.00	20.52	19.74	0.59
1.2.(b)(2)	1.70	22.59	24.09	24.66	24.72	24.55	24.03	24.03	0.69

All deflections in mm.

TABLE 4(a): DEFLECTIONS (Gauges 1-7) and TRANSVERSE EXPANSION (Gauges T1 & T2) RECORDED DURING TEST 1

LOAD CASE	Recorded Deflection (Average)	Calculated Deflection (Test Conditions)	% Difference	Calculated Deflection (U.D.L. Conditions)	Recorded Transverse Expansion
1.1.(1)	10.51	10.23	2.7	9.77	0.92
1.1.(2)	10.17	9.75	4.3	9.77	0.90
1.2.(a)(1)	20.86	18.63	12.0	18.03	2.06
1.2.(a)(2)	20.59	18.08	13.9	18.03	2.01
1.2.(b)(1)	20.41	17.92	13.9	15.10	2.16
1.2.(b)(2)	23.95	21.91	9.3	15.10	2.39

All deflections in mm.

TABLE 4(b): BARE FORMWORK DEFLECTIONS

	CONCRETE			STEEL FORMWORK			REINFORCEMENT	
	Cube Strength f_{cu} (N/mm^2)	Young's Modulus E_c (N/mm^2)	Tensile Strength f_t (N/mm^2)	Yield Stress σ_{ys} (N/mm^2)	Ultimate Tensile Strength σ_t (N/mm^2)	Young's Modulus E_s (kN/mm^2)	Yield Stress σ_{ys} (N/mm^2)	Ultimate Tensile Strength σ_{tR} (N/mm^2)
TEST 2	64.7 66.6 66.6 66.2 65.9 AVERAGE 66.0	37500	3.75	307 291 285 295 297 298 AVERAGE 295 (Both Tests)	425 421 422 416 418 419 AVERAGE 420 (Both Tests)	201.0 200.0 199.9 202.0 200.1 200.0 AVERAGE 200.5 (Both Tests)	438.0	670.0
TEST 3	64.2 64.5 64.4 65.7 68.6 AVERAGE 66.0	37500	3.75				(Tension Reinforcement) 444.0	 635.0

TABLE 5: COMPOSITE STATIC TESTS - MATERIAL PROPERTIES

ELEVATION OF OUTER FLANGES PRIOR TO CASTING

Measured at 300 mm intervals along length — All figures in mm

Specimen		1	2	3	4 Loading Point	5	6	7 Midspan	8	9	10 Loading Point	11	12	13
4	EAST EDGE	0	-2	-3.5	-5	-8.5	-10	-10	-8	-5.5	-3.5	-2	-0.5	0
	WEST EDGE	0	-2	-2.5	-4	-6	-10	-13	-14	-13	-9	-4	-2	0
6	EAST EDGE	0	-4	-8	-11	-13	-17	-17	-20	-20	-15	-10	-4	0
	WEST EDGE	0	-4	-8	-12	-14	-17	-14	-12	-12	-9	-3	0	0
8	EAST EDGE	0	-5	-8	-10	-15	-16	-14	-12	-9	-6	-4	-2	0
	WEST EDGE	0	-3	-5	-7	-8	-10	-15	-20	-19	-16	-10	-6	0

OVERALL DEPTH OF SPECIMENS

Specimen													
4	251	253	256	261	264	265	265	265	263	260	254	251	250
5	251	253	256	258	263	265	265	265	264	259	255	254	251
6	252	253	256	259	264	269	269	266	264	258	256	253	251
7	250	252	253	255	258	257	257	257	253	252	252	250	250
8	250	253	258	259	262	264	267	267	264	262	260	258	254
9	252	254	258	261	264	258	270	268	264	261	256	253	251

TABLE 6: GEOMETRICAL PROPERTIES OF SPECIMENS

	STAGES I & II	STAGE III				STAGE IV			
				Load Range					
Test No.	Maximum Load (kN)	Min. Load (kN)	Max. Load (kN)	(kN)	As % of Max. H.B.	Experimental Ultimate (kN)	Plastic Stress Block Theory Ultimate (kN)	σ_d * (N/mm^2)	η_u **
4	125.0	12.5	112.5	H.B. SPECTRUM (See Figure 33)		235.0	236.0	28.5	0.50
5	125.0	12.5	100.0	87.5	78.0	231.0	236.0	27.8	0.48
6	100.0	12.5	87.5	75.0	66.7	-	207.0	-	-
7	87.5	12.5	75.0	62.5	55.6	204.0	208.0	24.3	0.76
8	87.5	12.5	81.25	68.75	61.0	220.0	227.0	24.0	0.48
9	93.75	12.5	93.75	81.25	72.0	-	225.4	-	-

* Calculated value at failure

** Ratio of σ_d to concrete cube strength

All loads are given as kN per jack

TABLE 7: REPEATED LOADING TESTS - DETAILS OF LOADS APPLIED TO SPECIMENS

	CONCRETE				STEEL FORMWORK		REINFORCEMENT	
SPECIMEN No.	Cube Strength f_{cu}	Specimen Strength f_c*	Elastic Modulus E_c	Tensile Strength f_t	Yield Stress σ_{ys}	Ultimate Tensile Strength σ_t	Yield Stress σ_{yR}	Ultimate Tensile Strength σ_{tR}
4	57.0	38.0	32500	3.2	295.0	420.0	440.0	670.0
5	58.0	39.0	33500	3.2	295.0	420.0	440.0	670.0
6	30.0	20.0	28000	2.5	282.0	385.0	440.0	670.0
7	32.0	22.0	25750	2.5	275.0	380.0	440.0	670.0
8	50.0	34.0	30500	2.6	280.0	380.0	440.0	670.0
9	50.0	34.0	31000	2.6	282.0	385.0	440.0	670.0

*$f_c = 0.67\ f_{cu}$ All figures are in N/mm^2

TABLE 8: REPEATED LOADING TESTS - MATERIAL TEST RESULTS

TEST No.	CYCLES ($x10^6$)	Stress Range (N/mm^2)	
		Bottom Flange (Strain Gauge Group S/M/B)	Lower Web (Strain Gauge Group S/M/W4F)
5	1.26	140.0	125.0
6	1.70	128.0	106.0
7	5.00	100.0	83.0
8	5.00	110.0	93.0
9	1.22	136.0	114.0

TABLE 9: STRESS RANGES IN CONSTANT AMPLITUDE TESTS

SPECIMEN GROUP	STRESSES IN TERMS OF $(\sigma_v)_{ave}$				STRESSES IN TERMS OF $(\sigma_v)_{max}$			
	Min.	Max.	Mean	Range	Min.	Max.	Mean	Range
VS1	20.0	60.0	40.0	40.0	30.6	91.8	61.2	61.2
VS2	20.0	80.0	50.0	60.0	30.6	122.4	76.5	91.8
VS3	20.0	100.0	60.0	80.0	30.6	153.0	91.8	122.4
VS4	20.0	120.0	70.0	100.0	30.6	183.6	107.1	153.0
VS5	20.0	140.0	80.0	120.0	30.6	214.2	122.4	183.6

All values are in N/mm^2

TABLE 10: STRESS LEVELS IN VIBROPHORE TESTS

SPECIMEN GROUP	STRESS RANGE $(\sigma_v)_{ave}$ (N/mm^2)	N to failure ($\times 10^6$) * Run-out (five specimens in each group)					Mean Value of Log N in each Group	Standard Deviation of Log N (=log 1/Δ)	Δ
		1	2	3	4	5			
VS2	60.0	74.25*	100.56*	85.26*	124.0*	90.0*	7.9703	0.0836	0.825
VS3	80.0	15.46	65.45*	2.71	65.35*	45.0*	7.3813	0.5889	0.258
VS4	100.0	1.40	0.95	0.92	0.97	1.0	6.0149	0.0745	0.8424
VS5	120.0	0.338	0.332	0.63	1.28	0.61	5.7484	0.2411	0.5740

TABLE 11: VIBROPHORE TEST RESULTS

	WET CONCRETE LOAD ONLY WITHOUT PONDING EFFECTS				WET CONCRETE LOAD ONLY WITH PONDING EFFECTS				WET CONCRETE PLUS ADDITIONAL CONSTRUCTION LOAD	
	Midspan Deflection (mm)	Midspan Bending Moment (kNm)	Top Flange Stress (N/mm^2)	Bottom Flange Stress (N/mm^2)	Midspan Deflection (mm)	Midspan Bending Moment (kNm)	Top Flange Stress (N/mm^2)	Bottom Flange Stress (N/mm^2)	Top Flange Stress (N/mm^2)	Bottom Flange Stress (N/mm^2)
FULLY EFFECTIVE SECTION	9.77	1.61	-62.4	+62.4	10.20	1.67	-64.7	+64.7	-120.0	+120.0
EFFECTIVE SECTION	11.25	1.61	-78.0	+64.4	11.88	1.68	-81.3	+67.2	-152.0	+123.0
APPROXIMATE EFFECTIVE SECTION	11.91	1.61	-85.9	+64.7	12.57	1.69	-90.2	+67.9	-166.0	+125.0

Note Values for the wet concrete load have been calculated assuming a simply supported span of 3.33 m and a nominal design slab depth of 250 mm.

TABLE 12: BARE FORMWORK - CALCULATED DEFLECTIONS AND STRESSES

	Dead Load*	Steel Strain Hardening Factor μ	Partial Interaction η_u	. Ultimate Load in kN, for slab width = test specimen width				
				TEST 2	TEST 4	TEST 5	TEST 7	TEST 8
EXPERIMENTAL	-	-	-	254.0	235.0	231.0	204.0	220.0
(i) Plastic Stress Block Theory	-	-	-	240.0	236.0	236.0	208.0	227.0
(ii) Complete Interaction	zero	0.0	-	237.0	235.0	234.0	210.0	222.0
	Max.	0.0	-	232.0	230.0	230.5	207.0	218.0
	Max.	0.015	-	264.0	258.0	262.0	234.0	248.0
(iii) Partial Interaction Maximum Attainable Load (Values of max. concrete strain attained, are given in brackets in microstrain)	Max.	0.015	0.6	-	224.0 (3150)	221.0 (3120)	-	207.0 (3075)
			1.0	-	230.0 (3300)	228.0 (3450)	198.0 (3057)	-
			1.6	248.0 (3100)	230.0 (3230)	231.0 (3420)	-	-

*For Dead Load, Zero indicates that dead load is not considered and, Max. indicates simple supports assumed during casting.

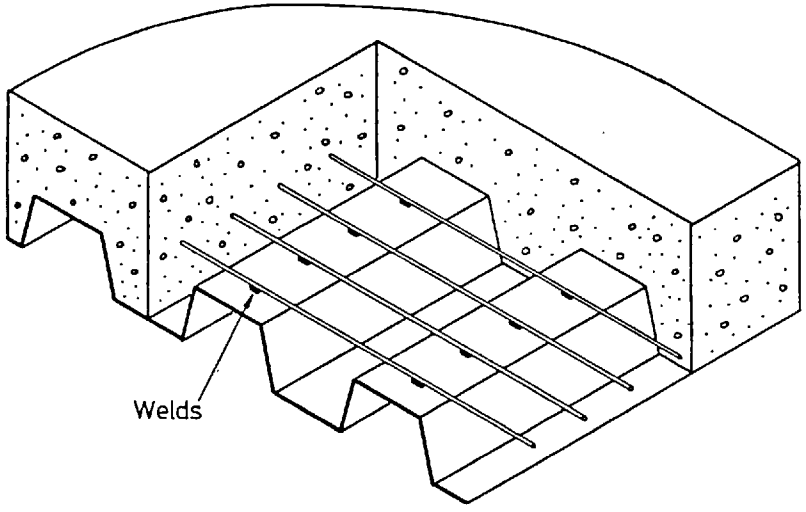
TABLE 13: COMPARISON OF THEORETICAL AND EXPERIMENTAL ULTIMATE LOADS

LIST OF FIGURES

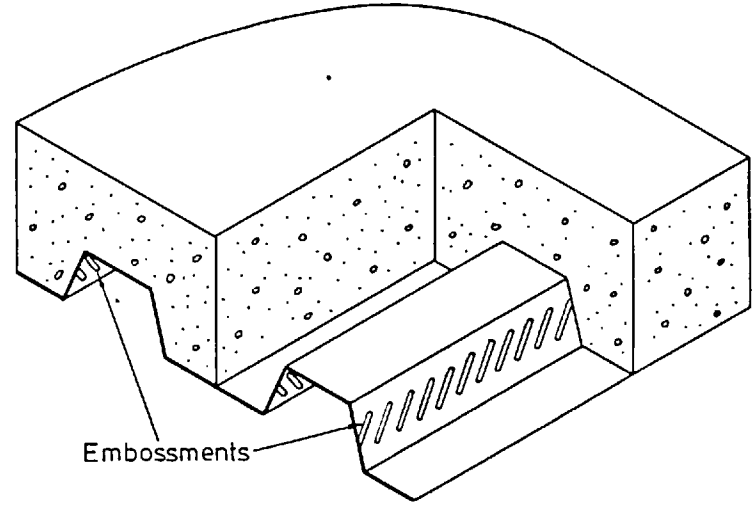
1. Types of Permanent Composite Steel Formwork
2. Cross-section of Prototype Formwork Unit
3. Schematic Definition of Notation for Table 1
4. Cross-sections of Embossment
5. Longitudinal Profile of Typical Formwork Unit
6. Push-out Test Specimen Details
7. Load-slip Curves, Push-out Test Series 1
8. Load-slip Curves, Push-out Test Series 2
9. Load-slip Curves, Push-out Test Series 3
10. Load-slip Curves, Push-out Test Series 4
11. Load-slip Curves, Push-out Test Series 5
12. Load-Separation Curves, Push-out Test Series 4
13. Construction Loading Test - Instrumentation
14. Longitudinal Stress Distribution - Wet Concrete Load Only
15. Longitudinal Stress Distribution - Wet Concrete plus Additional Construction Load
16. Bare Formwork : Load-deflection Response, Ultimate
17. Bare Formwork : Load-strain Response, Ultimate
18. Nominal Composite Design Section (Sagging Bending)
19. Nominal Composite Design Section (Hogging Bending)
20. Strain Gauge Instrumentation at Midspan
21. Slip and Separation Gauge Points
22. Test 2 : Curvature Comparison at Midspan
23. " : Load .v. Midspan Deflection
24. " : Load .v. Midspan Curvature
25. " : Slip Distributions at Loads of 100 kN and 244 kN
26. " : Separation Distributions at Loads of 100 kN and 244 kN
27. Test 3 : Load .v. Midspan Deflection
28. " : Load .v. Midspan Curvature
29. " : Slip Distributions at Loads of 100 kN and 200 kN
30. " : Separation Distribution at Loads of 100 kN and 200 kN
31. Tests 6 - 9 : Strain Gauges in Shear Span
32. Tests 4 - 9 : Position of Strain Gauges
33. Test 4 : H.B. Load Spectrum

34. Test 4 : Midspan Deflection - Stages I, II & III
35. " : Midspan Curvature - Stages I & II
36. " : Slip Distribution at 125 kN - Stages I & II
37. " : Concrete Surface Strain - Stages I & II
38. " : Steel Bottom Flange Strain - Stages I & II
39. Test 5 : Midspan Deflection - Stages I, II & III
40. " : Midspan Curvature - Stages I, II & III
41. " : Maximum Slip - Stages I & II
42. " : Slip Distribution at 100 kN, Before and After Stage III
43. " : Steel Bottom Flange Strain - Stage III
44. " : Concrete Surface Strain - Stage III
45. Test 6 : Midspan Deflection - Stages I, II & III
46. " : Midspan Curvature - Stages I, II & III
47. " : Maximum Slip - Stages II & III
48. " : Steel Bottom Flange Strain - Stage III
49. " : Steel Lower Web Strain - Stage III
50. " : Propagation of Fatigue Crack
51. Test 7 : Midspan Deflection - Stages I, II & III
52. " : Maximum Slip - Stages II & III
53. " : Slip Distribution at 75 kN - Stages II & III
54. " : Steel Bottom Flange Strain - Stage III
55. " : Steel Lower Web Strain - Stage III
56. Test 8 : Midspan Deflection - Stages I, II & III
57. " : Slip Distribution at 81.25 kN - Stages II & III
58. " : Steel Bottom Flange Strain - Stage III
59. " : Steel Lower Web Strain - Stage III
60. Test 9 : Midspan Deflection - Stages I, II & III
61. " : Slip Distribution at 93.75 kN - Stages II & III
62. " : Steel Bottom Flange Strain - Stage III
63. " : Propagation of Fatigue Crack
64. Test 4 : Deflections - Stage IV
65. " : Midspan Curvature - Stage IV
66. " : Slip Distributions - Stage IV
67. Test 5 : Deflections - Stage IV
68. " : Steel Bottom Flange Strain - Stage IV

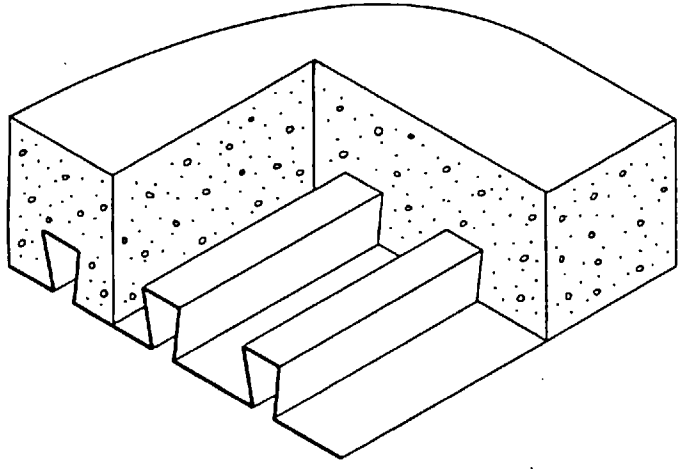
69. Test 5 : Concrete Surface Strain - Stage IV
70. Test 7 : Deflections - Stage IV
71. " : Slip Distributions - Stage IV
72. Test 8 : Deflections - Stage IV
73. " : Midspan Curvature - Stage IV
74. " : Steel Bottom Flange Strain - Stage IV
75. " : Concrete Surface Strain - Stage IV
76. " : Slip Distribution - Stage IV
77. Mean S-N Relationships and Composite Test Results
78. H.A. Spectrum Fatigue Life (Transverse Members)
79. H.B. Spectrum Fatigue Life (Transverse Members)
80. Vibrophore Specimen and Instrumentation
81. Stress Distribution in Vibrophore Specimen
82. Vibrophore Specimen - Plot of Load Against $(\sigma_v)_{max}$
83. Vibrophore Test Results
84. Fatigue Life Based on Vibrophore Results
85. Bare Formwork Cross-Sections
86. Bare Formwork - Analysis of Ponding Effect
87. Derivation of Partial Interaction Equations
88. Load Slip Curves and Theoretical Representation
89. Stress-Strain Curves for Steel
90. Stress-Strain Curve for Concrete
91. Test 2 : Midspan Deflection Response - Theory
92. " : Theoretical Slip Distribution at 100 kN
93. " : Theoretical Slip Distribution at 200 kN
94. " : Theoretical Slip Distribution at 248 kN
95. " : Theoretical Maximum Strain Distribution at 220 kN
96. Test 4 : Midspan Deflection Response - Theory
97. Test 5 : Midspan Deflection Response - Theory
98. Test 4 : Theoretical Slip Distributions at 180 kN
99. Test 5 : Theoretical Slip Distributions at 190 kN
100. Test 4 : Theoretical Maximum Strain Distribution at 180 kN
101. Effect of End Overhang on Slip Distribution
102. Effect of Embossment Spacing on Load-Deflection Response
103. Effect of Embossment Spacing on Slip Distribution
104. Effect of Embossment Spacing on Strain Distribution
105. Proposed Connection Details for Formwork



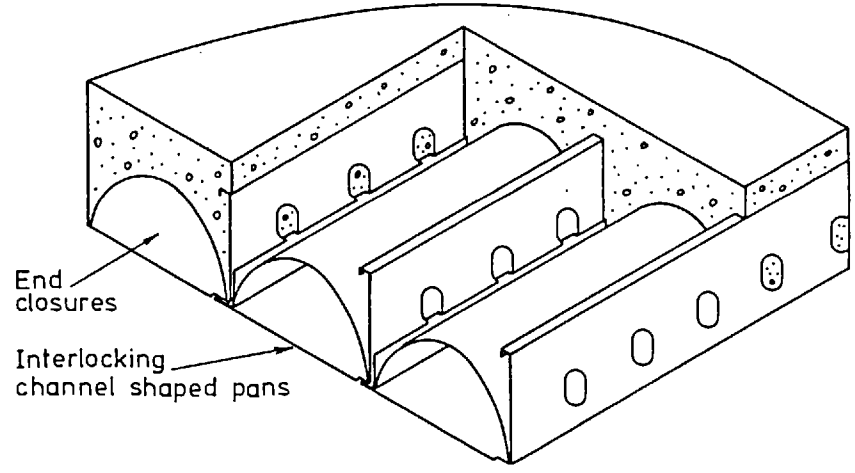
1(a). Example of Type I



1(b). Example of Type II



1(c). Example of Type III



1(d). Example of Alternative Type [see Ref. 5]

FIGURE 1: TYPES OF PERMANENT COMPOSITE STEEL FORMWORK

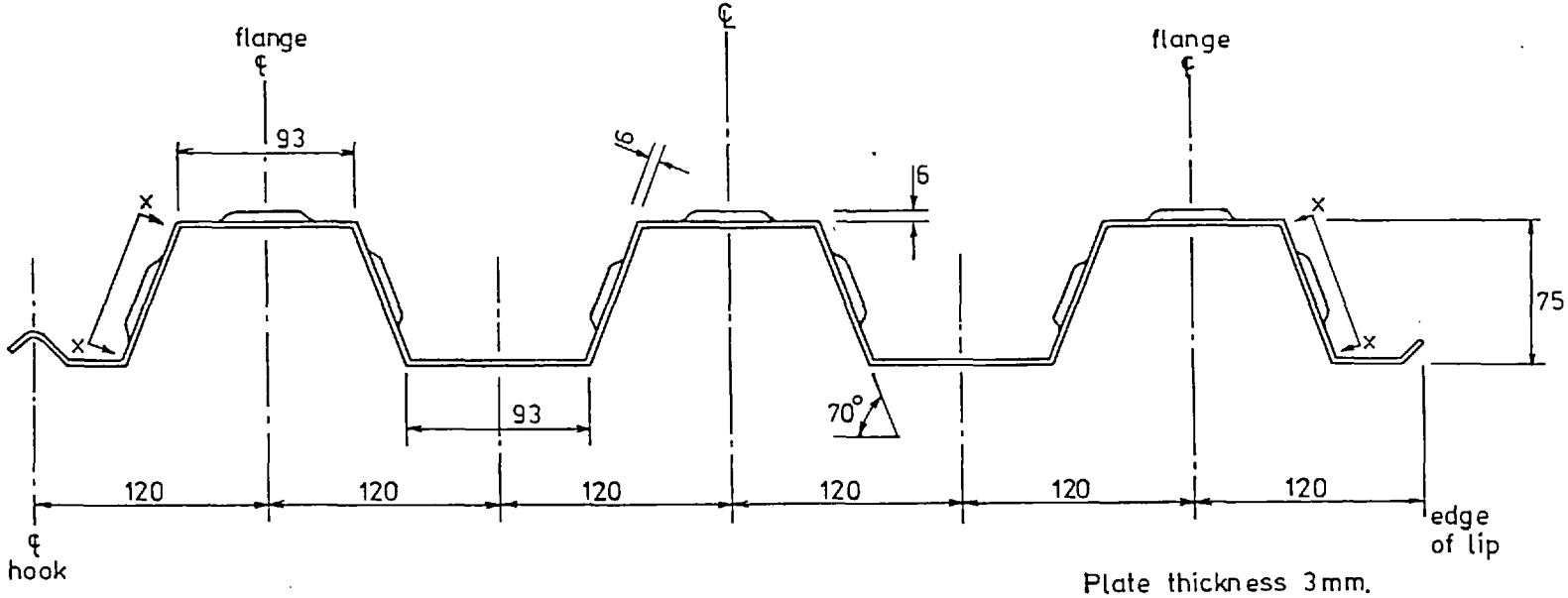
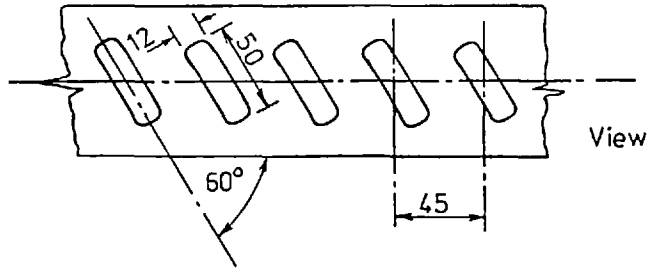


Plate thickness 3mm.

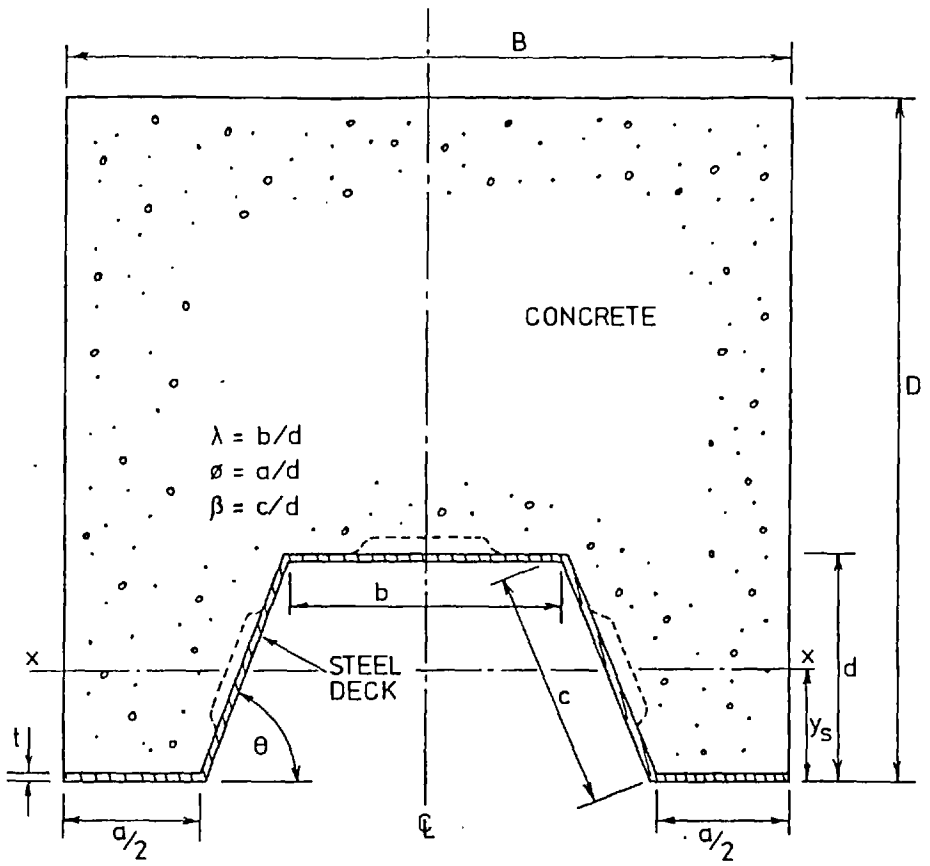
Length of unit 3·6m.

All dimensions in millimetres.

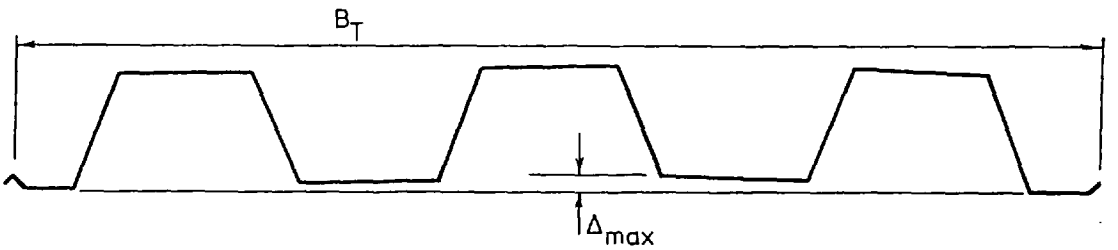


View on web plane xx

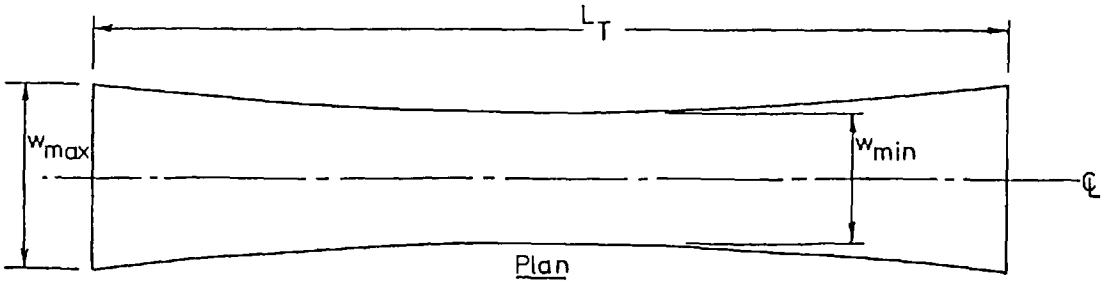
FIGURE 2: CROSS-SECTION OF PROTOTYPE FORMWORK UNIT



CROSS-SECTION NOTATION

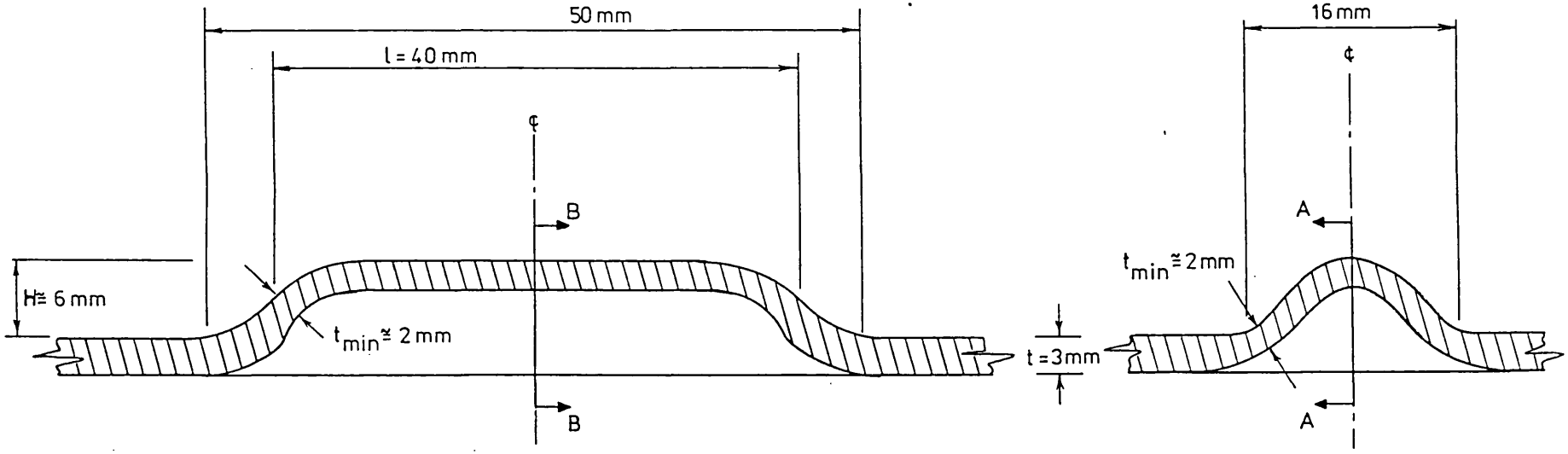


TRANSVERSE OUT-OF-FLATNESS Δ_{max}



VARIATION IN WIDTH $\delta_e = w_{max} - w_{min}$

FIGURE 3: SCHEMATIC DEFINITION OF NOTATION FOR TABLE 1



SECTION AA

SECTION BB

FIGURE 4: CROSS-SECTIONS OF EMBOSSMENT

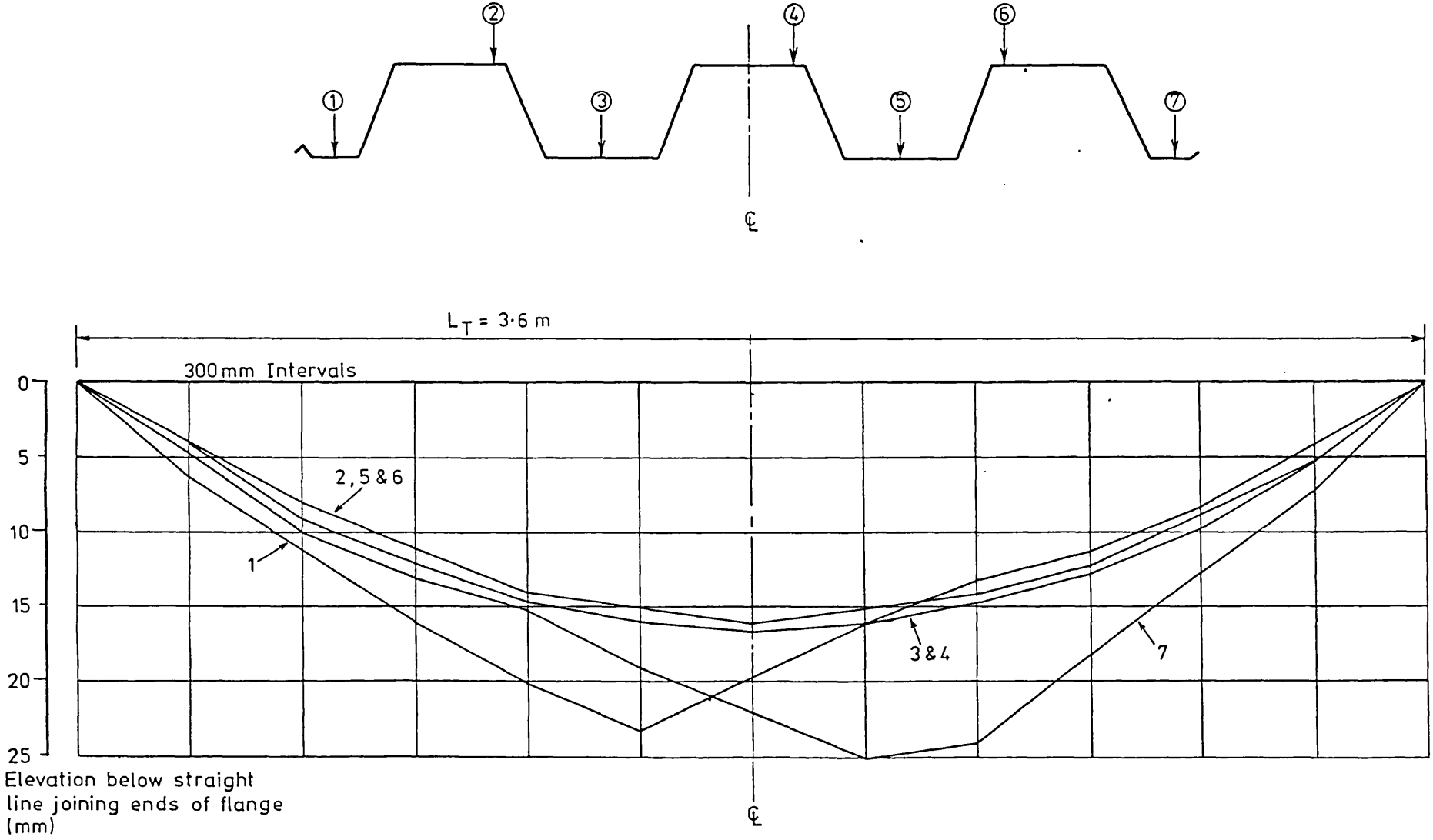
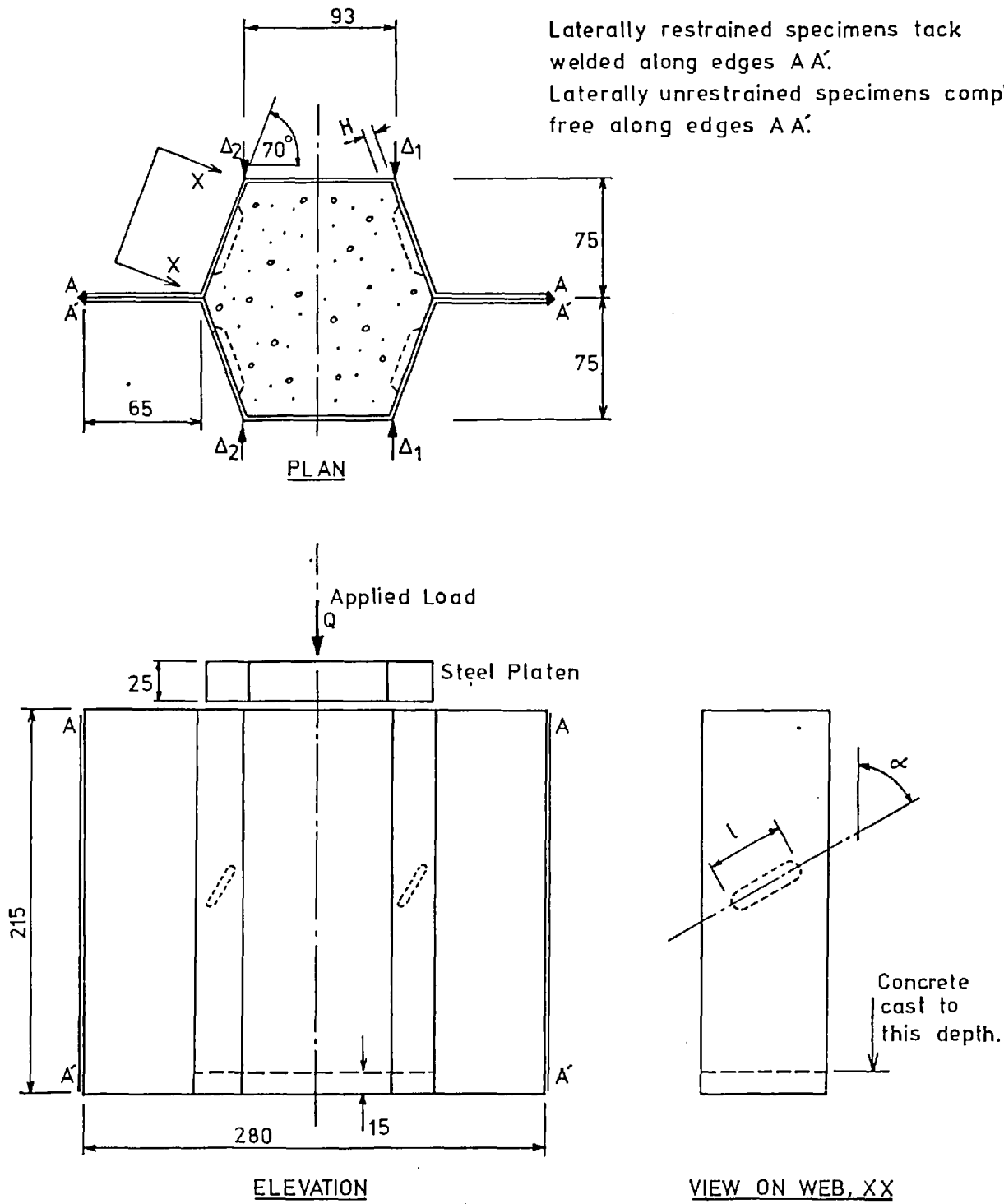


FIGURE 5: LONGITUDINAL PROFILE OF TYPICAL FORMWORK UNIT



All dimensions in millimetres.

FIGURE 6: PUSH-OUT TEST SPECIMEN DETAILS

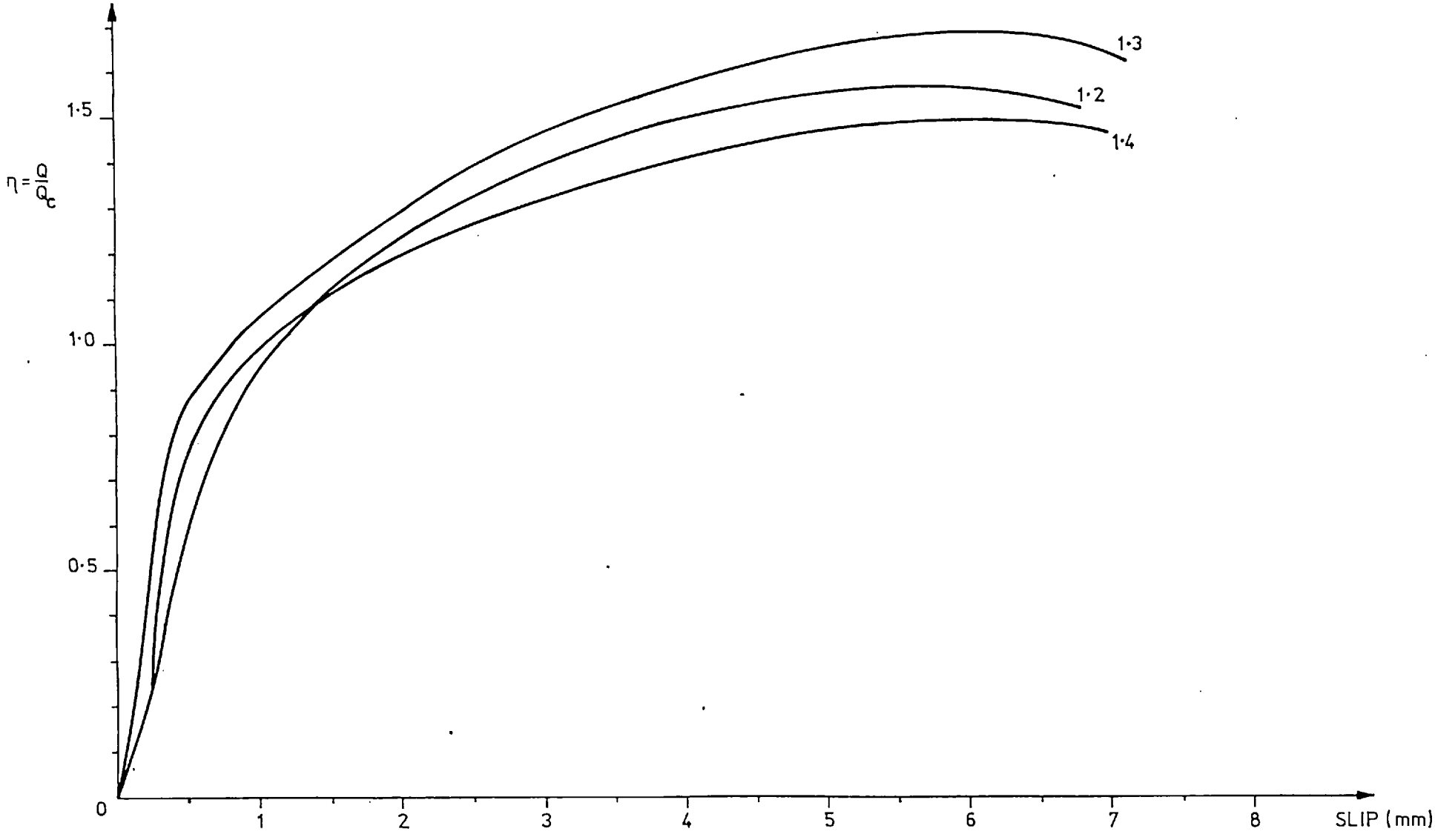


FIGURE 7: LOAD-SLIP CURVES, PUSH-OUT TEST SERIES 1

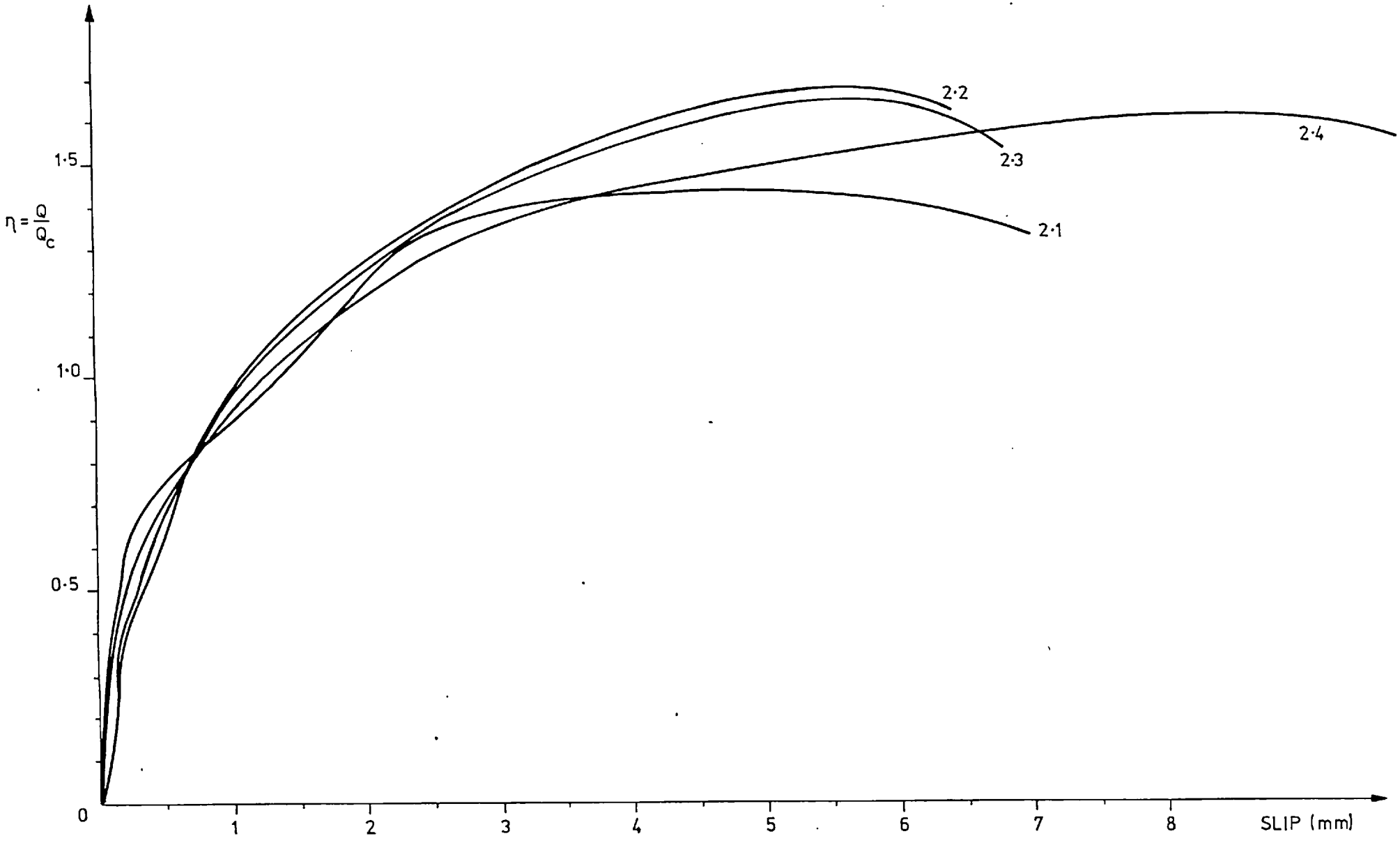


FIGURE 8: LOAD-SLIP CURVES, PUSH-OUT TEST SERIES 2

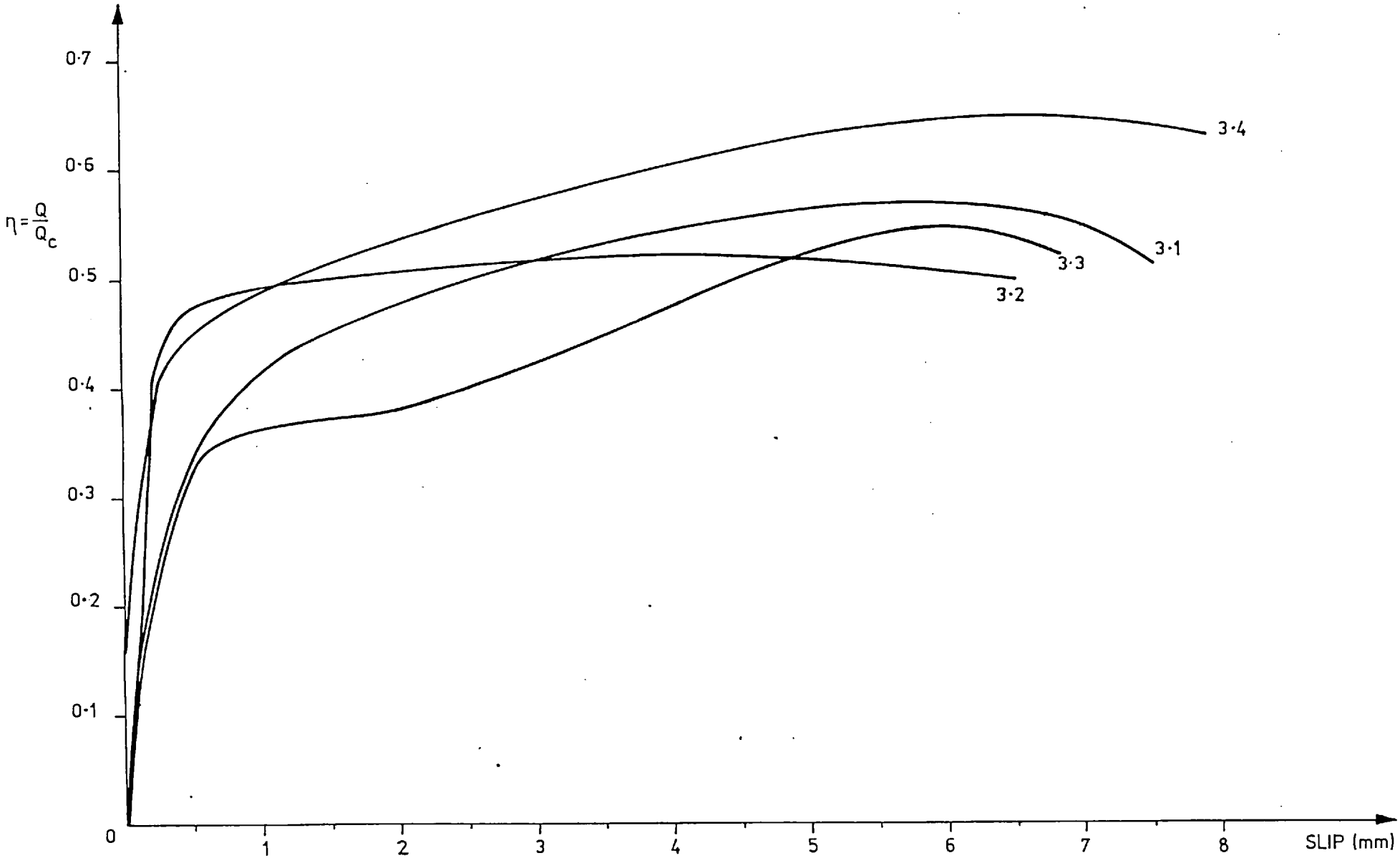


FIGURE 9: LOAD-SLIP CURVES, PUSH-OUT TEST SERIES 3

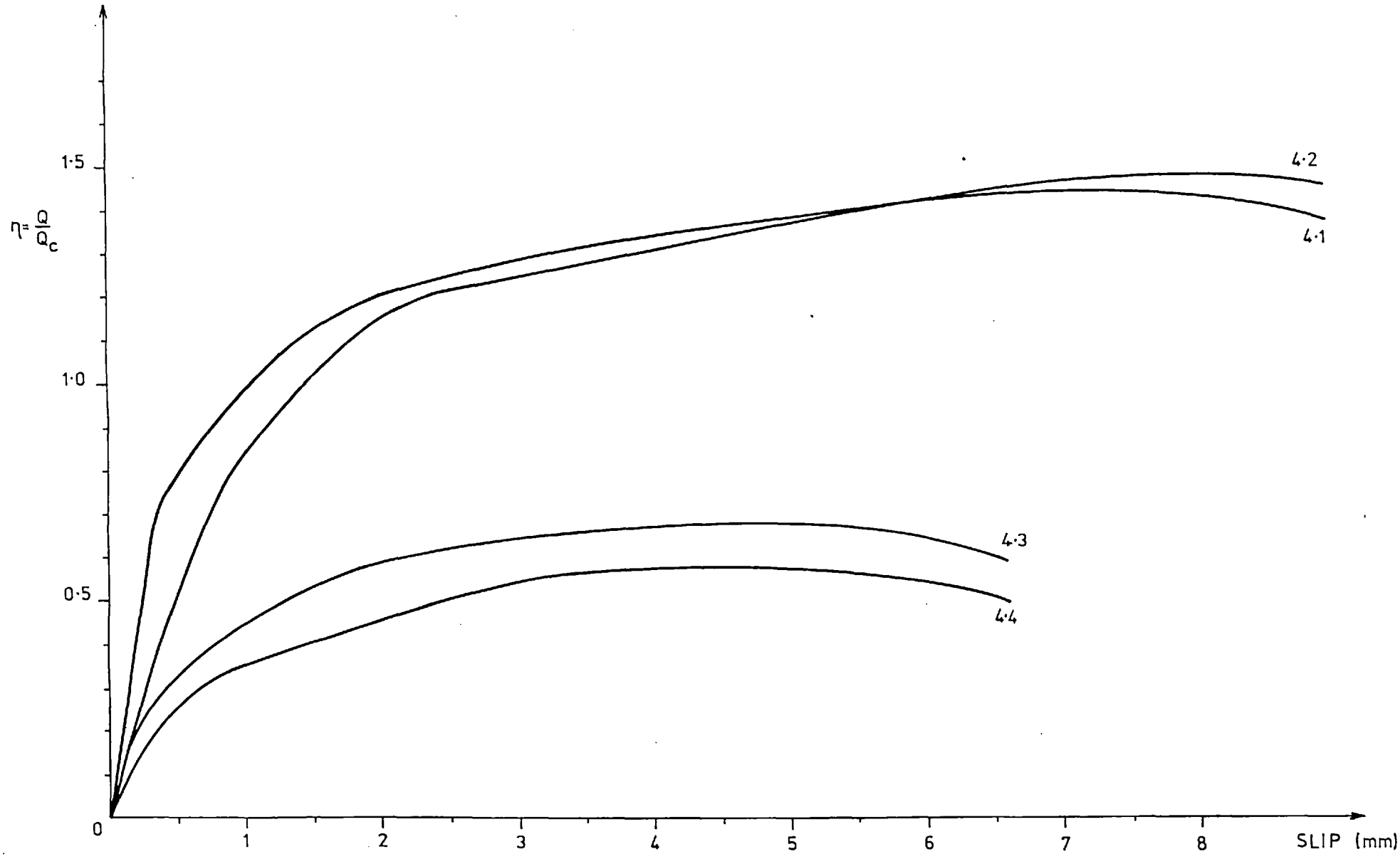


FIGURE 10: LOAD-SLIP CURVES, PUSH-OUT TEST SERIES 4

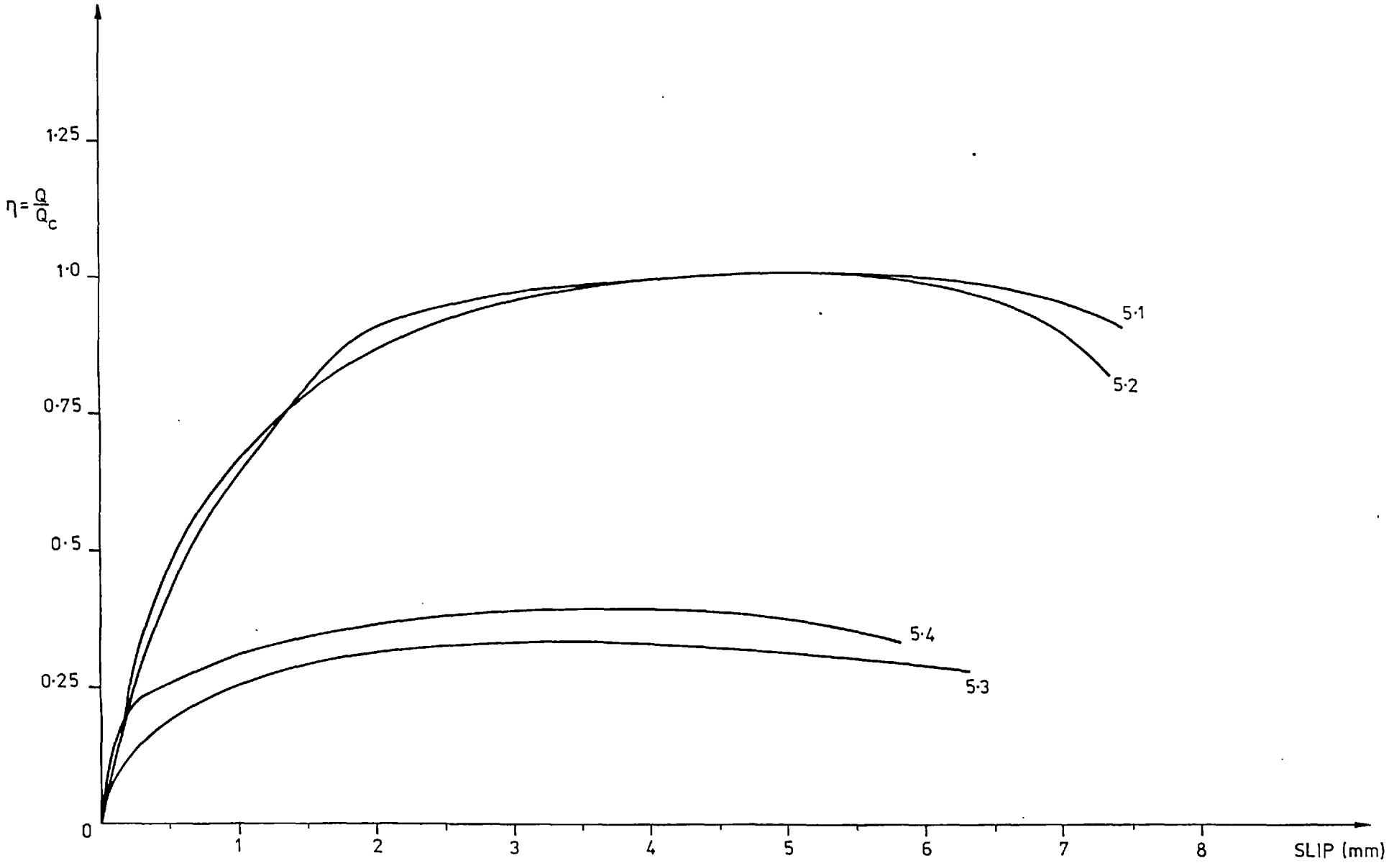


FIGURE 11: LOAD-SLIP CURVES, PUSH-OUT TEST SERIES 5

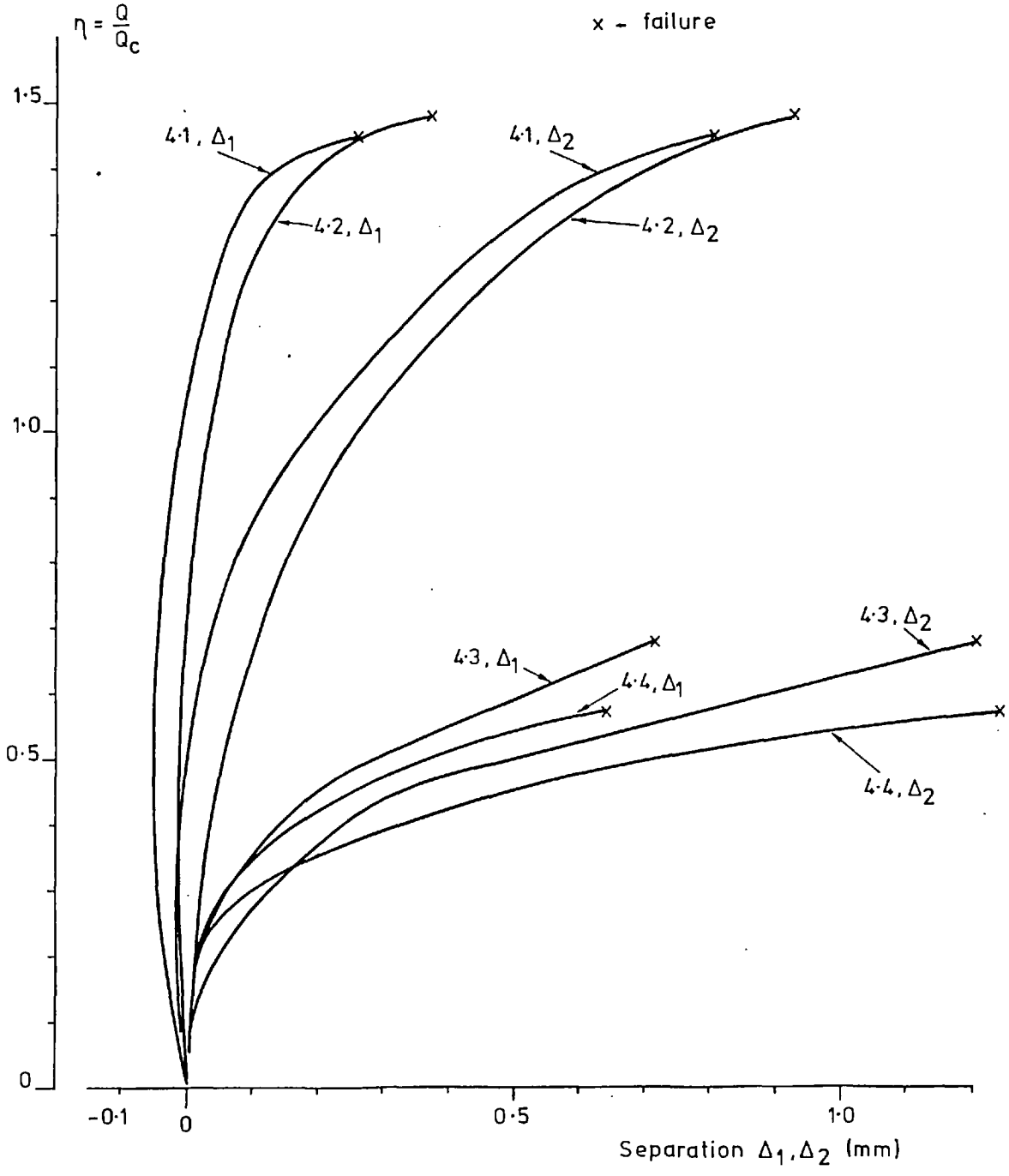


FIGURE 12: LOAD-SEPARATION CURVES, PUSH-OUT TEST SERIES 4

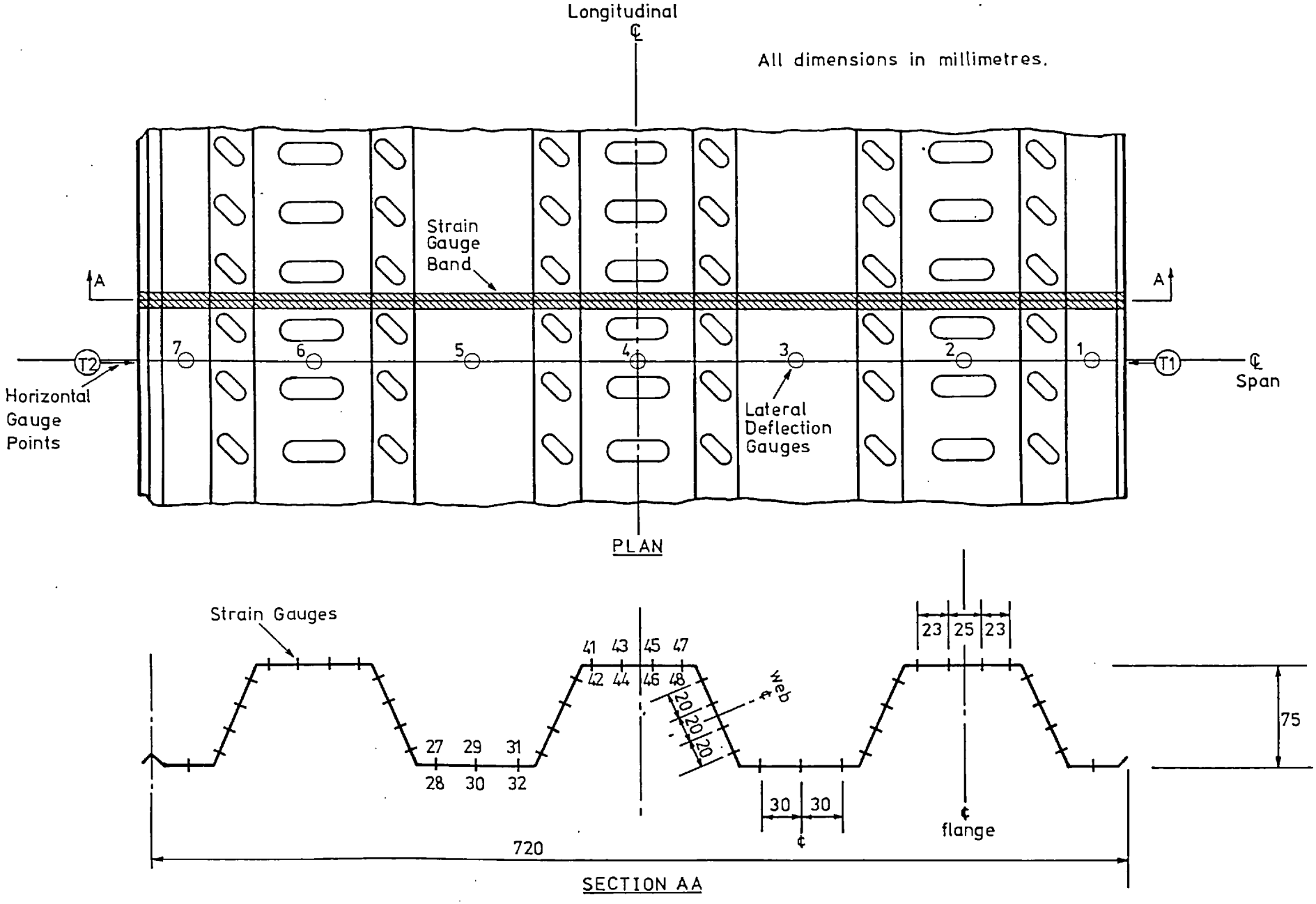


FIGURE 13: CONSTRUCTION LOADING TEST - INSTRUMENTATION

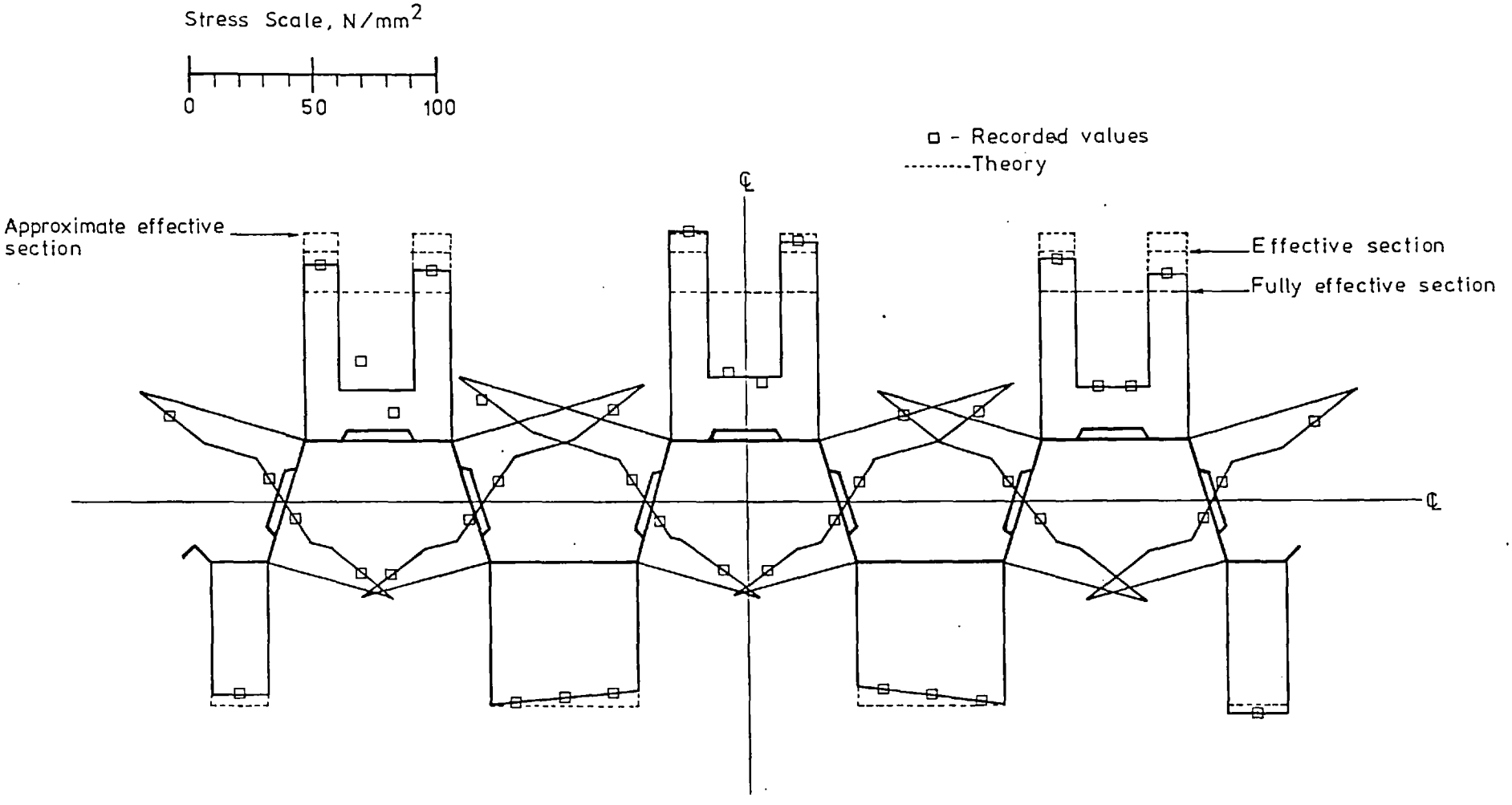


FIGURE 14: LONGITUDINAL STRESS DISTRIBUTION - WET CONCRETE LOAD ONLY

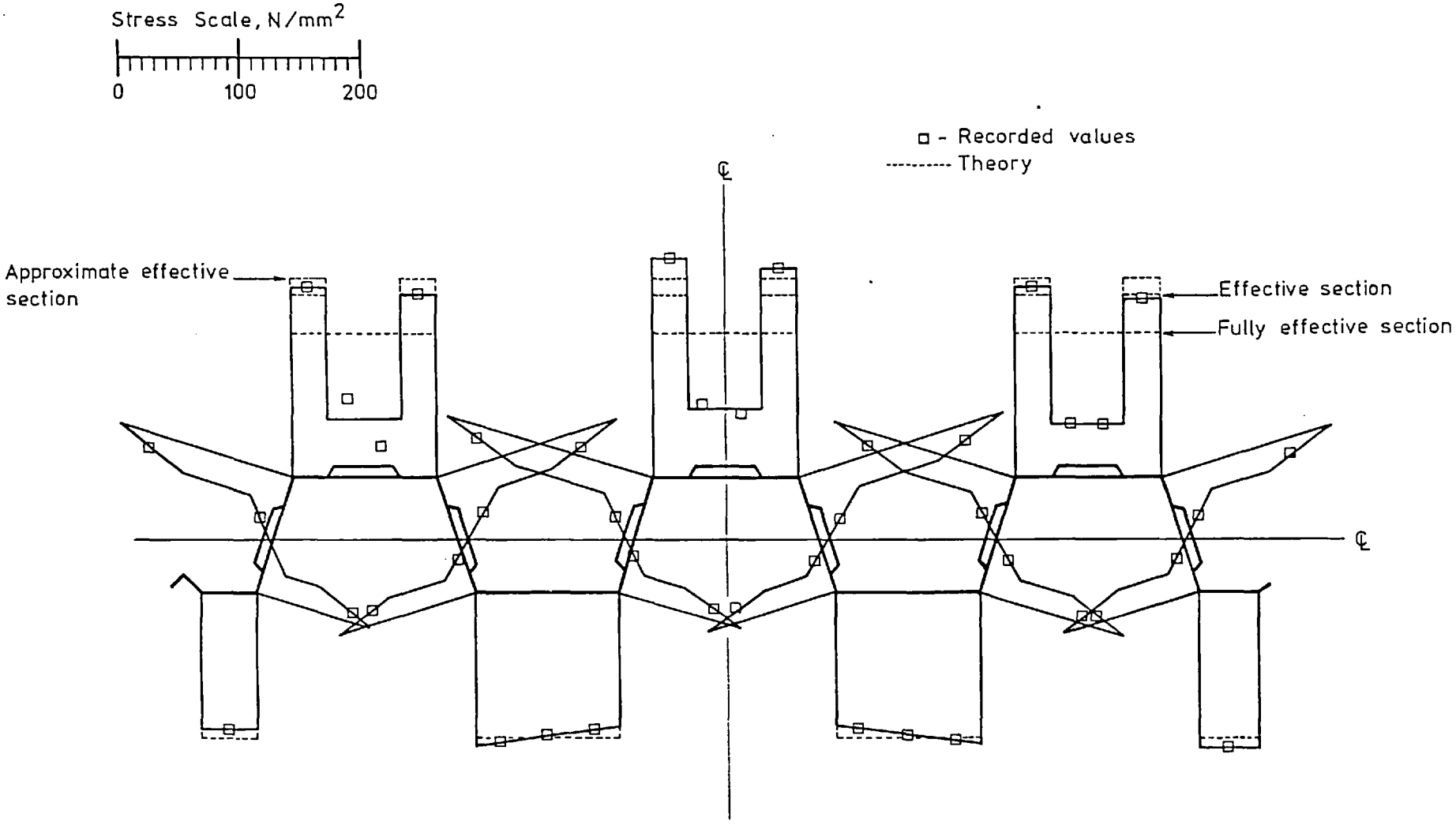


FIGURE 15: LONGITUDINAL STRESS DISTRIBUTION - WET CONCRETE PLUS ADDITIONAL CONSTRUCTION LOAD

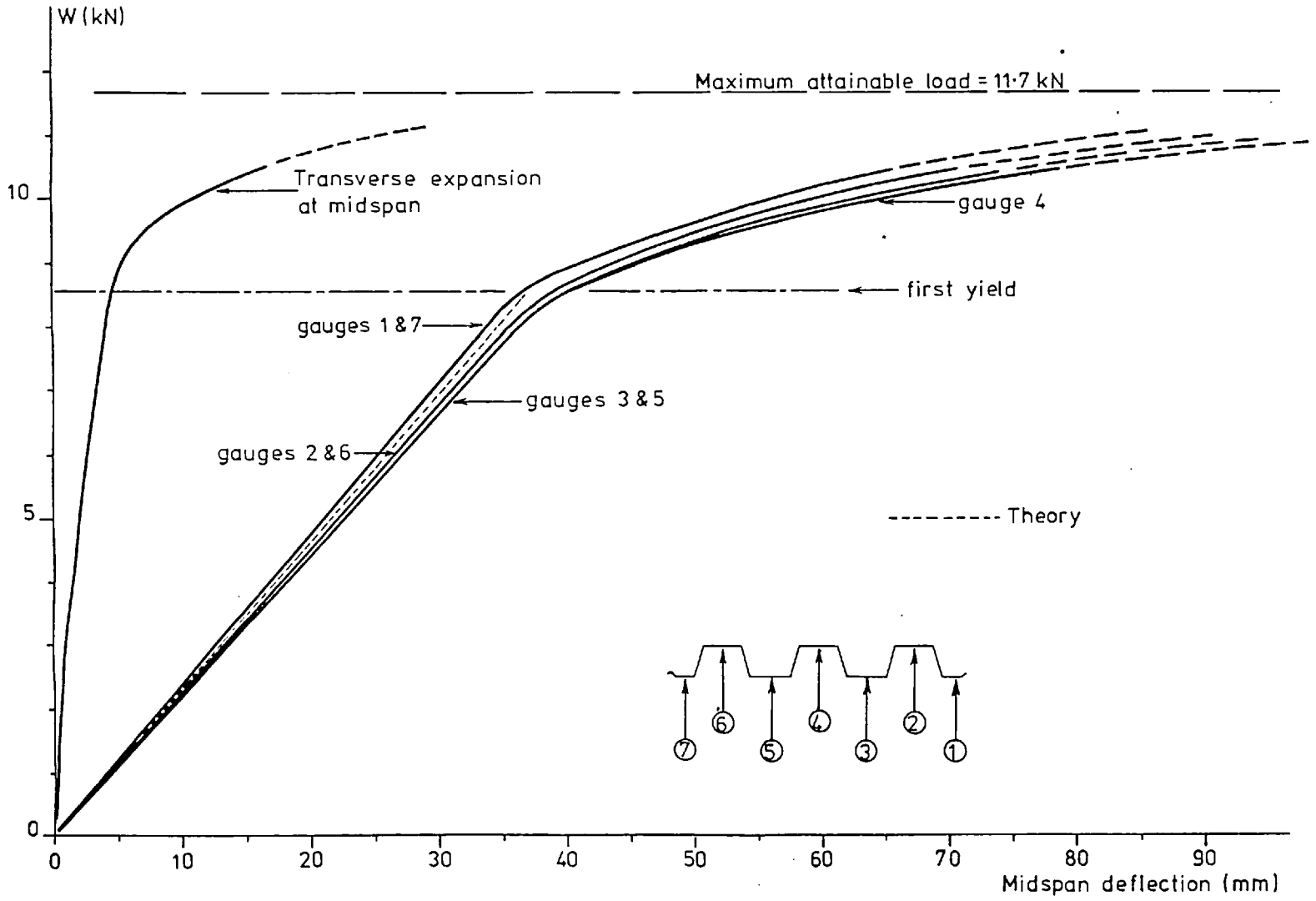


FIGURE 16: BARE FORMWORK : LOAD-DEFLECTION RESPONSE, ULTIMATE

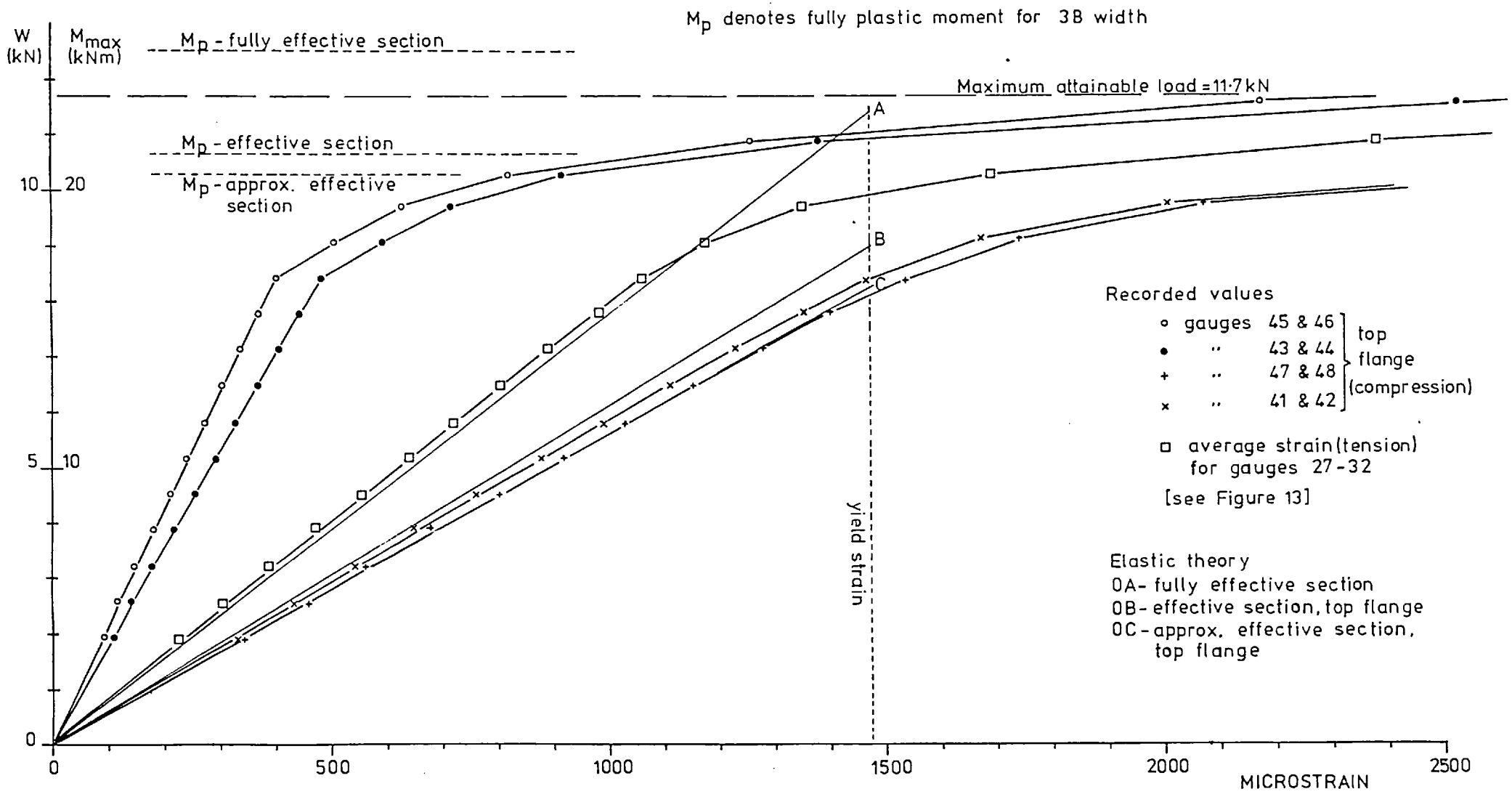
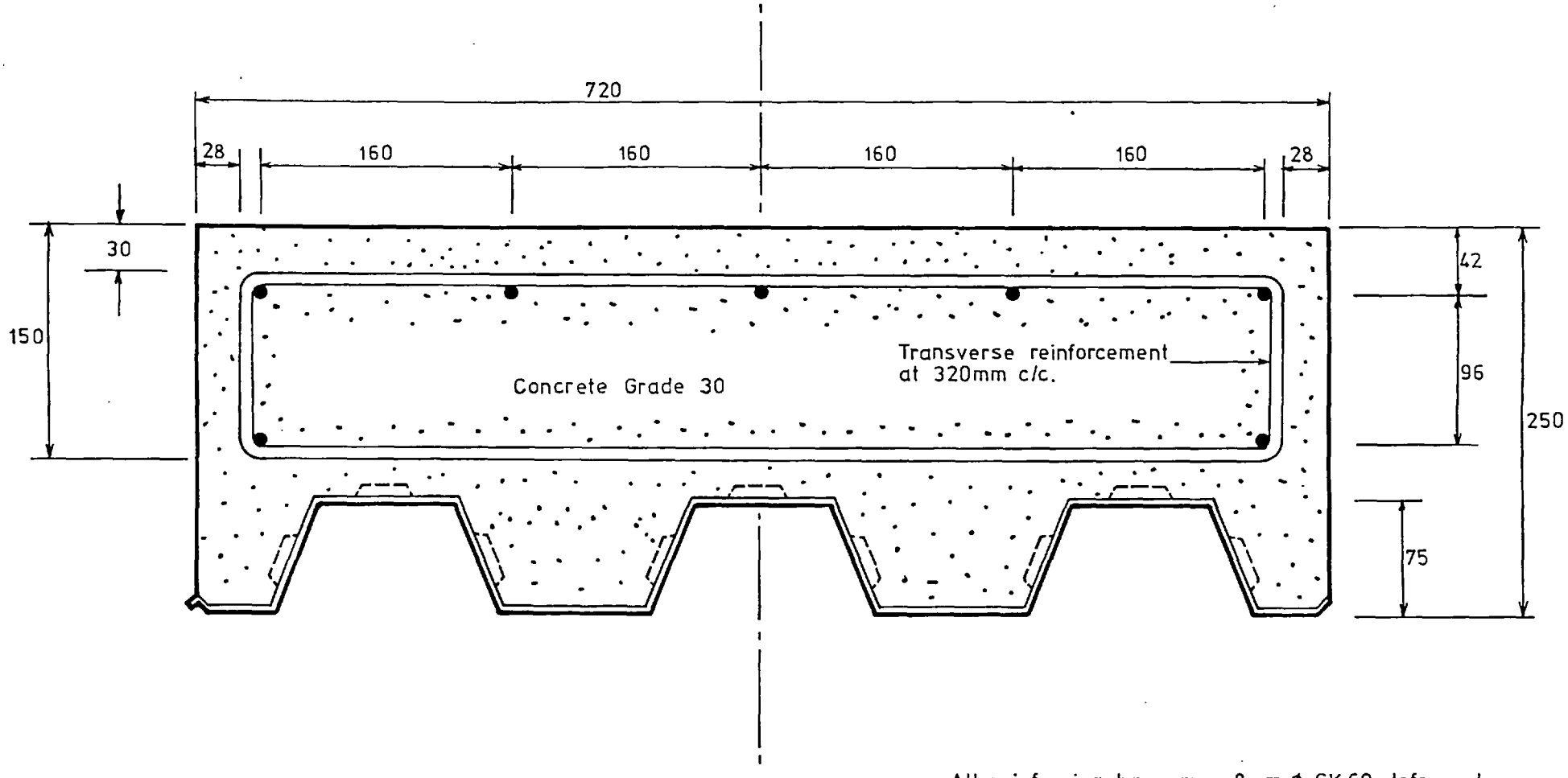


FIGURE 17: BARE FORMWORK : LOAD-STRAIN RESPONSE, ULTIMATE



All reinforcing bars are 8mm ϕ GK 60, deformed.

All dimensions in millimetres.

FIGURE 18: NOMINAL COMPOSITE DESIGN SECTION (Sagging Bending)

All dimensions in millimetres.

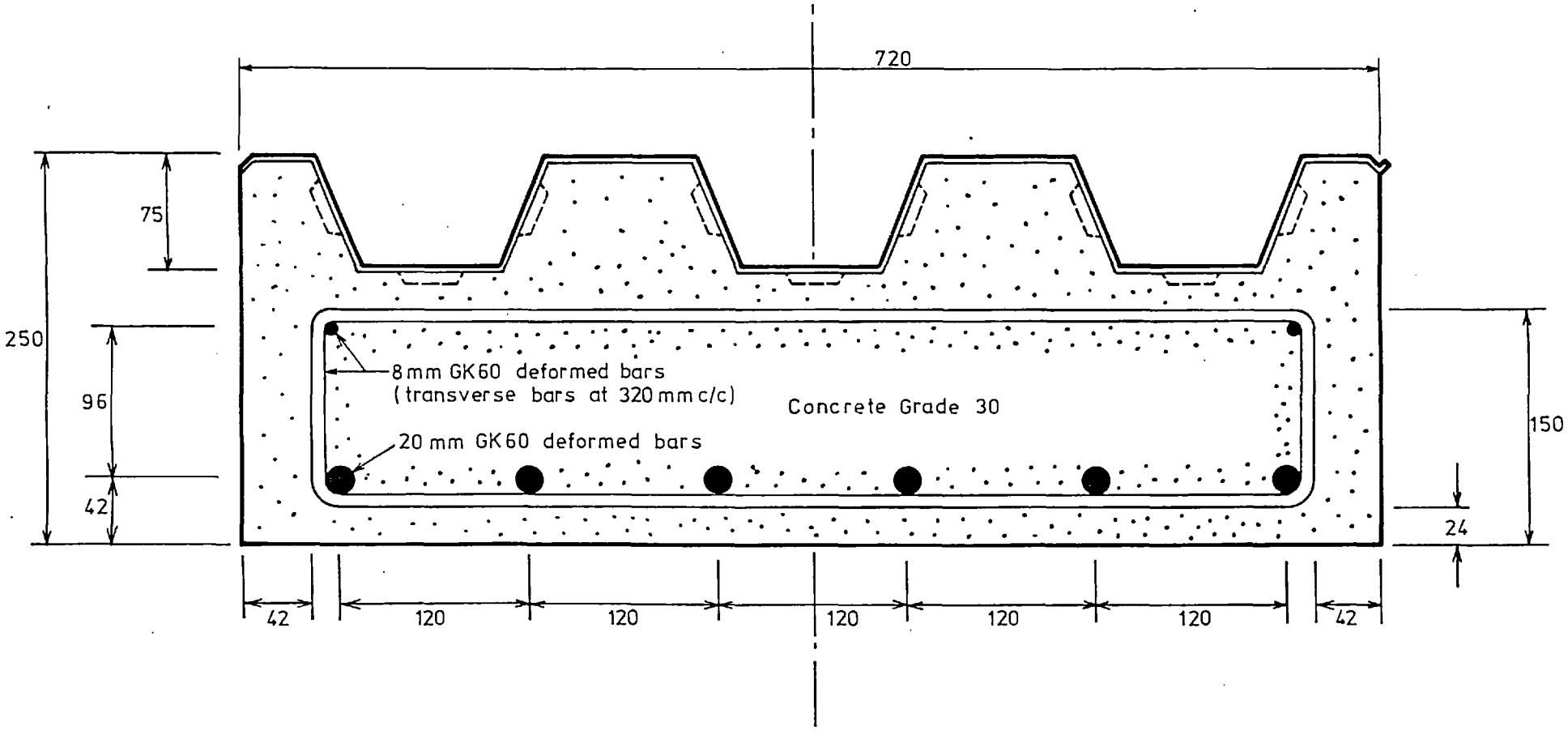


FIGURE 19: NOMINAL COMPOSITE DESIGN SECTION (Hogging Bending)

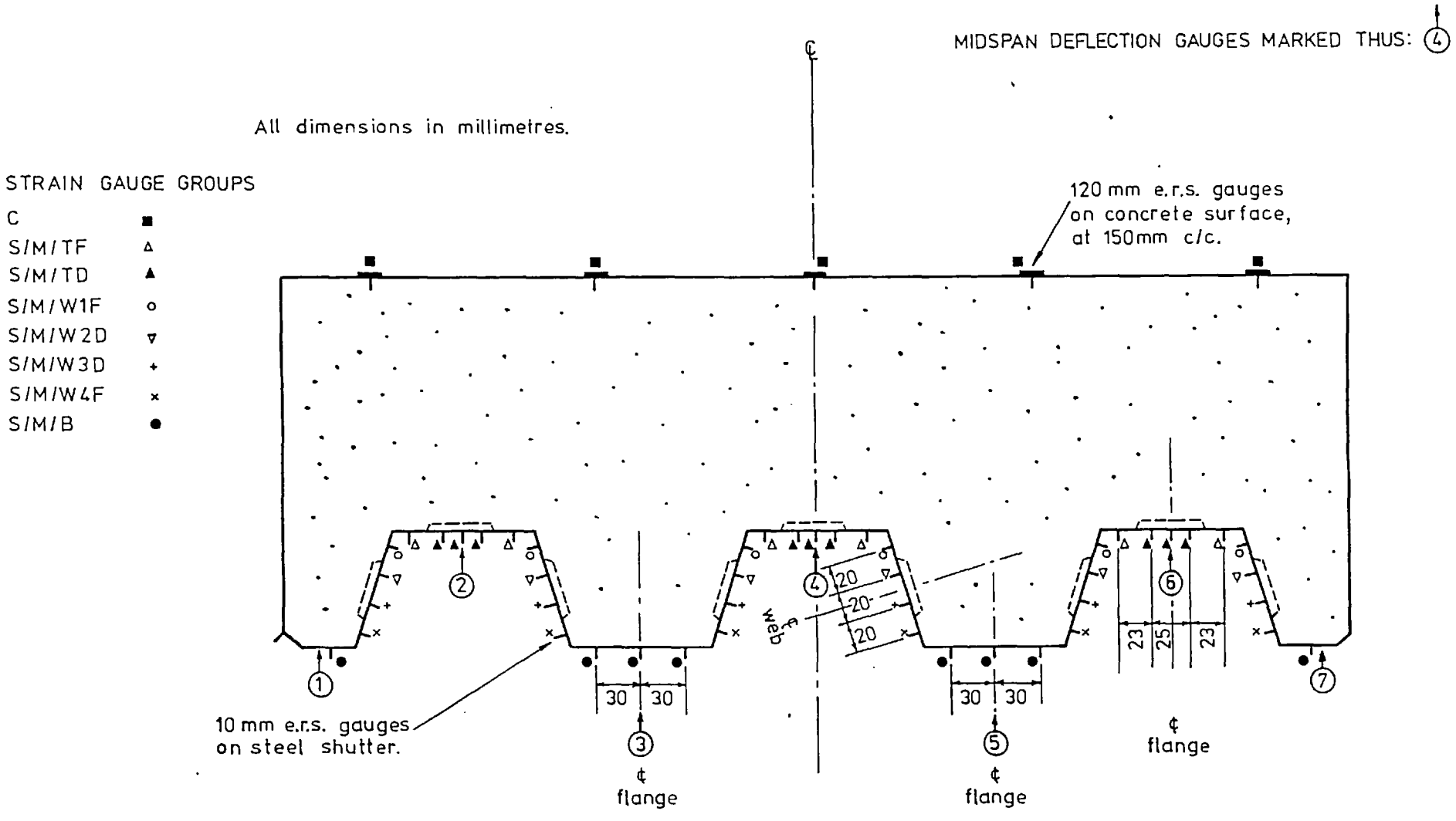


FIGURE 20: STRAIN GAUGE INSTRUMENTATION AT MIDSPAN

Even numbers are Slip

Odd numbers are Separation

All dimensions in millimetres

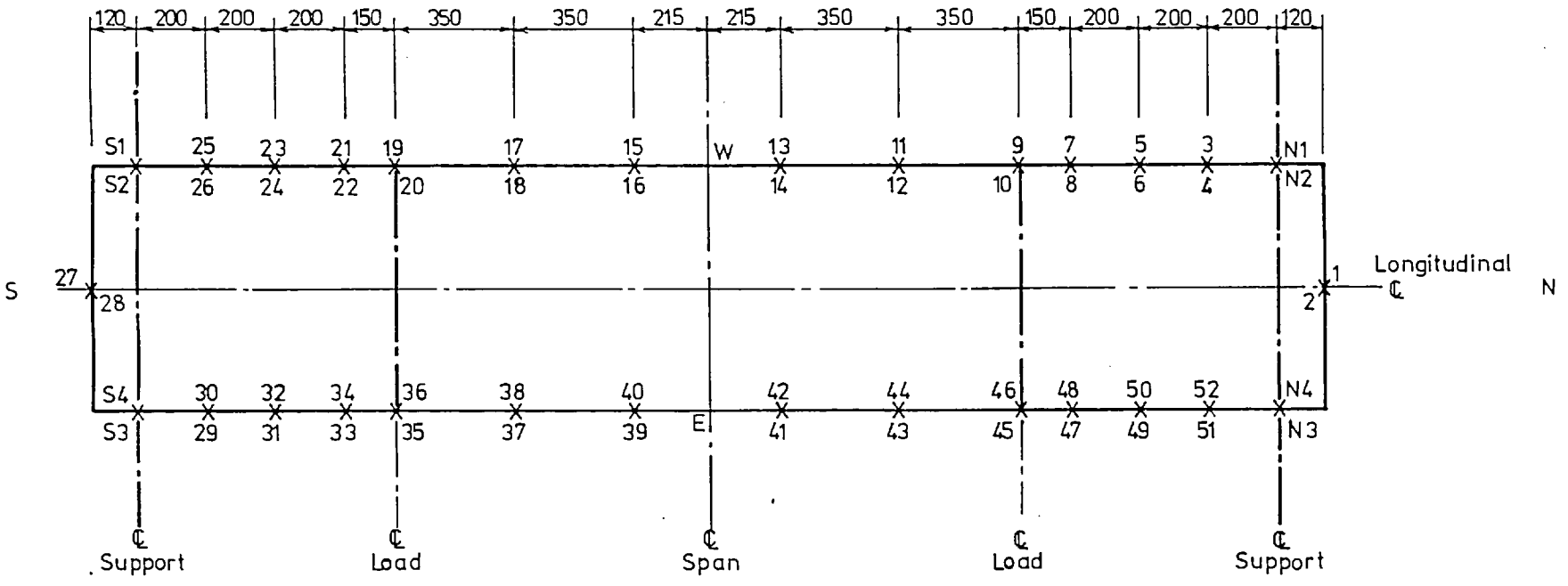


FIGURE 21: SLIP AND SEPARATION GAUGE POINTS

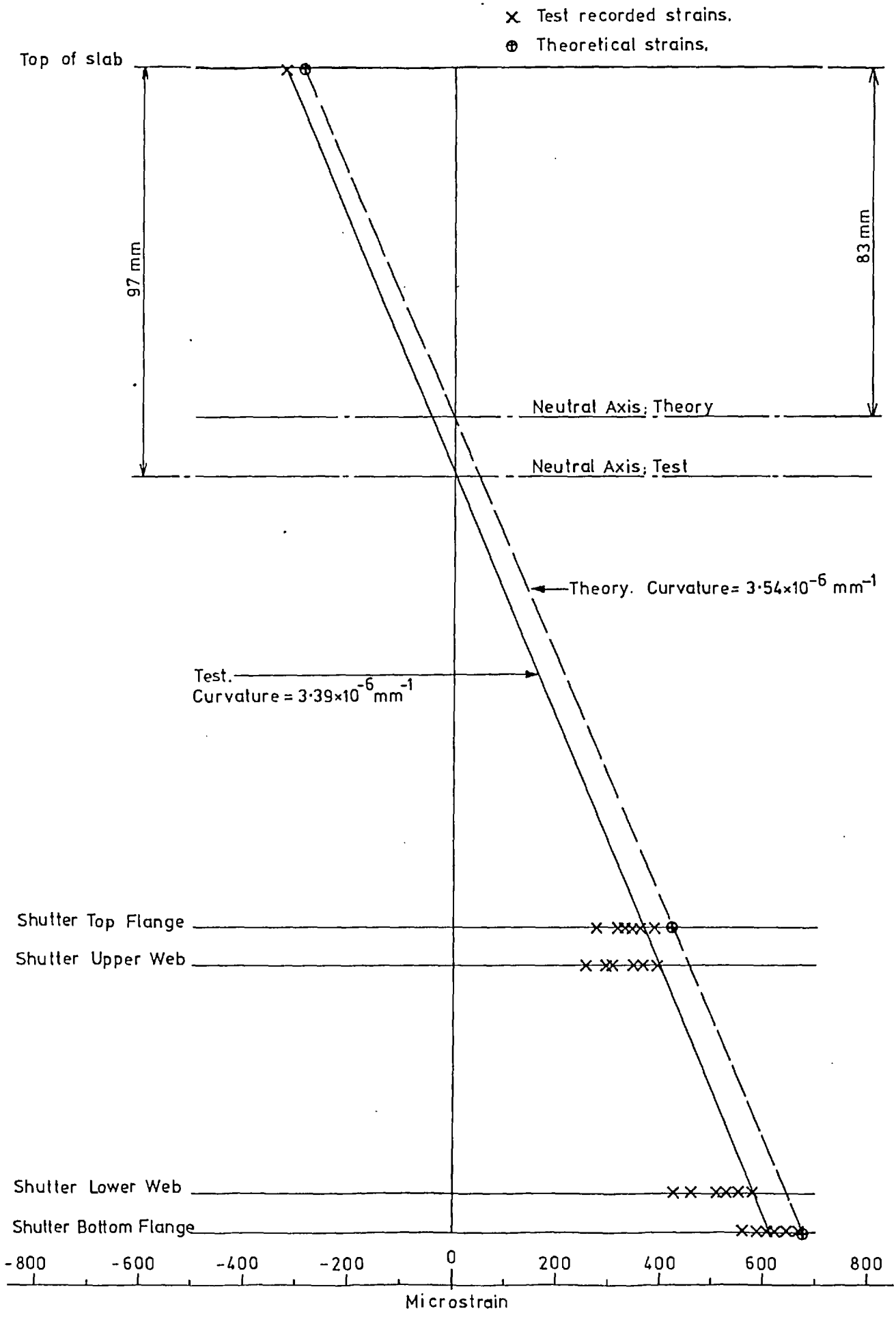


FIGURE 22: TEST 2 : CURVATURE COMPARISON AT MIDSPAN

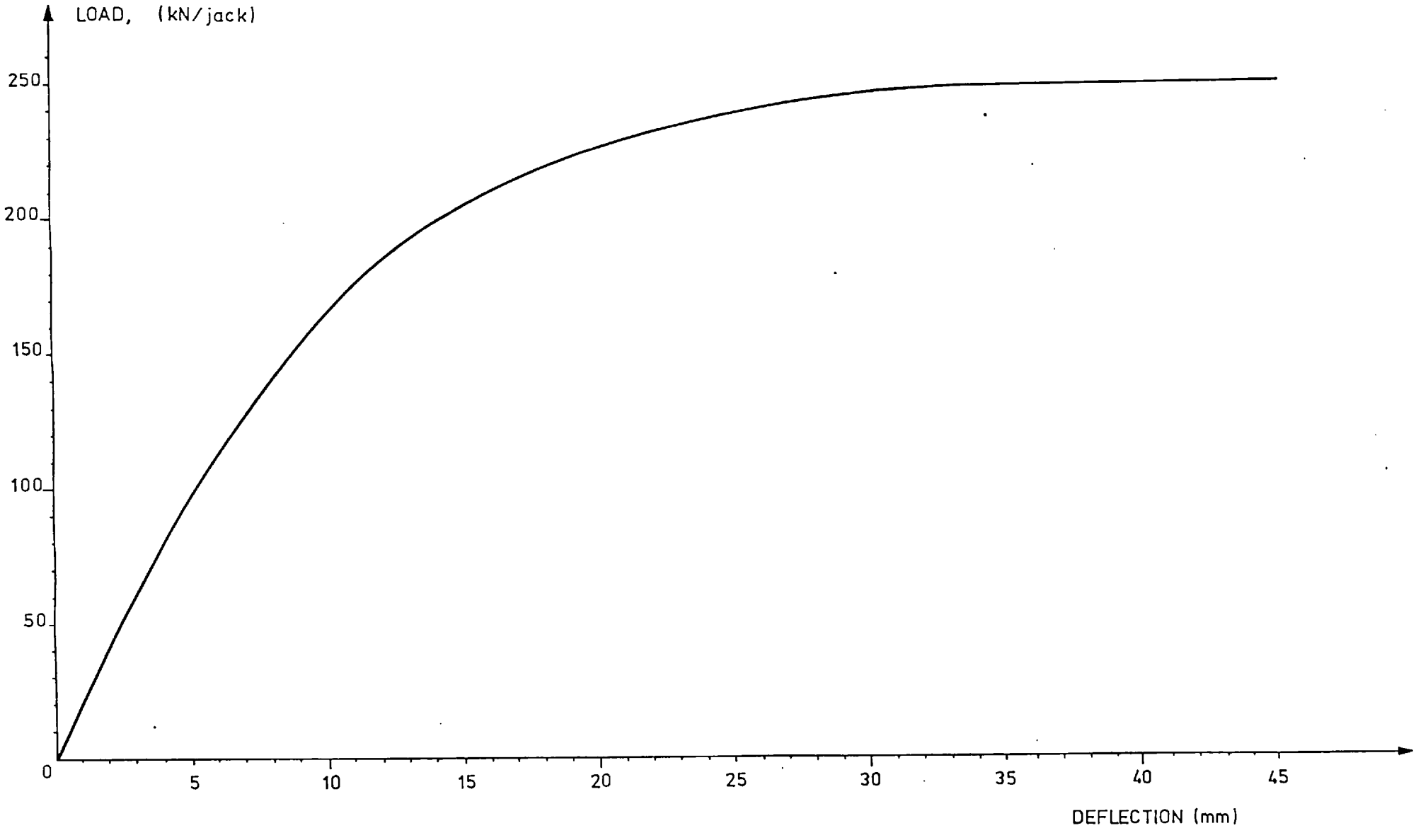


FIGURE 23: TEST 2 : LOAD .v. MIDSPAN DEFLECTION

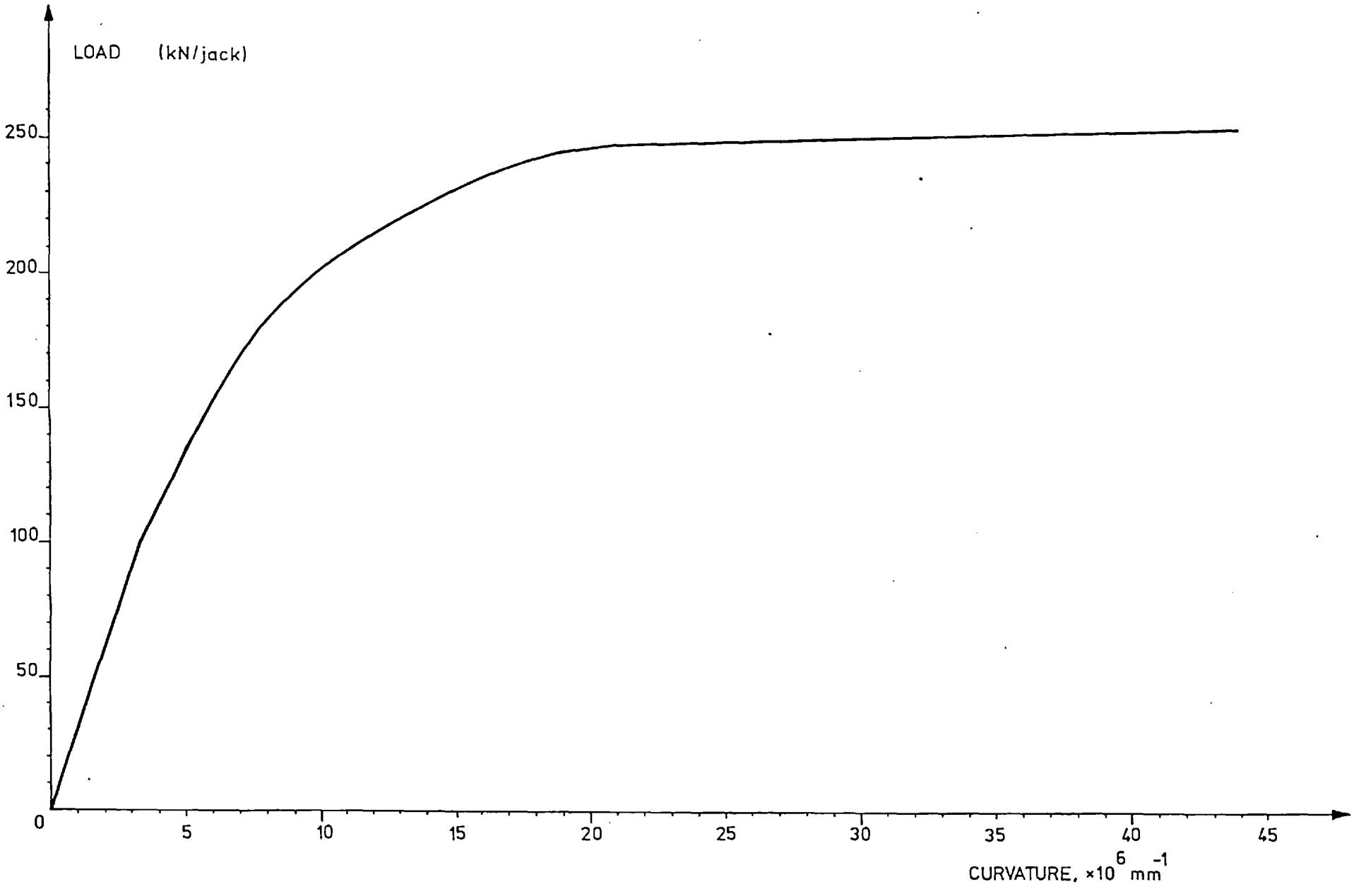


FIGURE 24: TEST 2 : LOAD .v. MIDSPAN CURVATURE

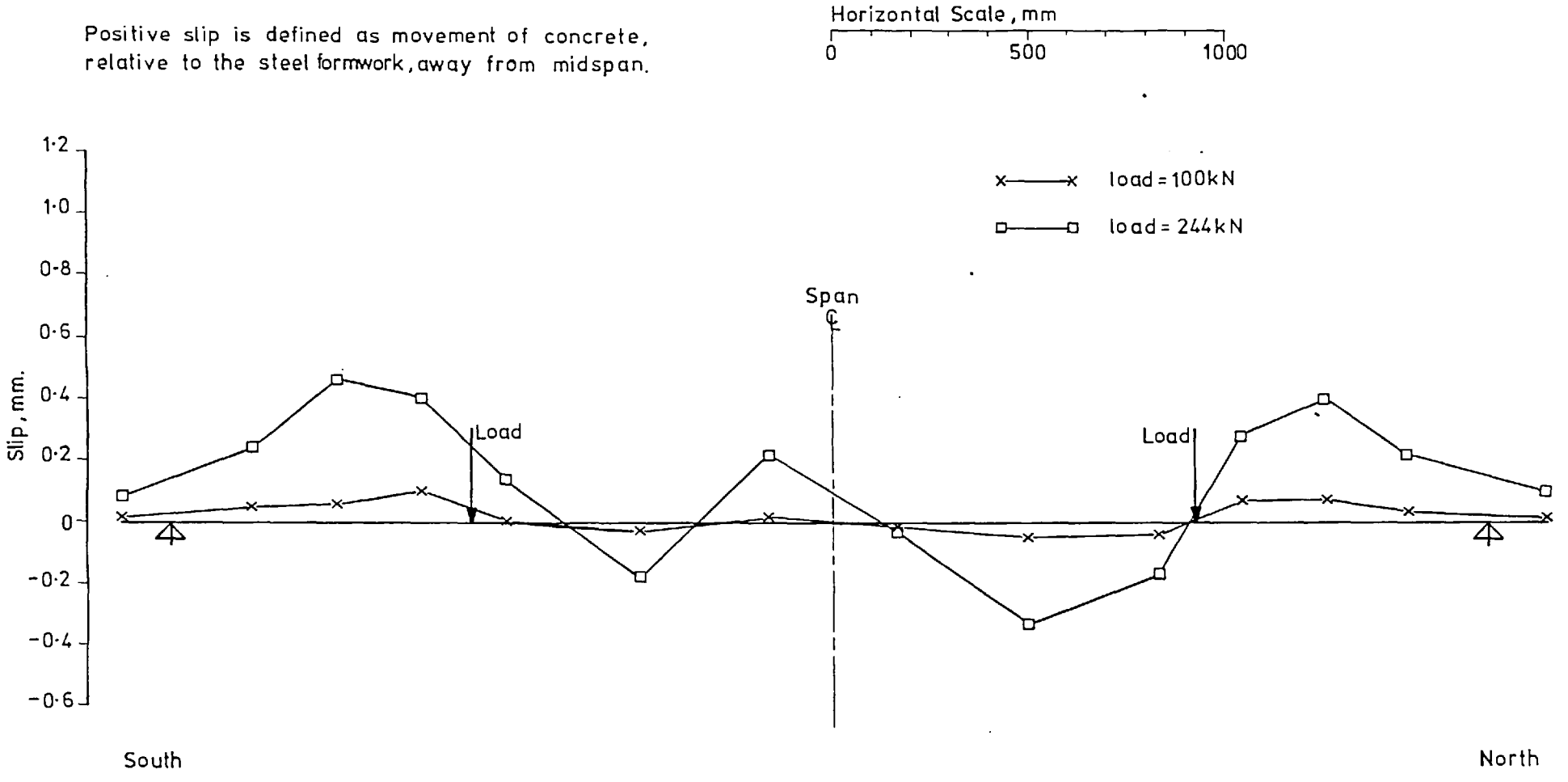


FIGURE 25: TEST 2 : SLIP DISTRIBUTIONS AT LOADS OF 100 kN & 244 kN

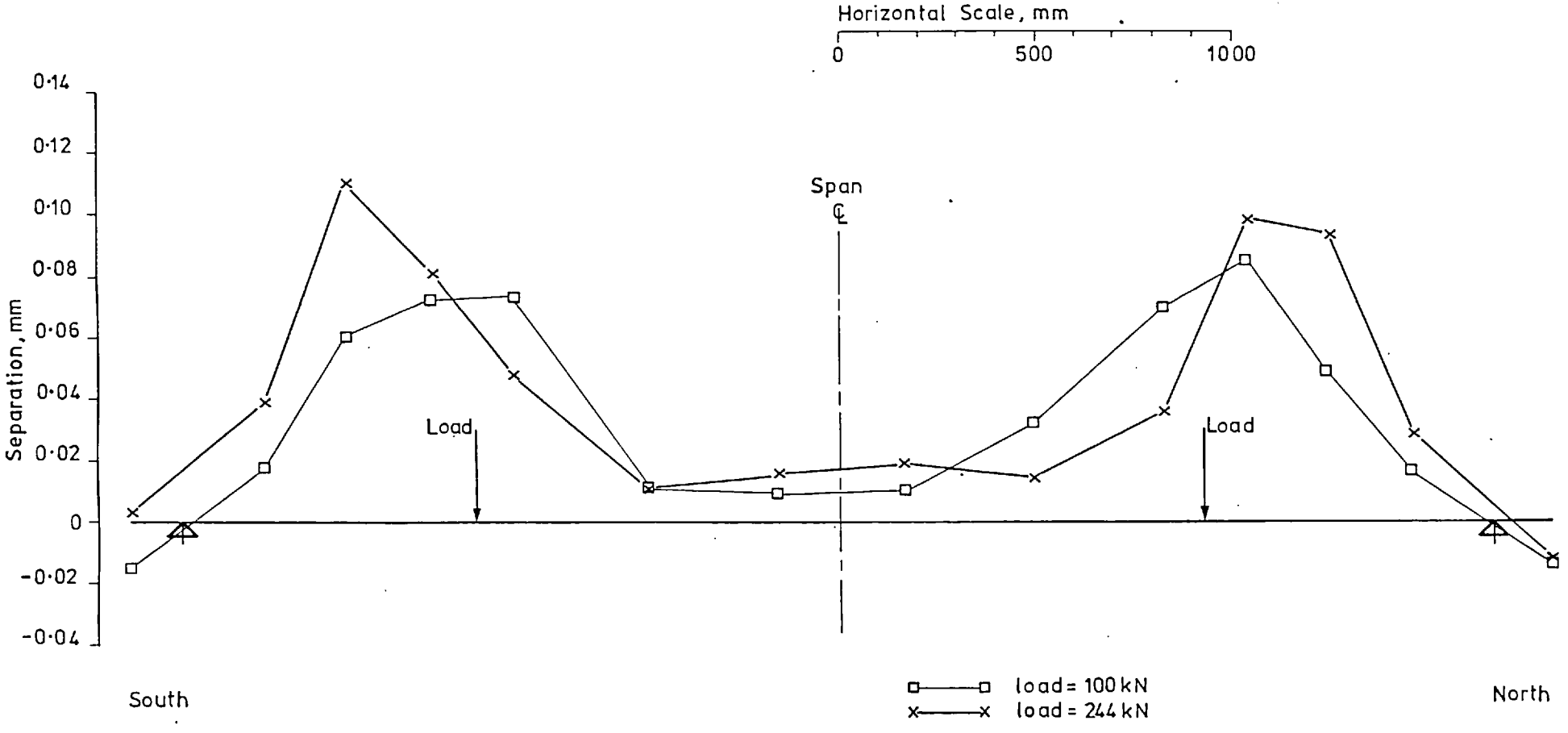


FIGURE 26: TEST 2 : SEPARATION DISTRIBUTIONS AT LOADS OF 100 kN & 244 kN

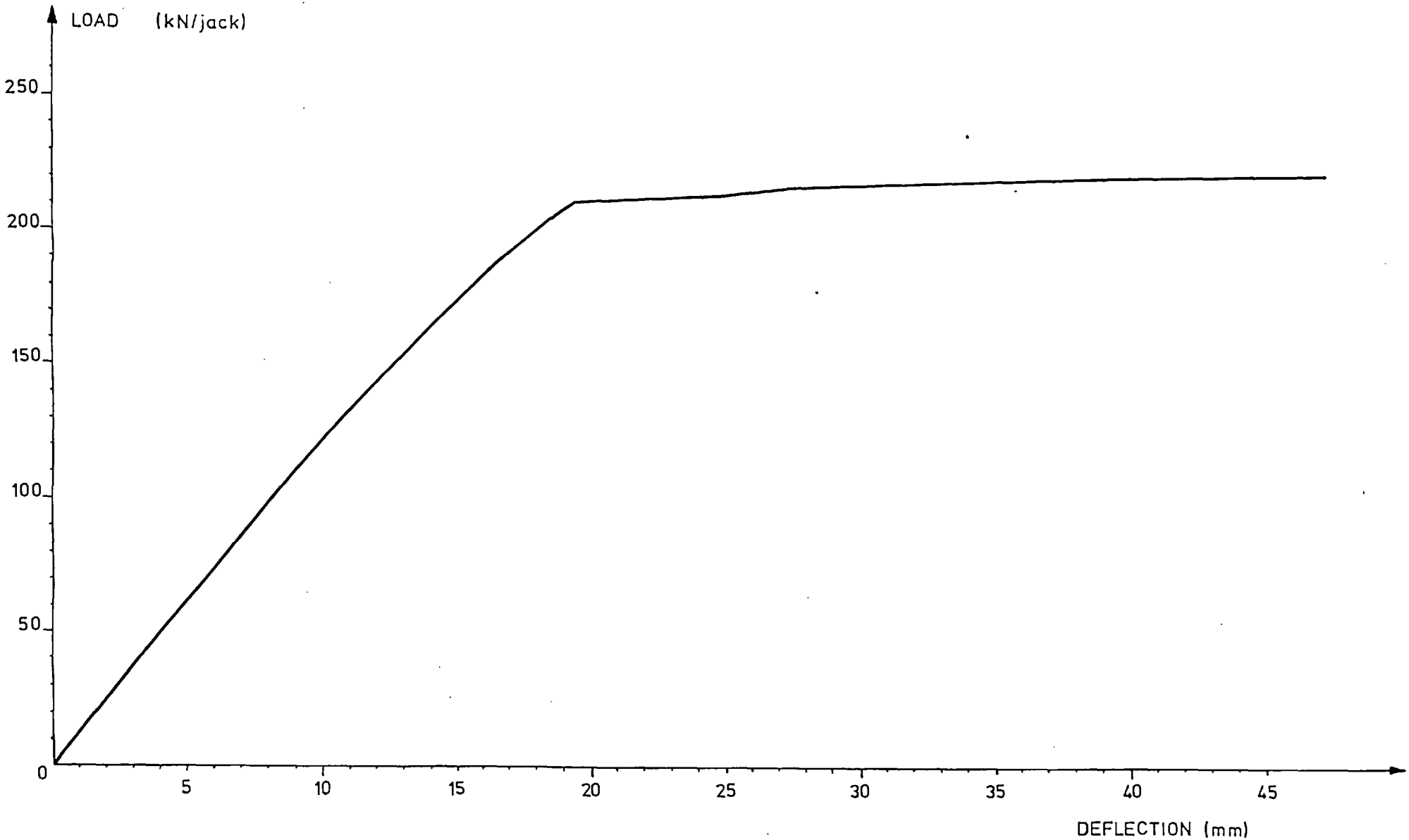


FIGURE 27: TEST 3 : LOAD .v. MIDSPAN DEFLECTION

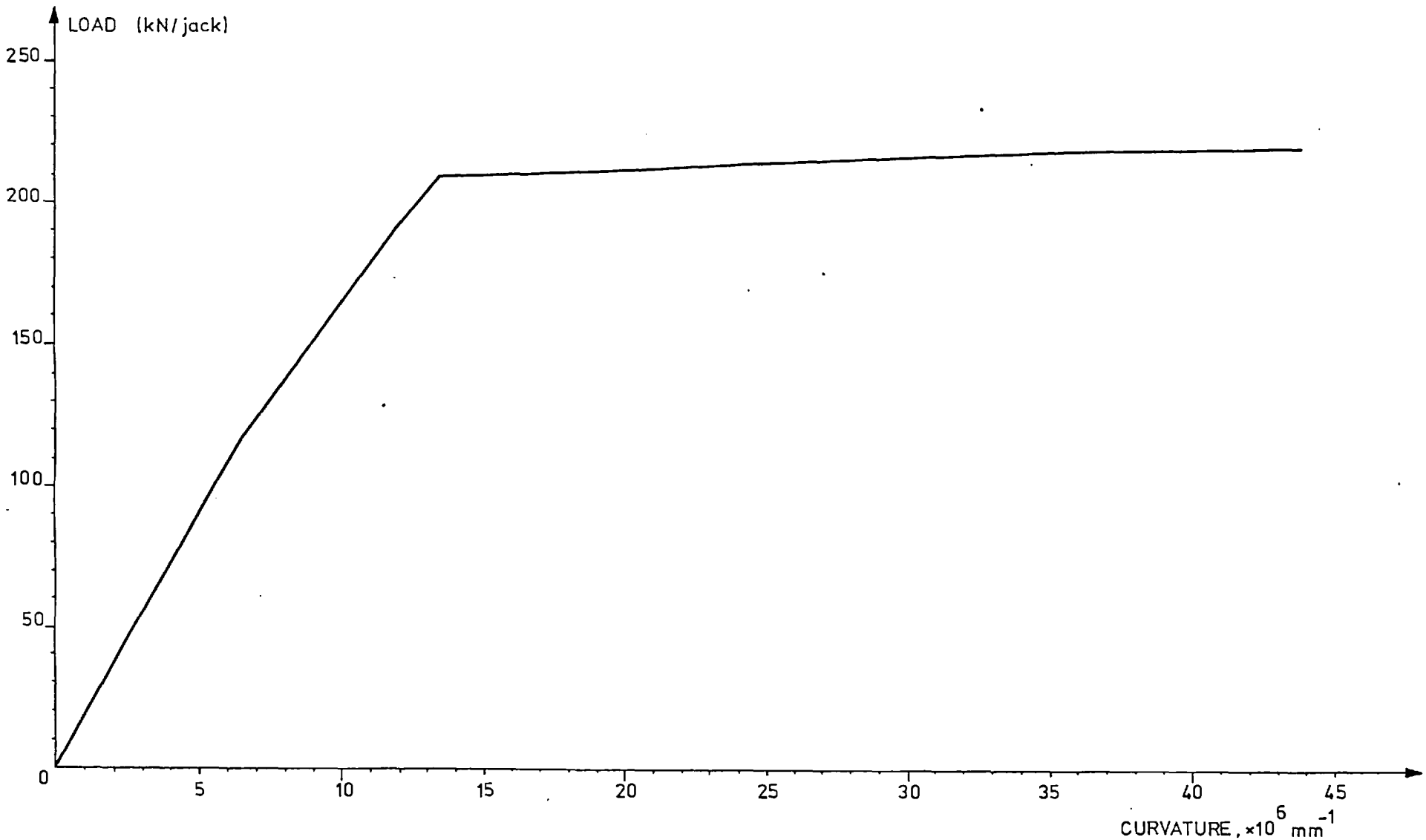


FIGURE 28: TEST 3 : LOAD .v. MIDSPAN CURVATURE

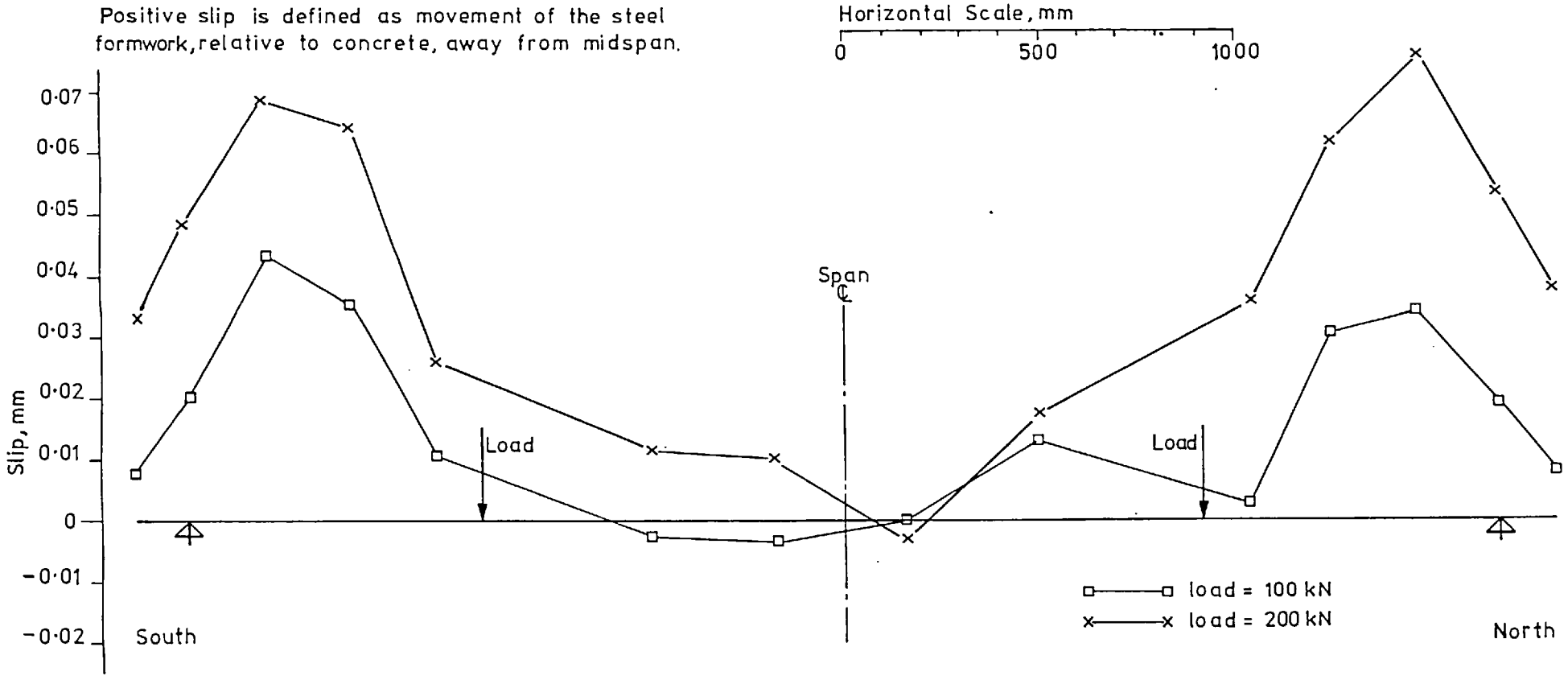


FIGURE 29: TEST 3 : SLIP DISTRIBUTIONS AT LOADS OF 100 kN & 200 kN

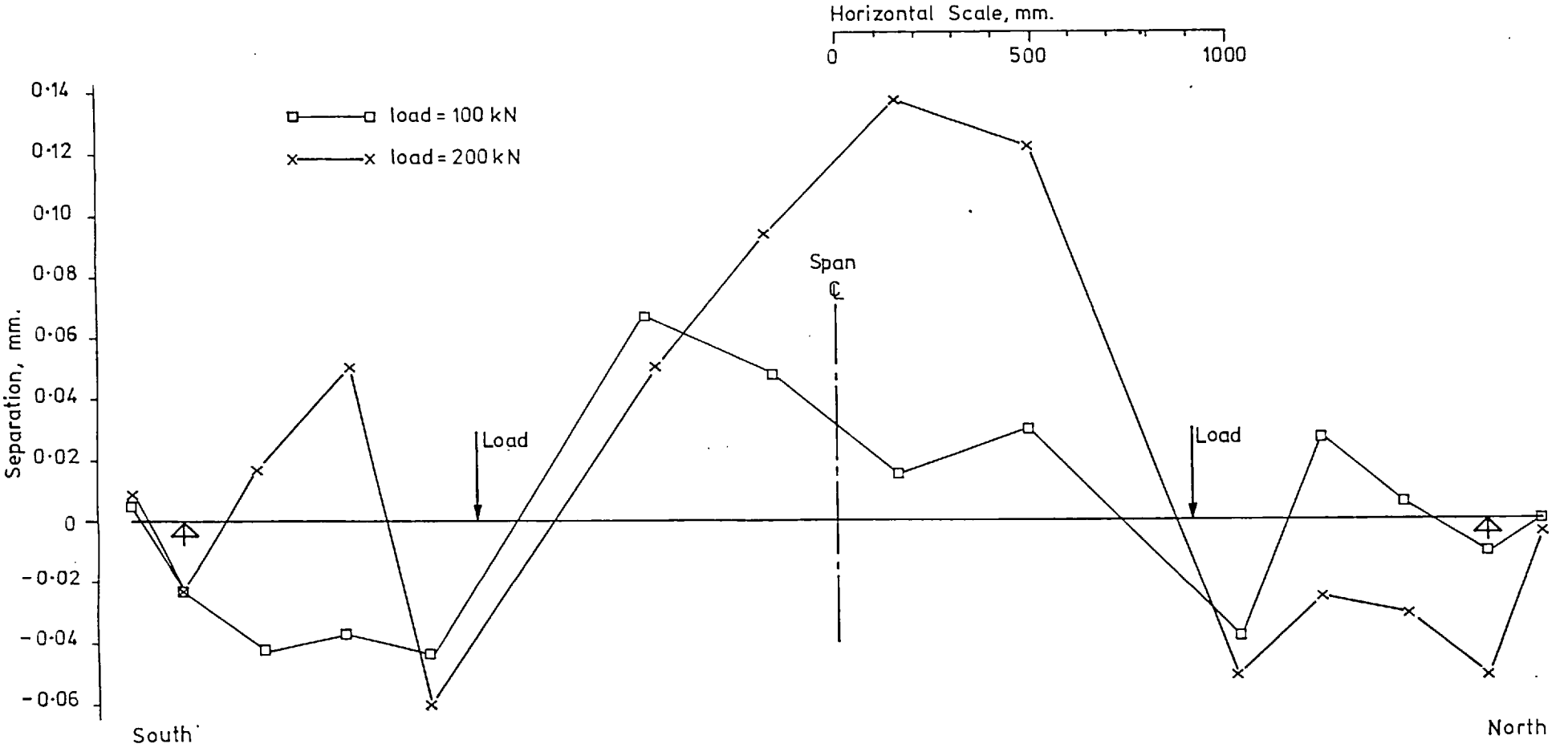


FIGURE 30: TEST 3 : SEPARATION DISTRIBUTION AT LOADS OF 100 kN & 200 kN

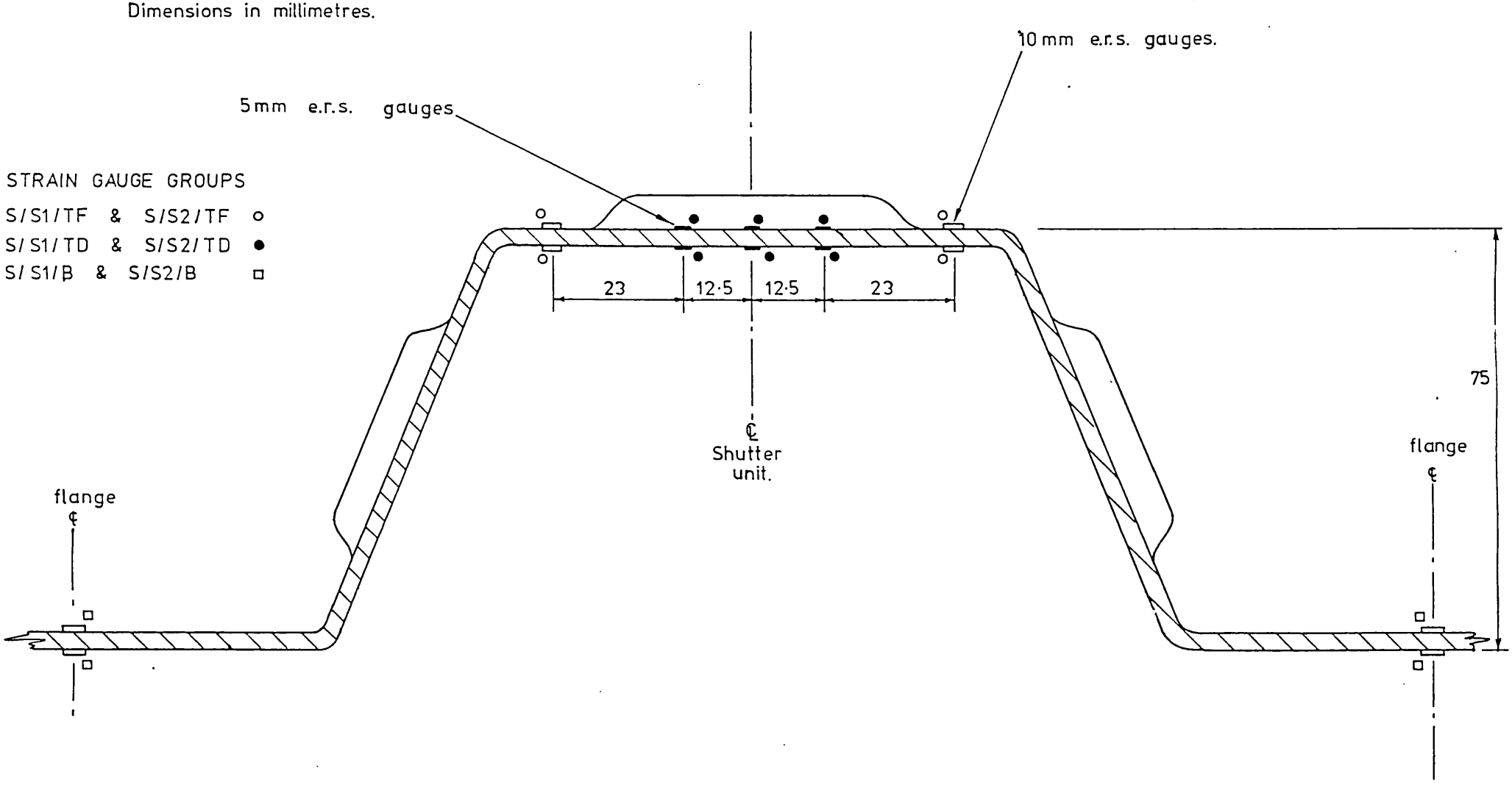


FIGURE 31: TESTS 6 - 9 : STRAIN GAUGES IN SHEAR SPAN

Section M - Midspan, all tests 2 - 9 inclusive. [Figure 20]

Sections S1 & S2 - Shear span, tests 6-9 inclusive. [Figure 31]

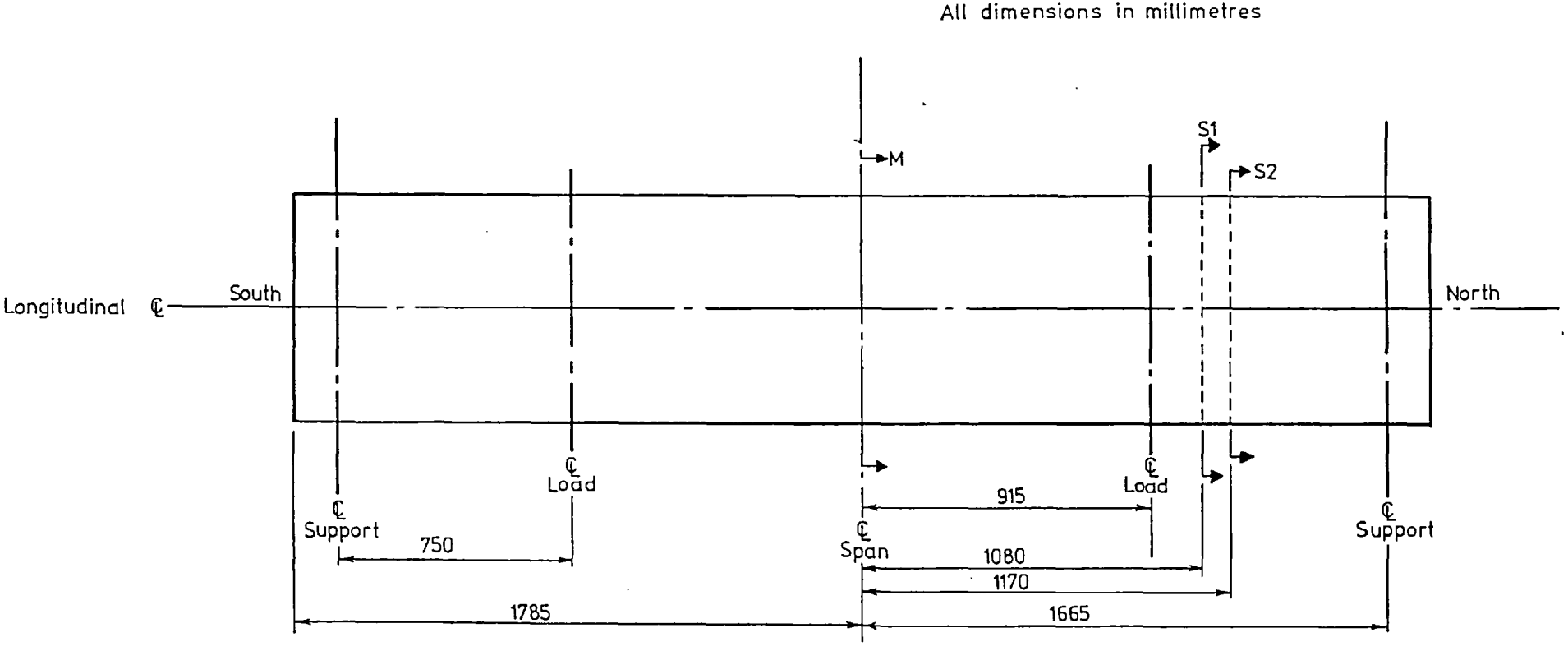


FIGURE 32: TESTS 4 - 9 : POSITION OF STRAIN GAUGES

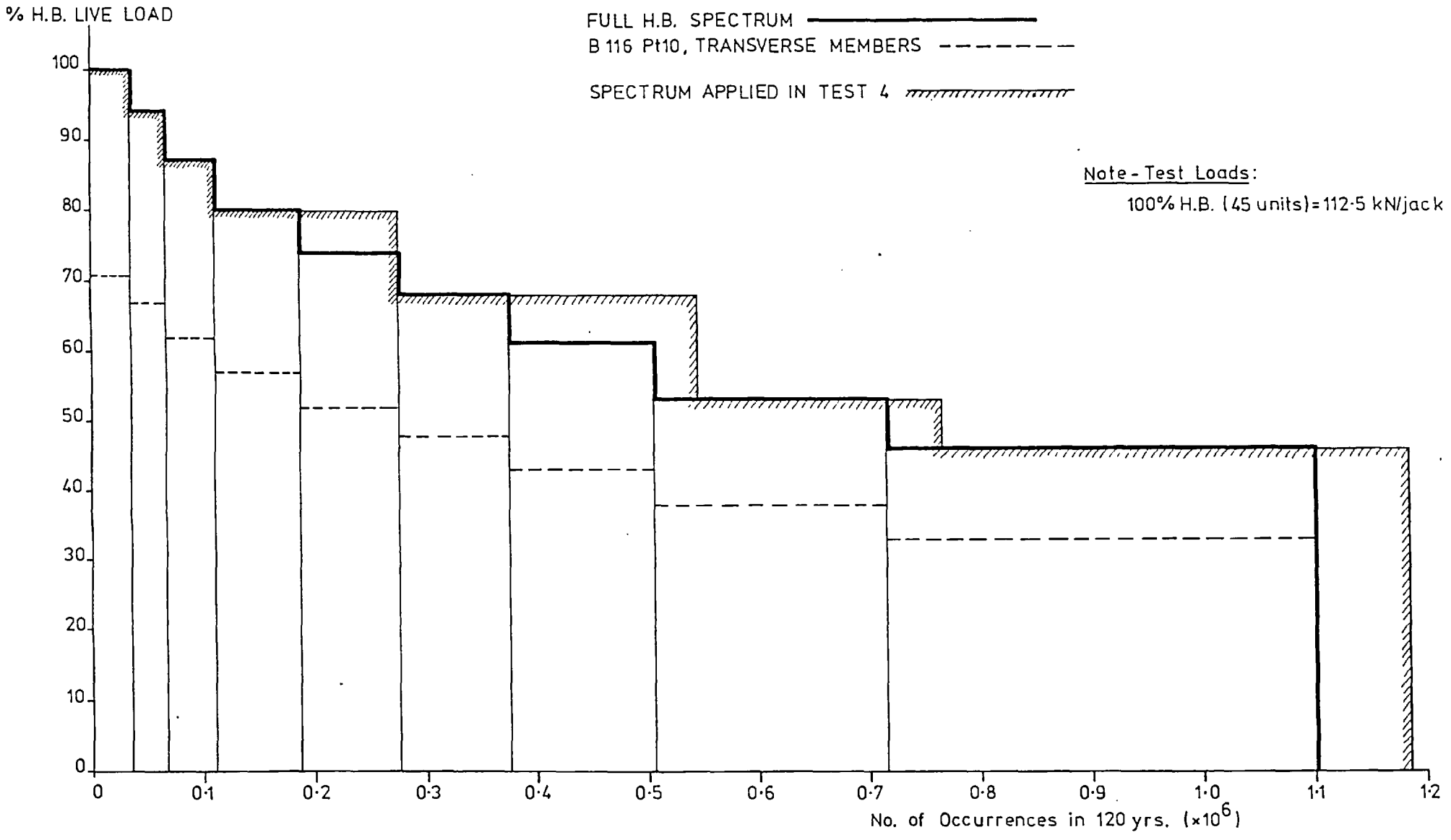


FIGURE 33: TEST 4 : H.B. LOAD SPECTRUM

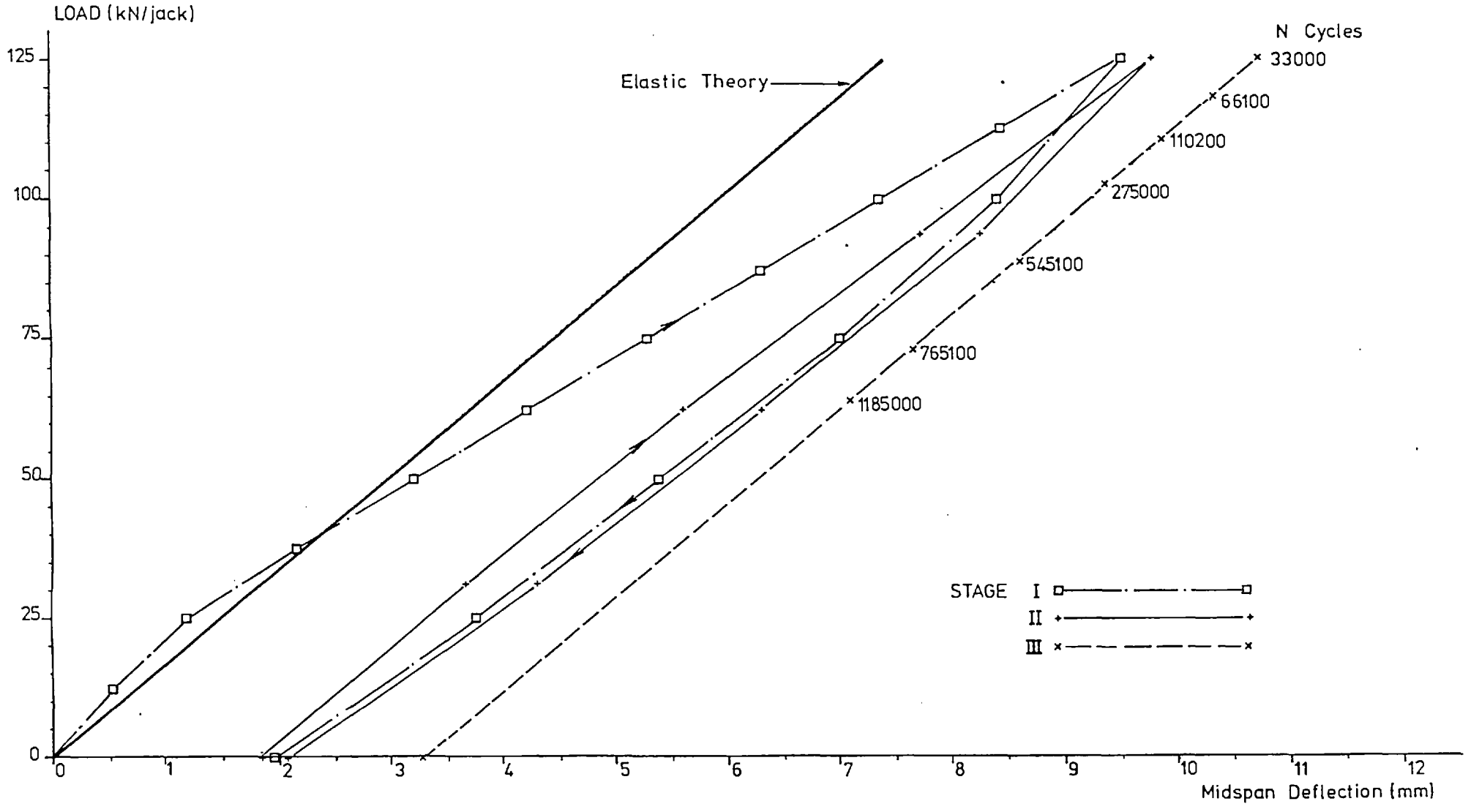


FIGURE 34: TEST 4 : MIDSPAN DEFLECTION - STAGES I, II & III

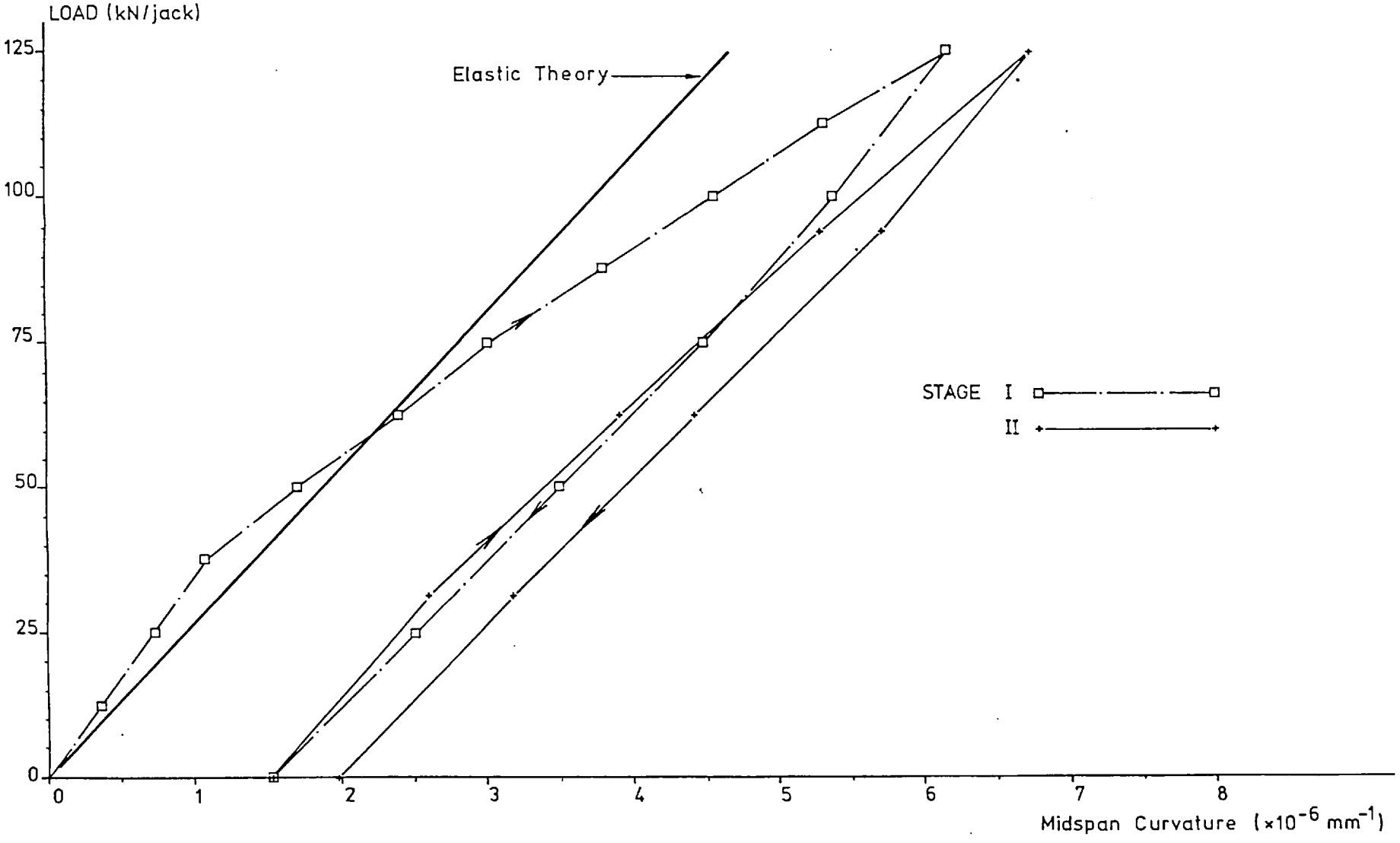


FIGURE 35: TEST 4 : MIDSPAN CURVATURE - STAGES I & II

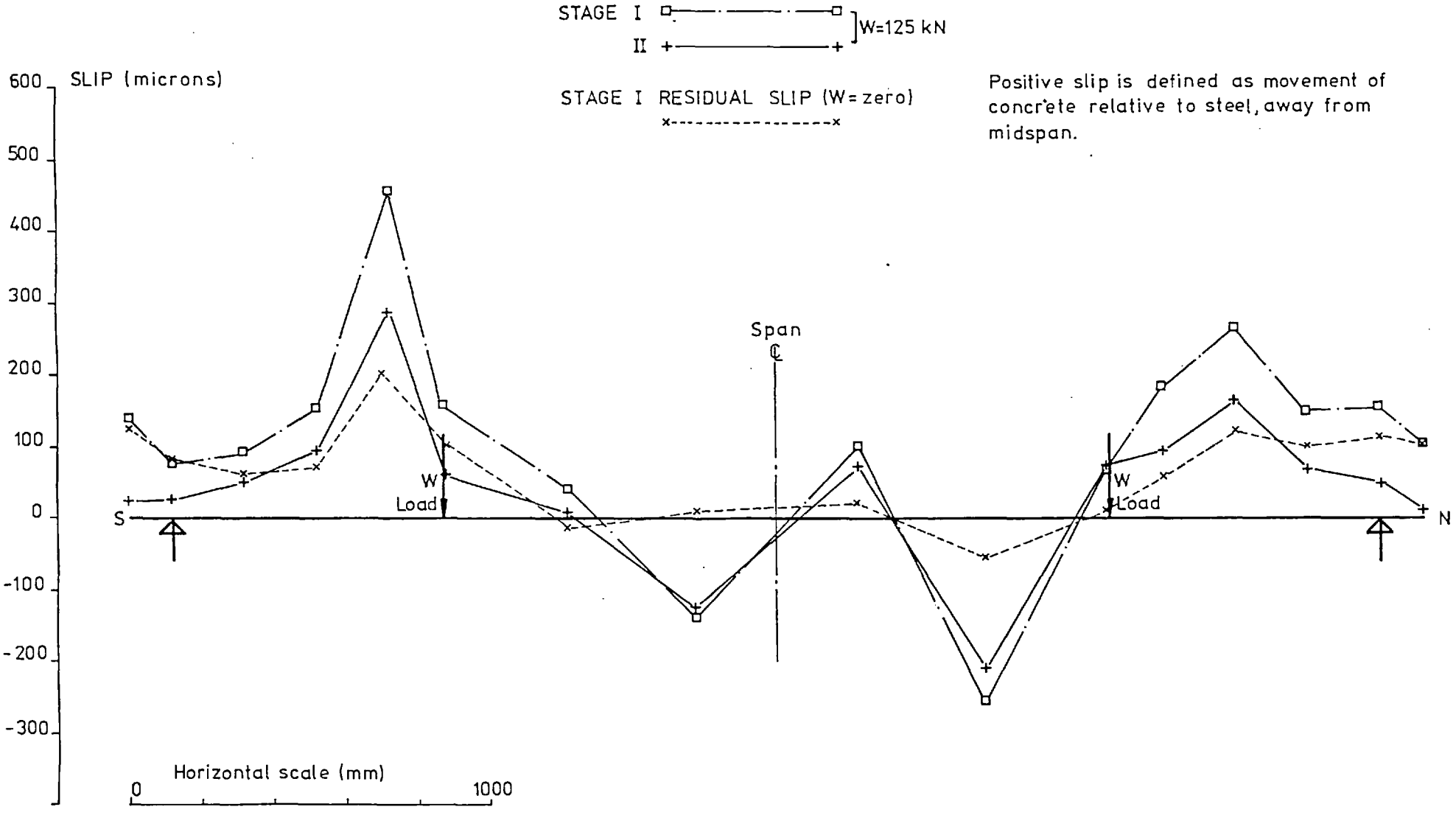


FIGURE 36: TEST 4: SLIP DISTRIBUTION AT 125 kN - STAGES I & II

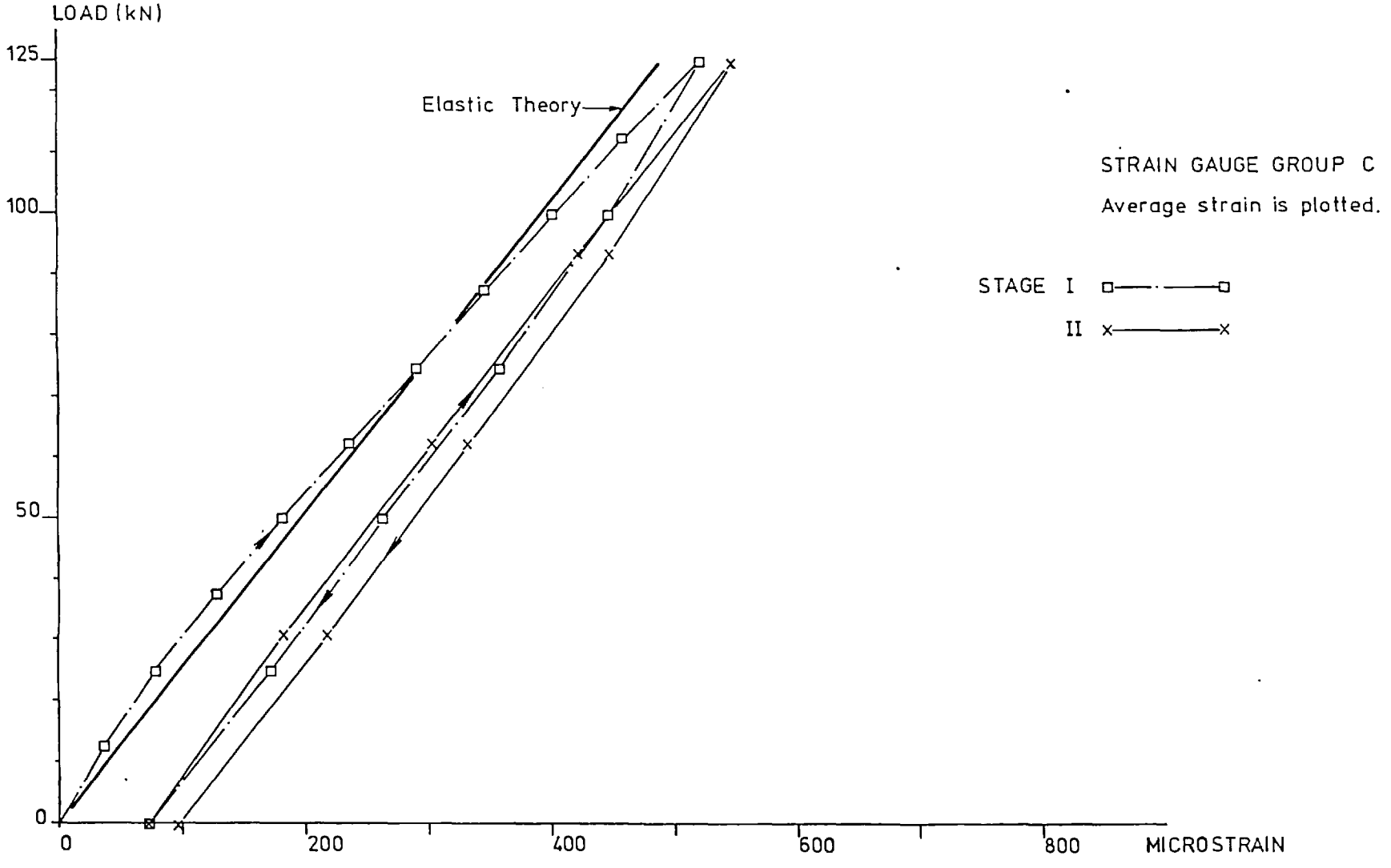


FIGURE 37: TEST 4 : CONCRETE SURFACE STRAIN - STAGES I & II

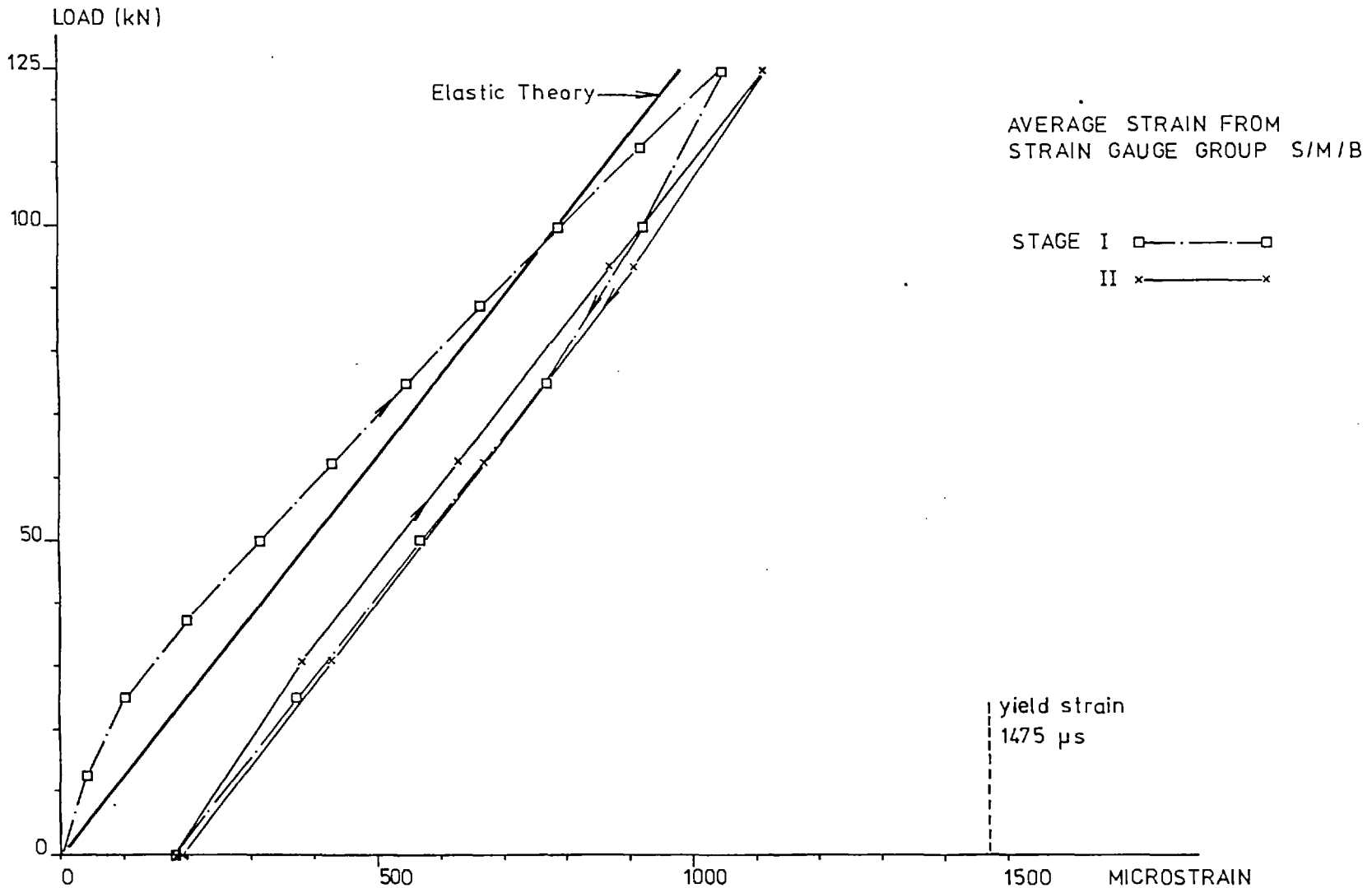


FIGURE 38: TEST 4 : STEEL BOTTOM FLANGE STRAIN - STAGES I & II

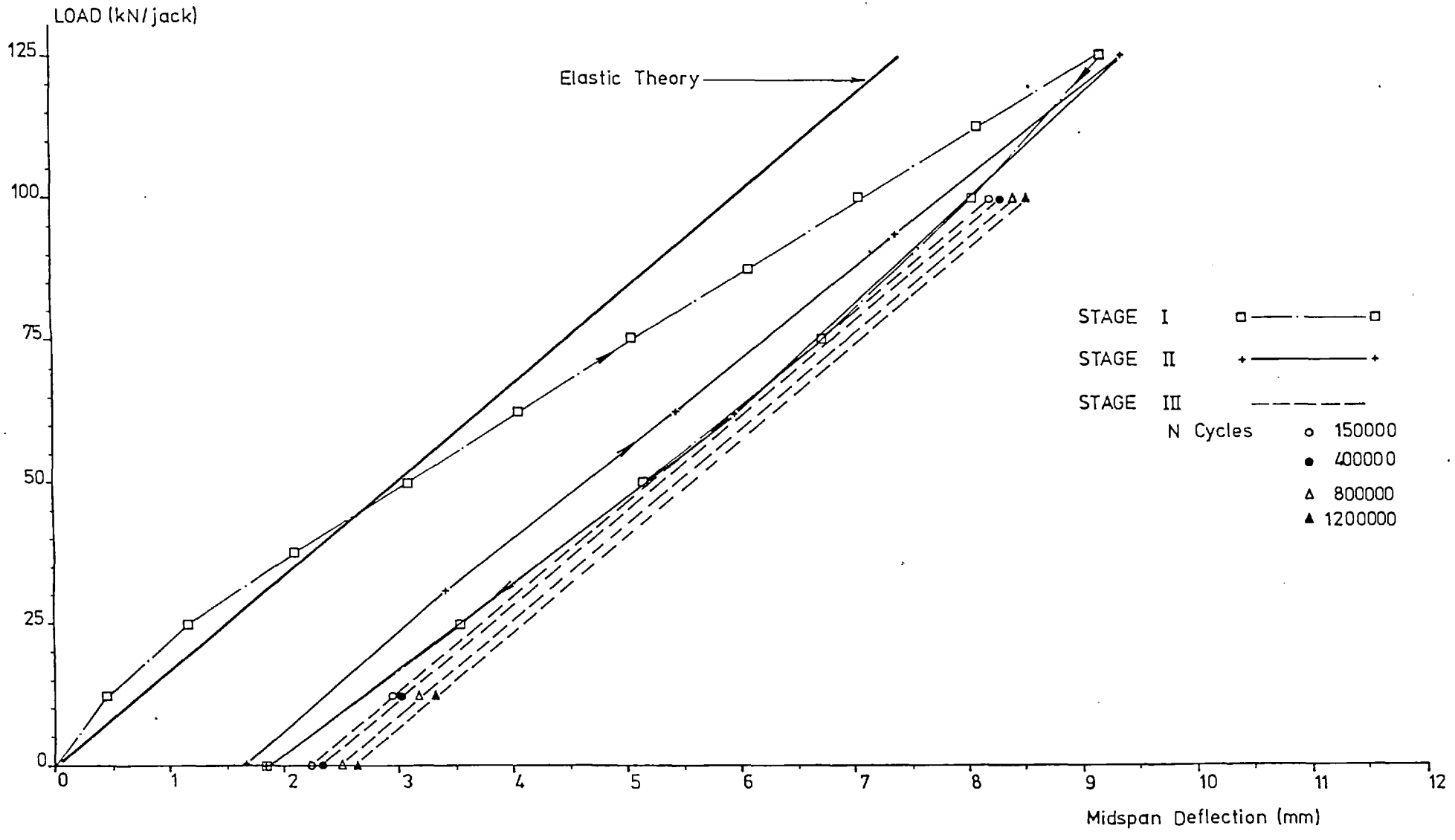


FIGURE 39: TEST 5 : MIDSPAN DEFLECTION - STAGES I, II & III

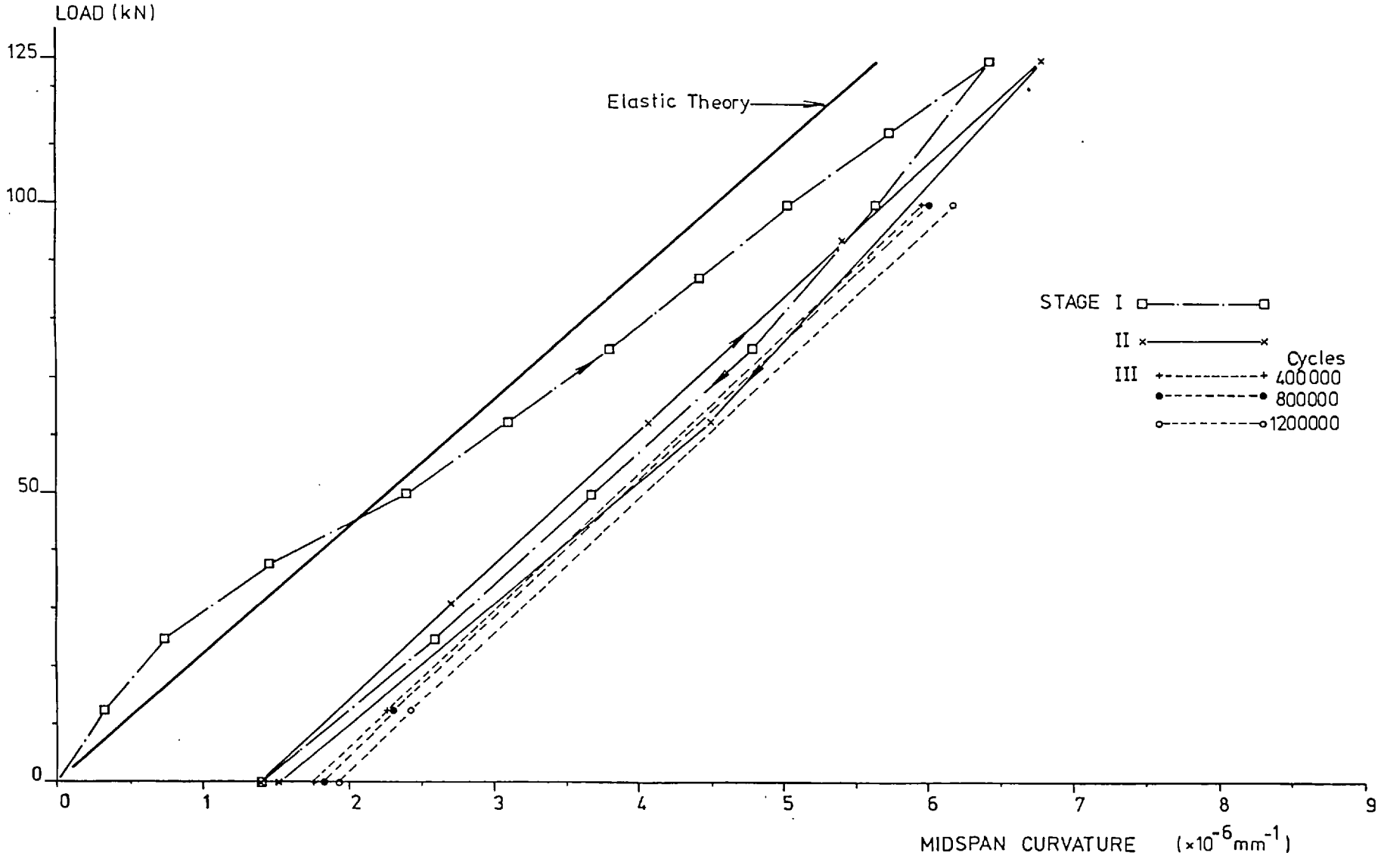


FIGURE 40: TEST 5 : MIDSPAN CURVATURE - STAGES I, II & III

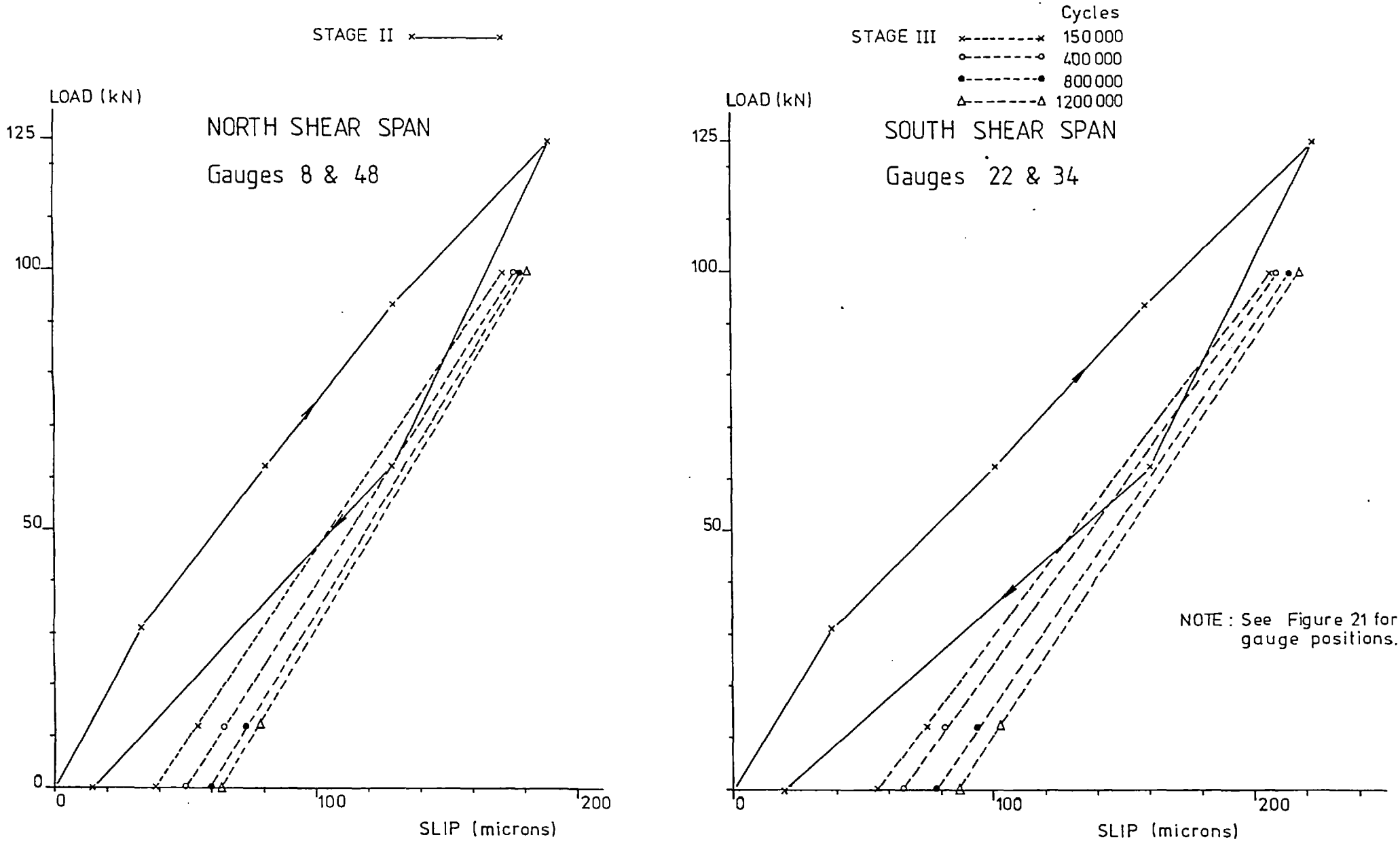


FIGURE 41: TEST 5 : MAXIMUM SLIP - STAGES I & II

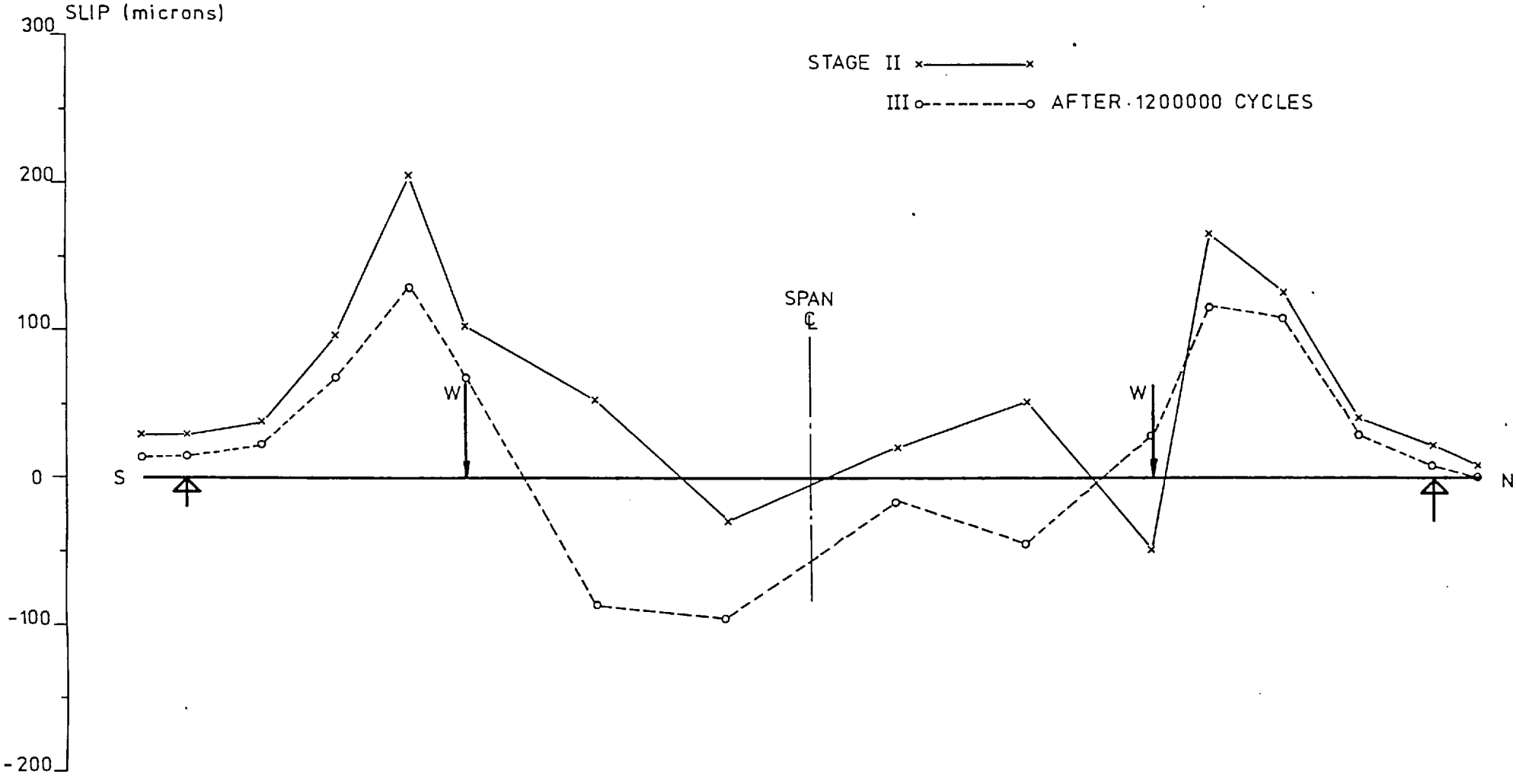


FIGURE 42: TEST 5 : SLIP DISTRIBUTION AT 100 kN, BEFORE AND AFTER STAGE III

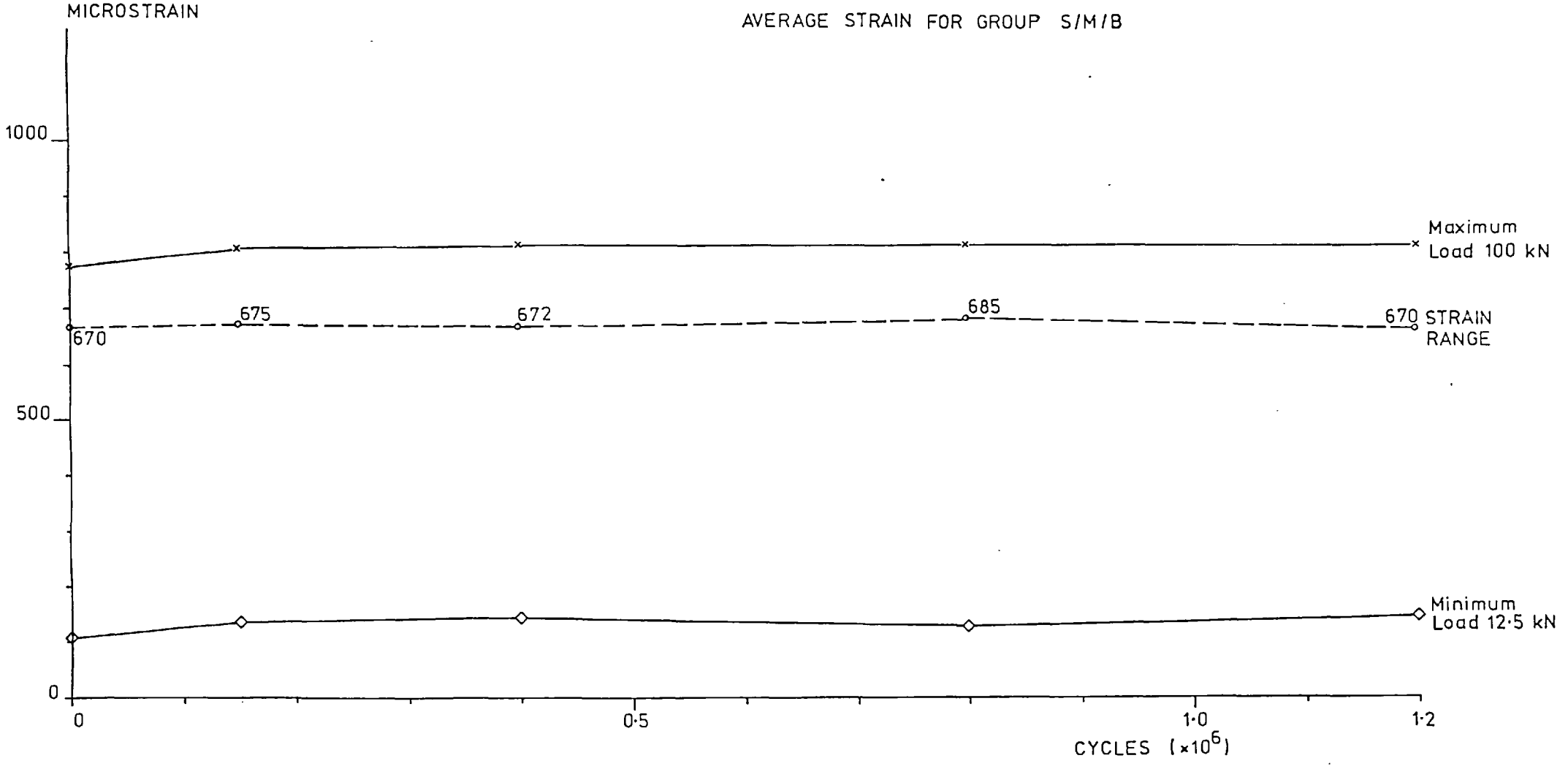


FIGURE 43: TEST 5 : STEEL BOTTOM FLANGE STRAIN - STAGE III

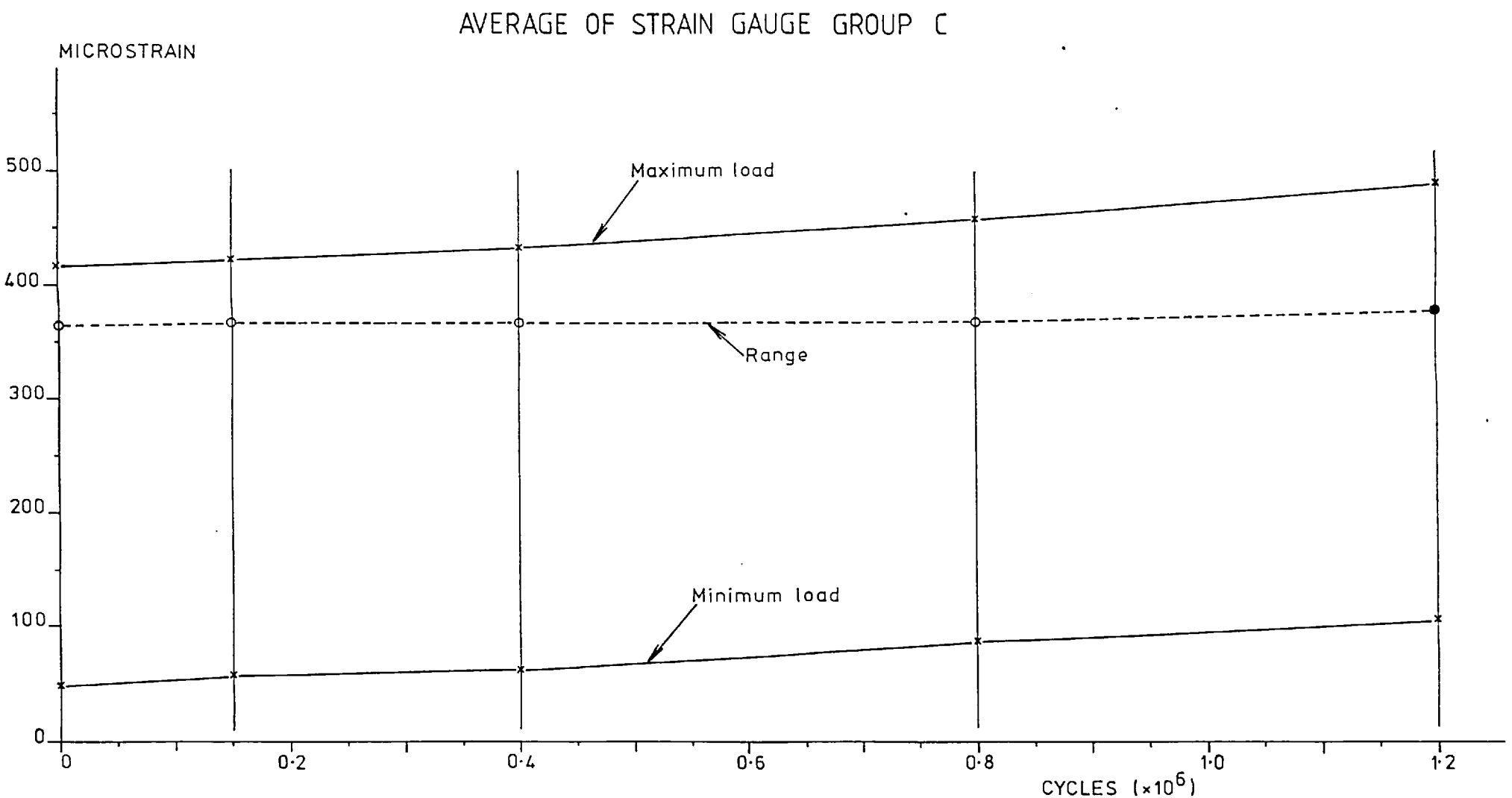


FIGURE 44: TEST 5 : CONCRETE SURFACE STRAIN - STAGE III

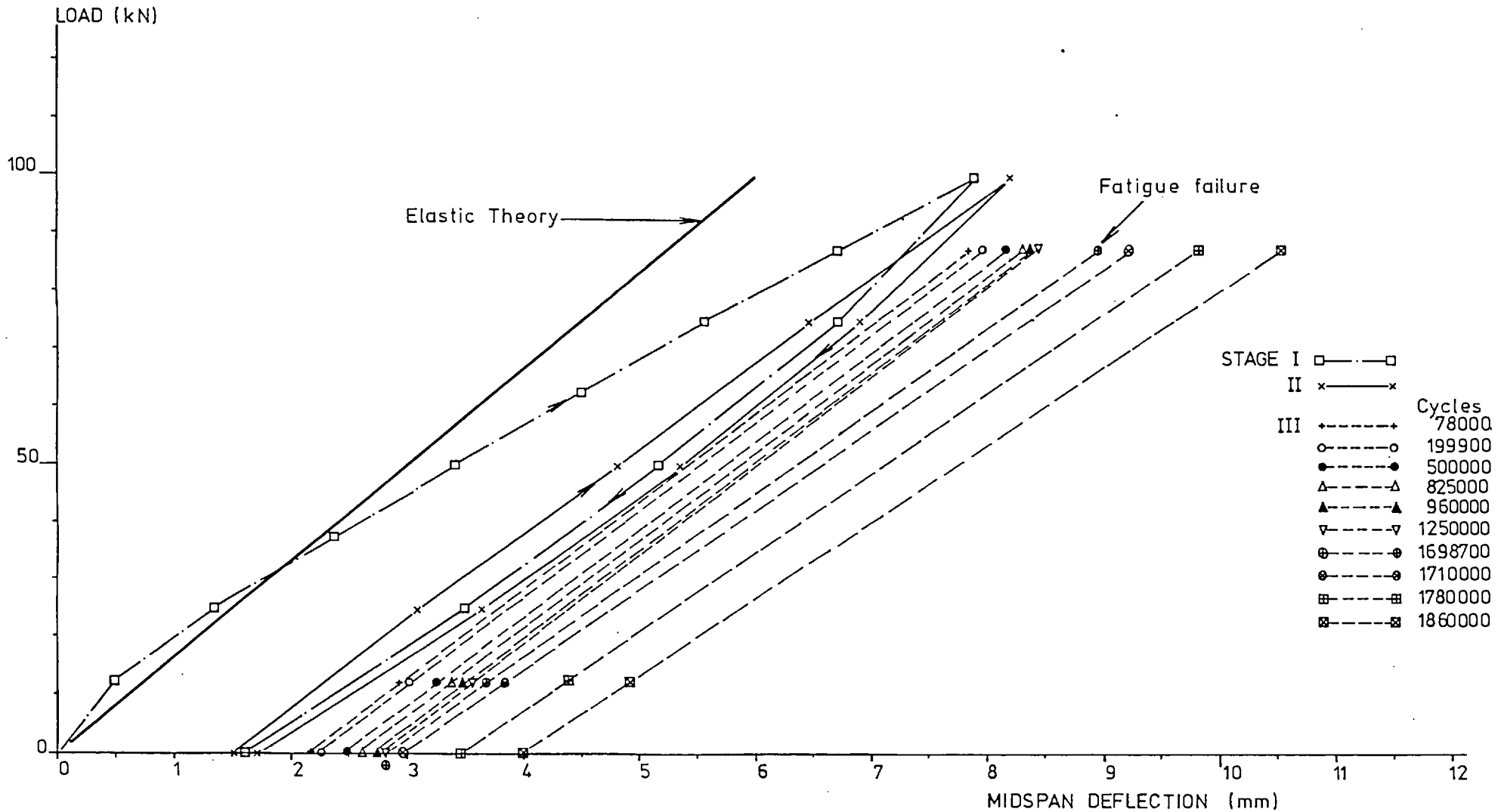


FIGURE 45: TEST 6 : MIDSPAN DEFLECTION - STAGES I, II & III

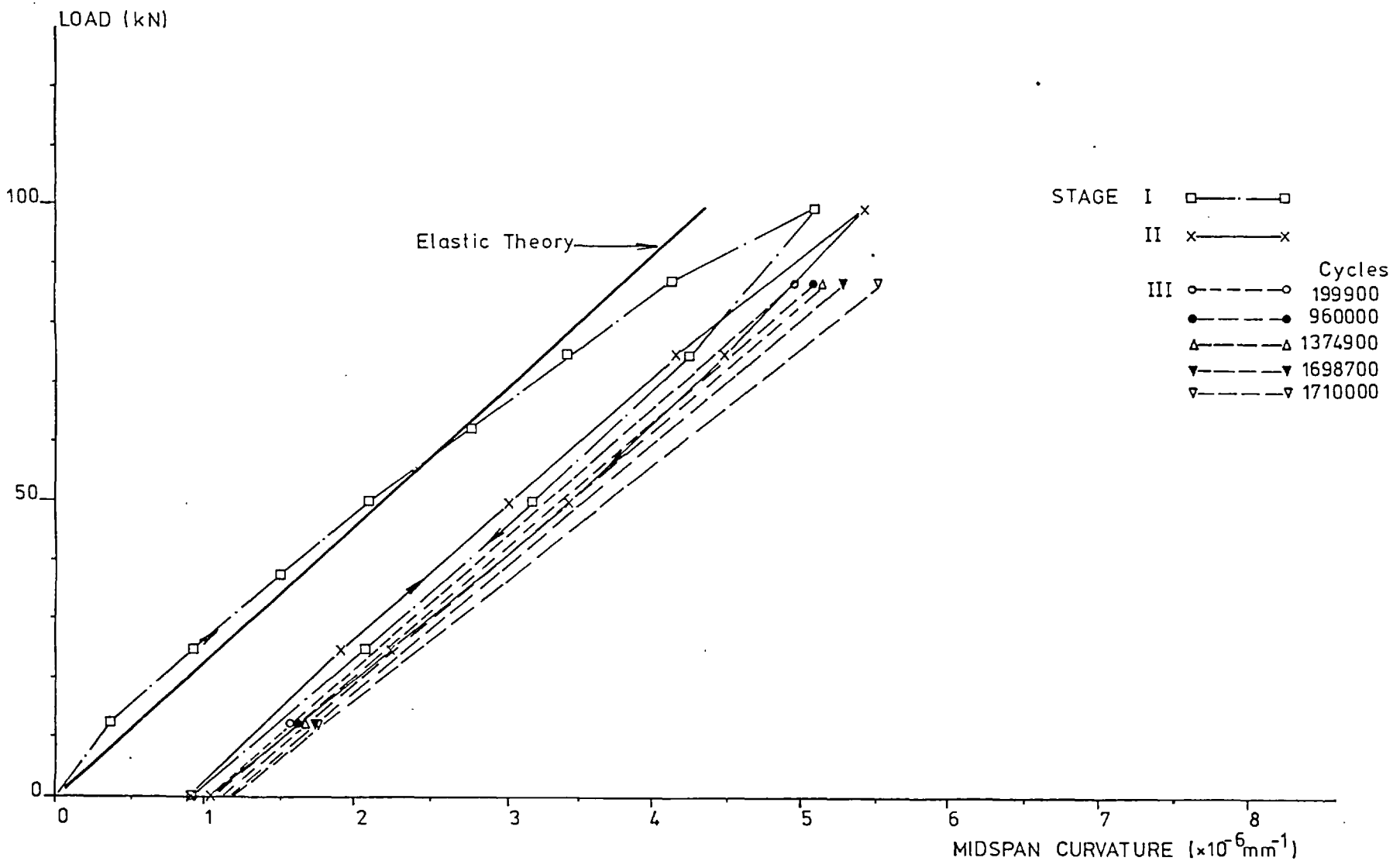


FIGURE 46: TEST 6 : MIDSPAN CURVATURE - STAGES I, II & III

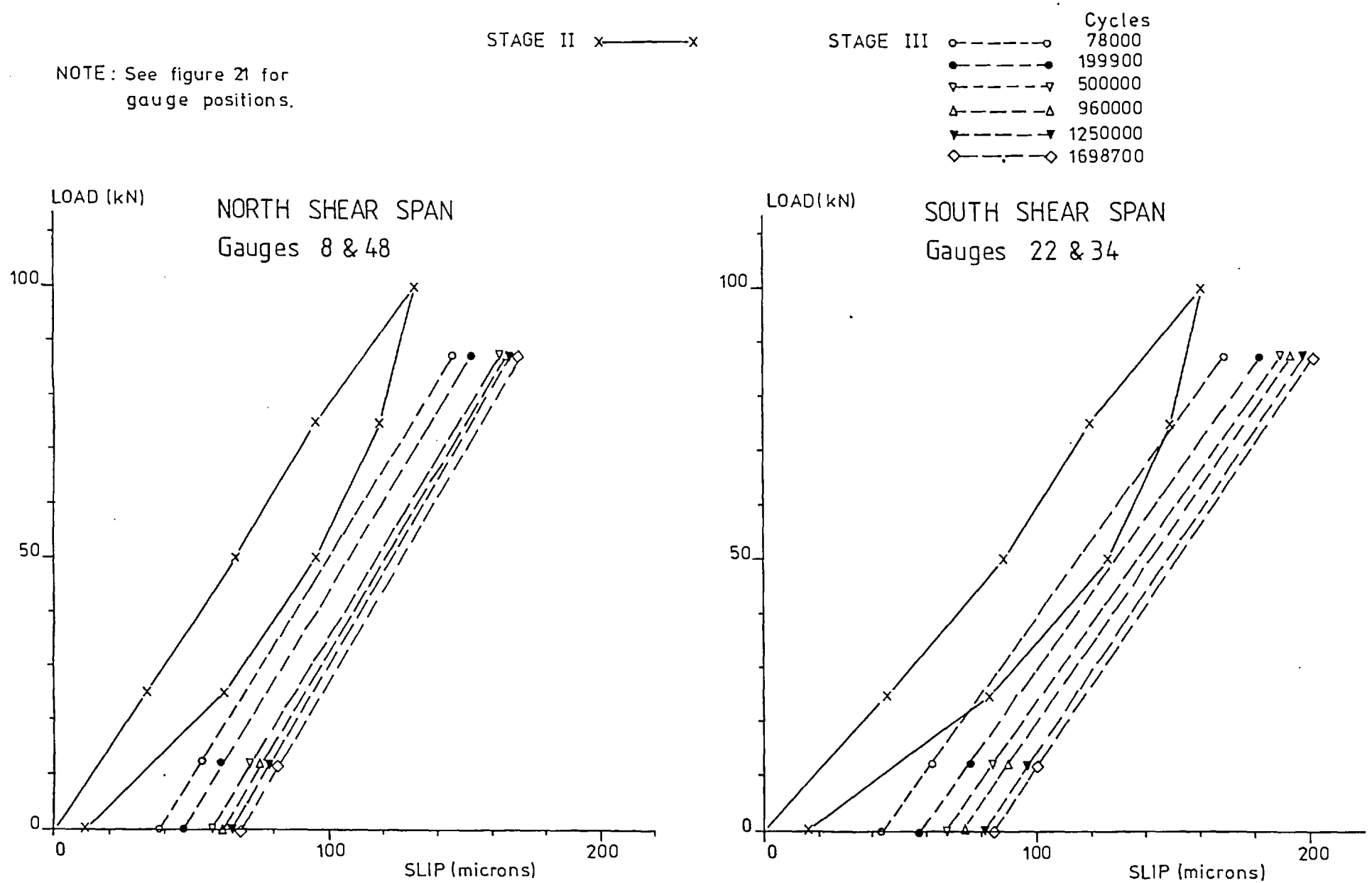


FIGURE 47: TEST 6 : MAXIMUM SLIP - STAGES II & III

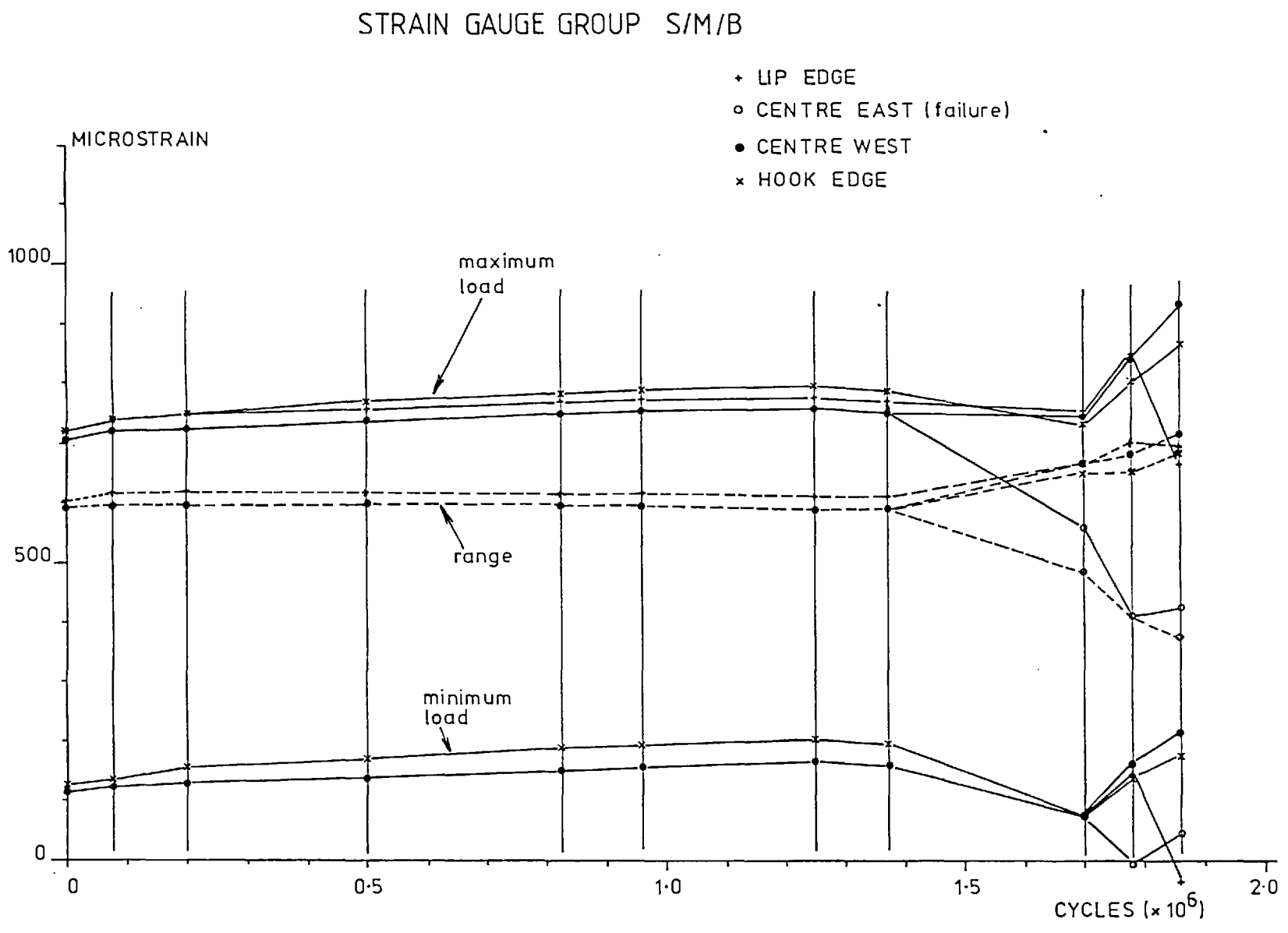


FIGURE 48: TEST 6 : STEEL BOTTOM FLANGE STRAIN - STAGE III

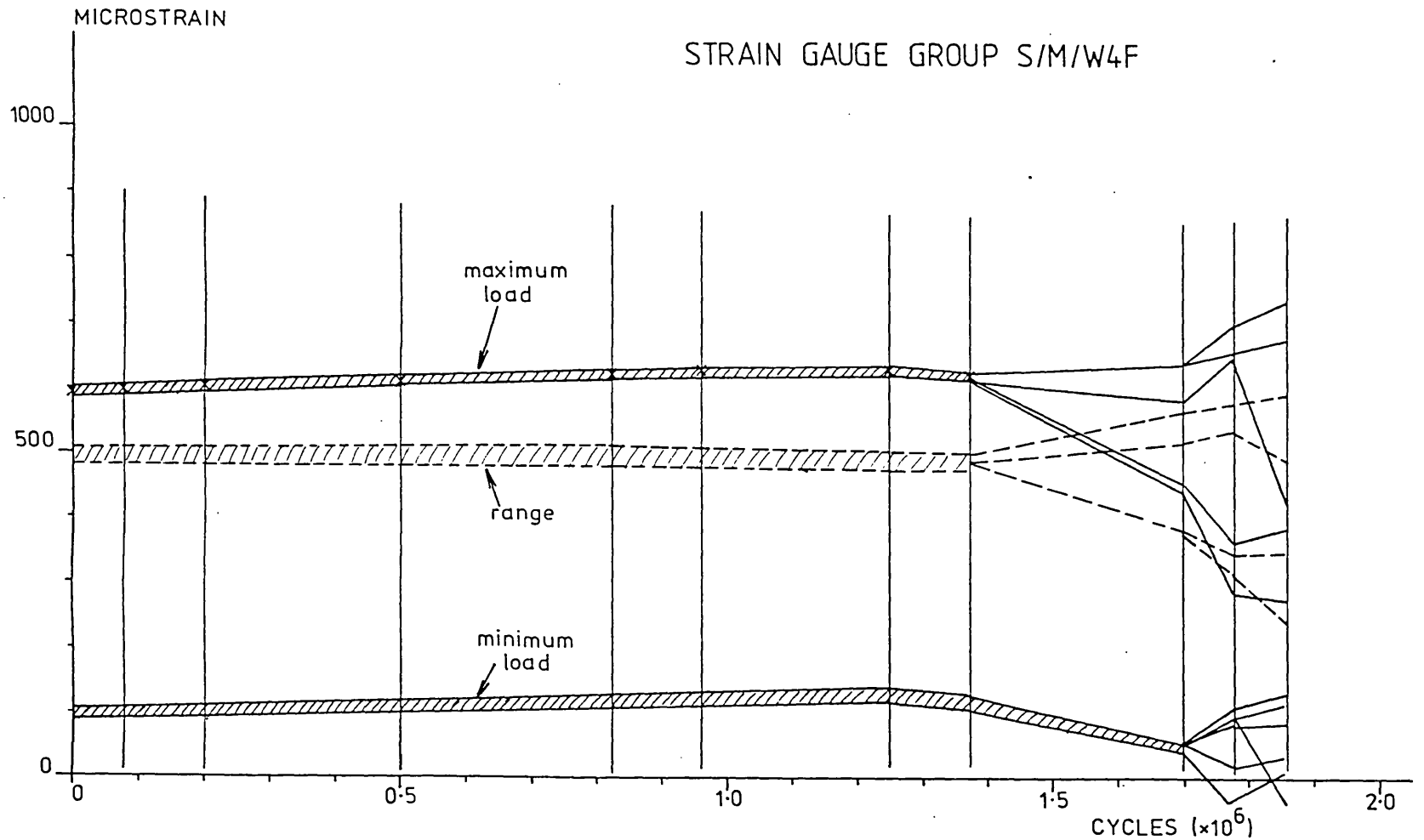
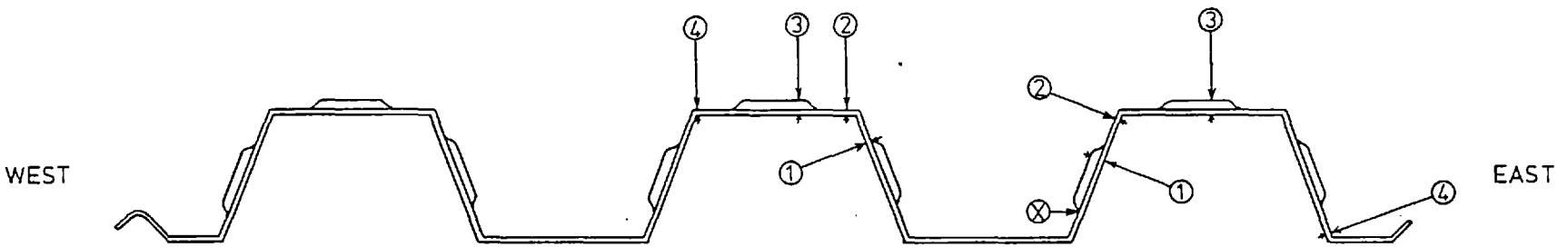


FIGURE 49: TEST 6 : STEEL LOWER WEB STRAIN - STAGE III

⊗ POINT OF ORIGIN OF CRACK



EXTENT OF FATIGUE CRACK AT N CYCLES

POSITION	1	1698700
	2	1710000
	3	1780000
	4	1860000

FIGURE 50: TEST 6 : PROPAGATION OF FATIGUE CRACK

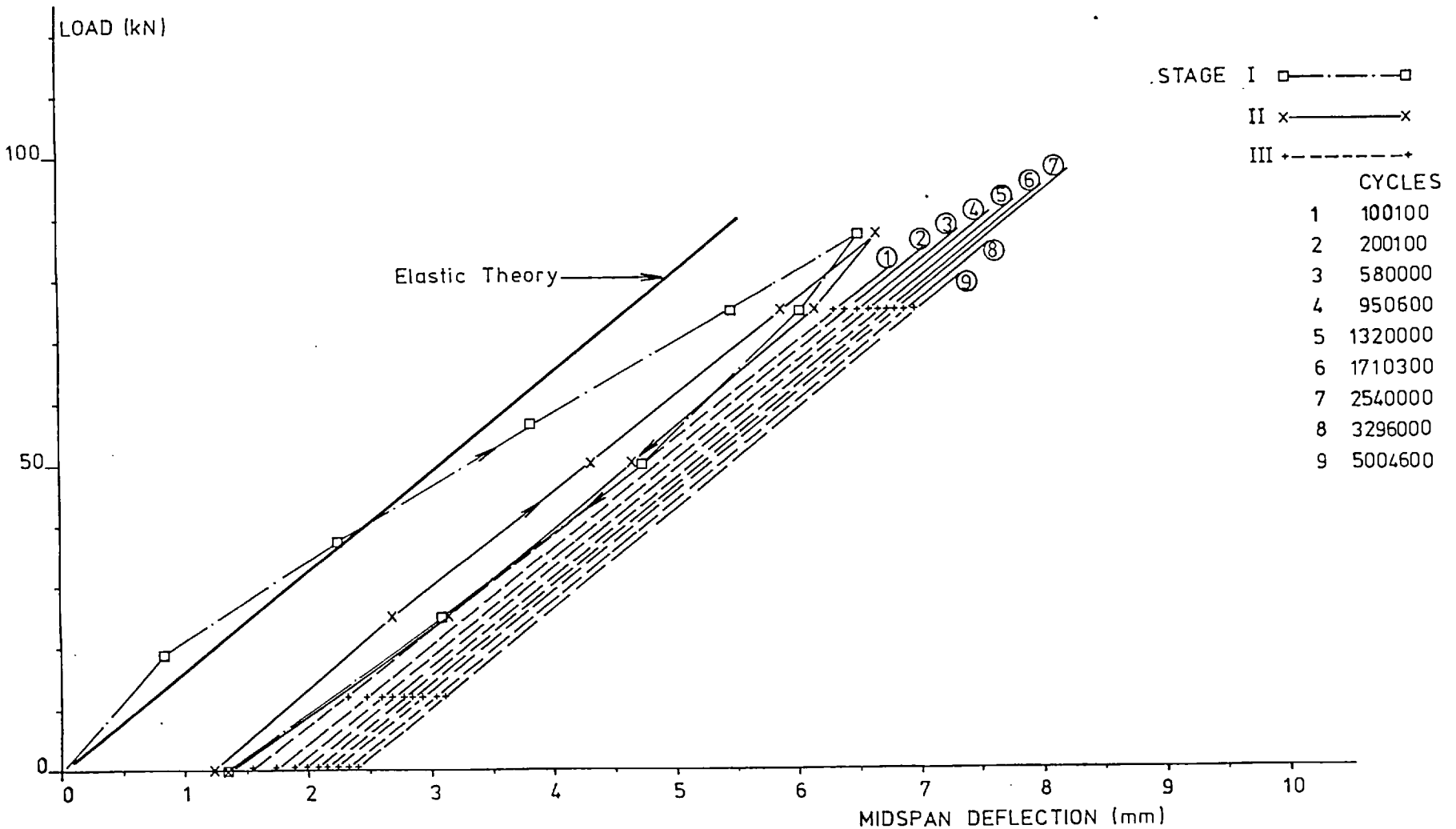
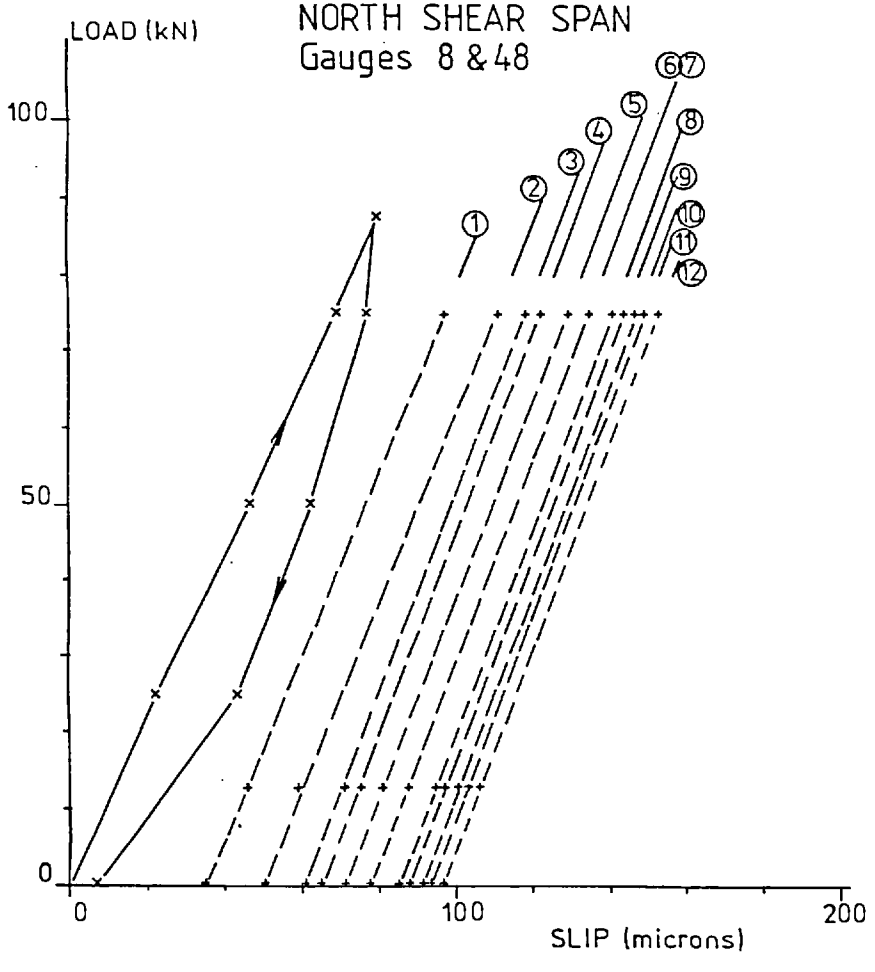


FIGURE 51: TEST 7 : MIDSPAN DEFLECTION - STAGES I, II & III

STAGE II ×——×

STAGE III +– – –+

	CYCLES		CYCLES
1	100100	7	1800200
2	200100	8	2180000
3	580000	9	2540000
4	950600	10	2900000
5	1320000	11	3296000
6	1710300	12	5004600



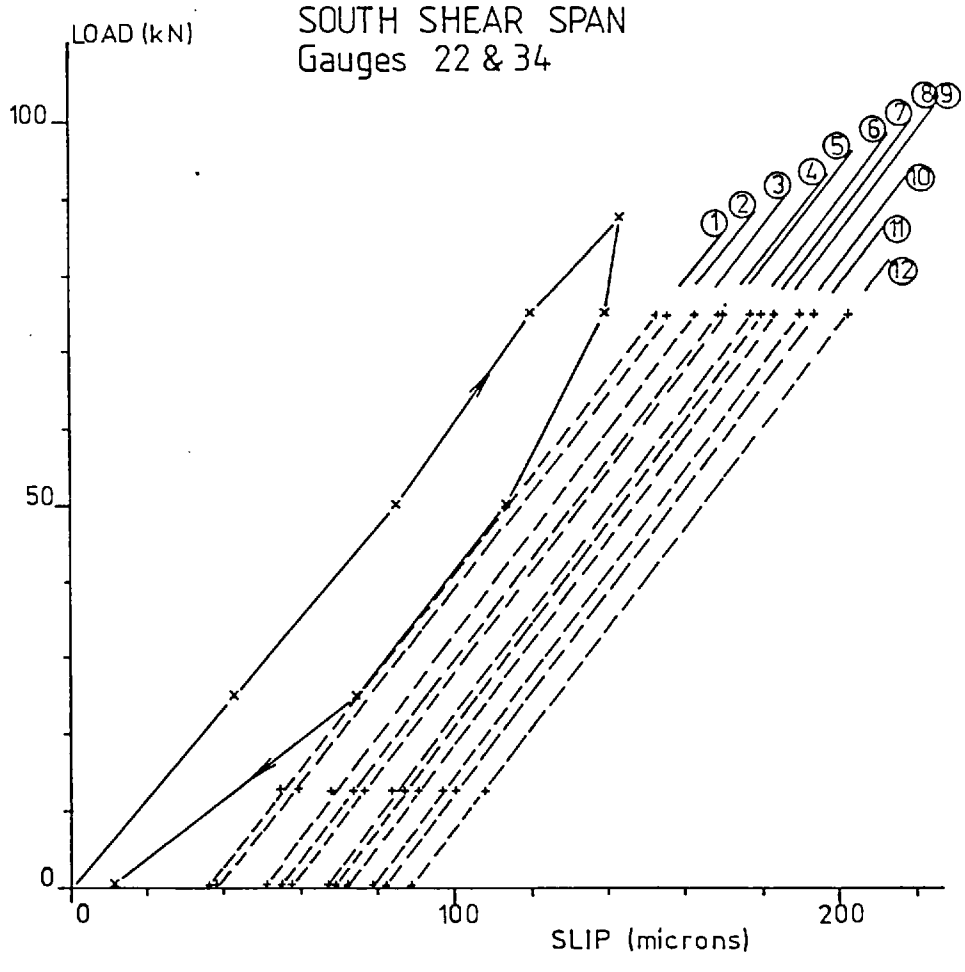


FIGURE 52: TEST 7 : MAXIMUM SLIP - STAGES II & III

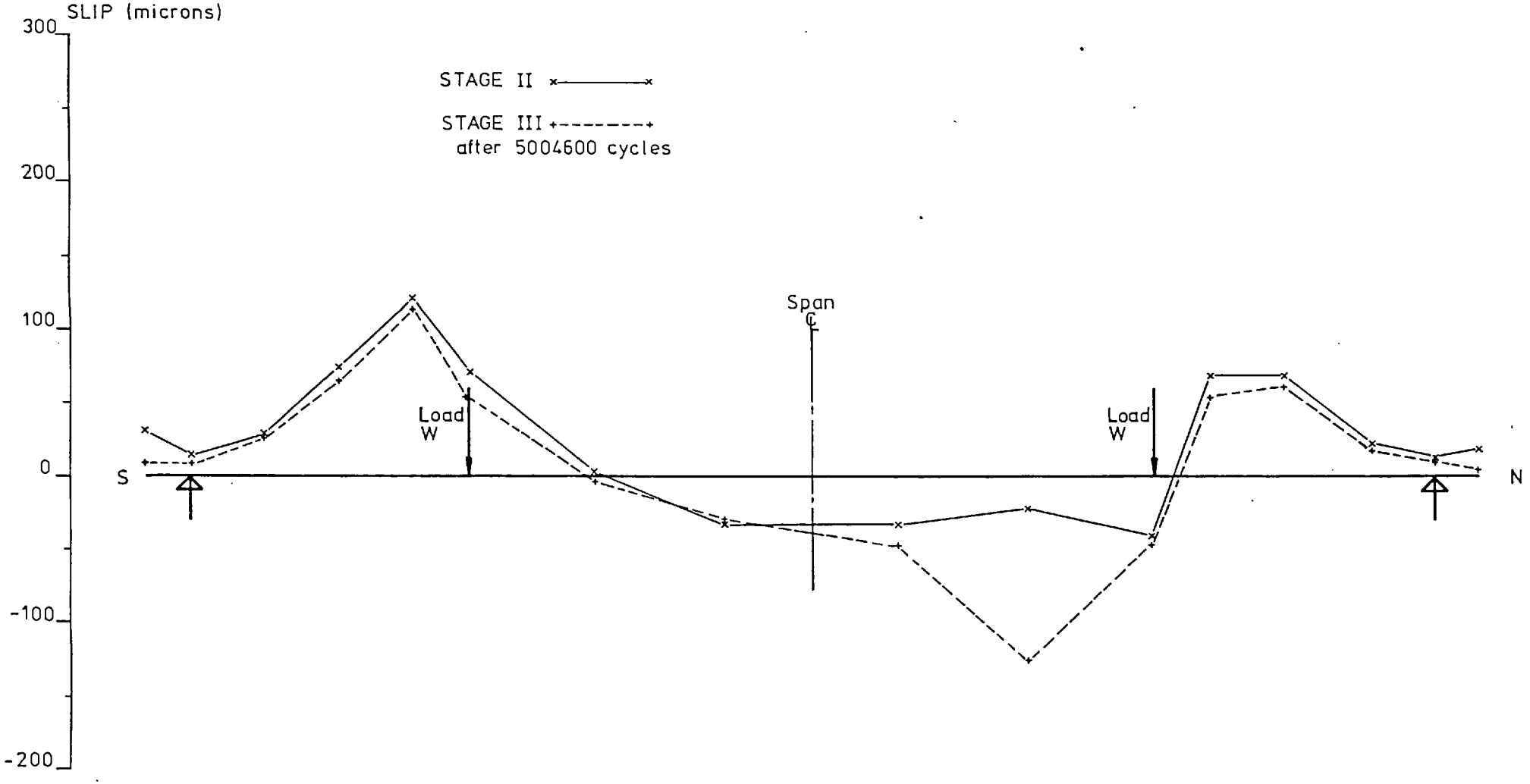


FIGURE 53: TEST 7 : SLIP DISTRIBUTION AT 75 kN - STAGES II & III

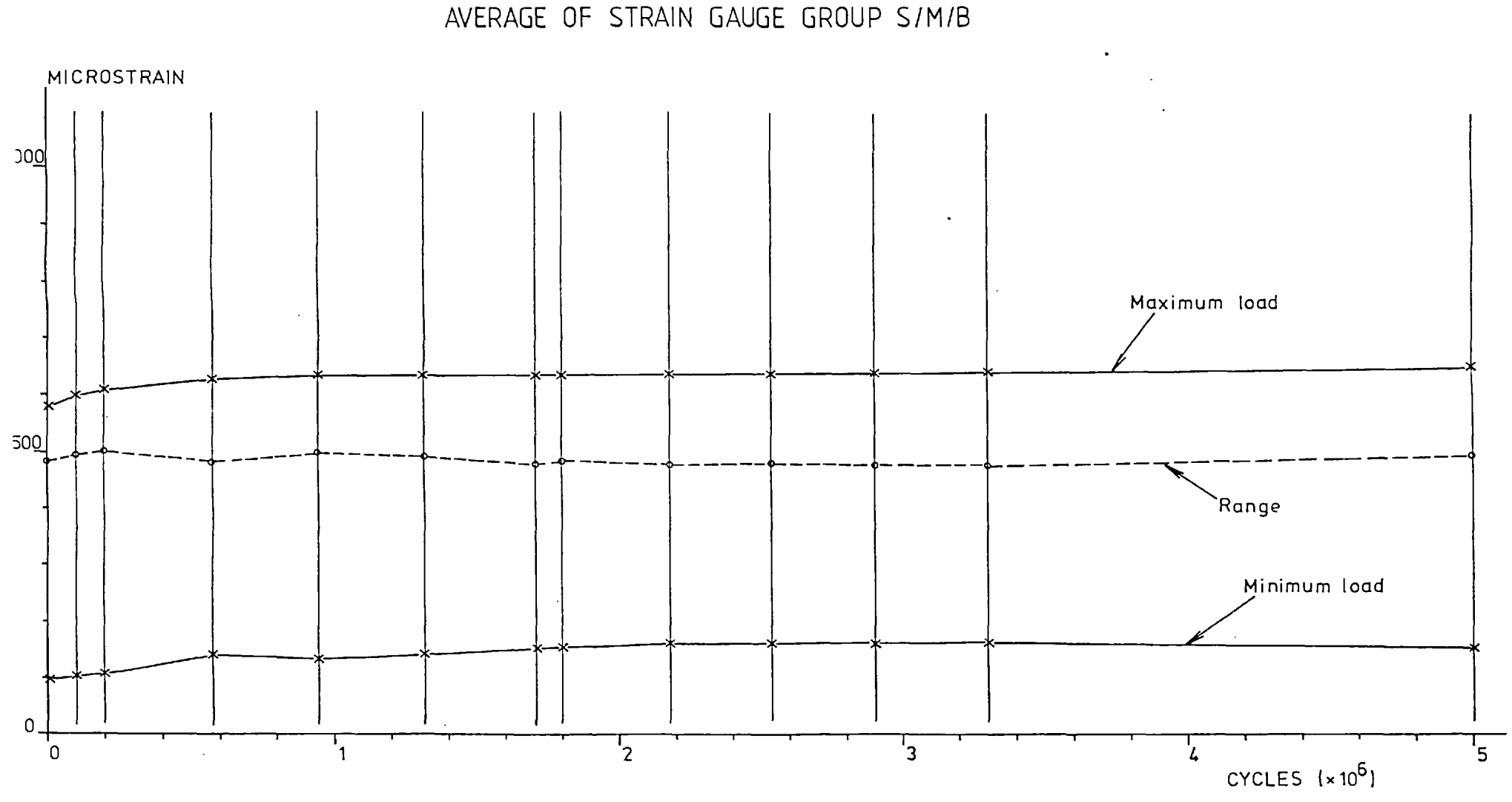


FIGURE 54: TEST 7 : STEEL BOTTOM FLANGE STRAIN - STAGE III

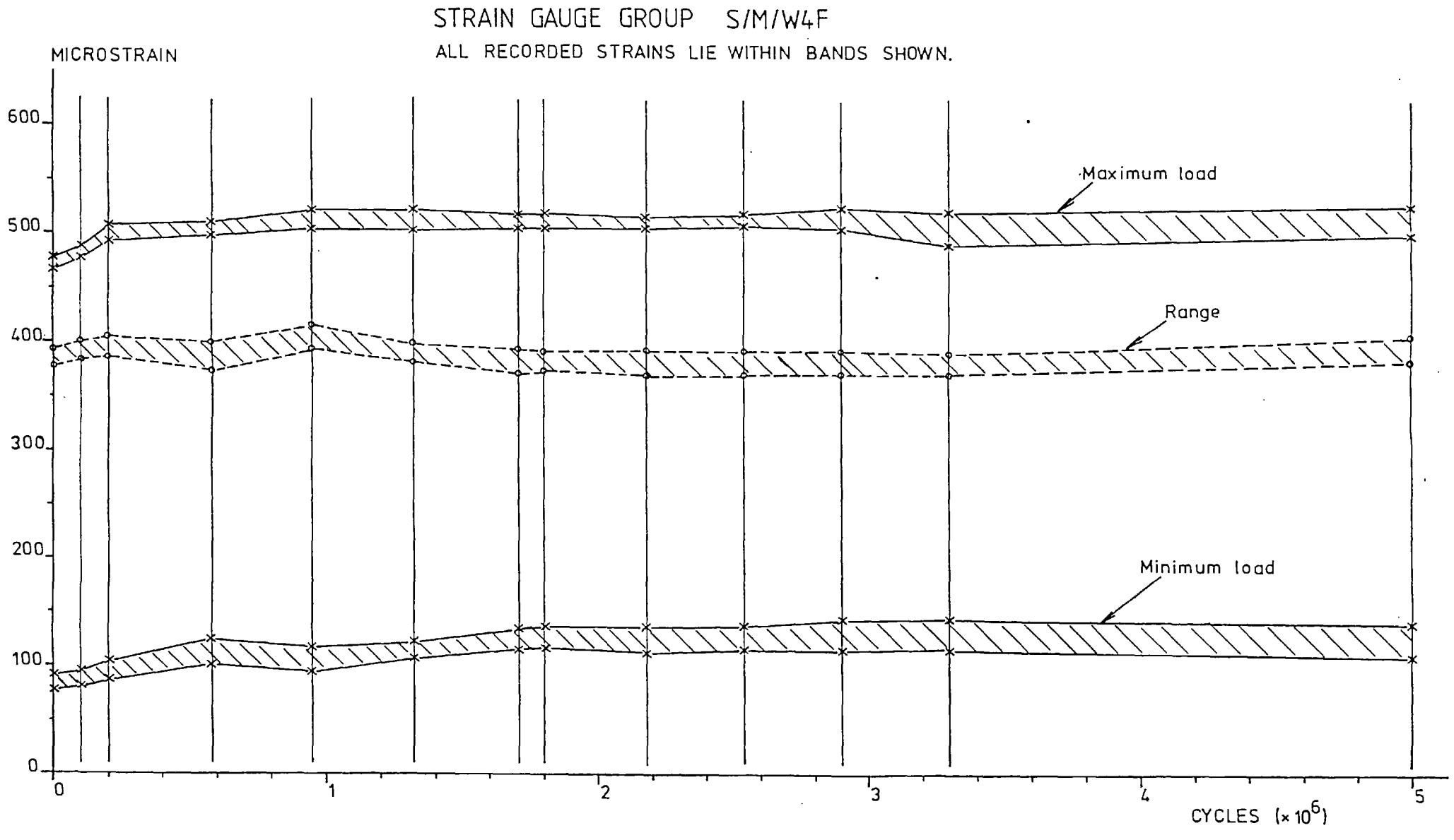


FIGURE 55: TEST 7 : STEEL LOWER WEB STRAIN - STAGE III

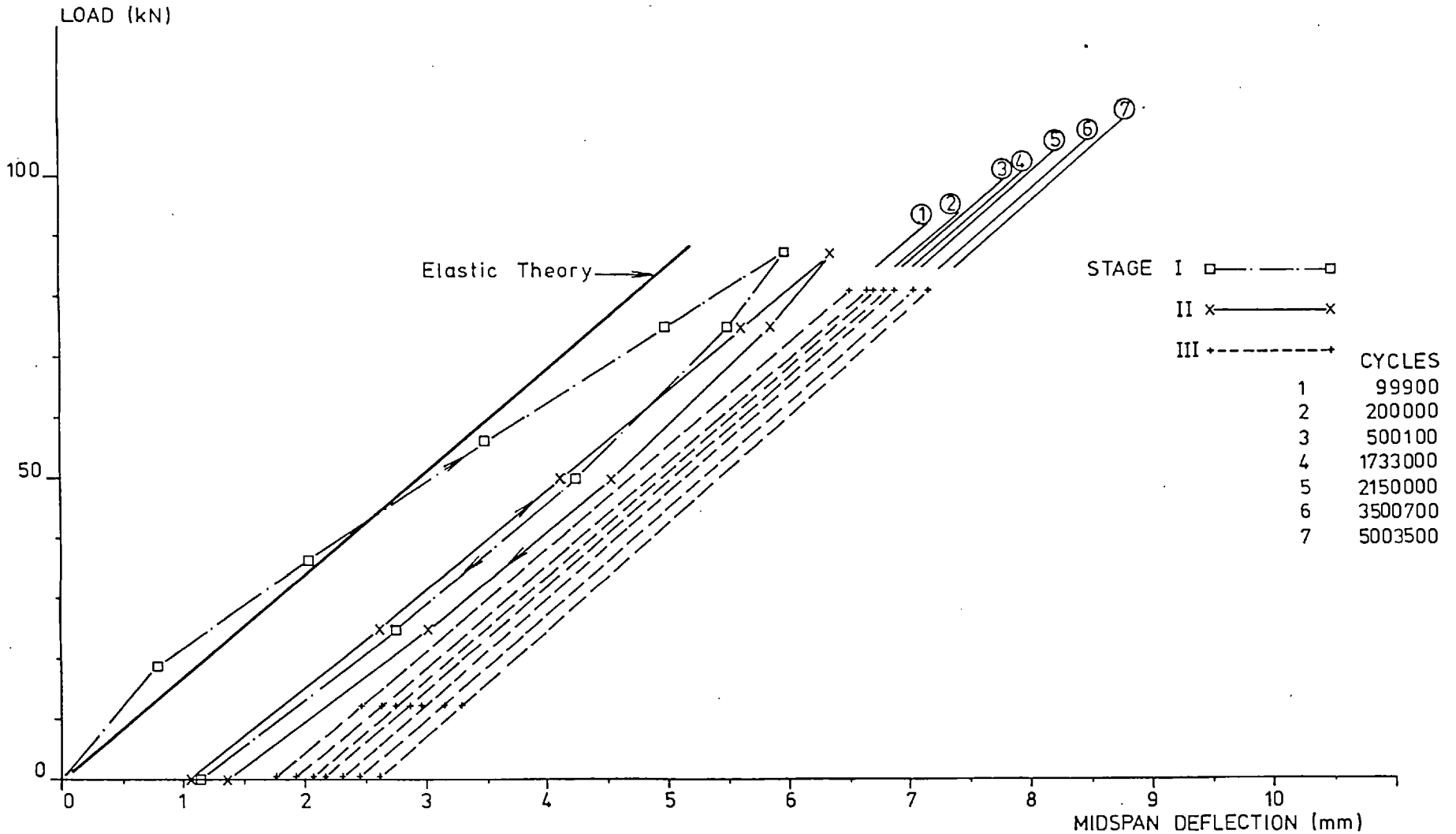


FIGURE 56: TEST 8 : MIDSPAN DEFLECTION - STAGES I, II & III

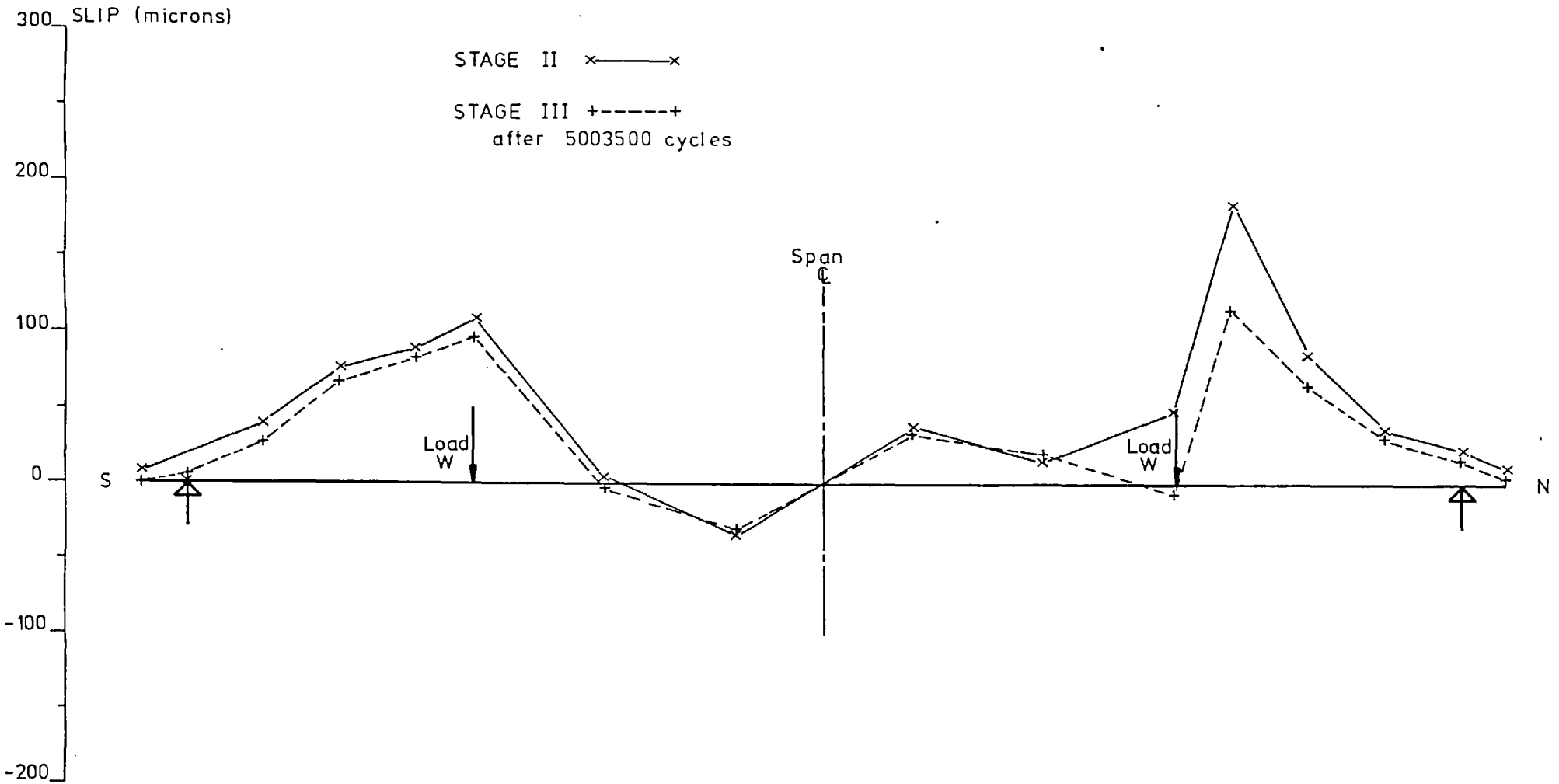


FIGURE 57: TEST 8 : SLIP DISTRIBUTION AT 81.25 kN - STAGES II & III

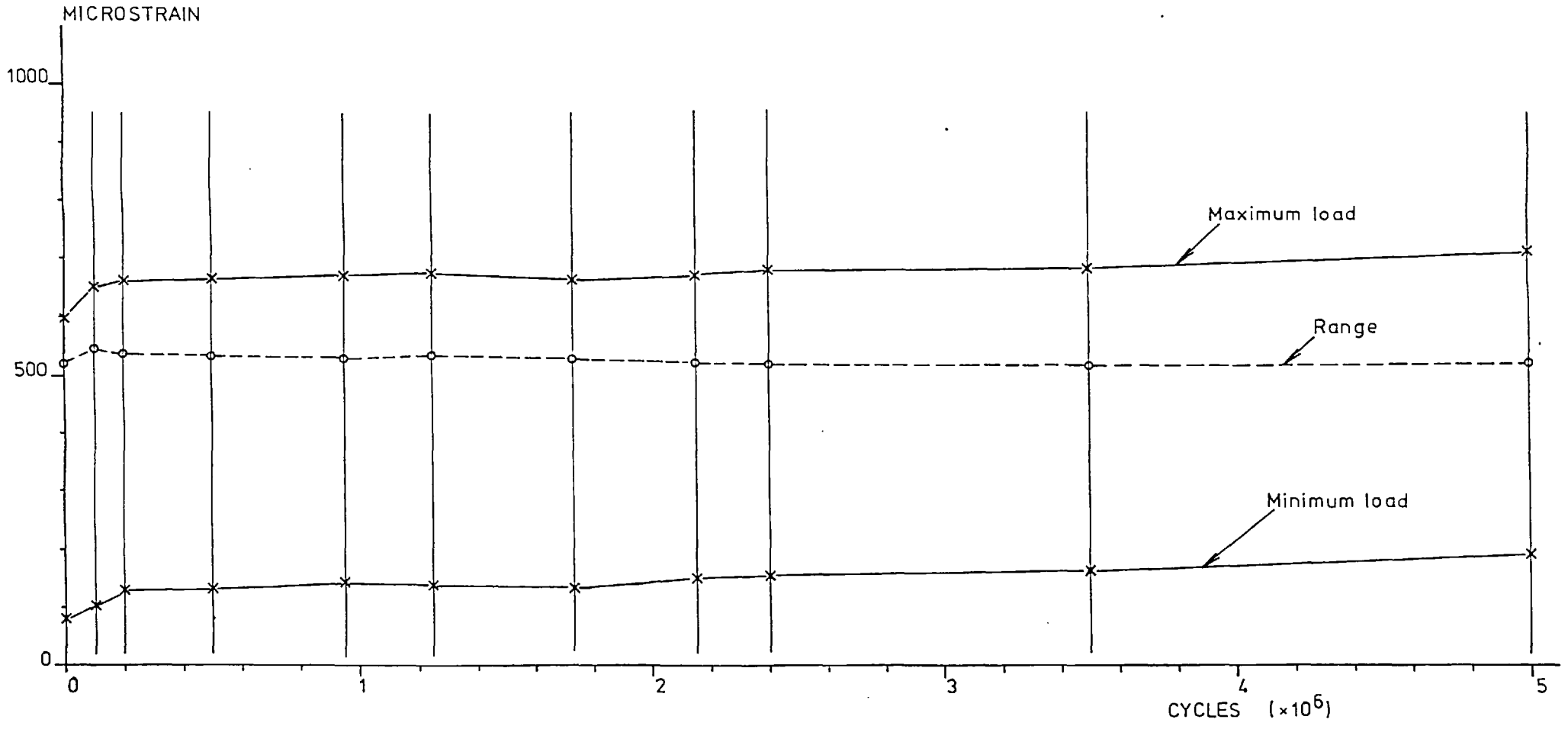


FIGURE 58: TEST 8 : STEEL BOTTOM FLANGE STRAIN - STAGE III

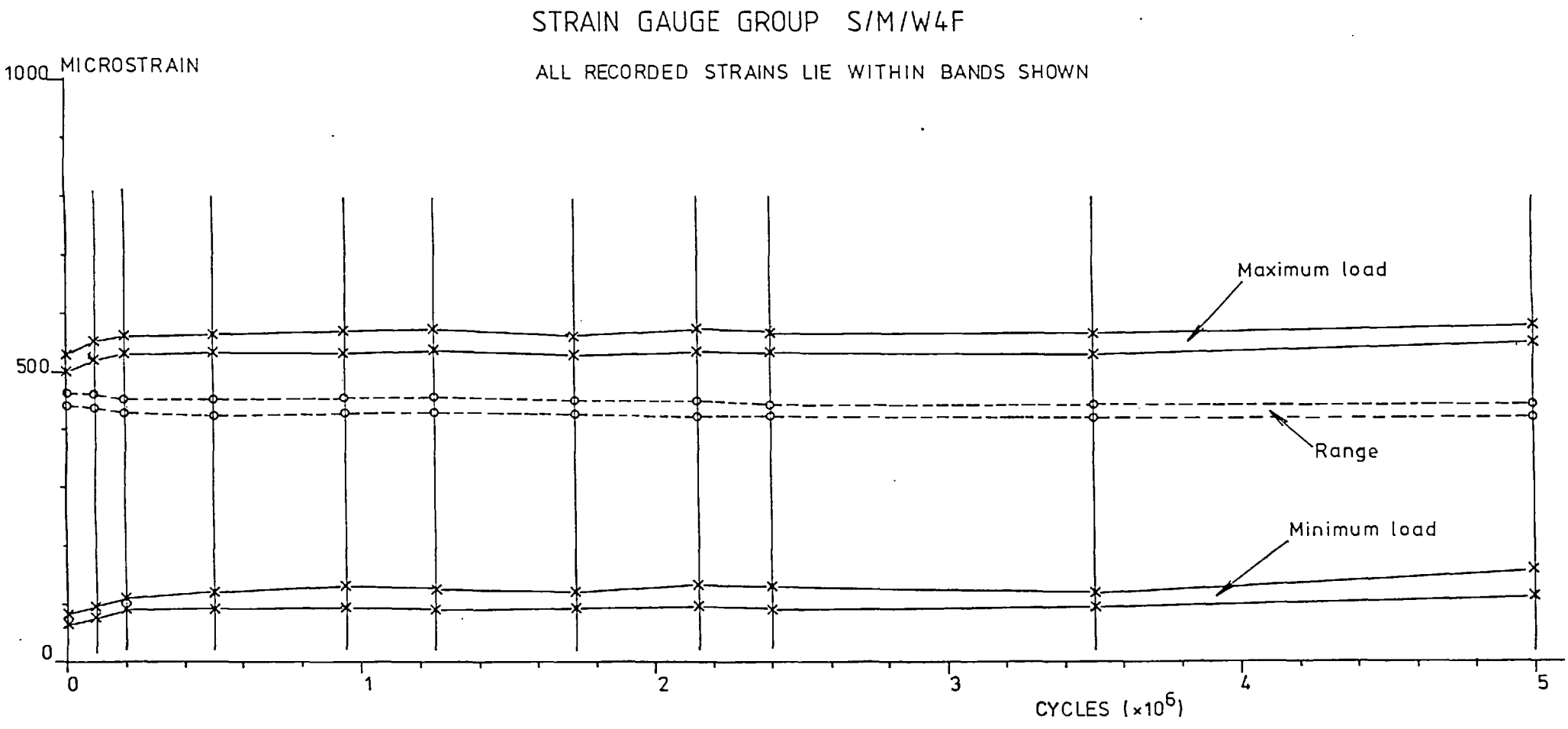


FIGURE 59: TEST 8 : STEEL LOWER WEB STRAIN - STAGE III

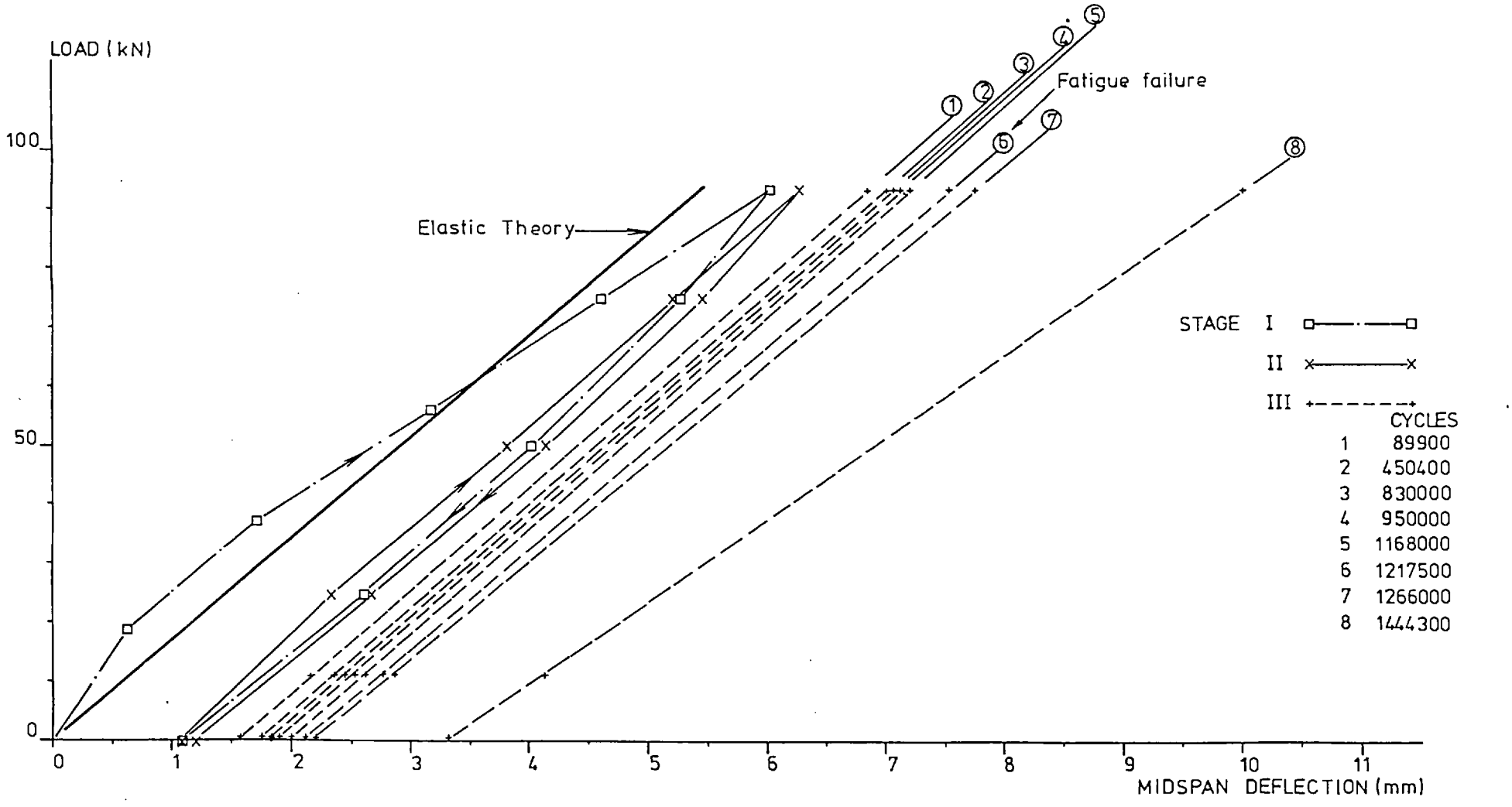


FIGURE 60: TEST 9 : MIDSPAN DEFLECTION - STAGES I, II & III

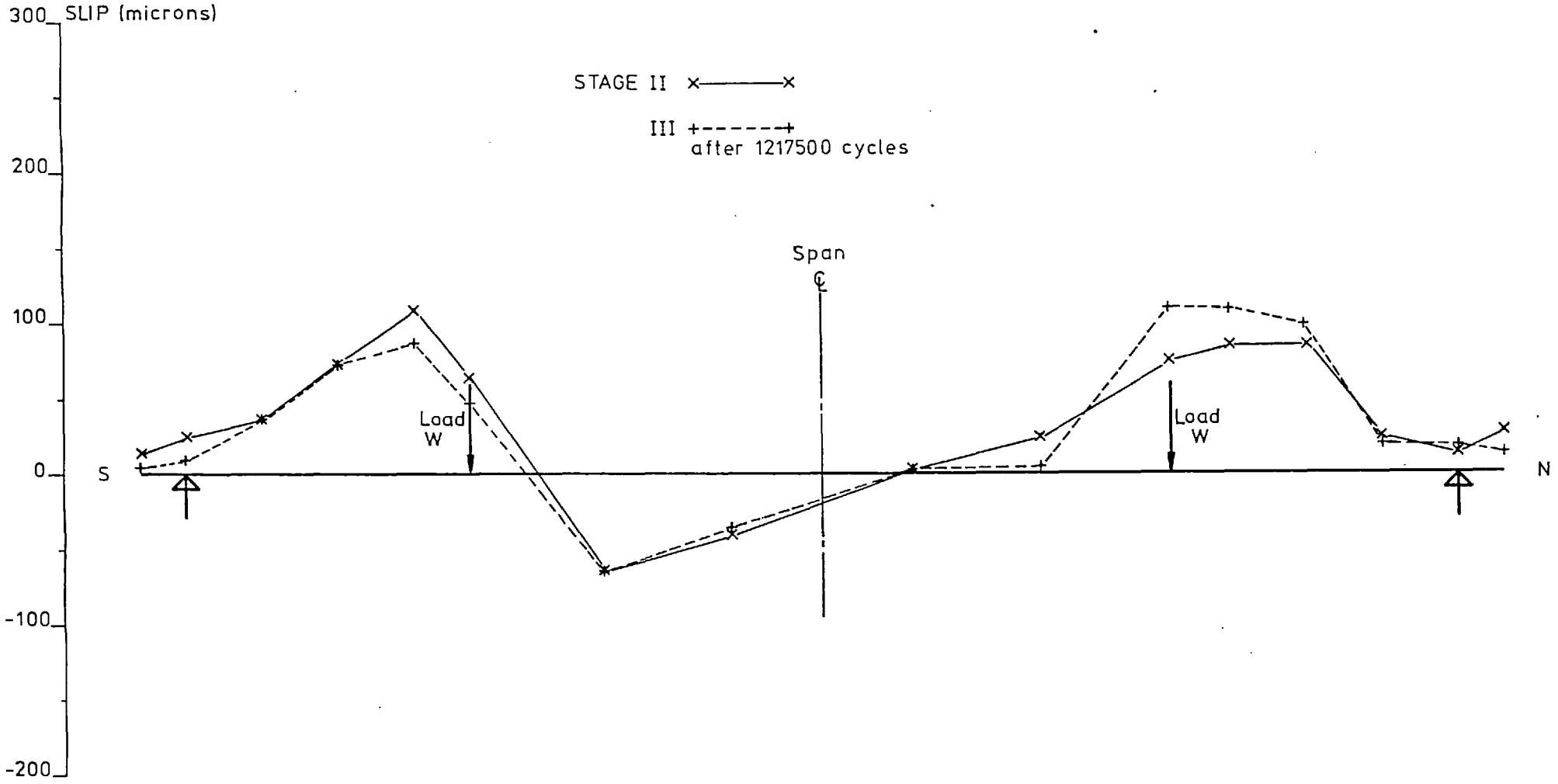


FIGURE 61: TEST 9 : SLIP DISTRIBUTION AT 93.75 kN - STAGES II & III

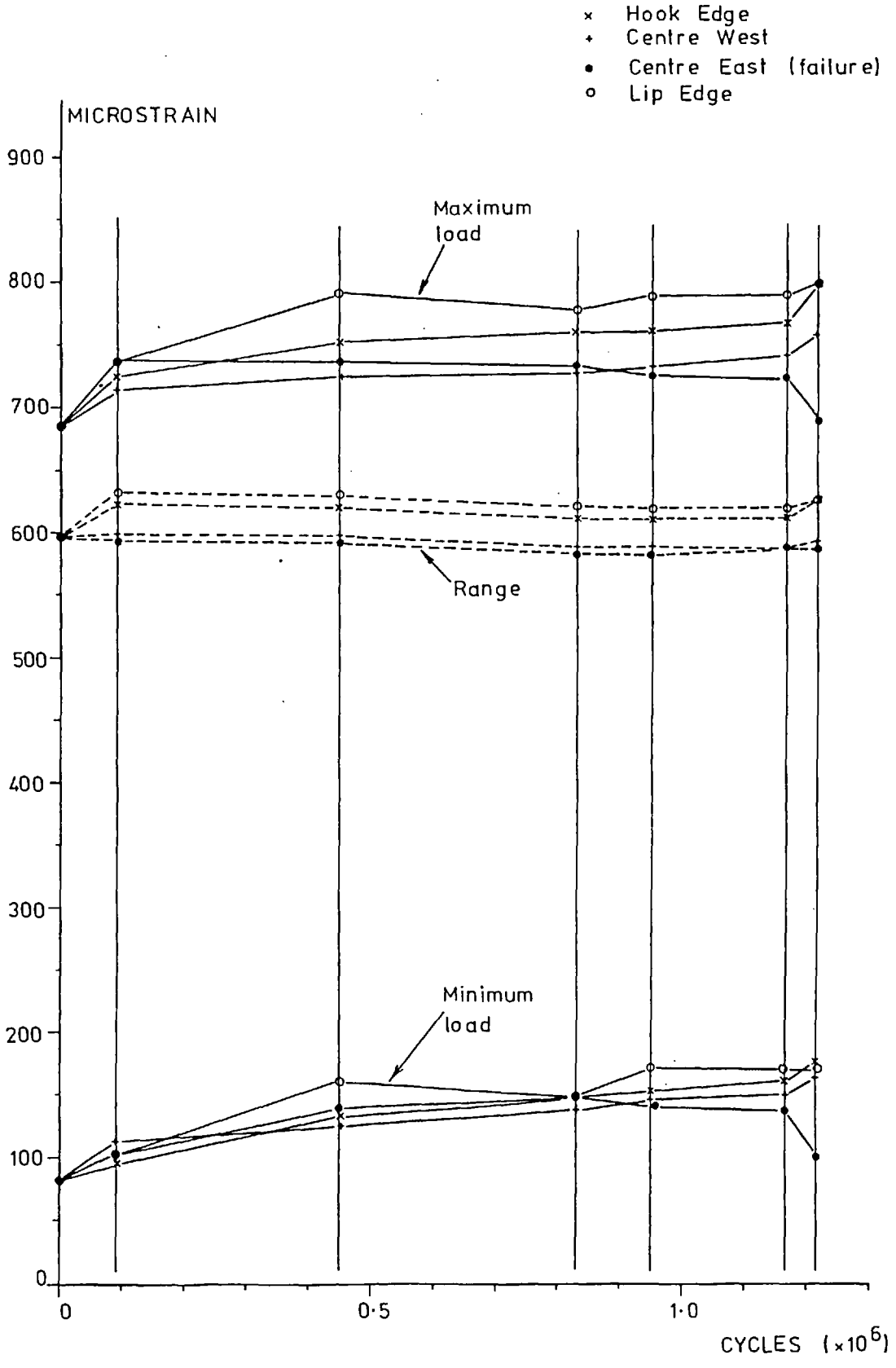
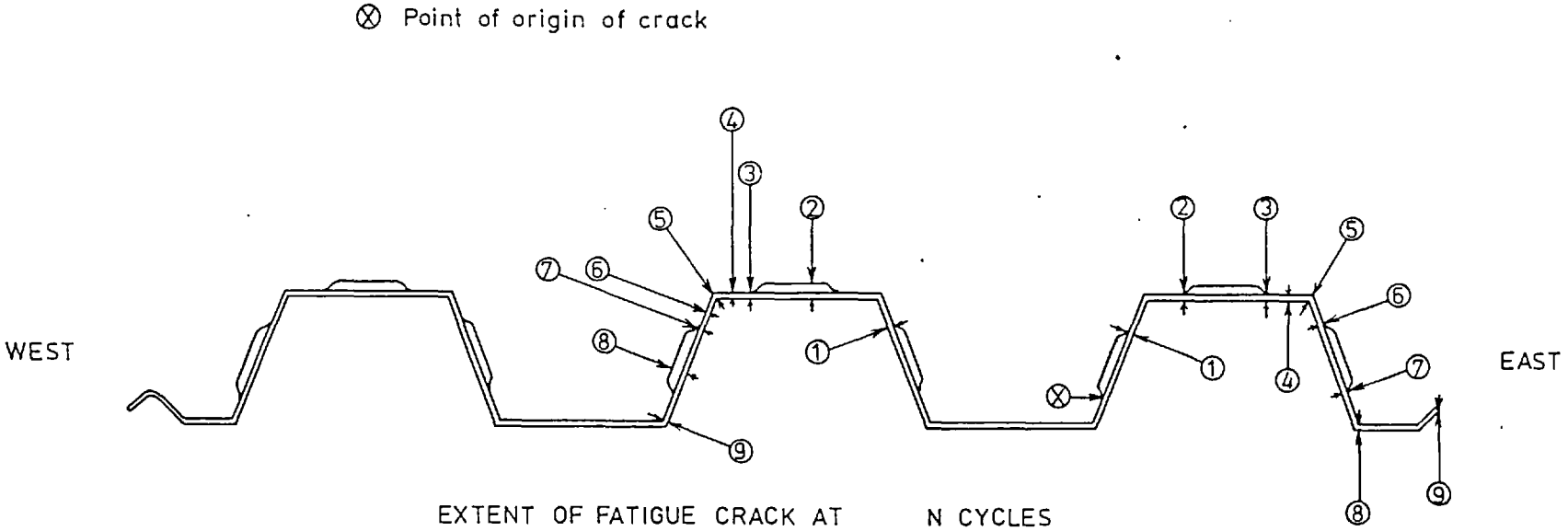


FIGURE 62: TEST 9 : STEEL BOTTOM FLANGE STRAIN - STAGE III



EXTENT OF FATIGUE CRACK AT POSITION	N CYCLES
1	1217500
2	1266000
3	1325000
4	1361300
5	1380300
6	1403300
7	1422400
8	1442000
9	1444300

FIGURE 63: TEST 9 : PROPAGATION OF FATIGUE CRACK

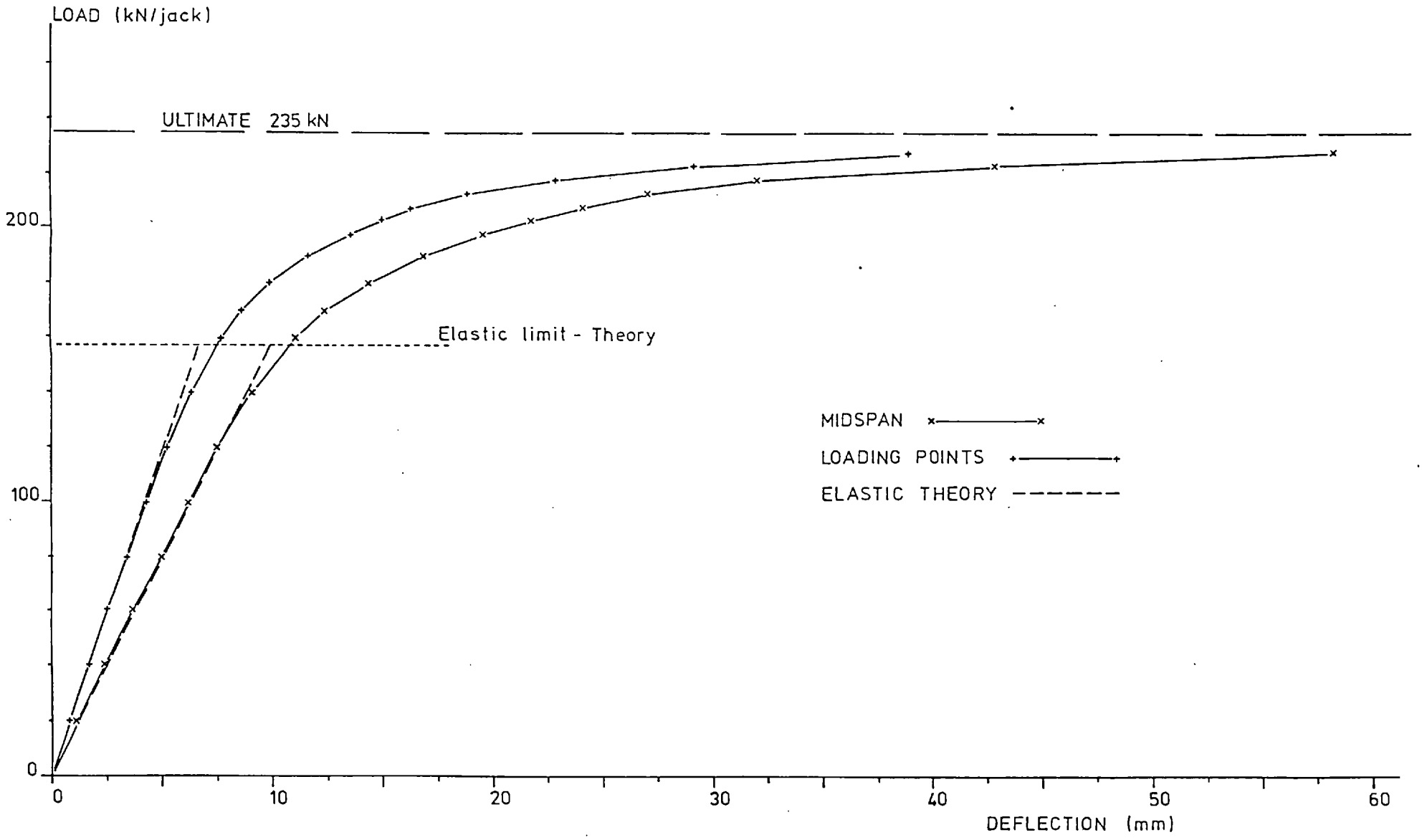


FIGURE 64: TEST 4 : DEFLECTIONS - STAGE IV

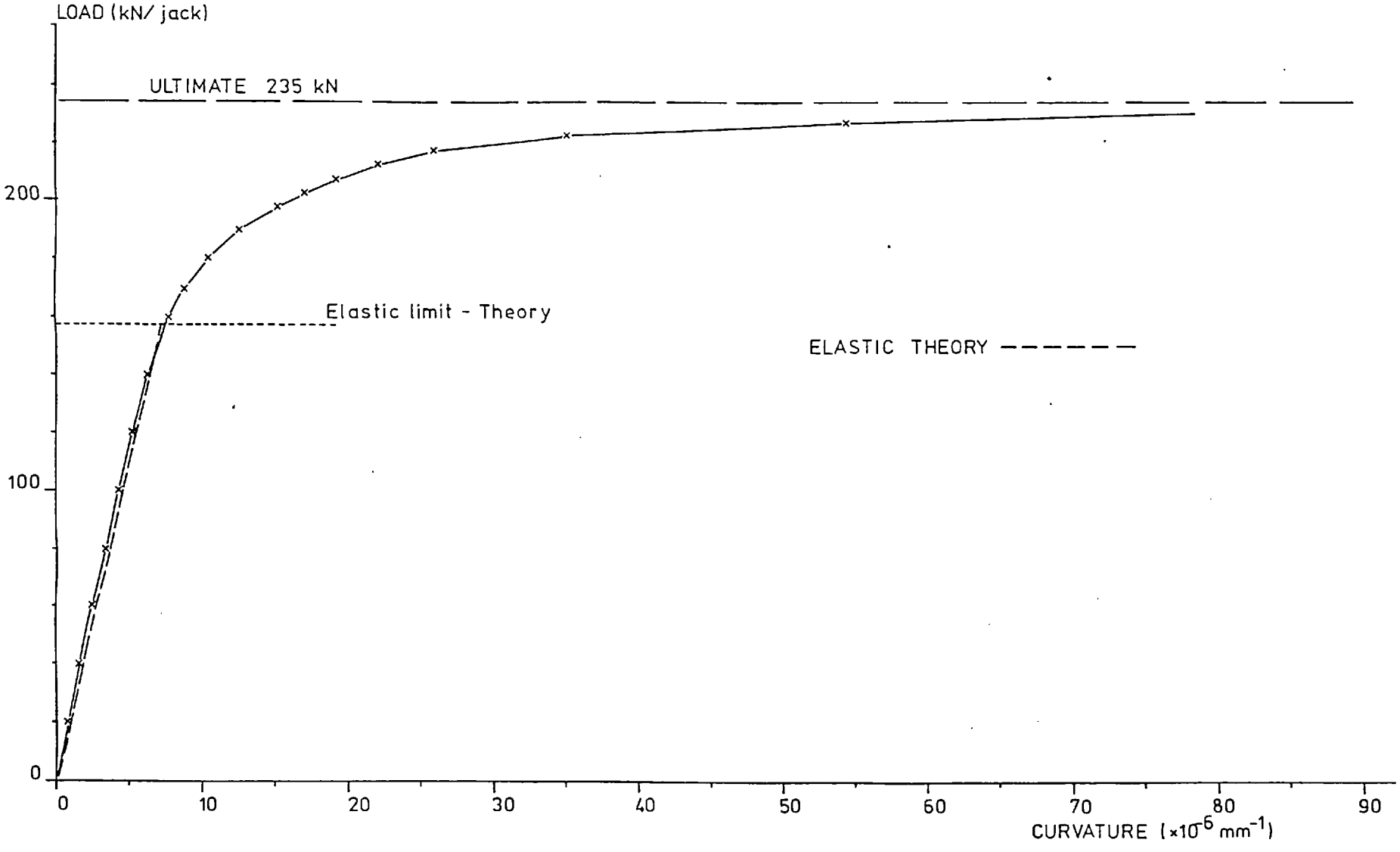


FIGURE 65: TEST 4 : MIDSPAN CURVATURE - STAGE IV

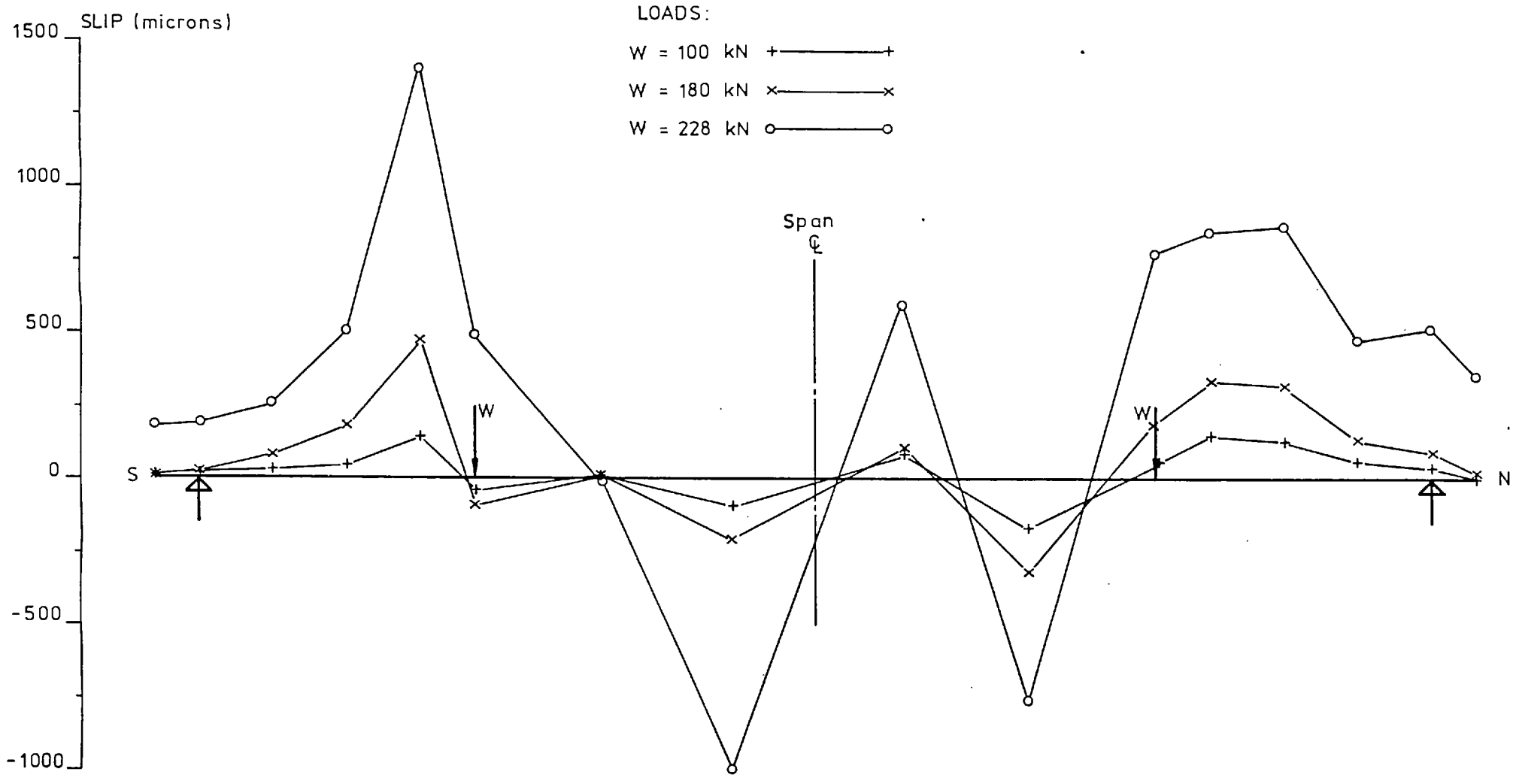


FIGURE 66: TEST 4 : SLIP DISTRIBUTIONS - STAGE IV

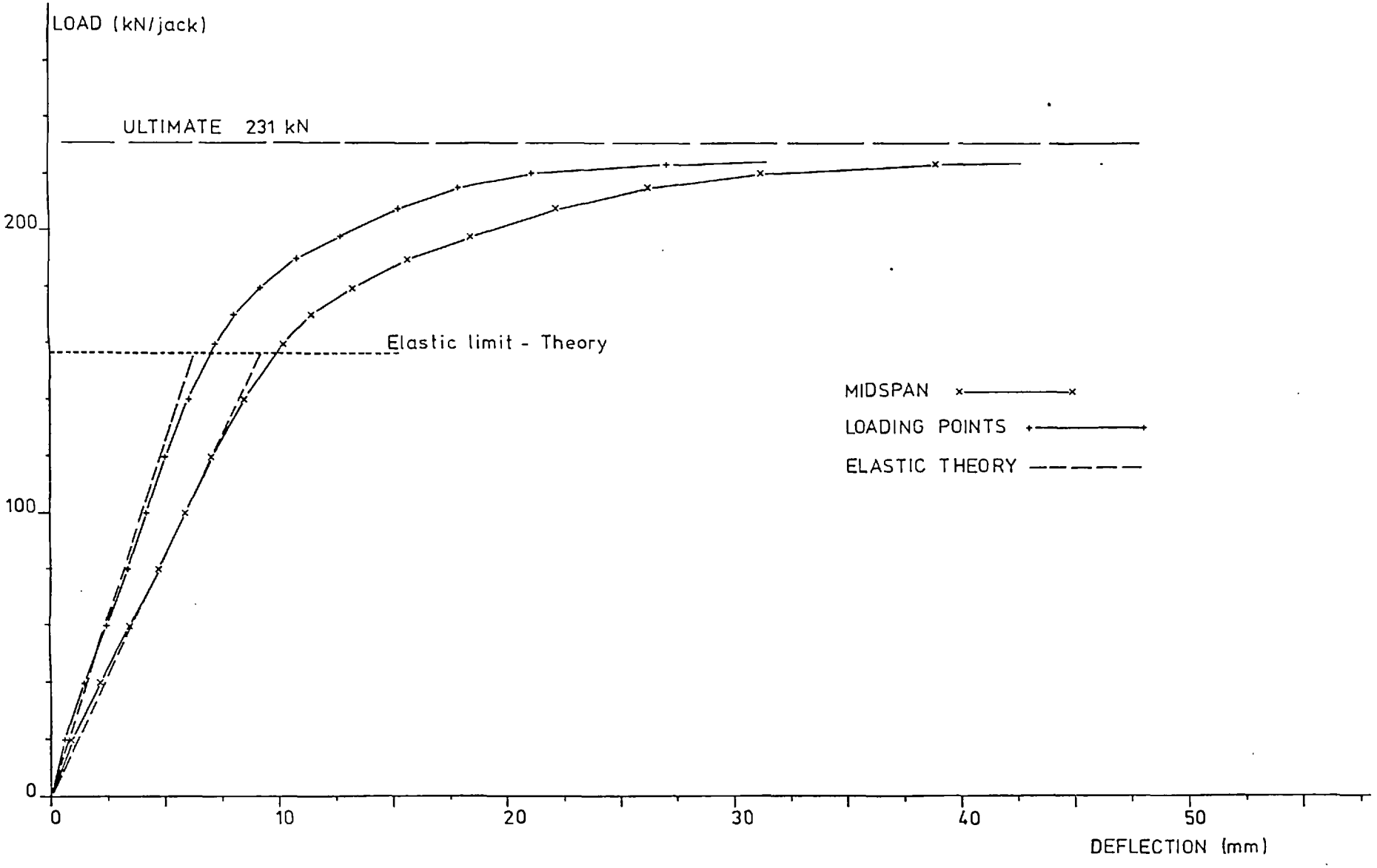


FIGURE 67: TEST 5 : DEFLECTIONS - STAGE IV

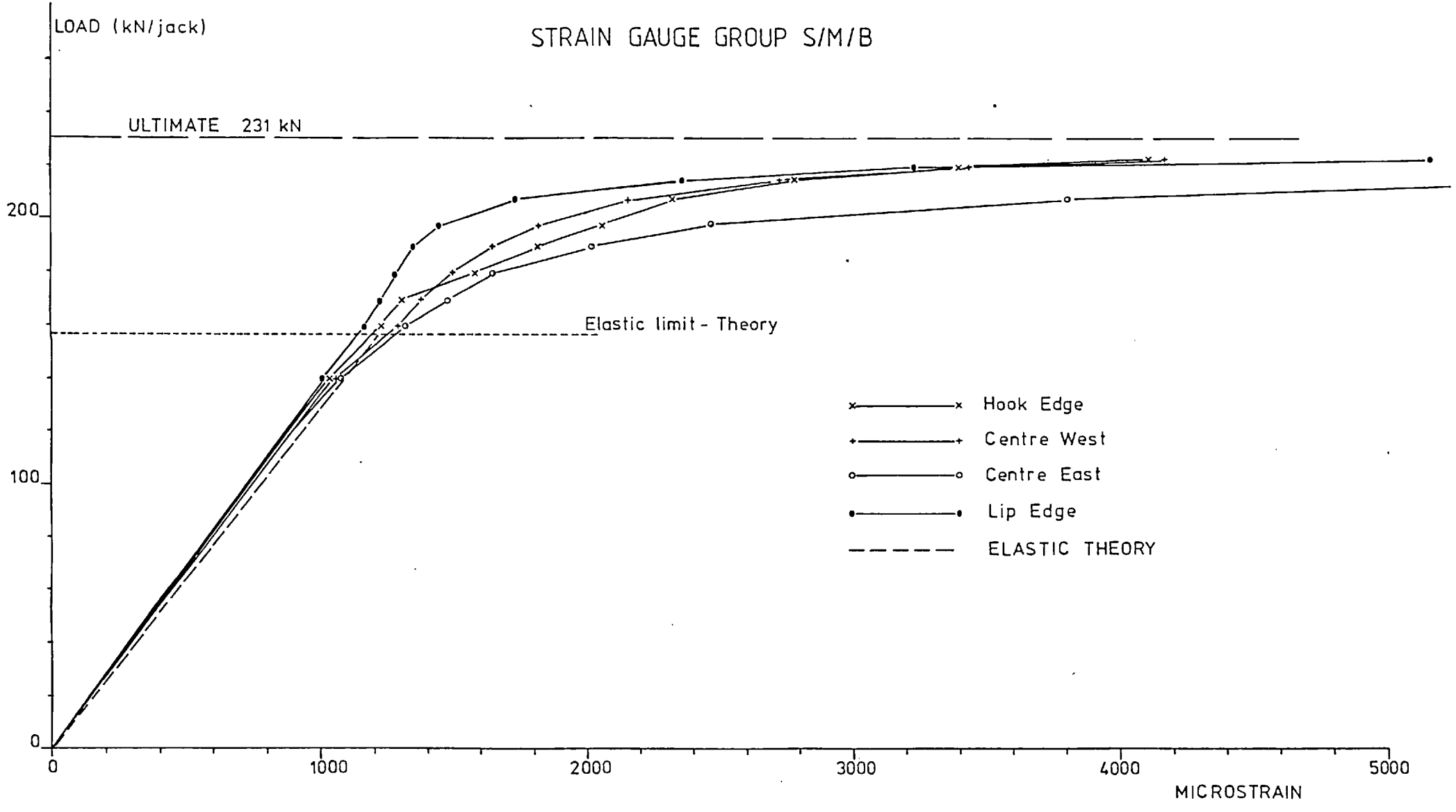


FIGURE 68: TEST 5 : STEEL BOTTOM FLANGE STRAIN - STAGE IV

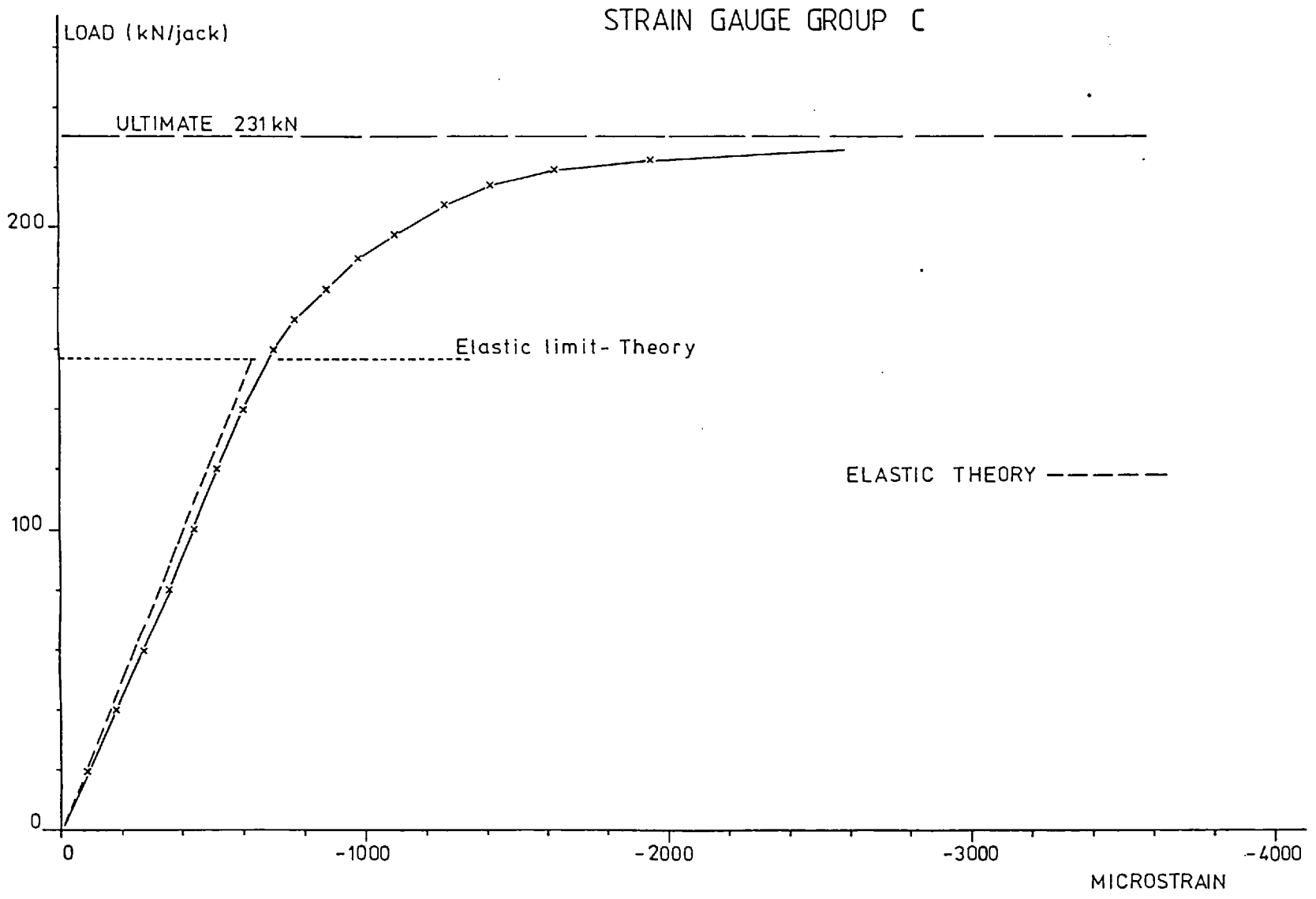


FIGURE 69: TEST 5 : CONCRETE SURFACE STRAIN - STAGE IV

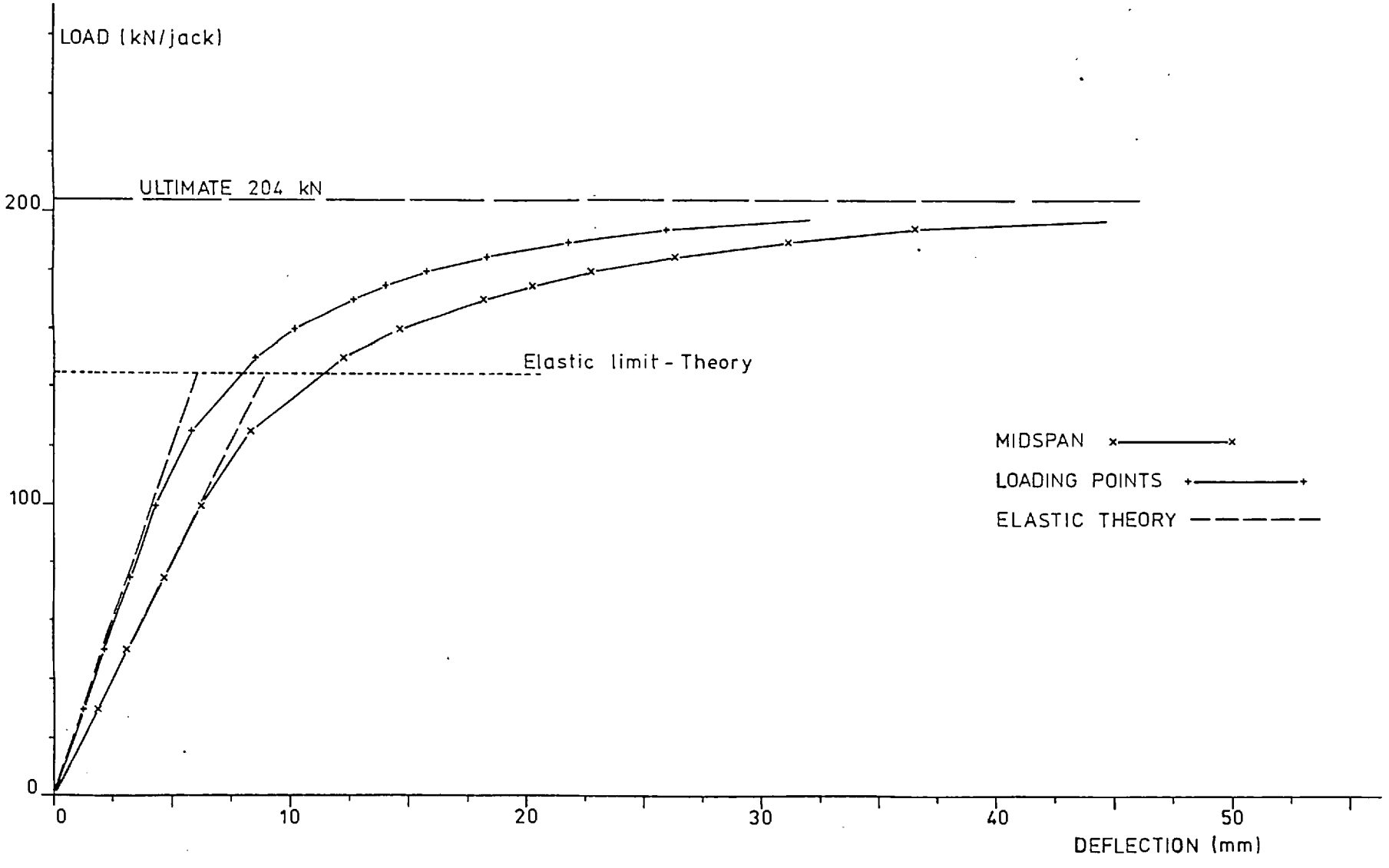


FIGURE 70: TEST 7 : DEFLECTIONS - STAGE IV

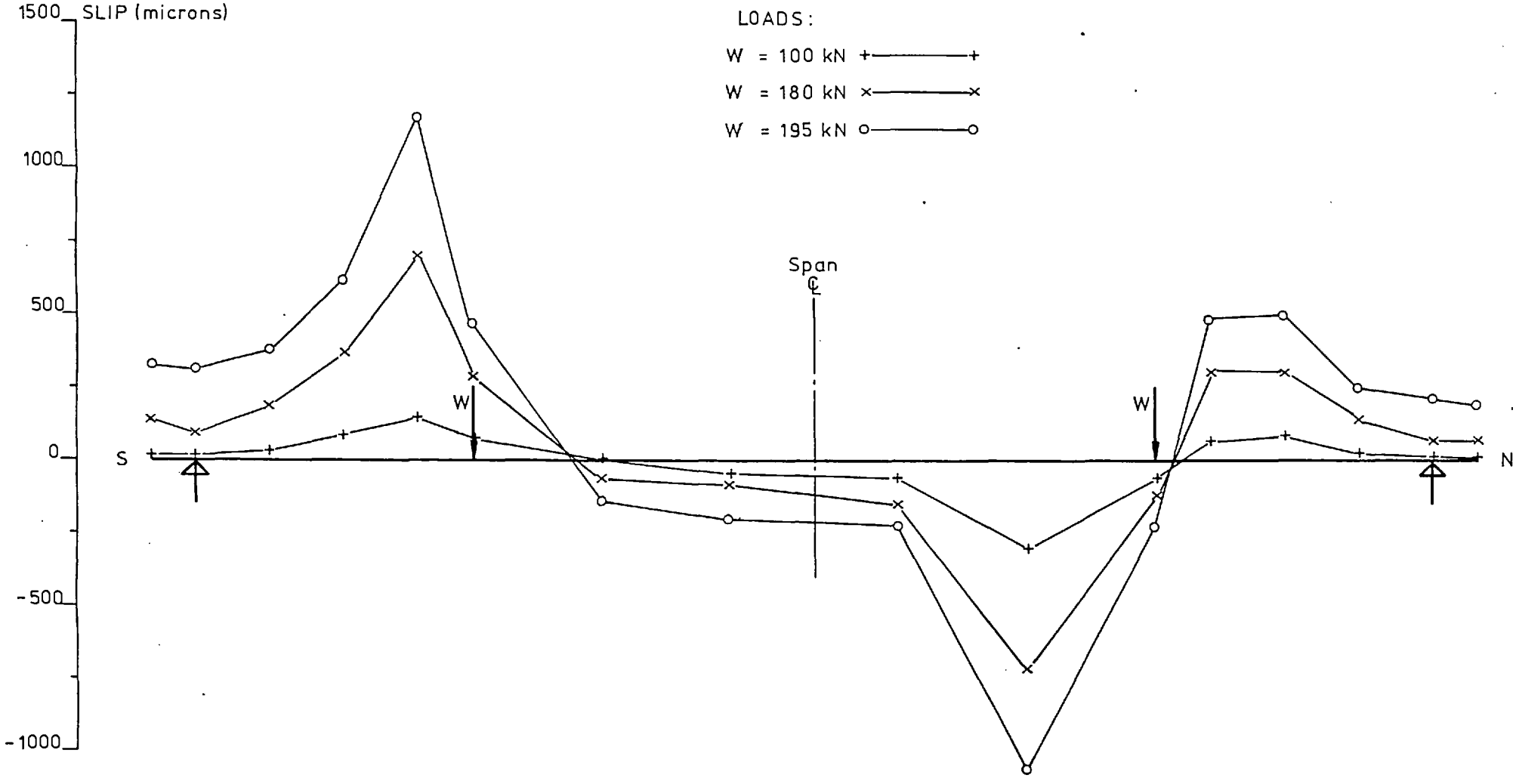


FIGURE 71: TEST 7 : SLIP DISTRIBUTIONS - STAGE IV

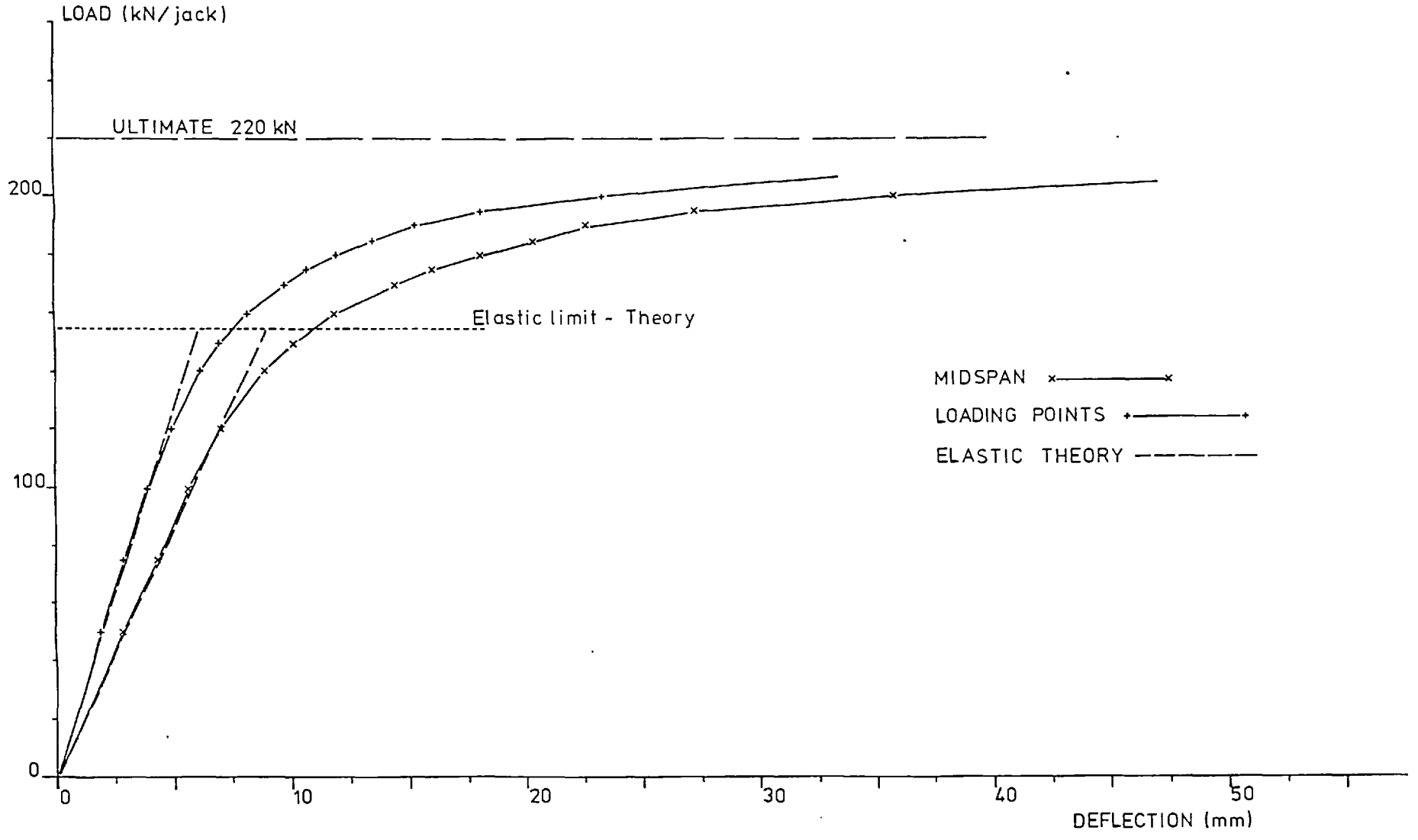


FIGURE 72: TEST 8 : DEFLECTIONS - STAGE IV

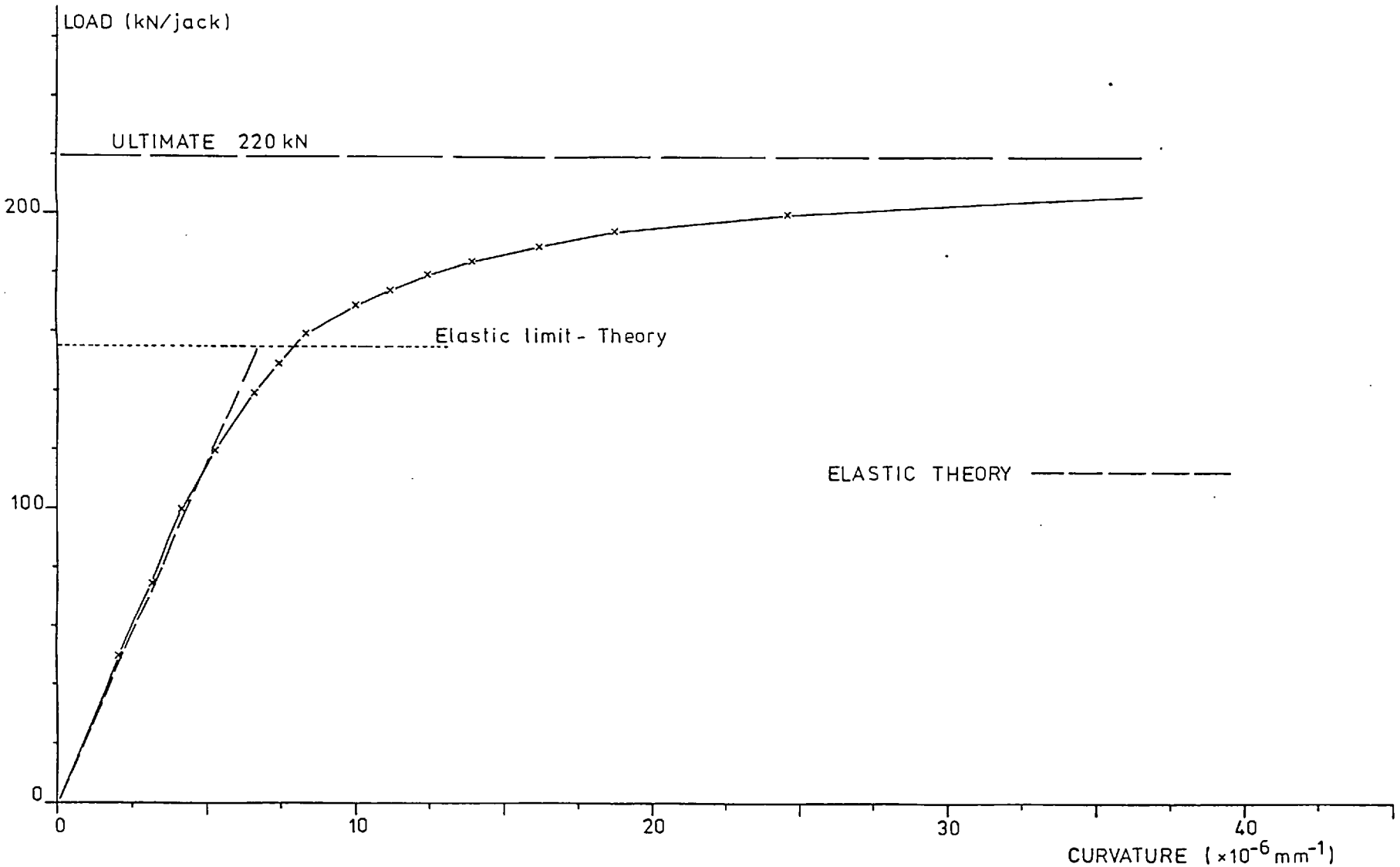


FIGURE 73: TEST 8 : MIDSPAN CURVATURE - STAGE IV

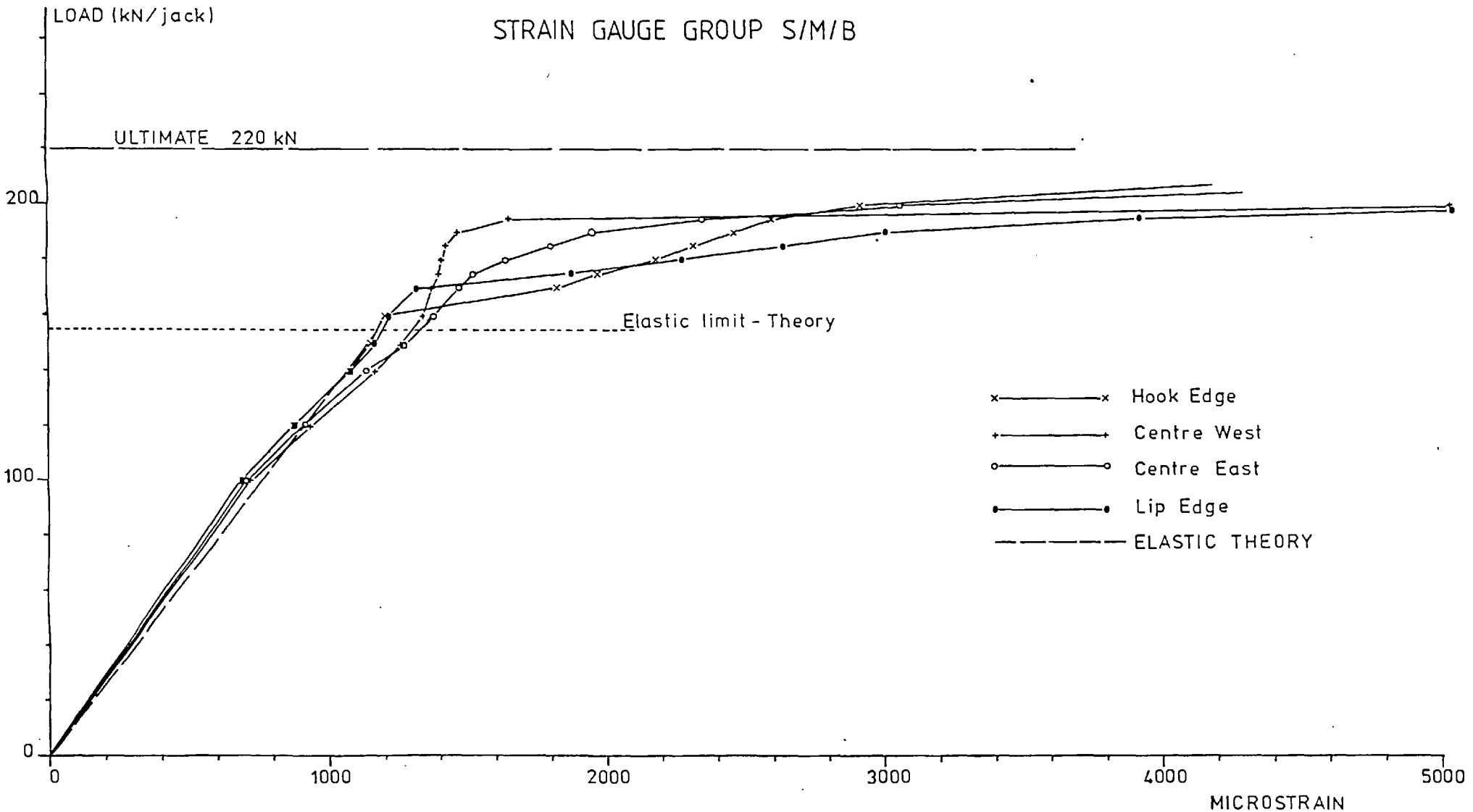


FIGURE 74: TEST 8 : STEEL BOTTOM FLANGE STRAIN - STAGE IV

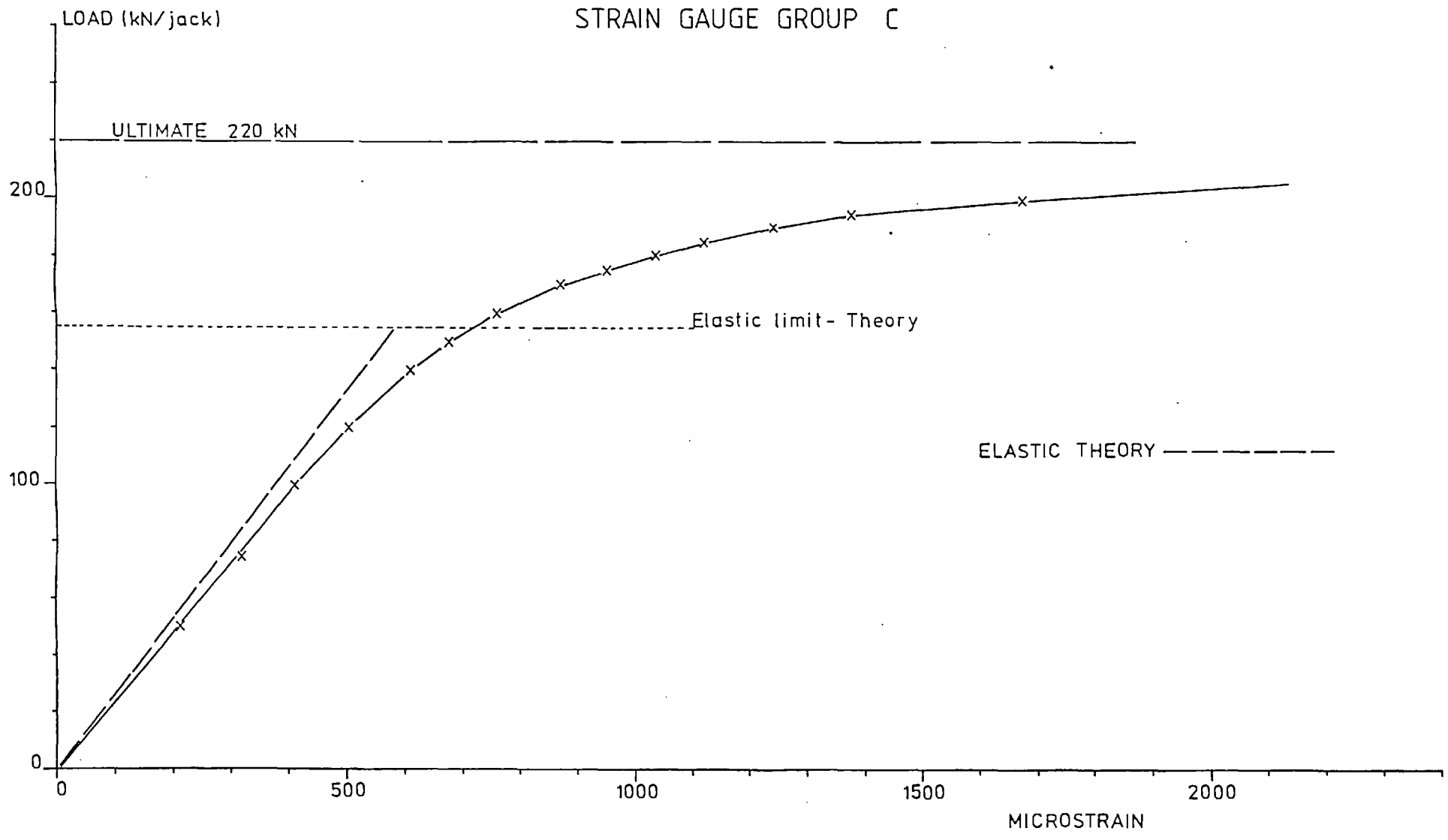


FIGURE 75: TEST 8 : CONCRETE SURFACE STRAIN - STAGE IV

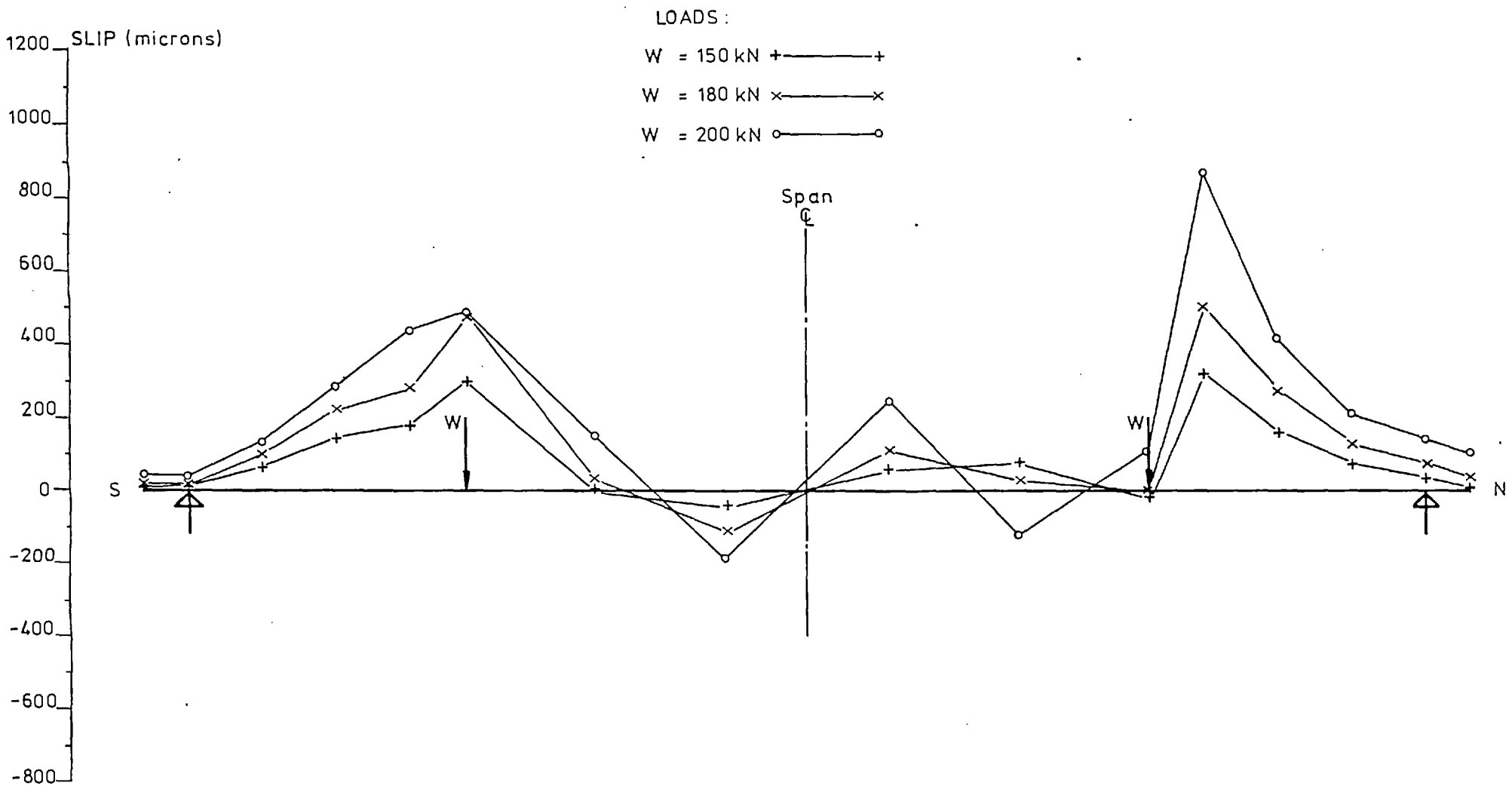


FIGURE 76: TEST 8 : SLIP DISTRIBUTION - STAGE IV

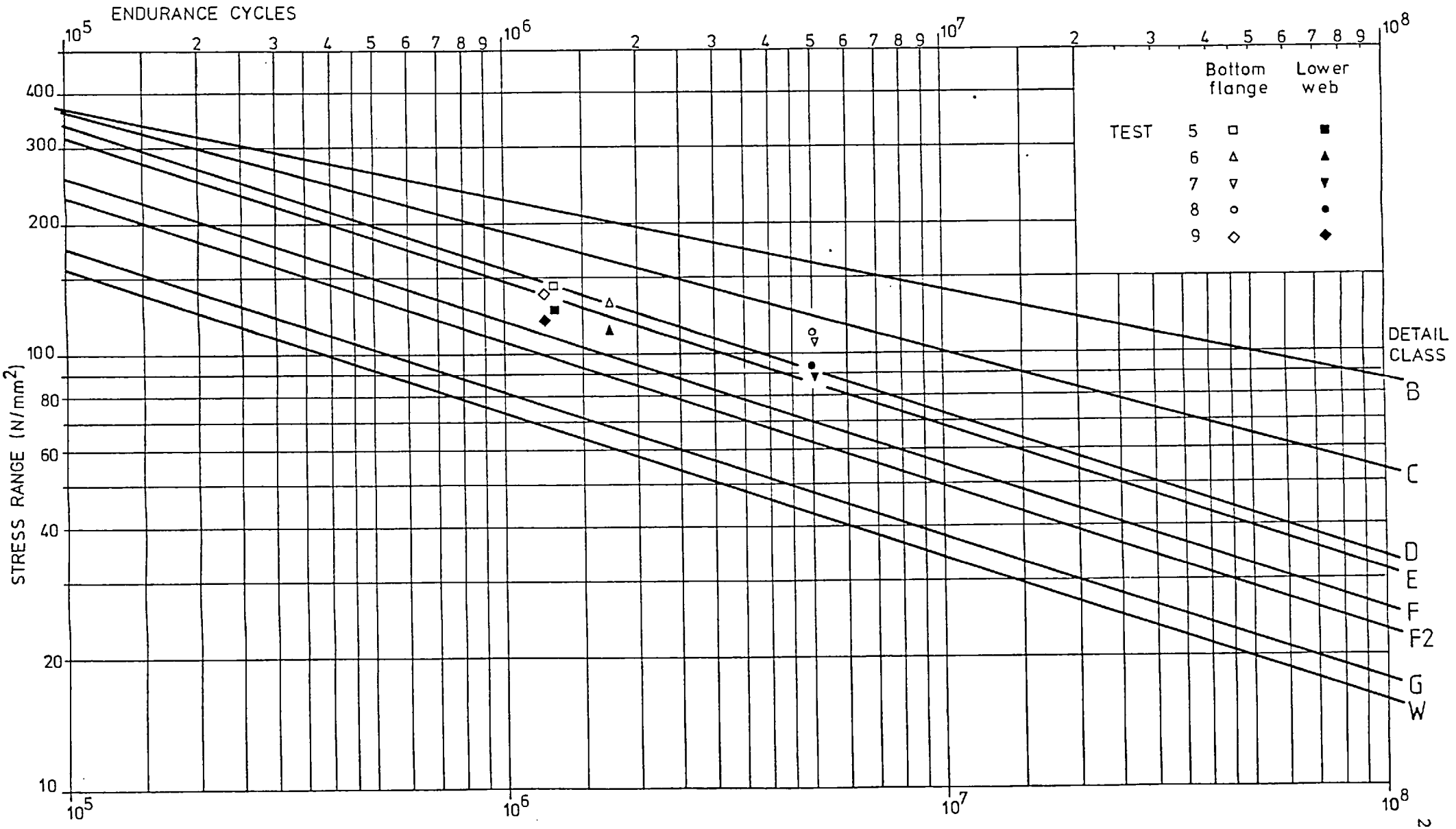


FIGURE 77: MEAN S-N RELATIONSHIPS AND COMPOSITE TEST RESULTS

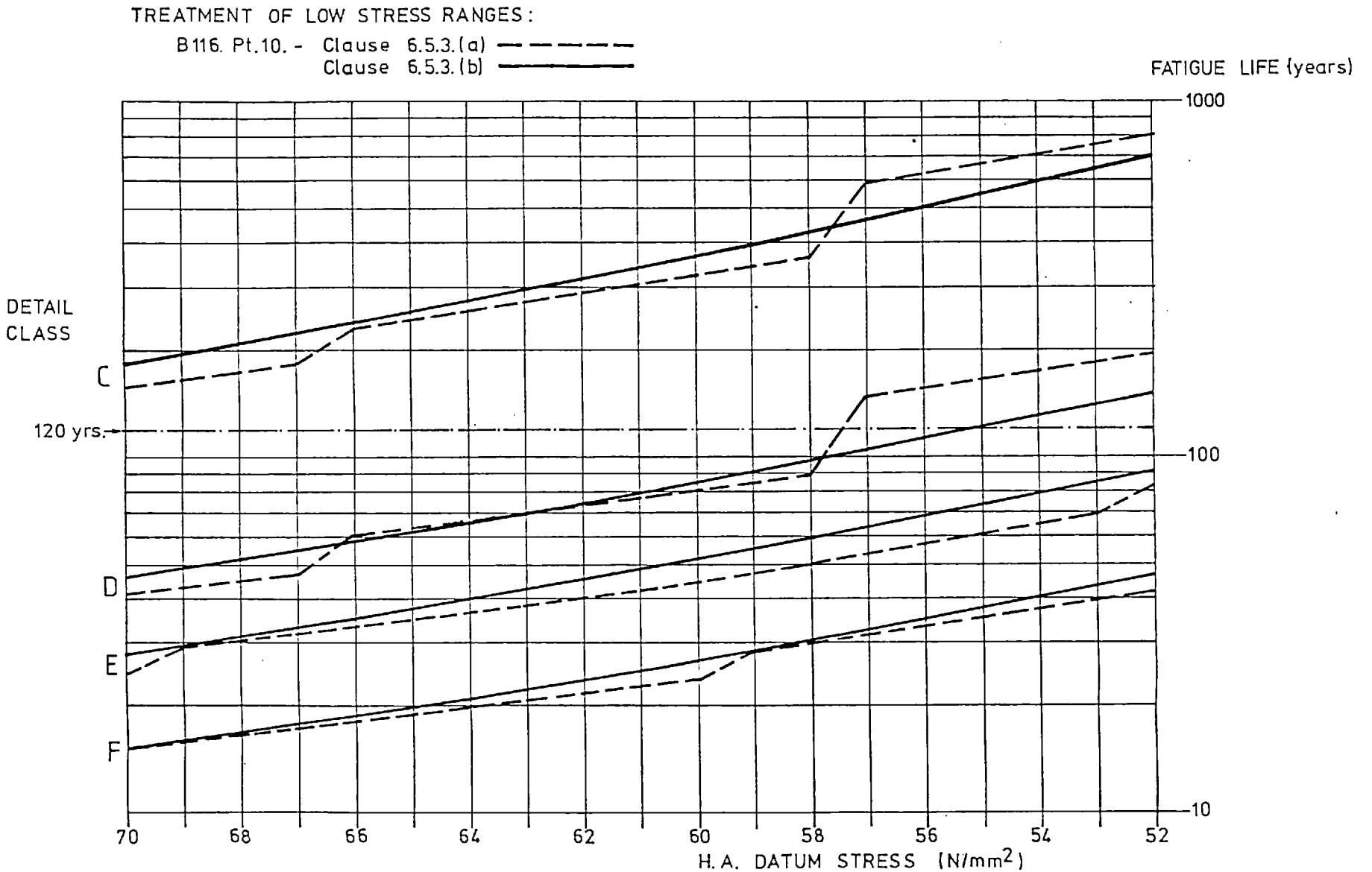


FIGURE 78: H.A. SPECTRUM FATIGUE LIFE (Transverse Members)

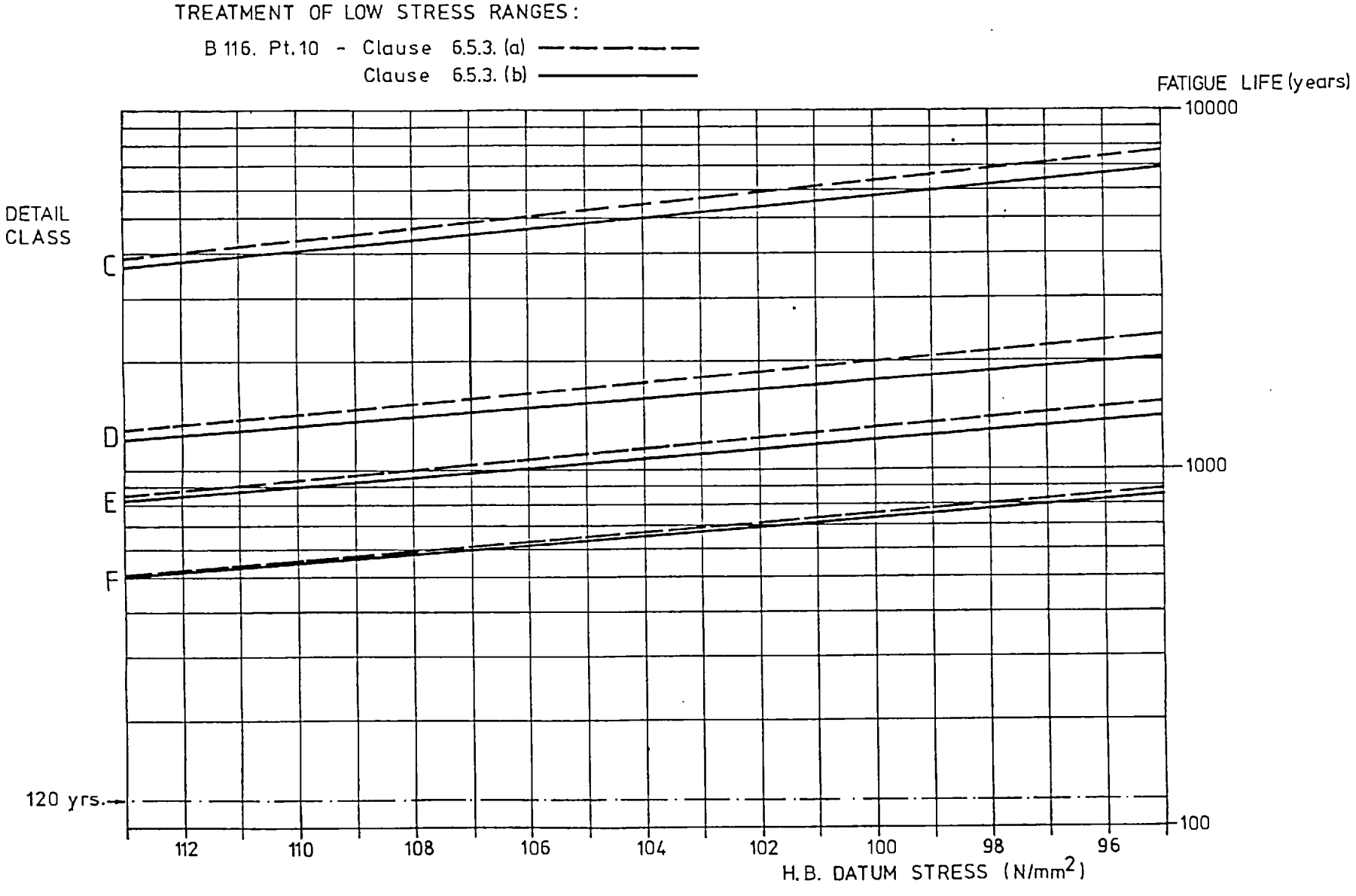
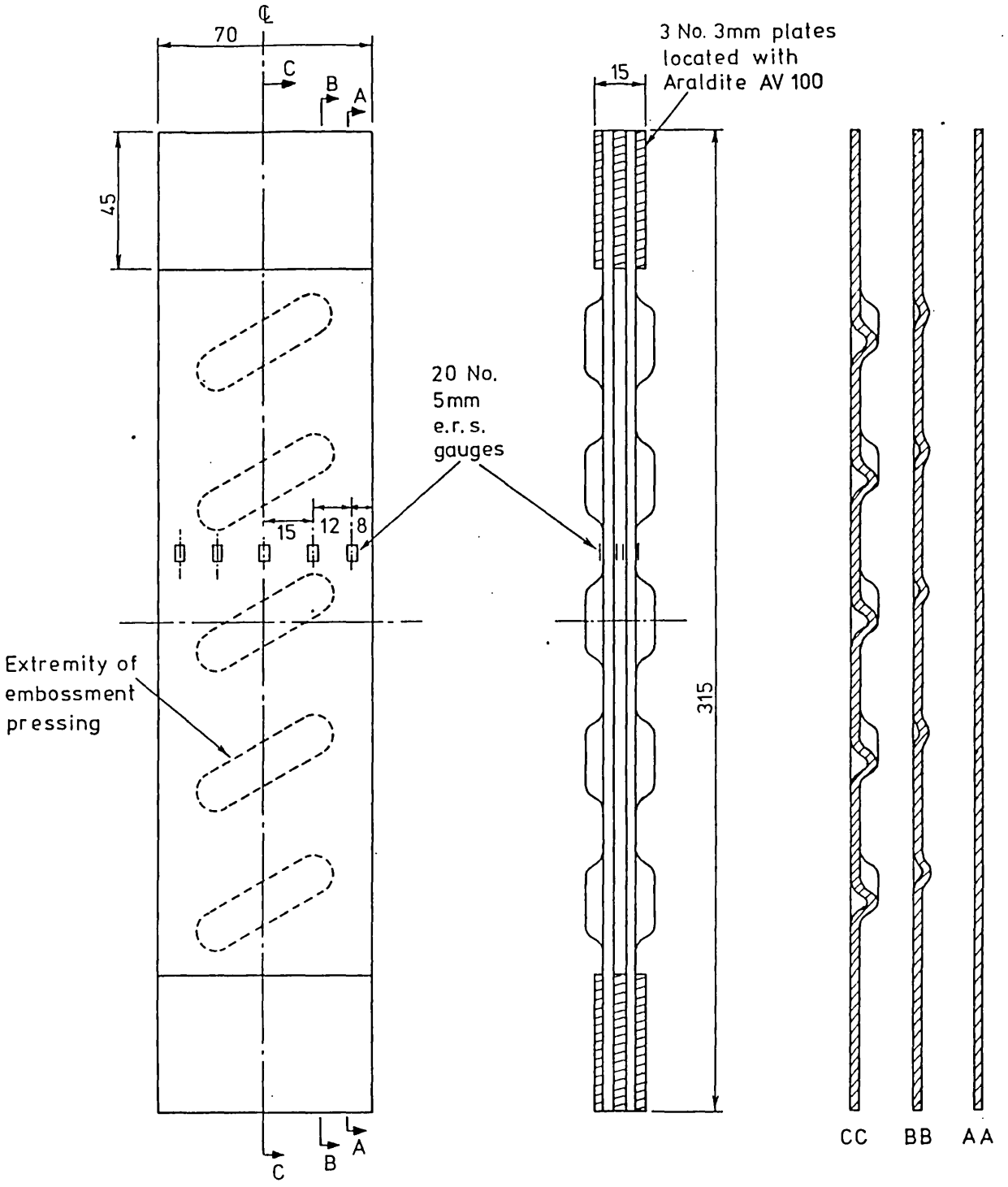


FIGURE 79: H.B. SPECTRUM FATIGUE LIFE (Transverse Members)



All dimensions in mm.

FIGURE 80: VIBROPHORE SPECIMEN AND INSTRUMENTATION

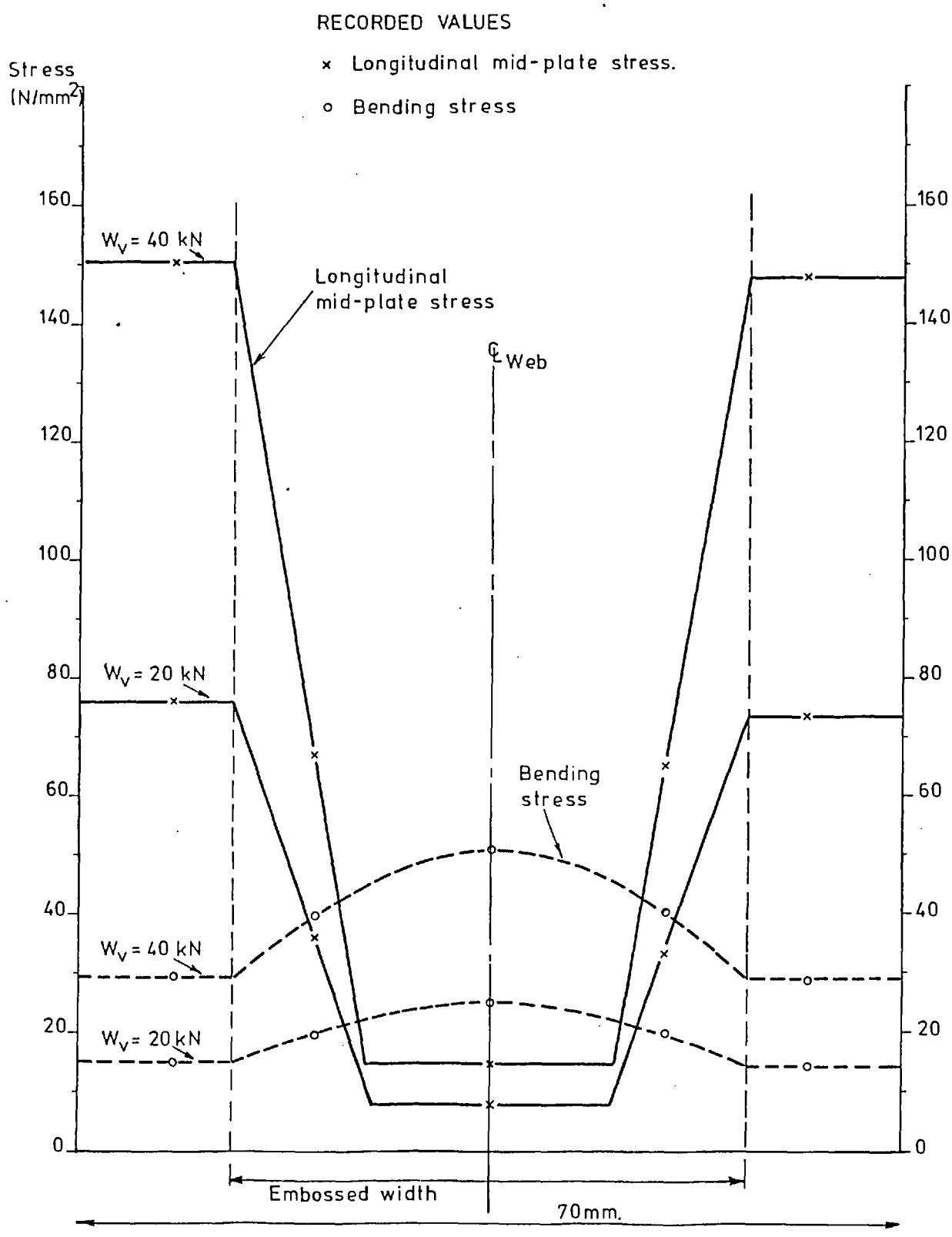


FIGURE 81: STRESS DISTRIBUTION IN VIBROPHORE SPECIMEN

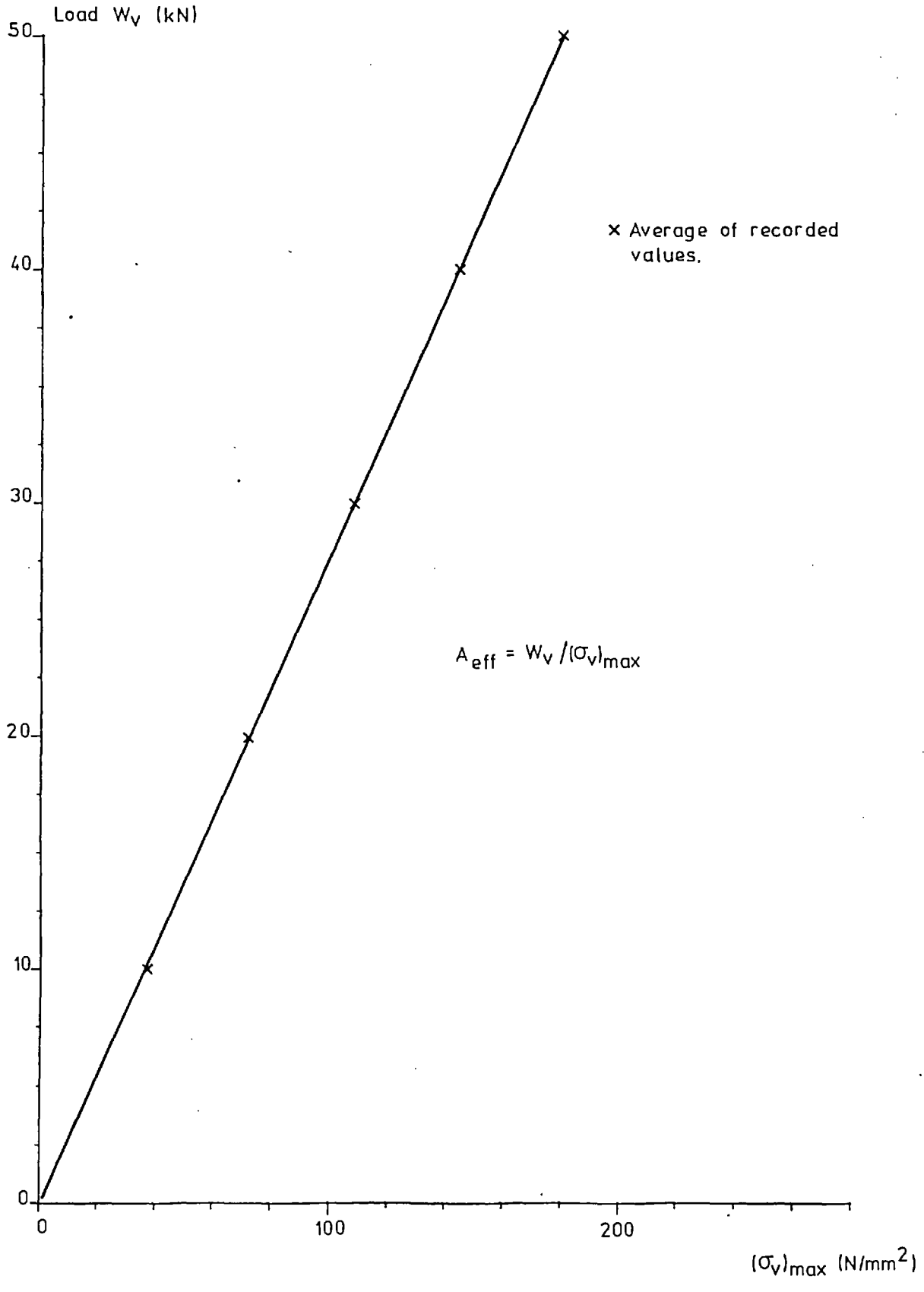


FIGURE 82: VIBROPHORE SPECIMEN - PLOT OF LOAD AGAINST $(\sigma_v)_{max}$.

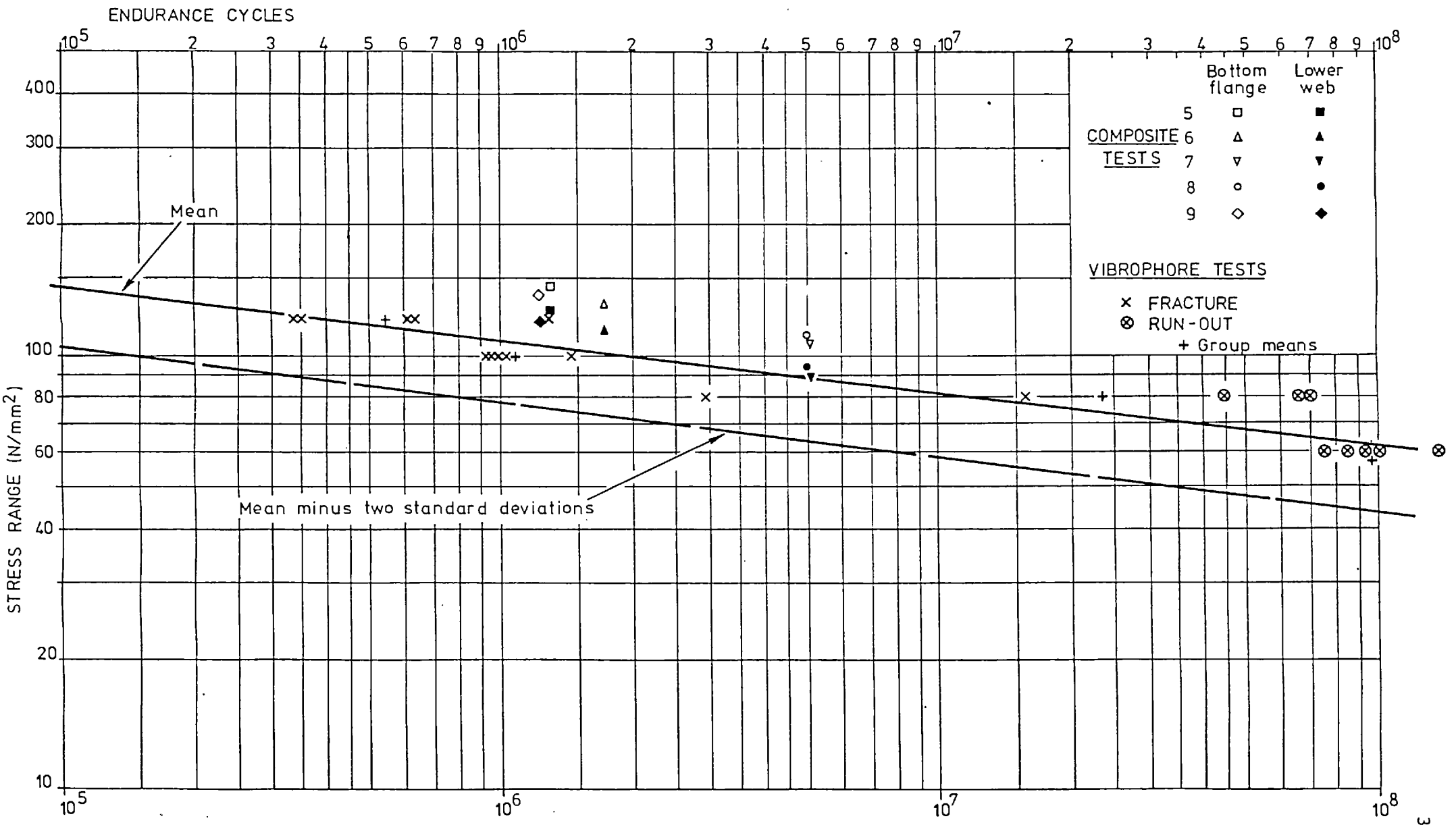


FIGURE 83: VIBROPHORE TEST RESULTS

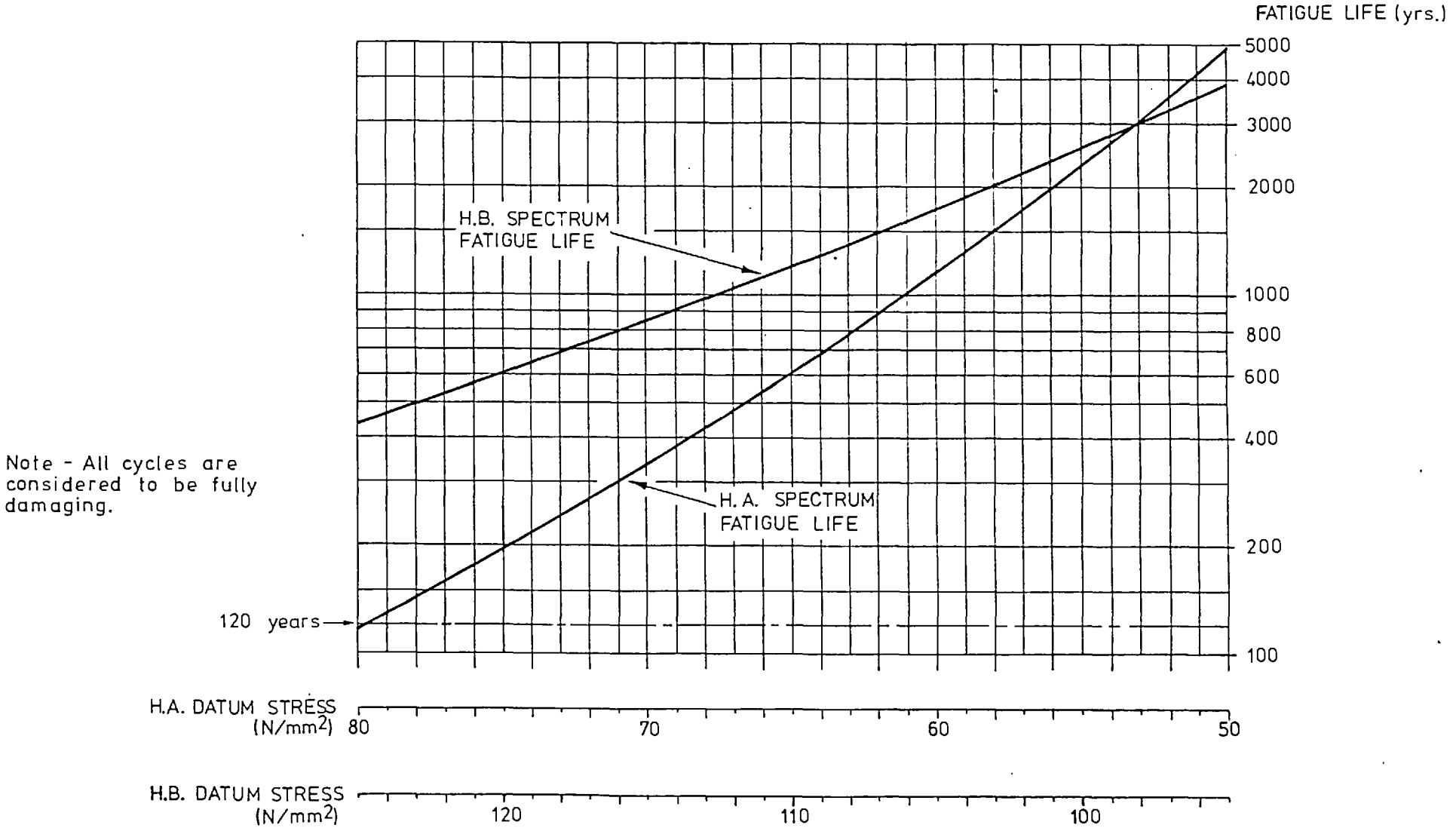
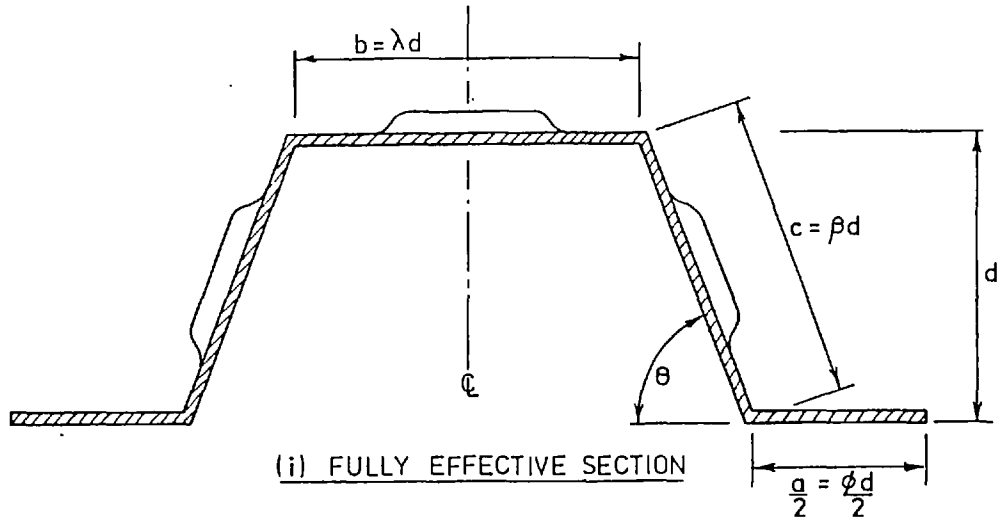
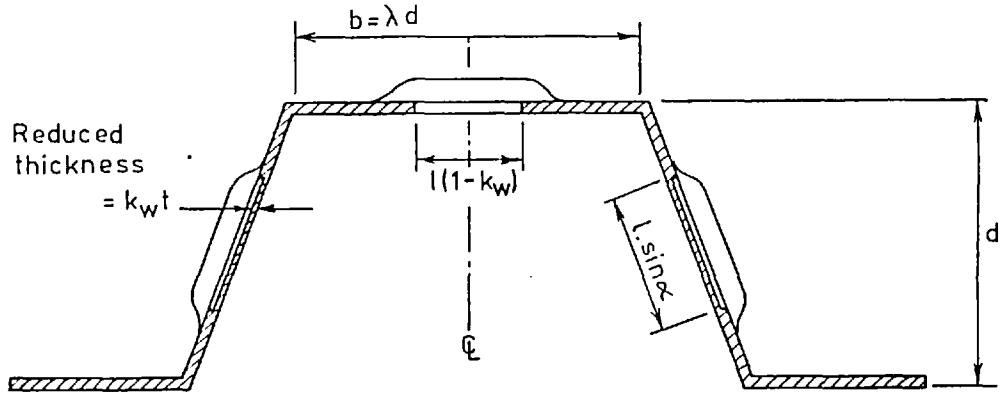


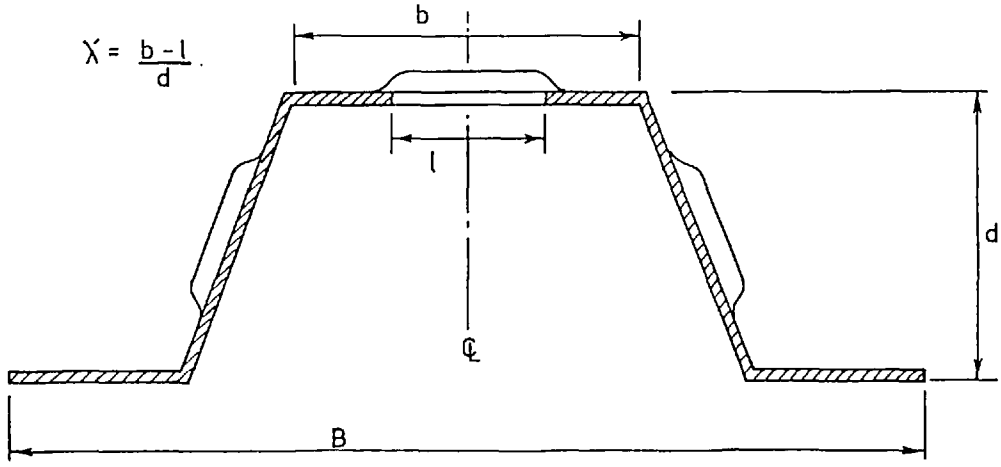
FIGURE 84: FATIGUE LIFE BASED ON VIBROPHORE RESULTS



(i) FULLY EFFECTIVE SECTION



(ii) EFFECTIVE SECTION



(iii) APPROXIMATE EFFECTIVE SECTION

FIGURE 85 : BARE FORMWORK CROSS-SECTIONS

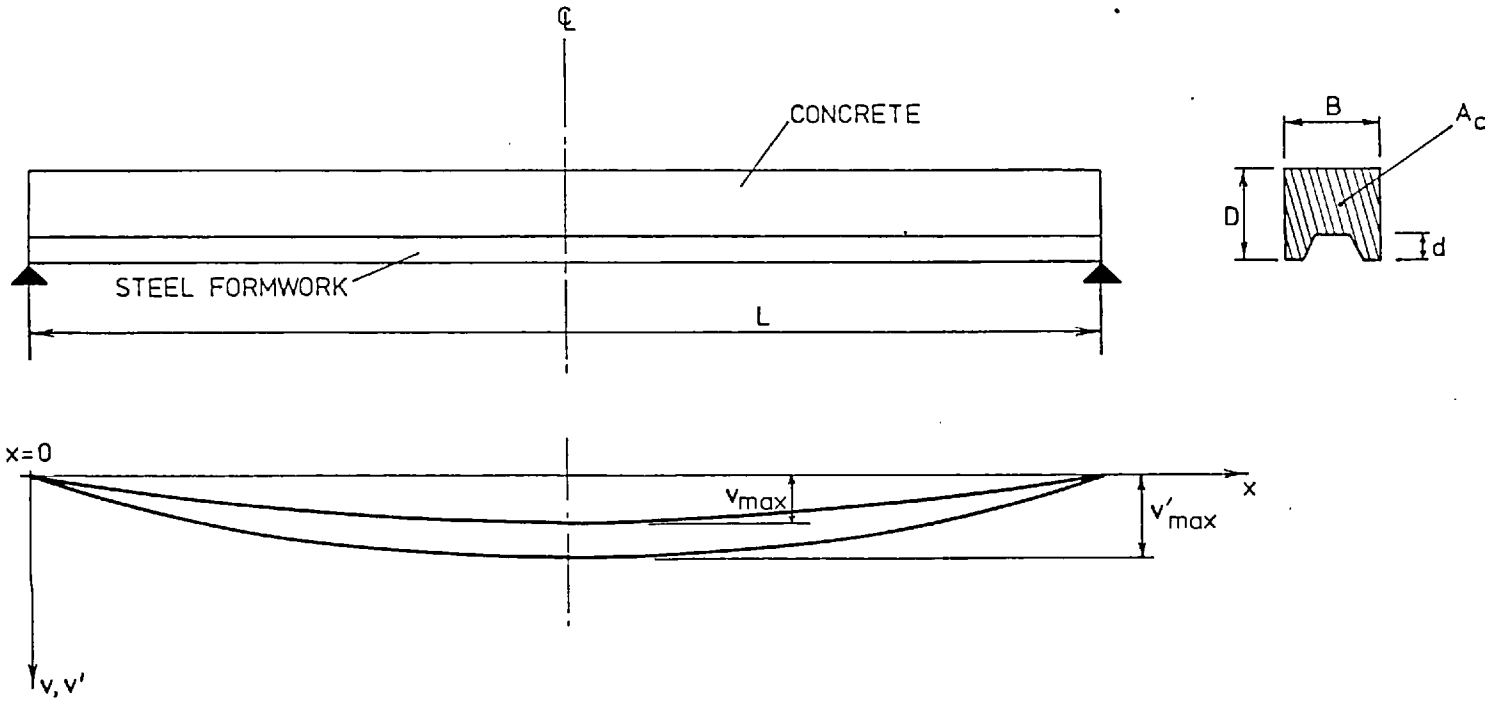


FIGURE 86: BARE FORMWORK - ANALYSIS OF PONDING EFFECT

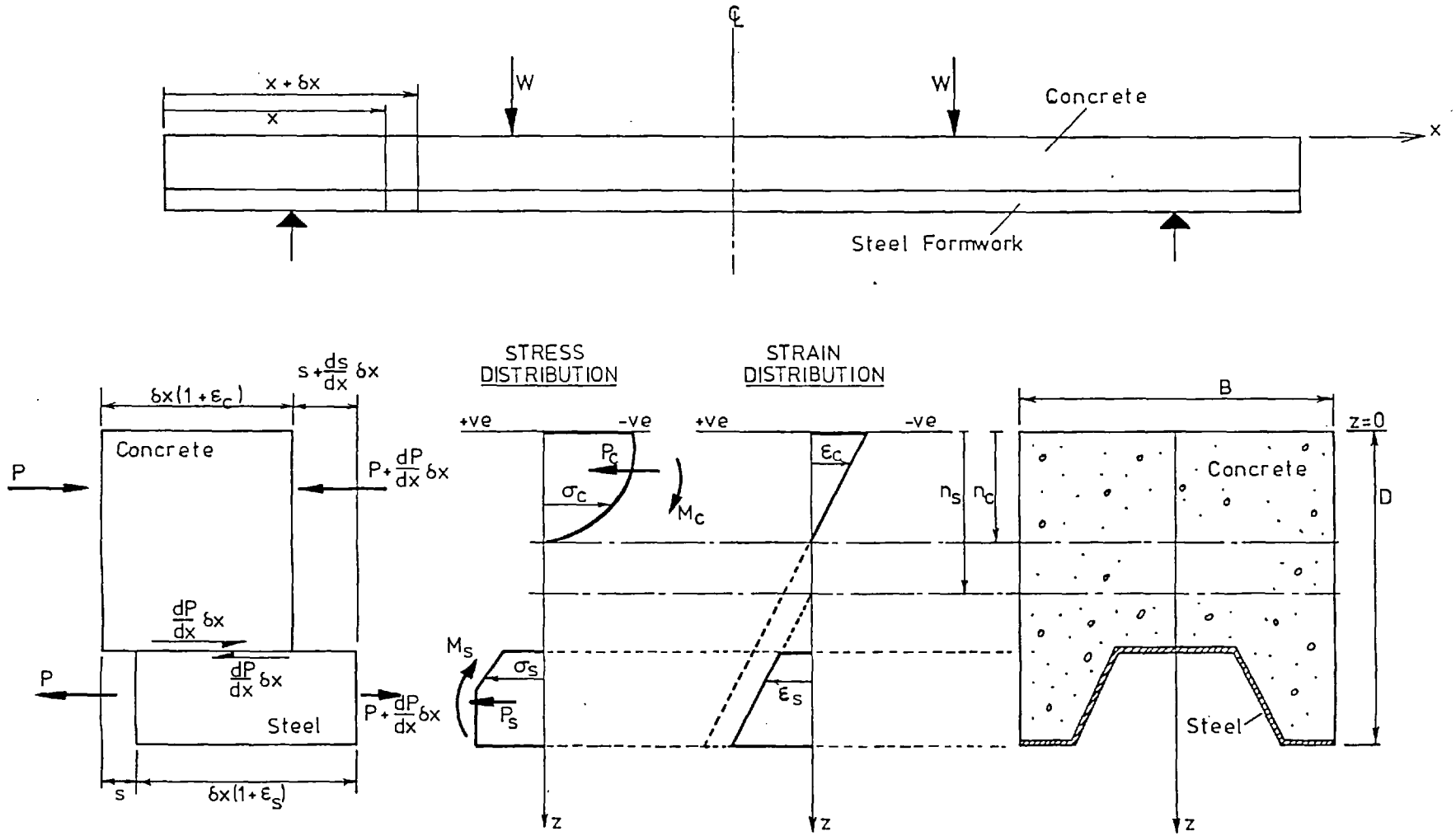


FIGURE 87: DERIVATION OF PARTIAL INTERACTION EQUATIONS

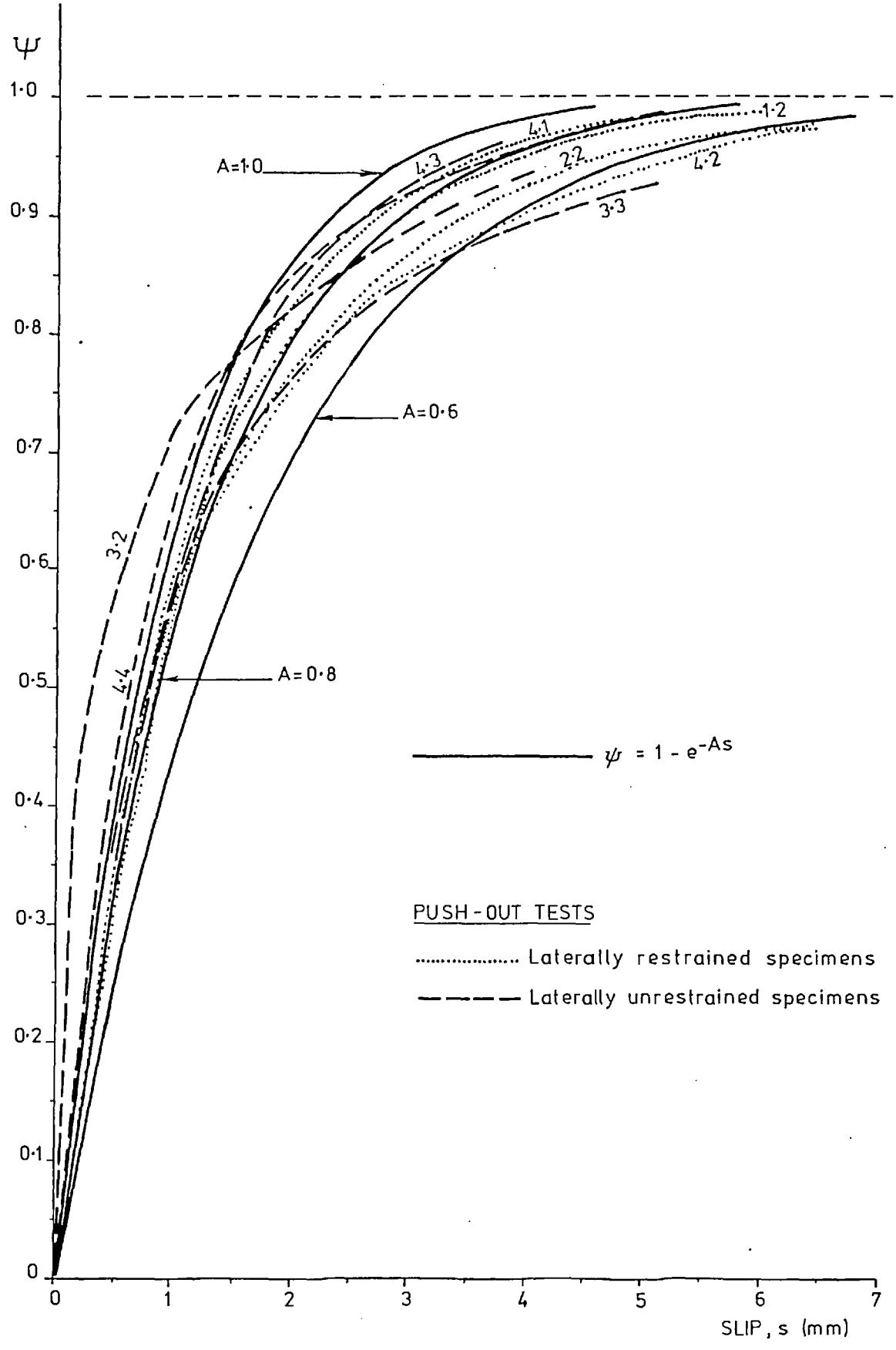


FIGURE 88: LOAD SLIP CURVES AND THEORETICAL REPRESENTATION

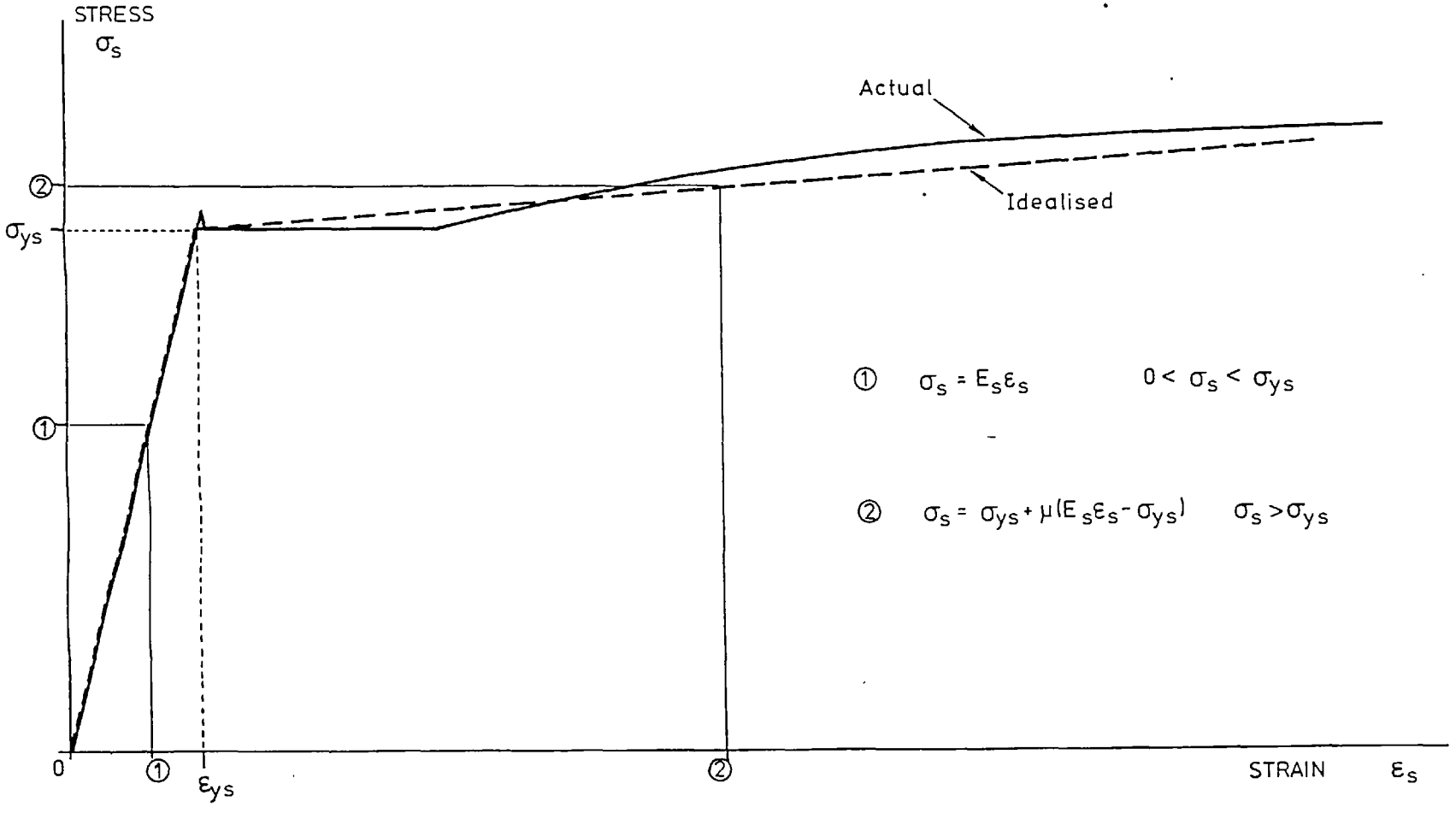


FIGURE 89: STRESS-STRAIN CURVES FOR STEEL

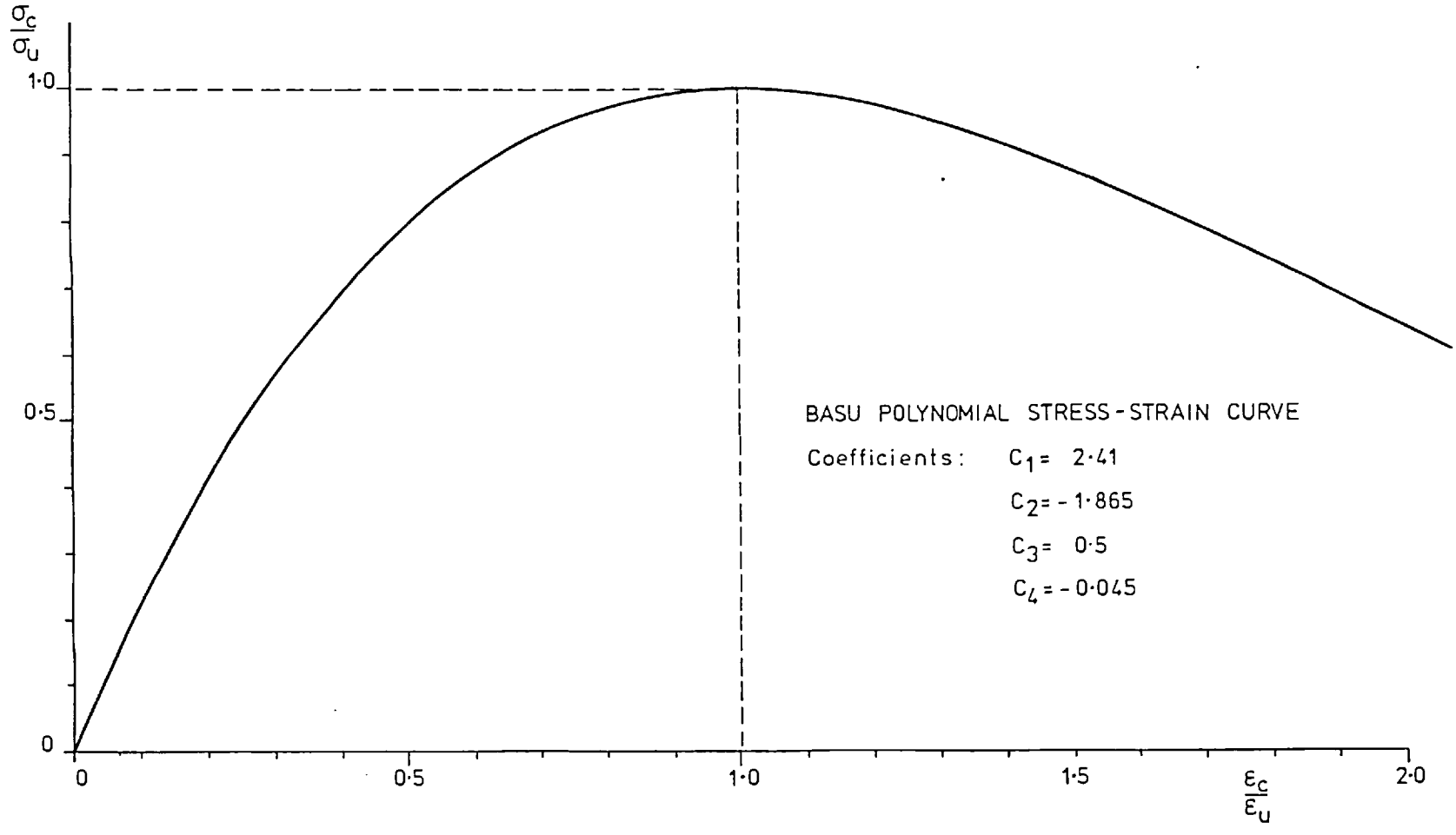


FIGURE 90: STRESS-STRAIN CURVE FOR CONCRETE

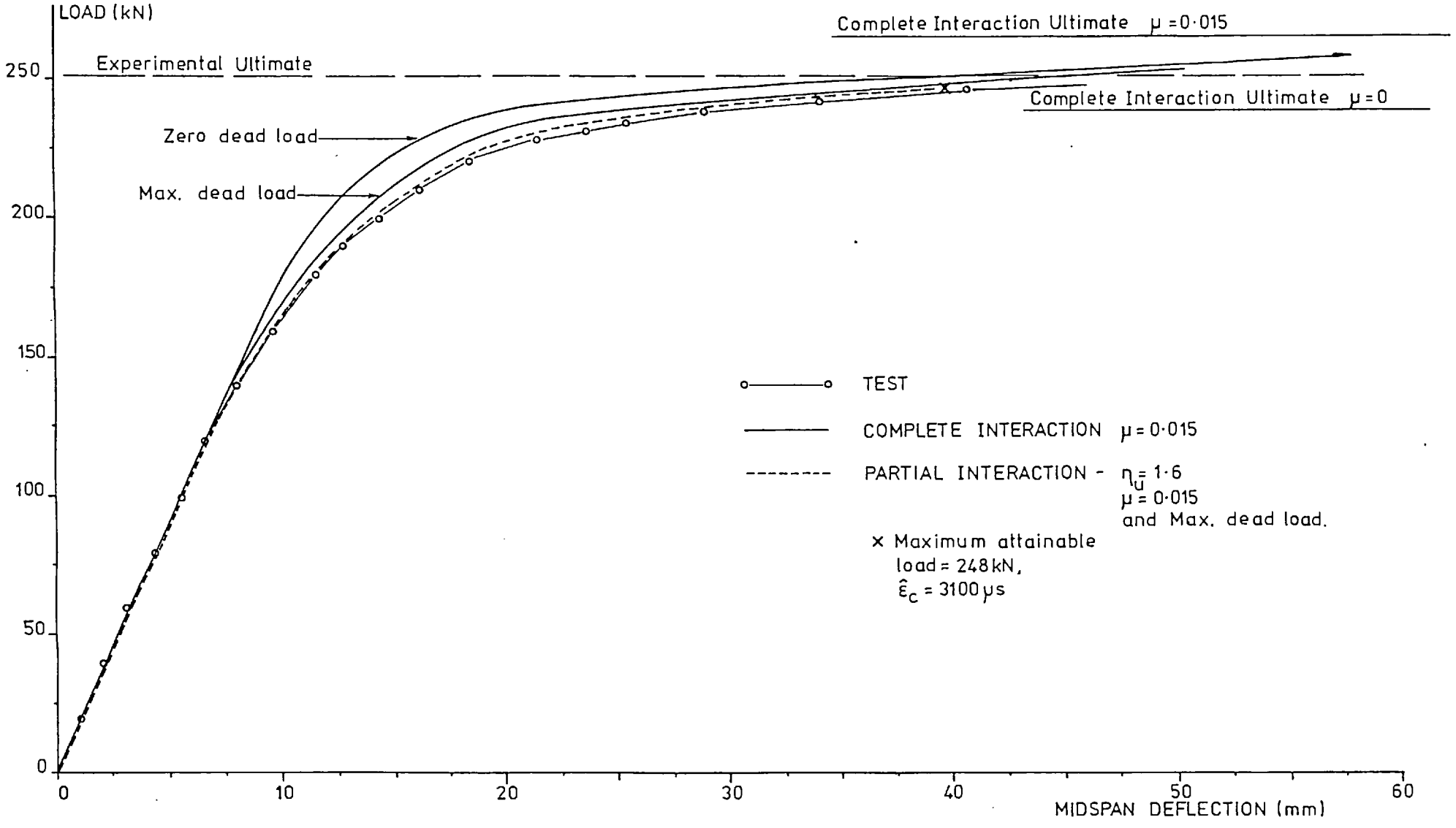


FIGURE 91: TEST 2 : MIDSPAN DEFLECTION RESPONSE - THEORY

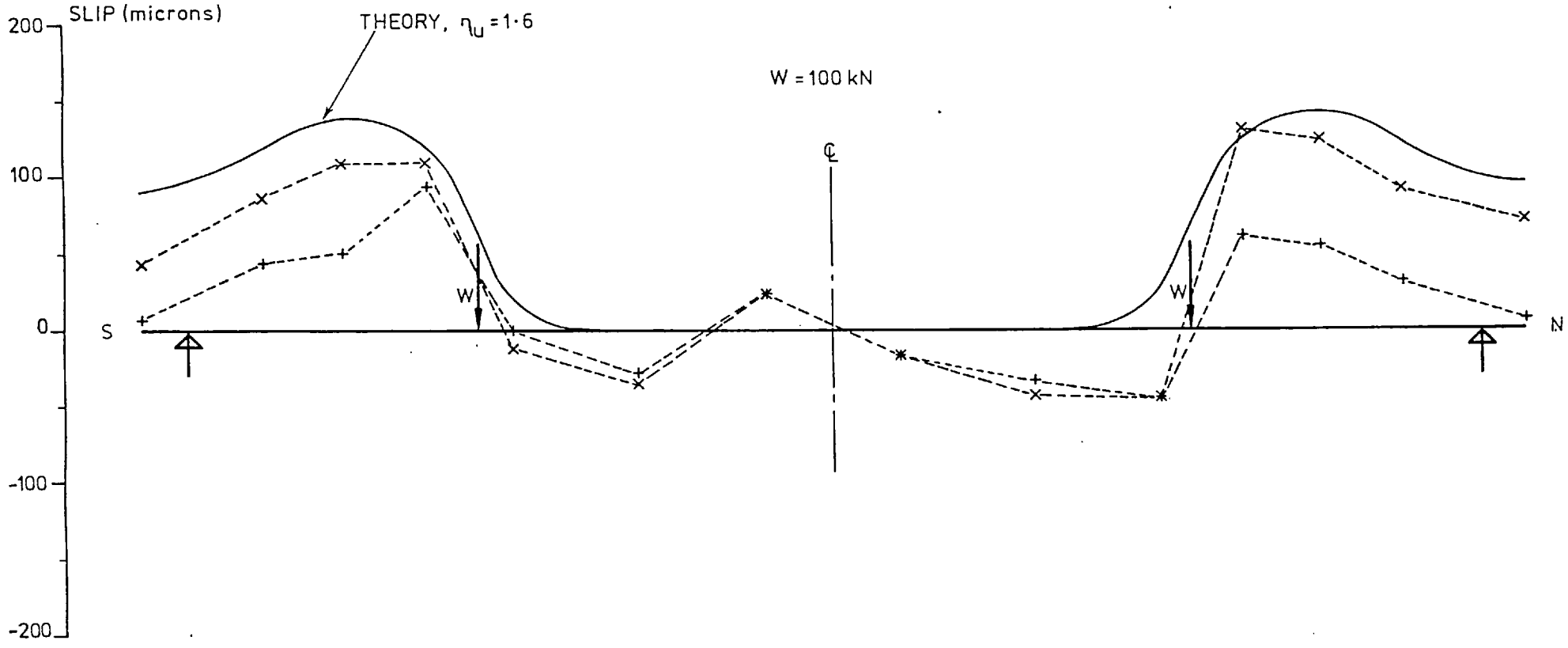


FIGURE 92: TEST 2 : THEORETICAL SLIP DISTRIBUTION AT 100 kN

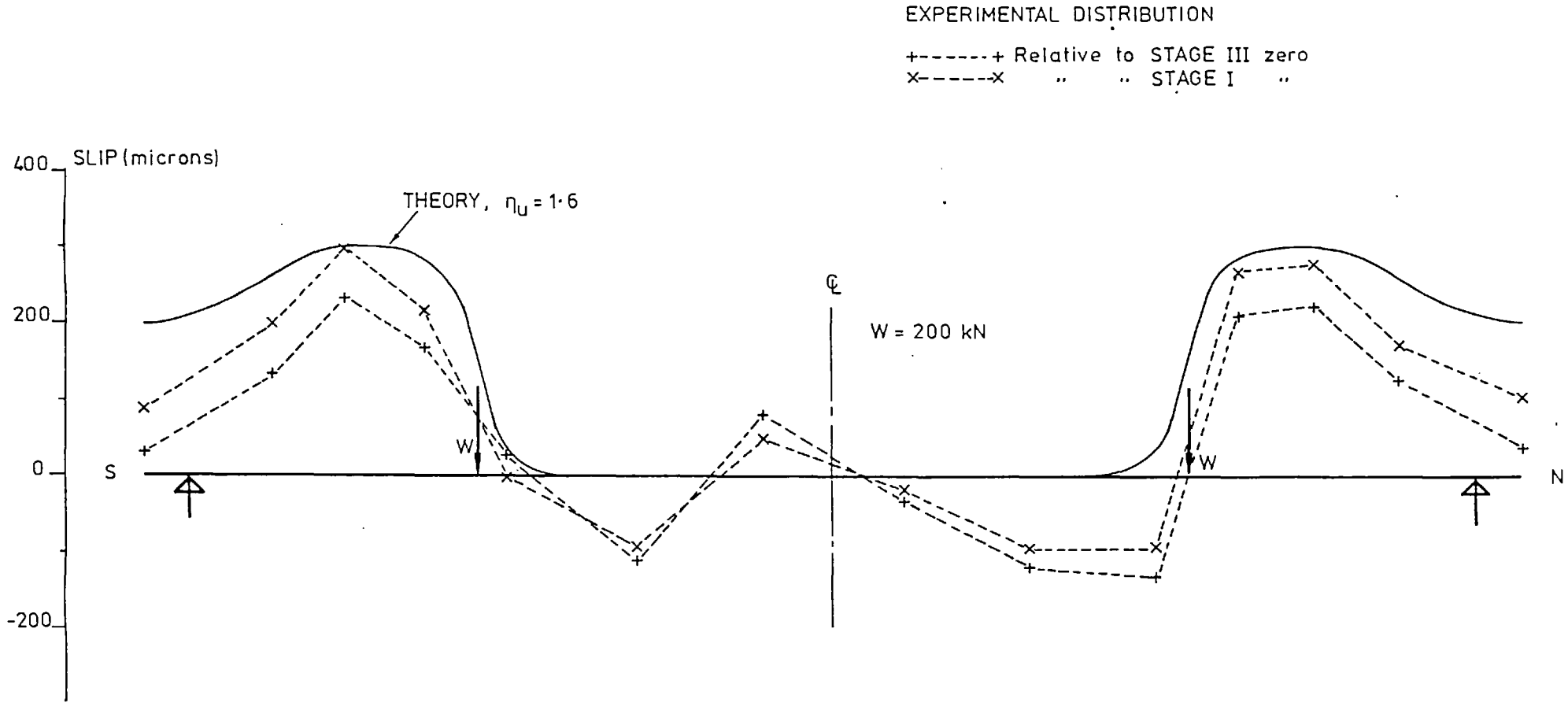


FIGURE 93 : TEST 2 : THEORETICAL SLIP DISTRIBUTION AT 200 kN

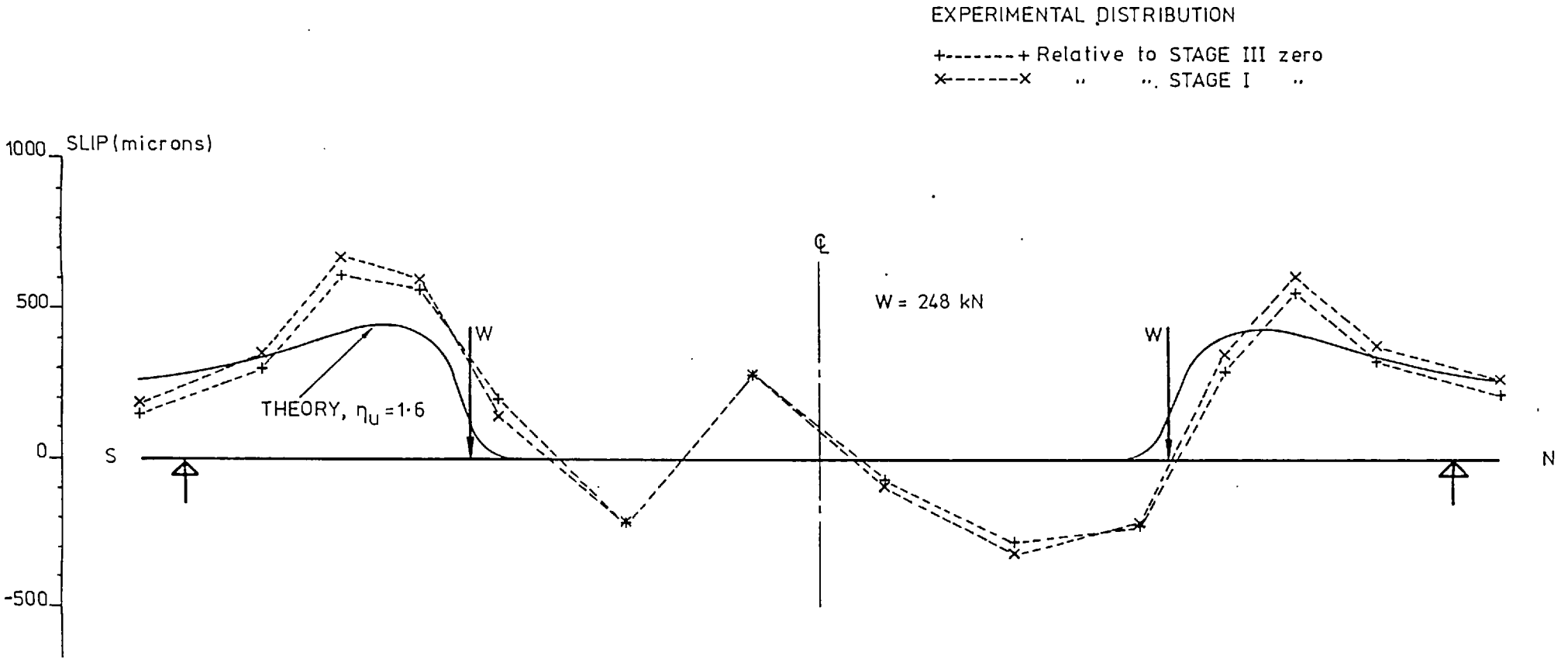


FIGURE 94: TEST 2 : THEORETICAL SLIP DISTRIBUTION AT 248 kN

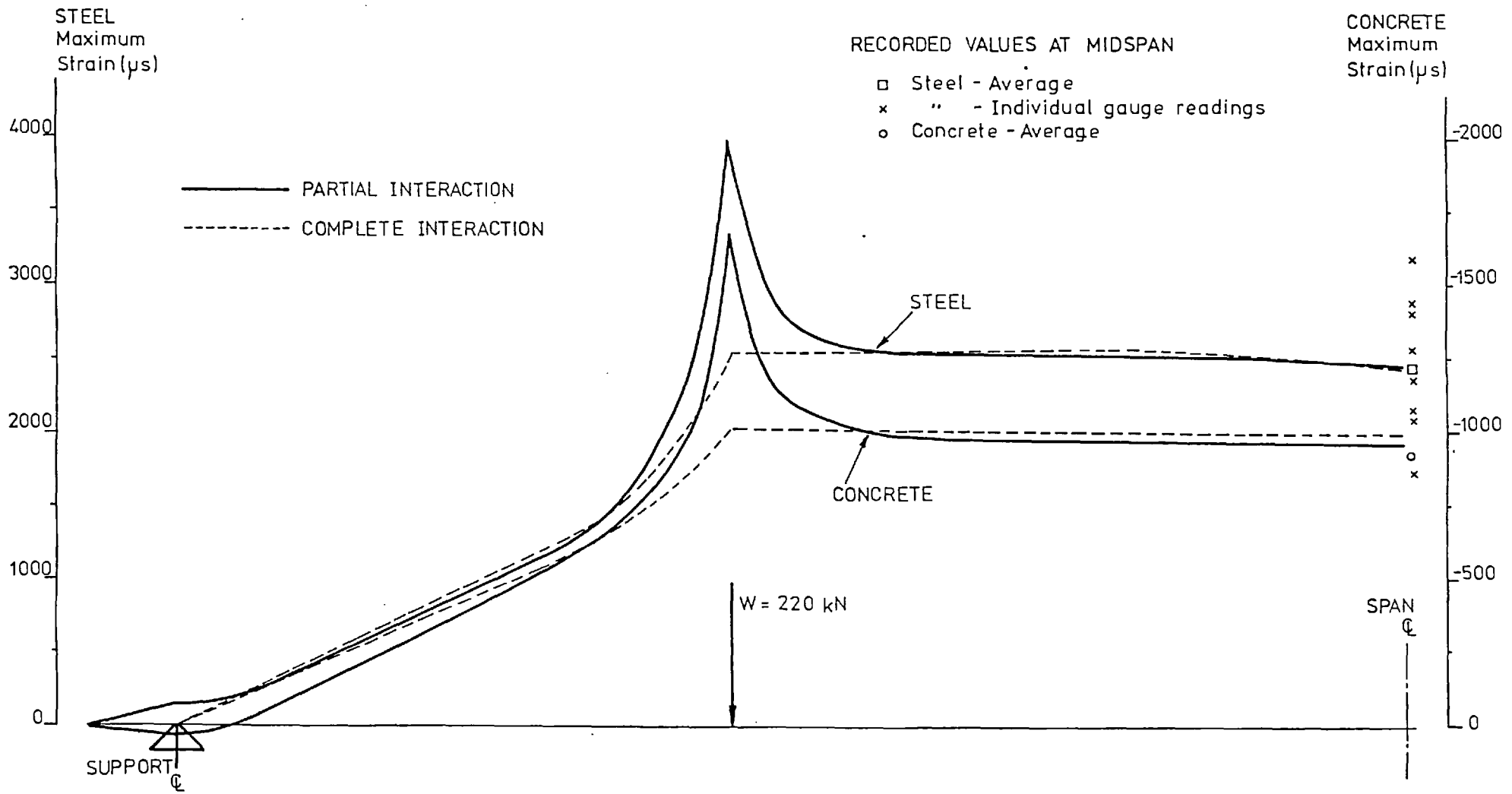


FIGURE 95: TEST 2 : THEORETICAL MAXIMUM STRAIN DISTRIBUTION AT 220 kN

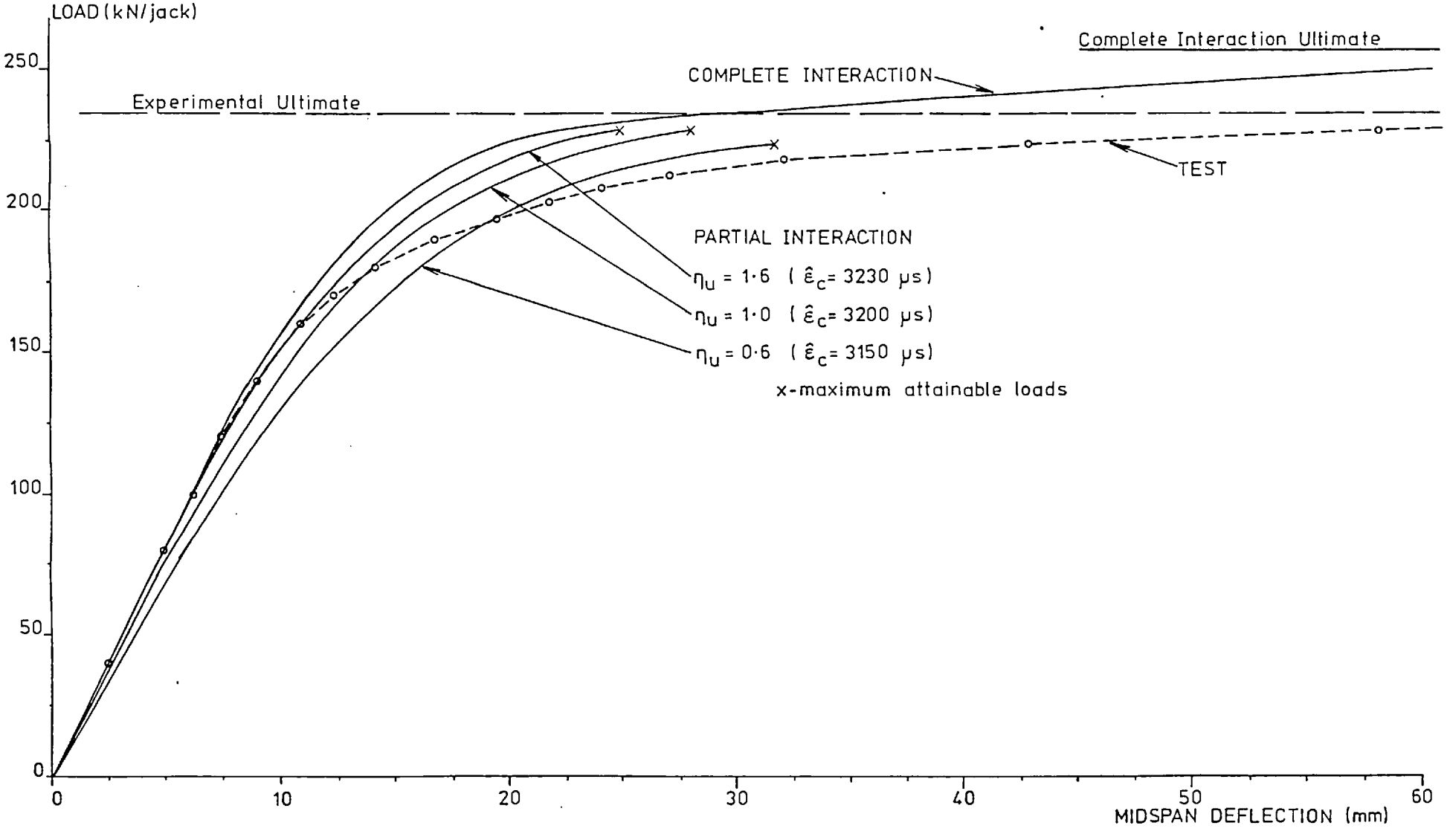


FIGURE 96: TEST 4 : MIDSPAN DEFLECTION RESPONSE - THEORY

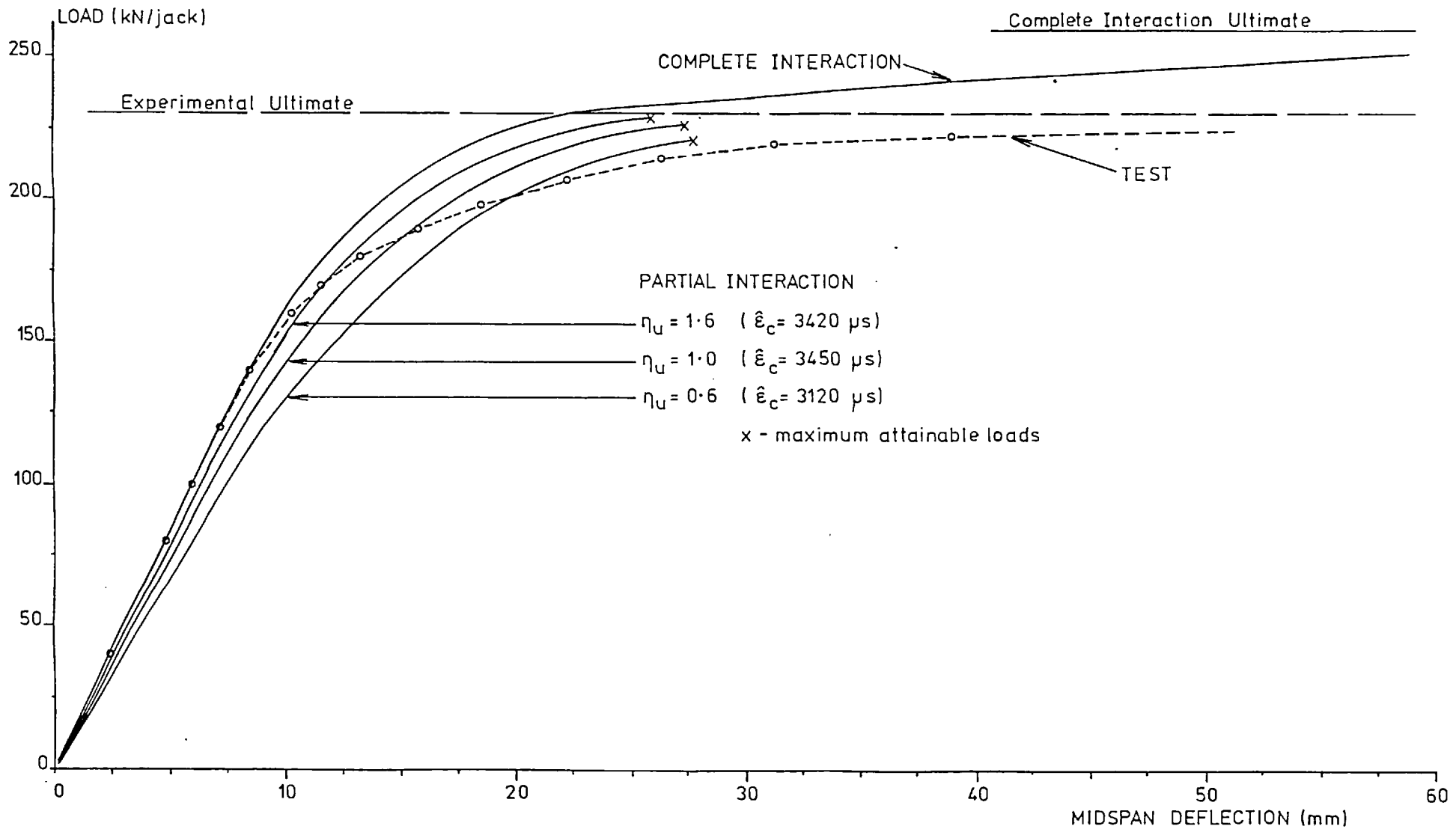


FIGURE 97: TEST 5 : MIDSPAN DEFLECTION RESPONSE - THEORY

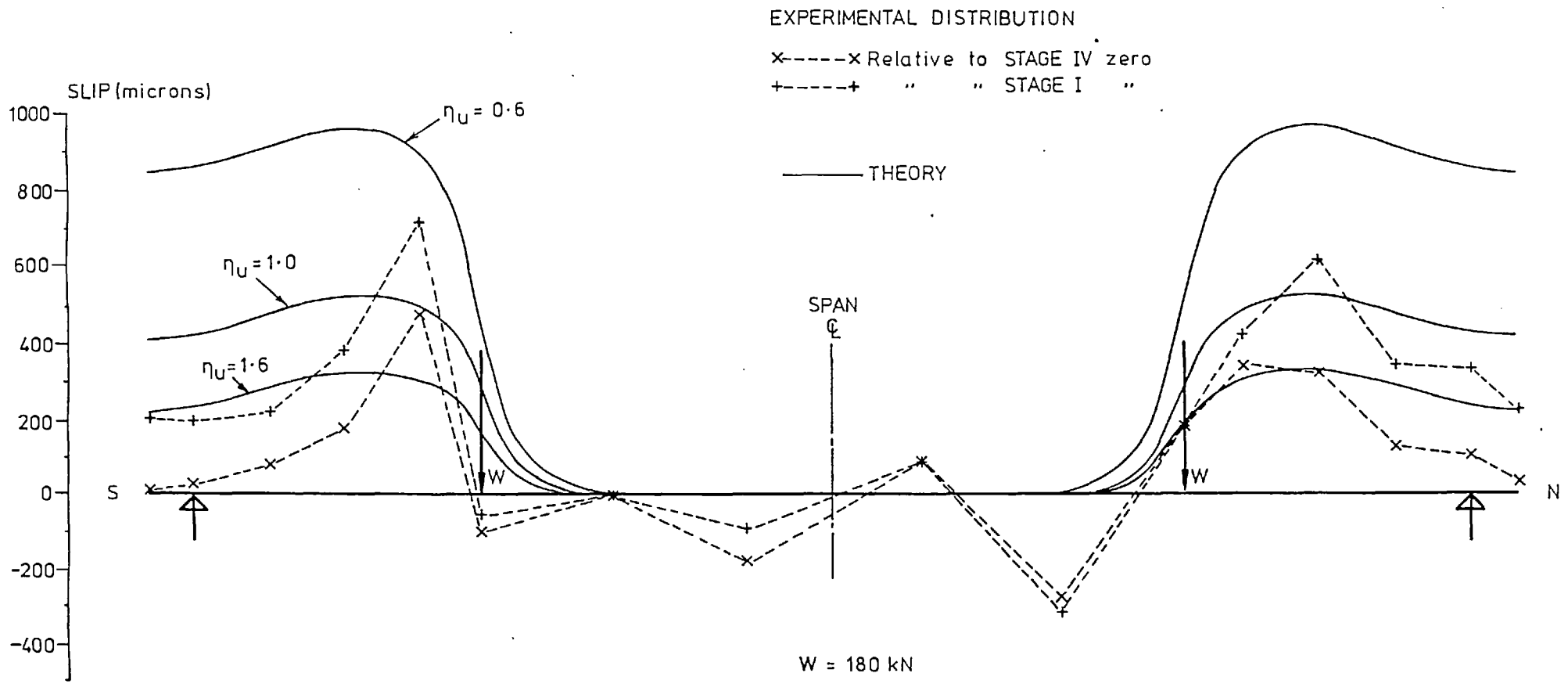


FIGURE 98: TEST 4 : THEORETICAL SLIP DISTRIBUTIONS AT 180 kN

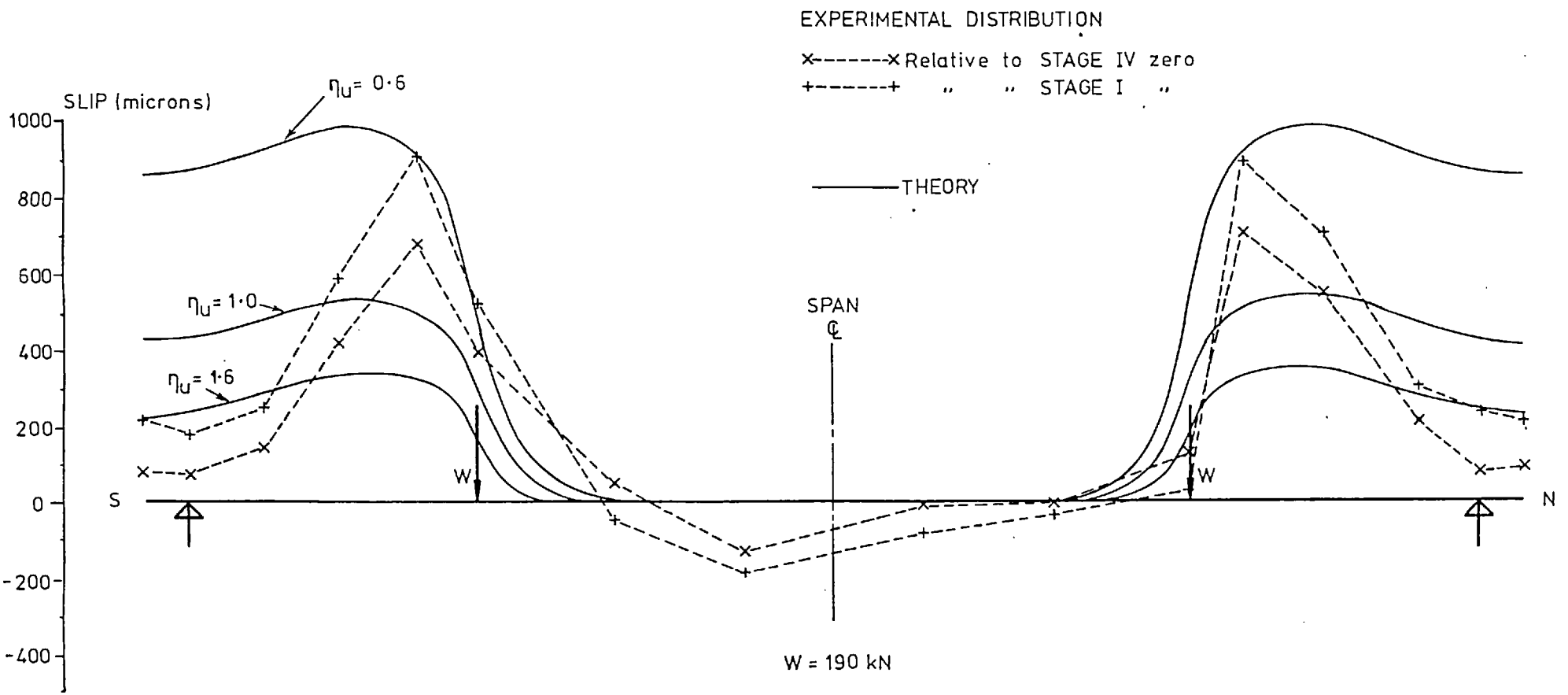


FIGURE 99: TEST 5 : THEORETICAL SLIP DISTRIBUTIONS AT 190 kN

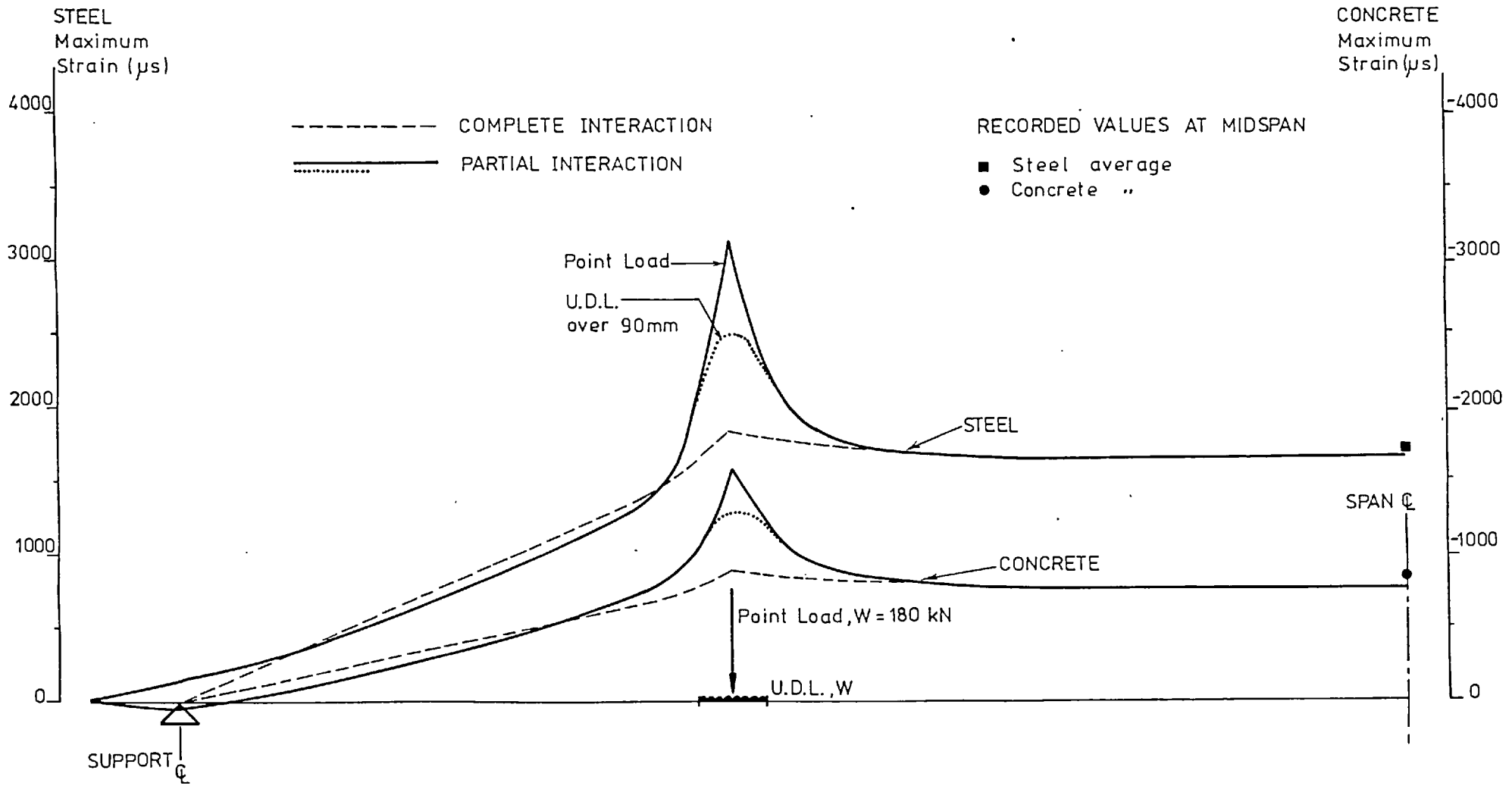


FIGURE 100: TEST 4 : THEORETICAL MAXIMUM STRAIN DISTRIBUTION AT 180 kN

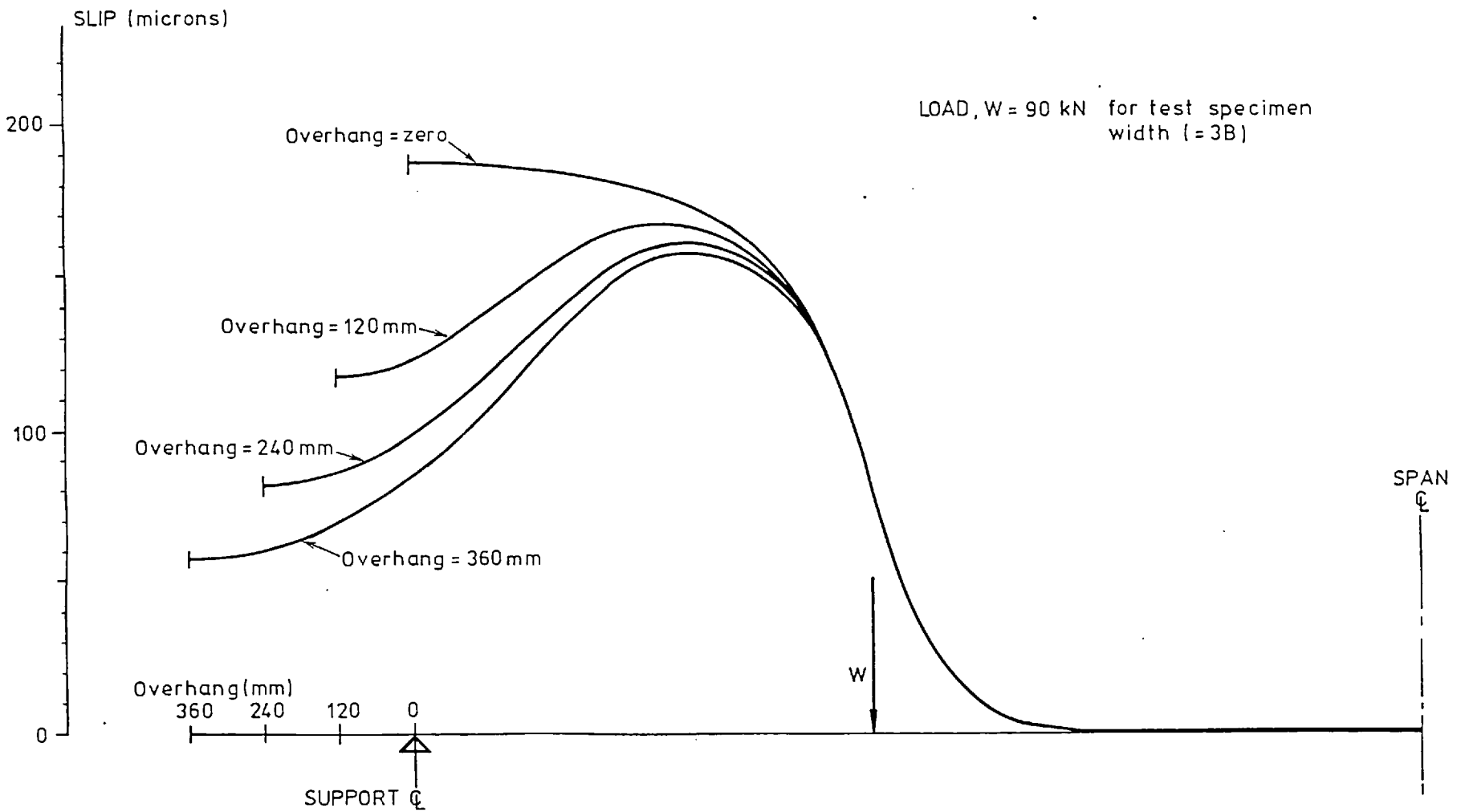


FIGURE 101: EFFECT OF END OVERHANG ON SLIP DISTRIBUTION

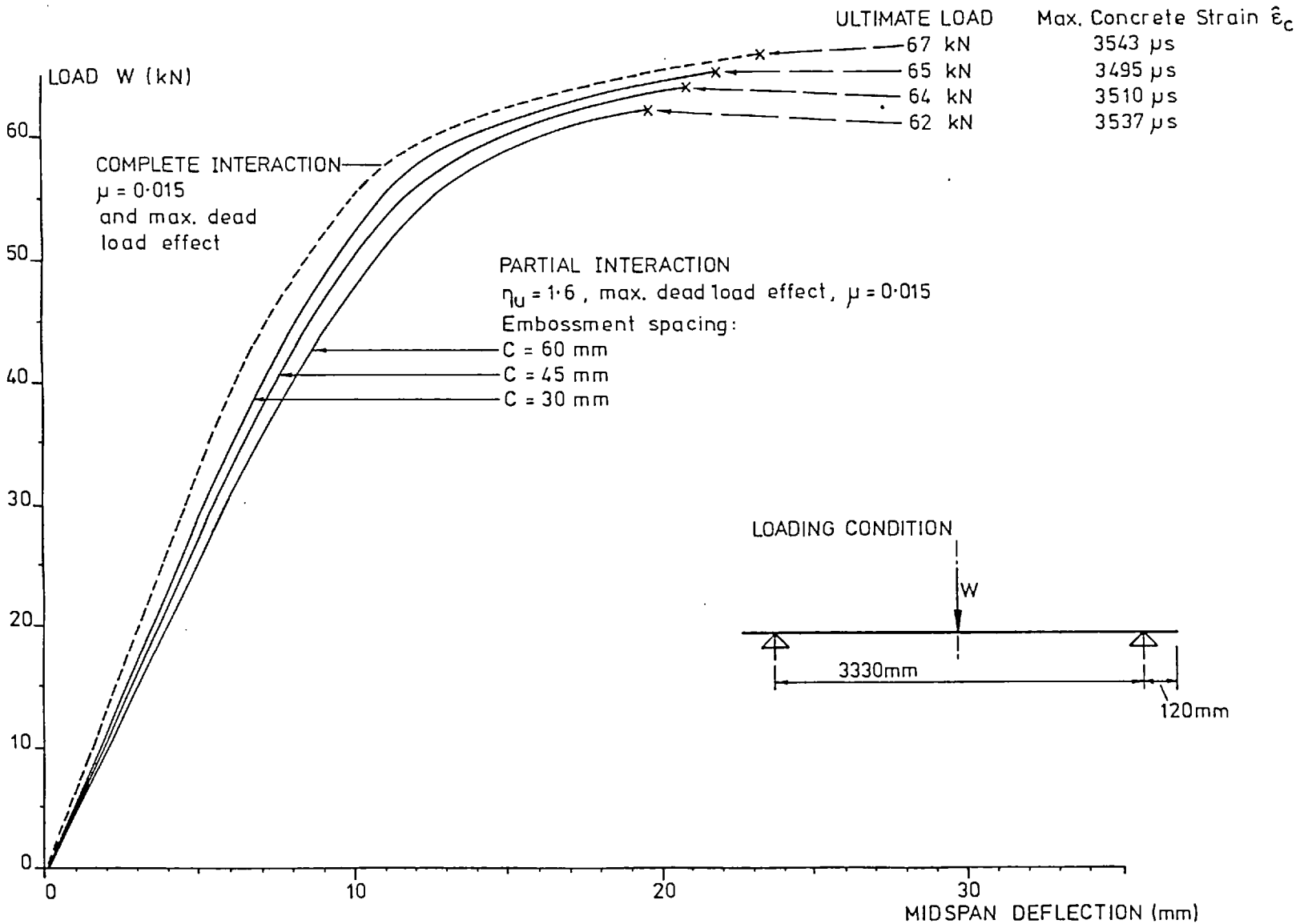


FIGURE 102: EFFECT OF EMBOSSMENT SPACING ON LOAD-DEFLECTION RESPONSE

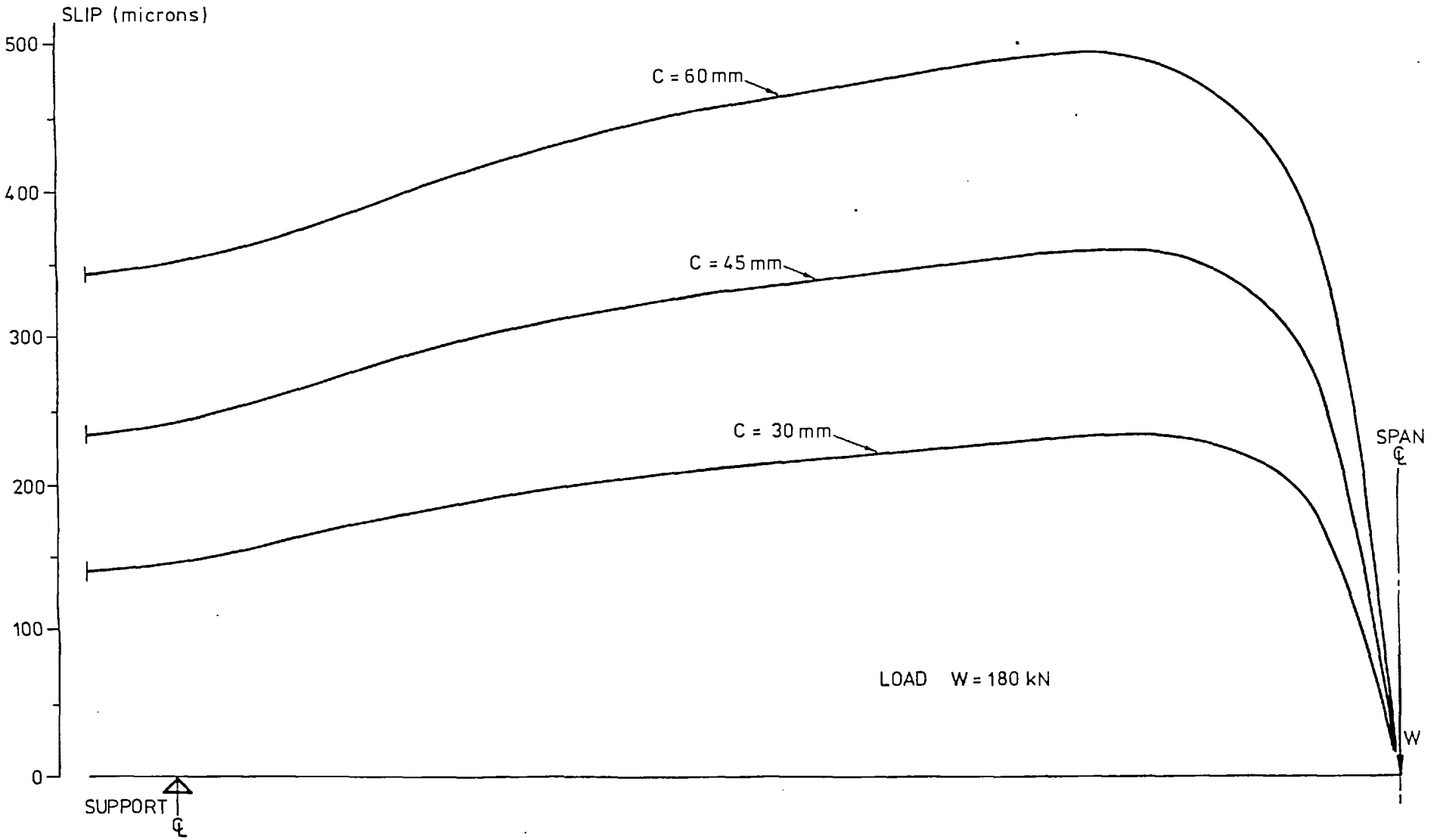


FIGURE 103: EFFECT OF EMBOSSMENT SPACING ON SLIP DISTRIBUTION

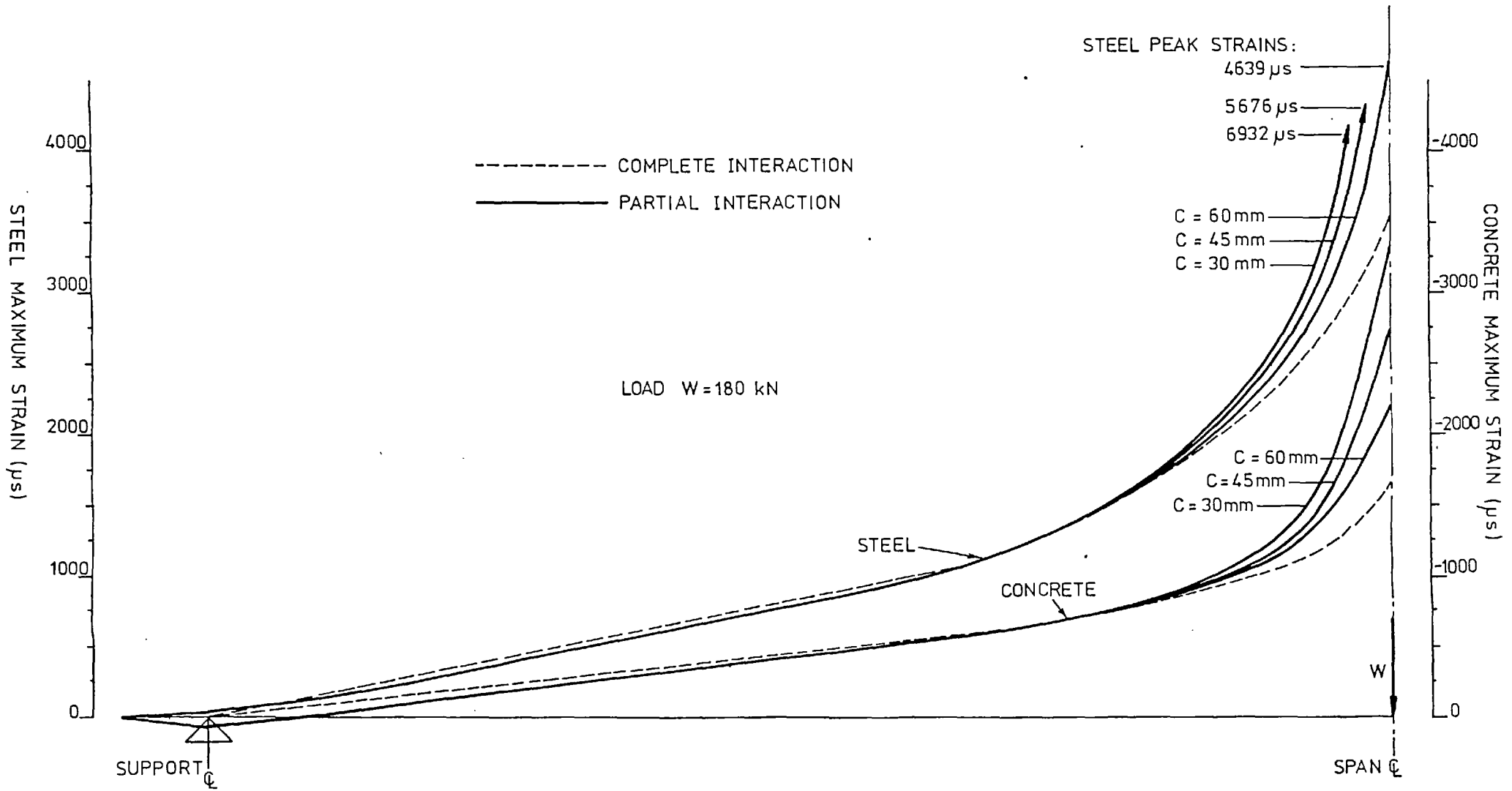
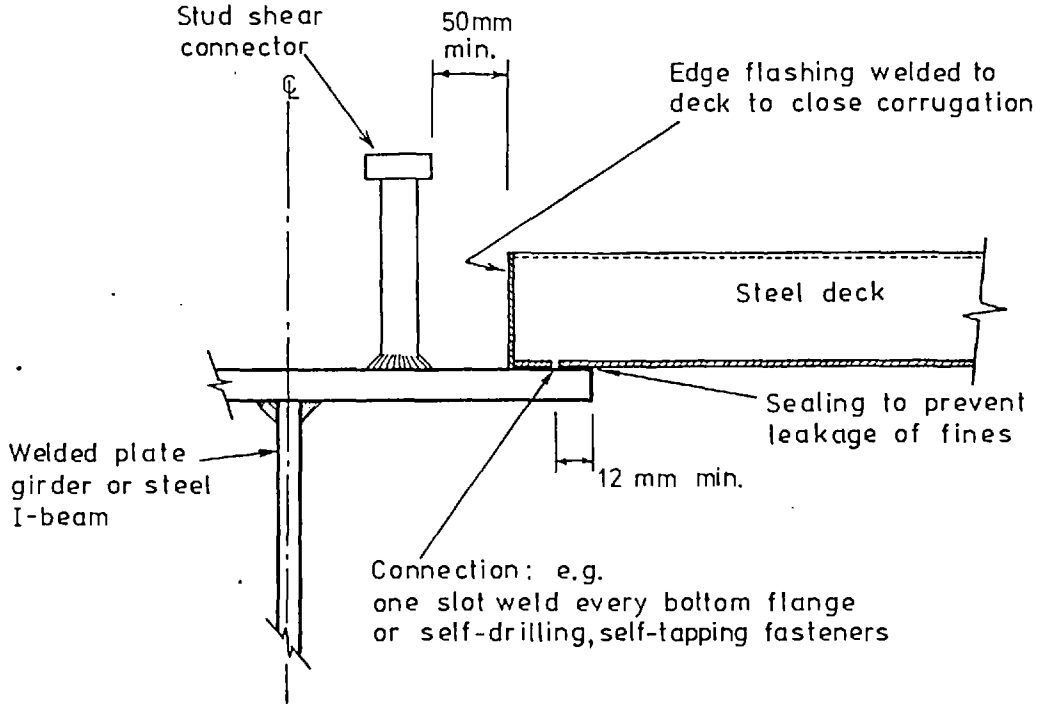
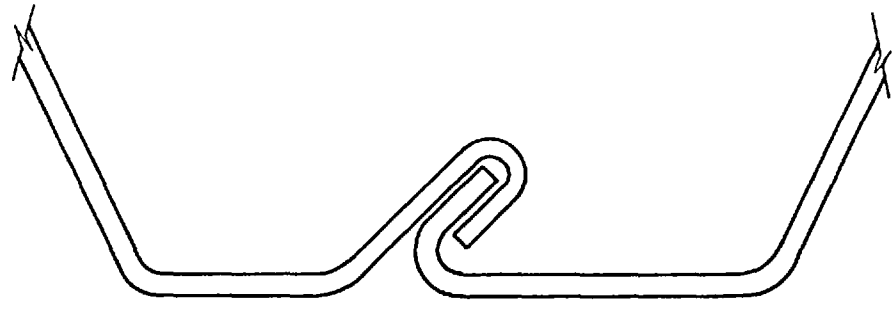


FIGURE 104: EFFECT OF EMBOSSMENT SPACING ON STRAIN DISTRIBUTION



END CONNECTION DETAILS FOR STEEL BEAMS.



POSSIBLE ALTERNATIVE LONGITUDINAL EDGE CONNECTION

FIGURE 105: PROPOSED CONNECTION DETAILS FOR FORMWORK

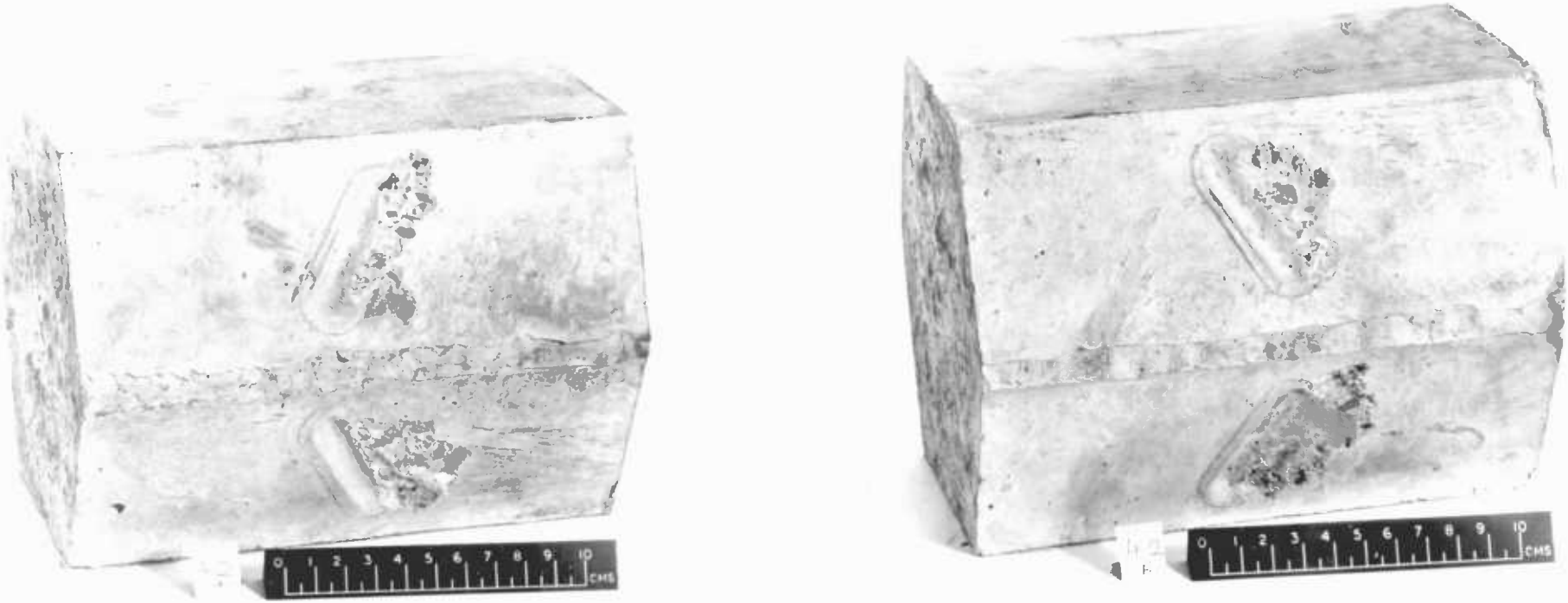


PLATE 1. PUSH-OUT SPECIMEN 4.2.

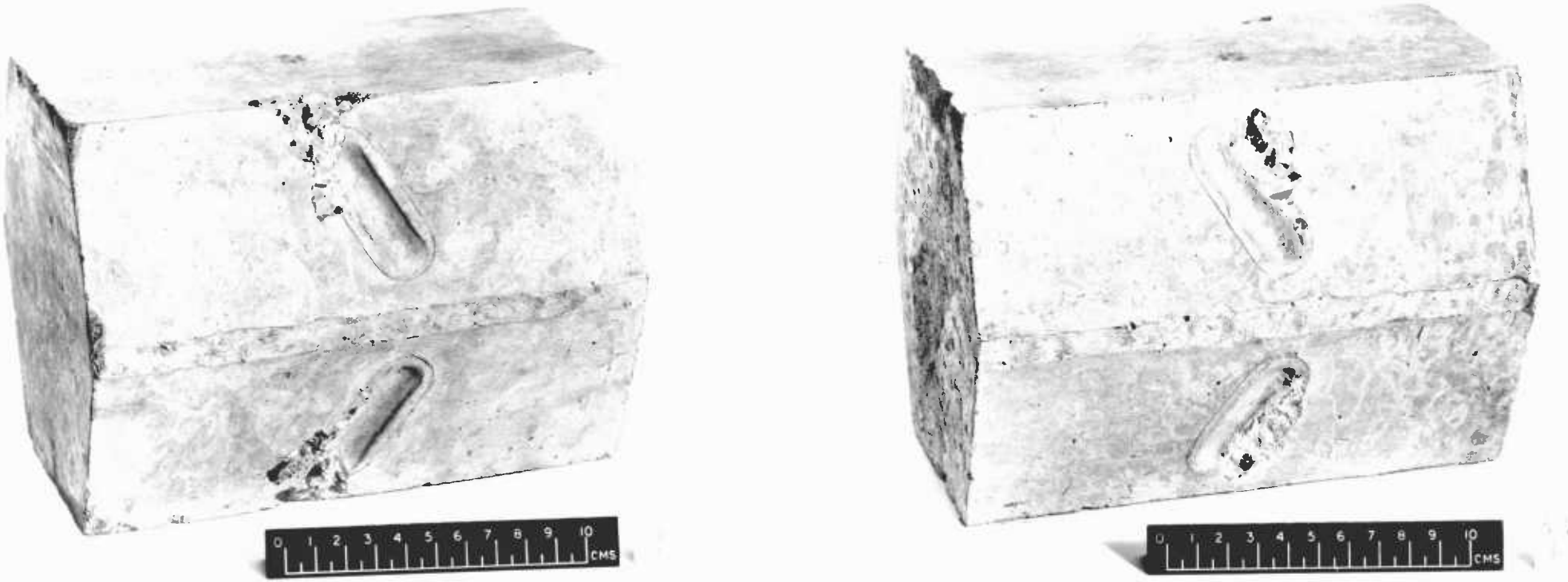


PLATE 2. PUSH-OUT SPECIMEN 4.4.



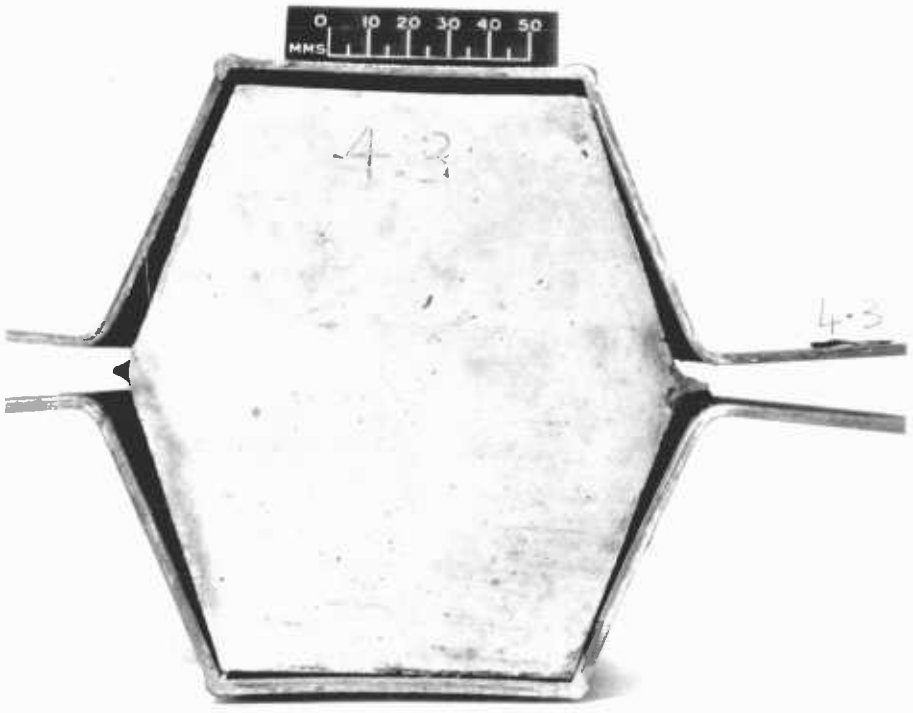


PLATE 3. PUSH-OUT SPECIMENS 1.3. AND 4.3.

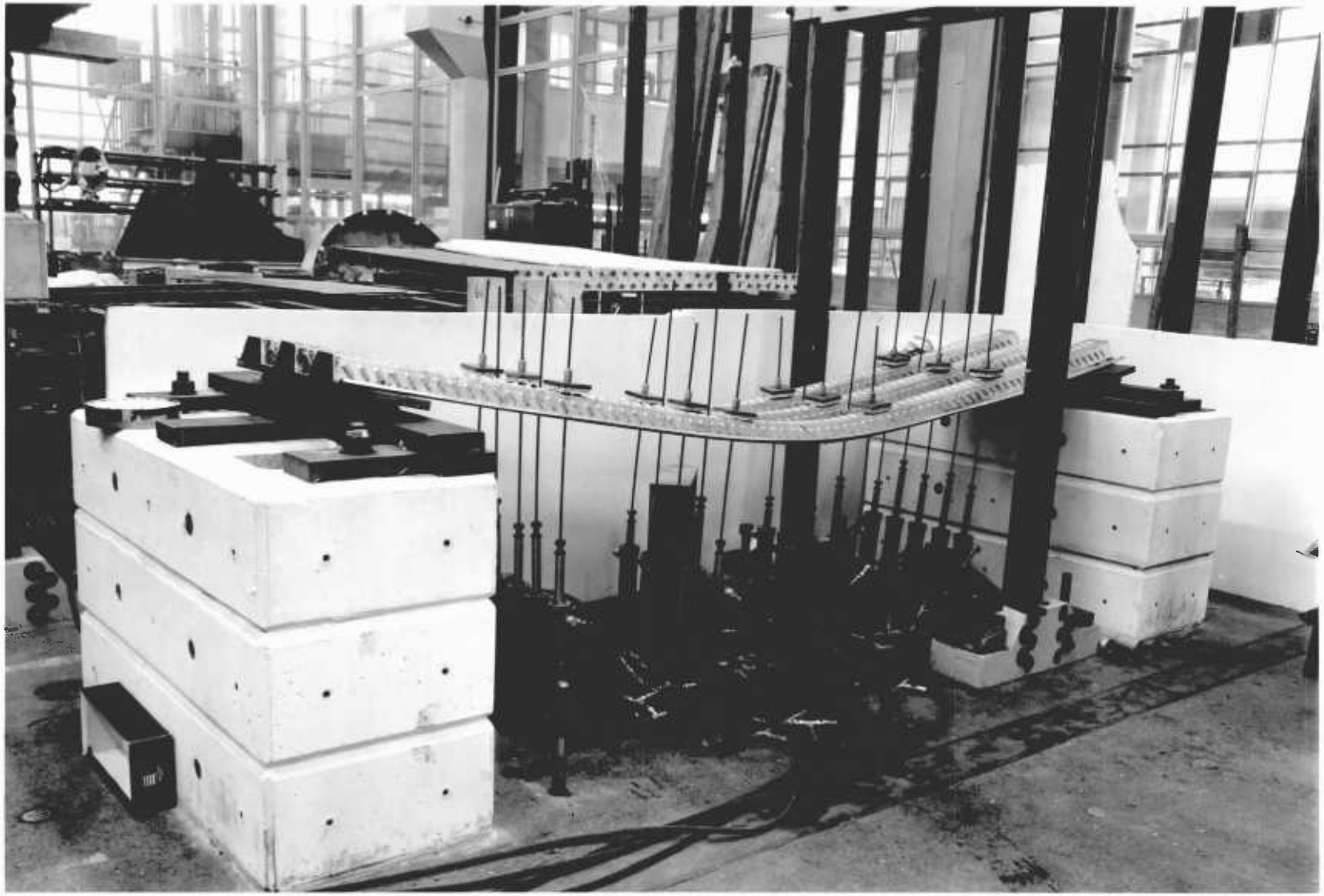


PLATE 4. CONSTRUCTION LOADING TEST RIG

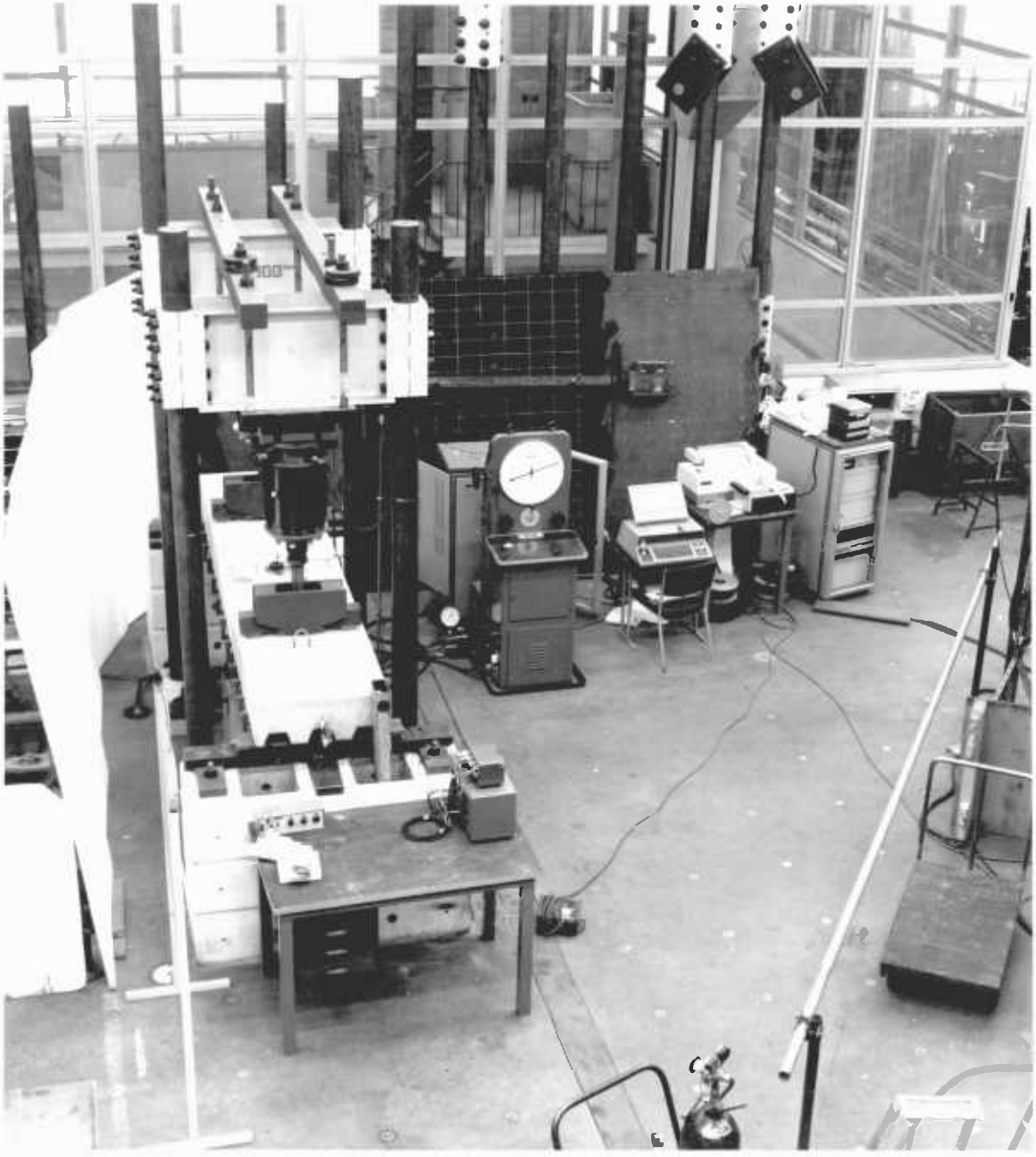


PLATE 5. GENERAL VIEW OF STATIC TEST RIG

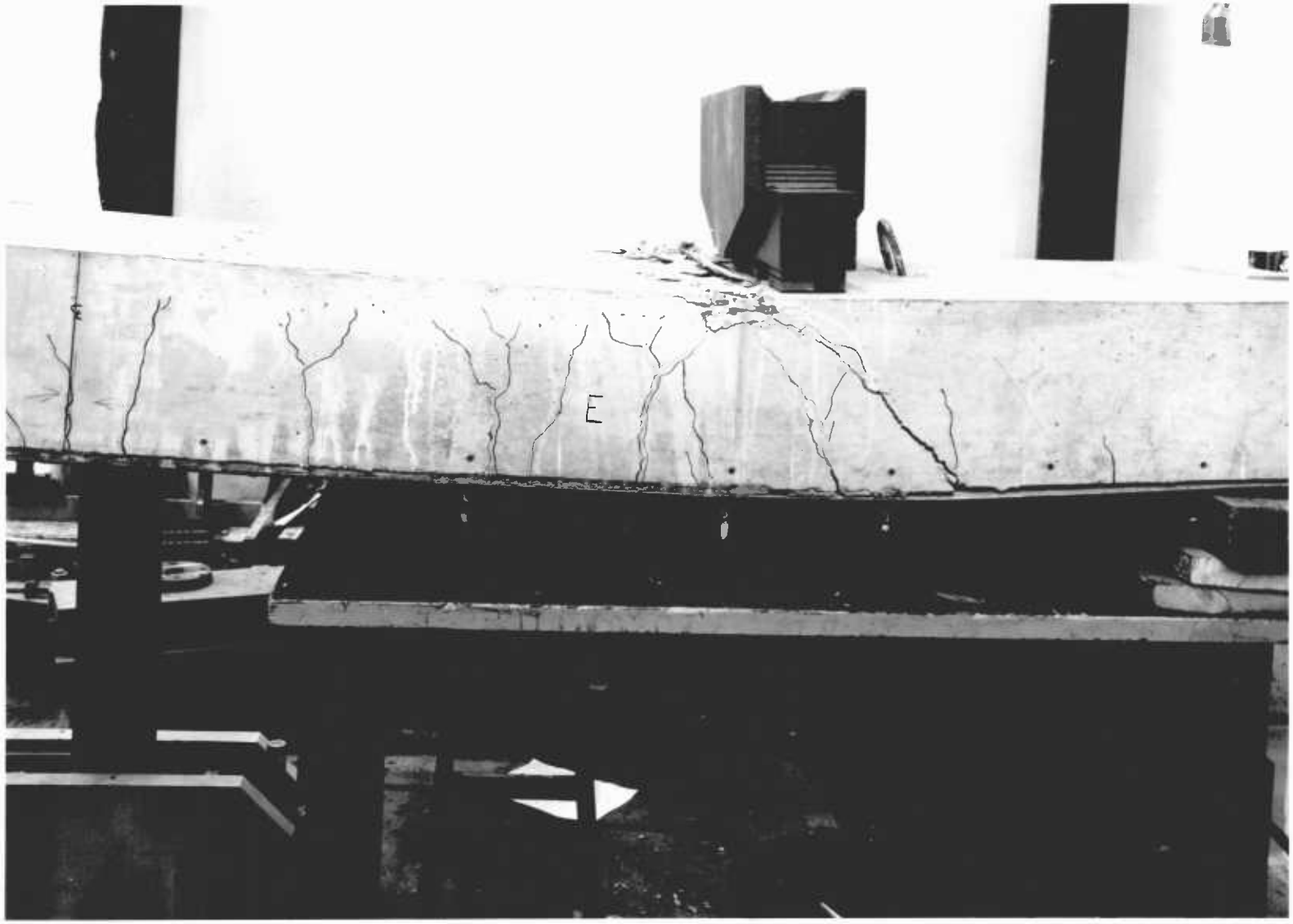


PLATE 6. FAILURE OF SPECIMEN IN TEST 2

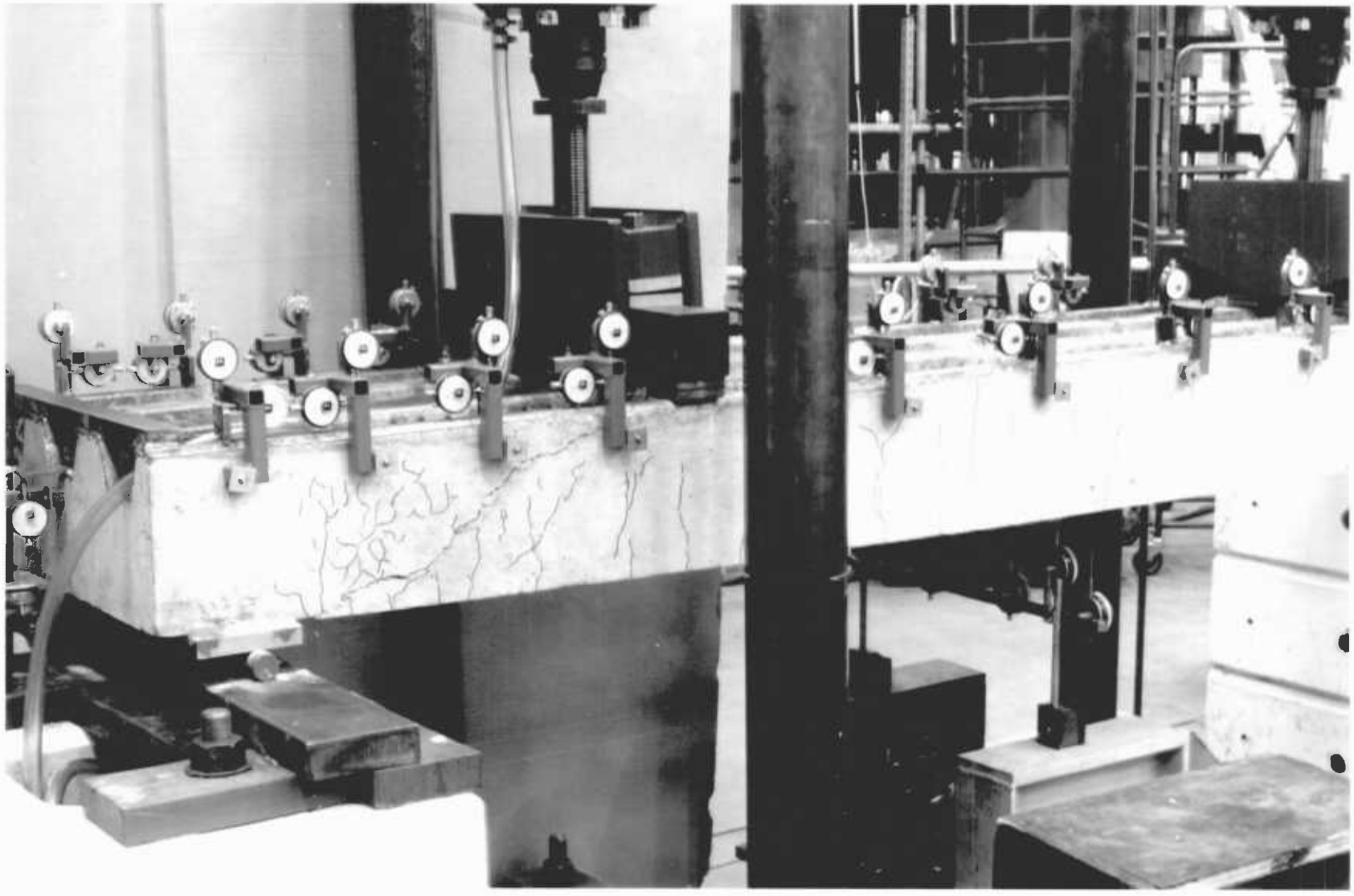


PLATE 7. FAILURE OF SPECIMEN IN TEST 3

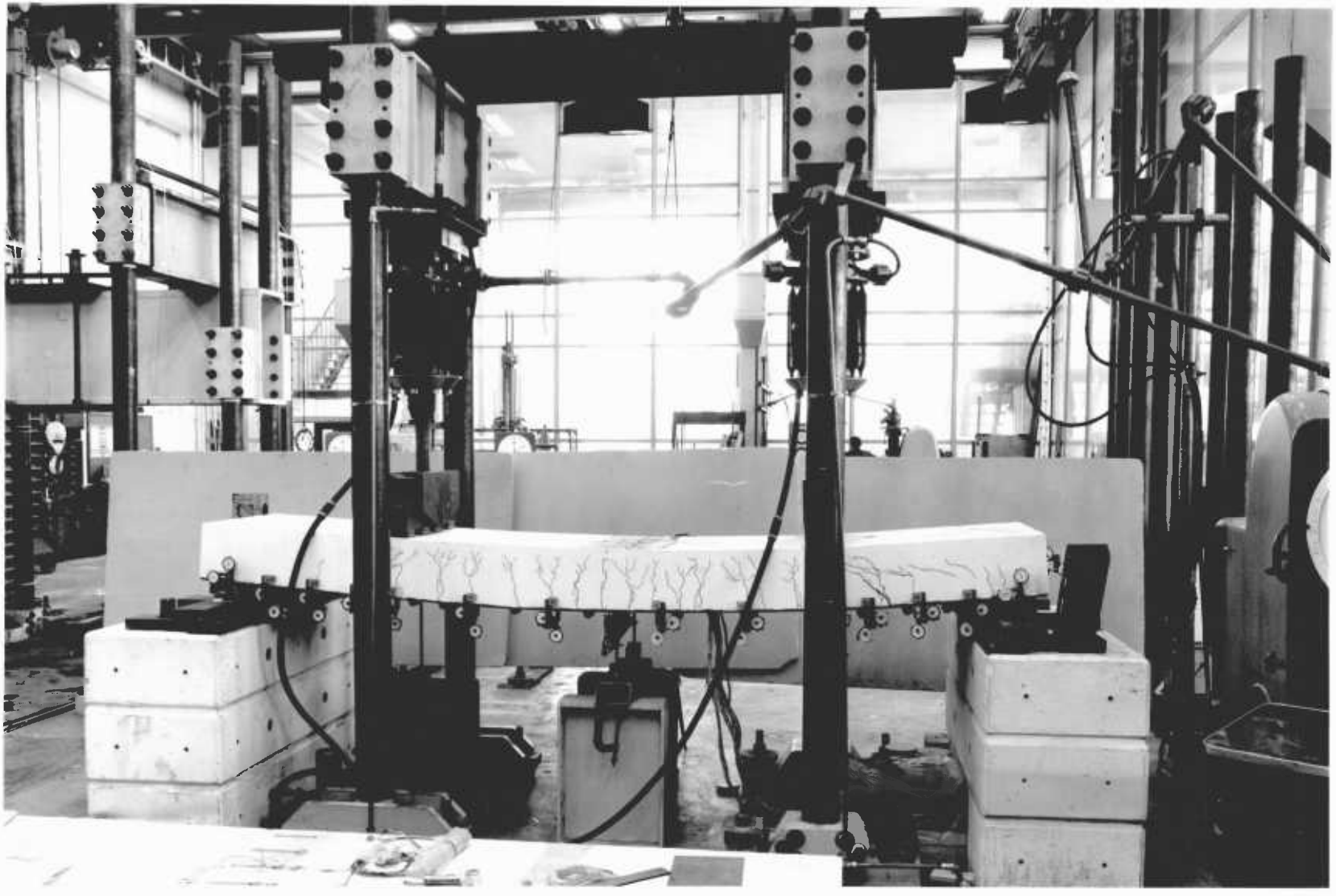


PLATE 8. TEST RIG FOR REPEATED LOADING

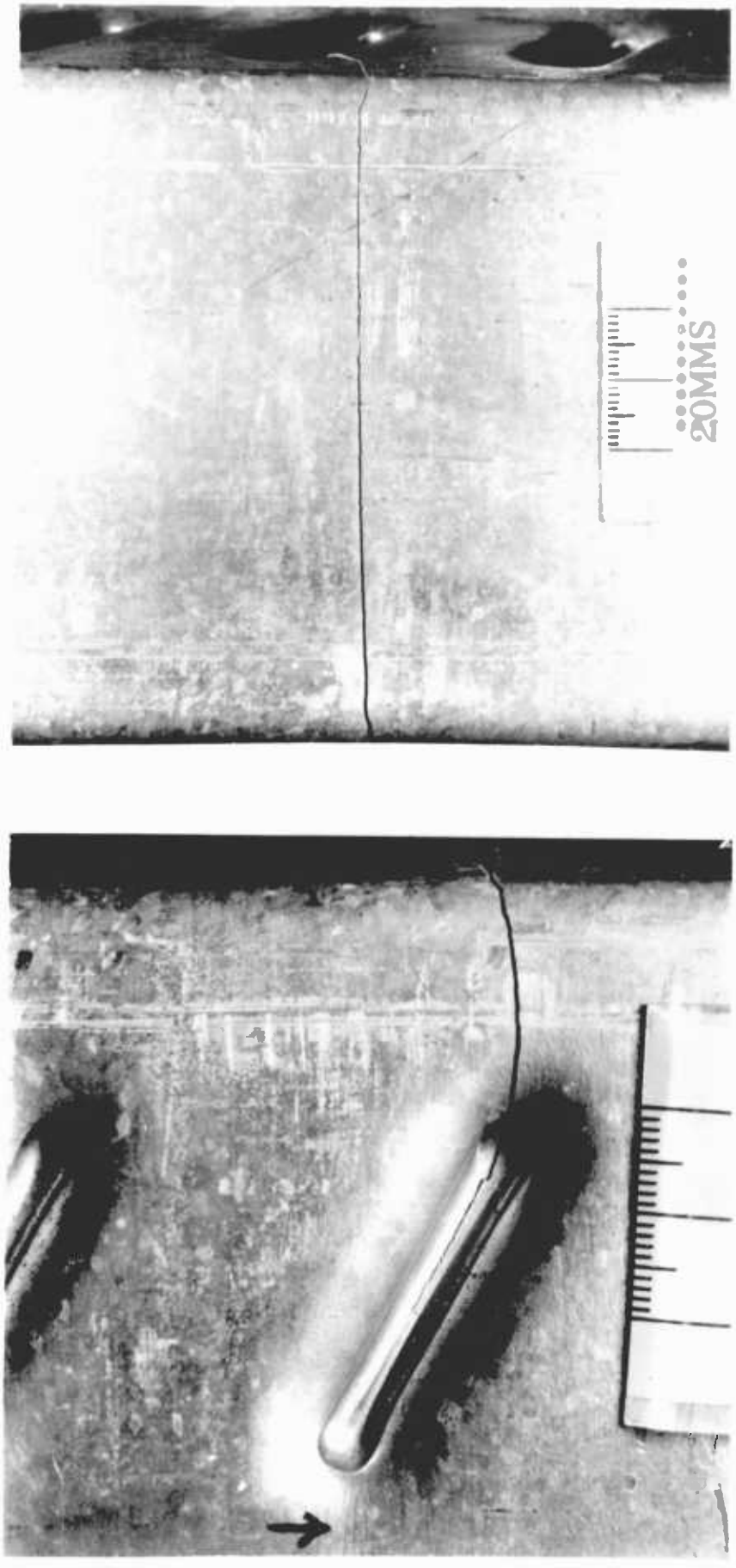


PLATE 9. TEST 6 - FATIGUE CRACK

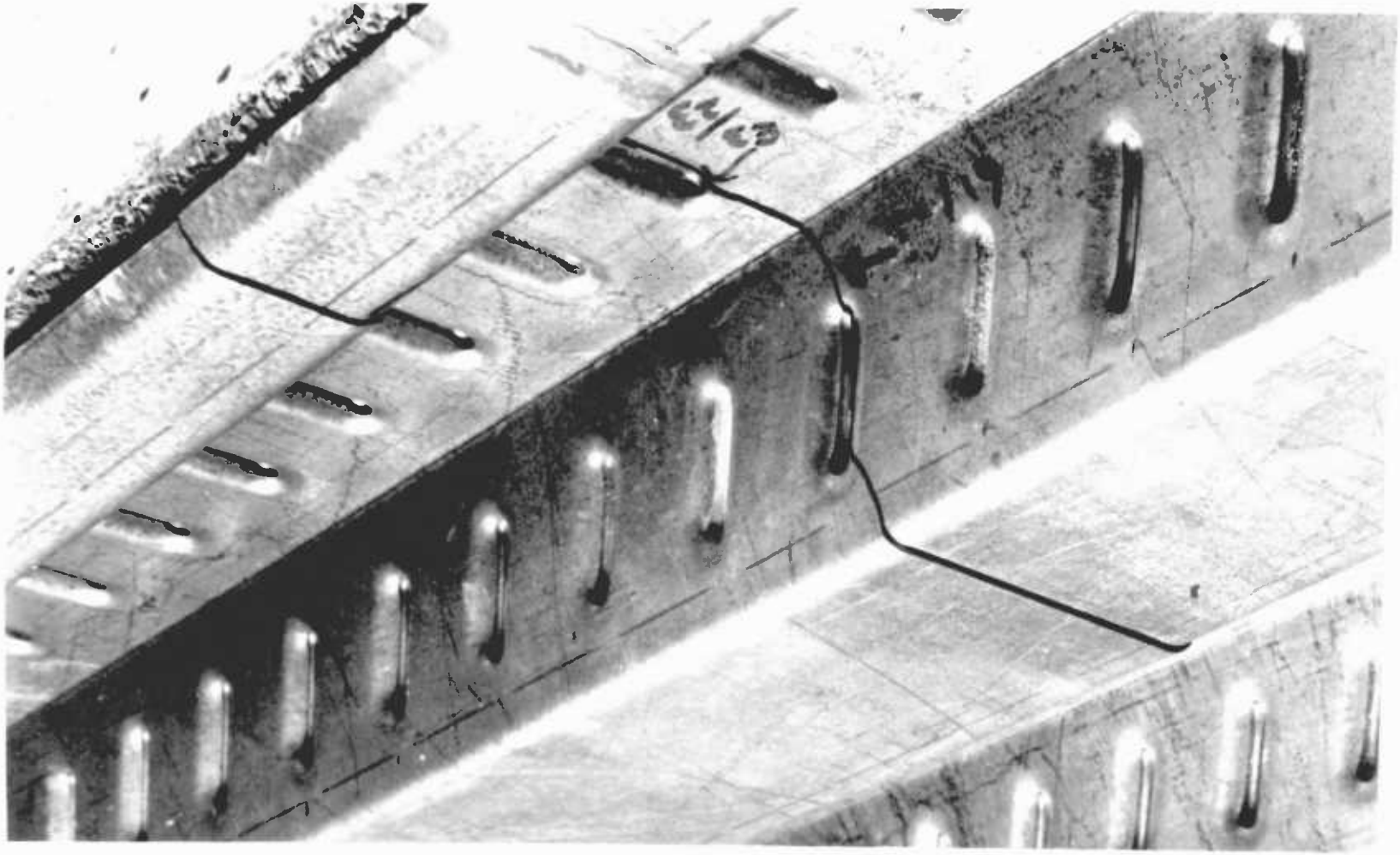


PLATE 10. TEST 9 - FINAL EXTENT OF FATIGUE CRACK

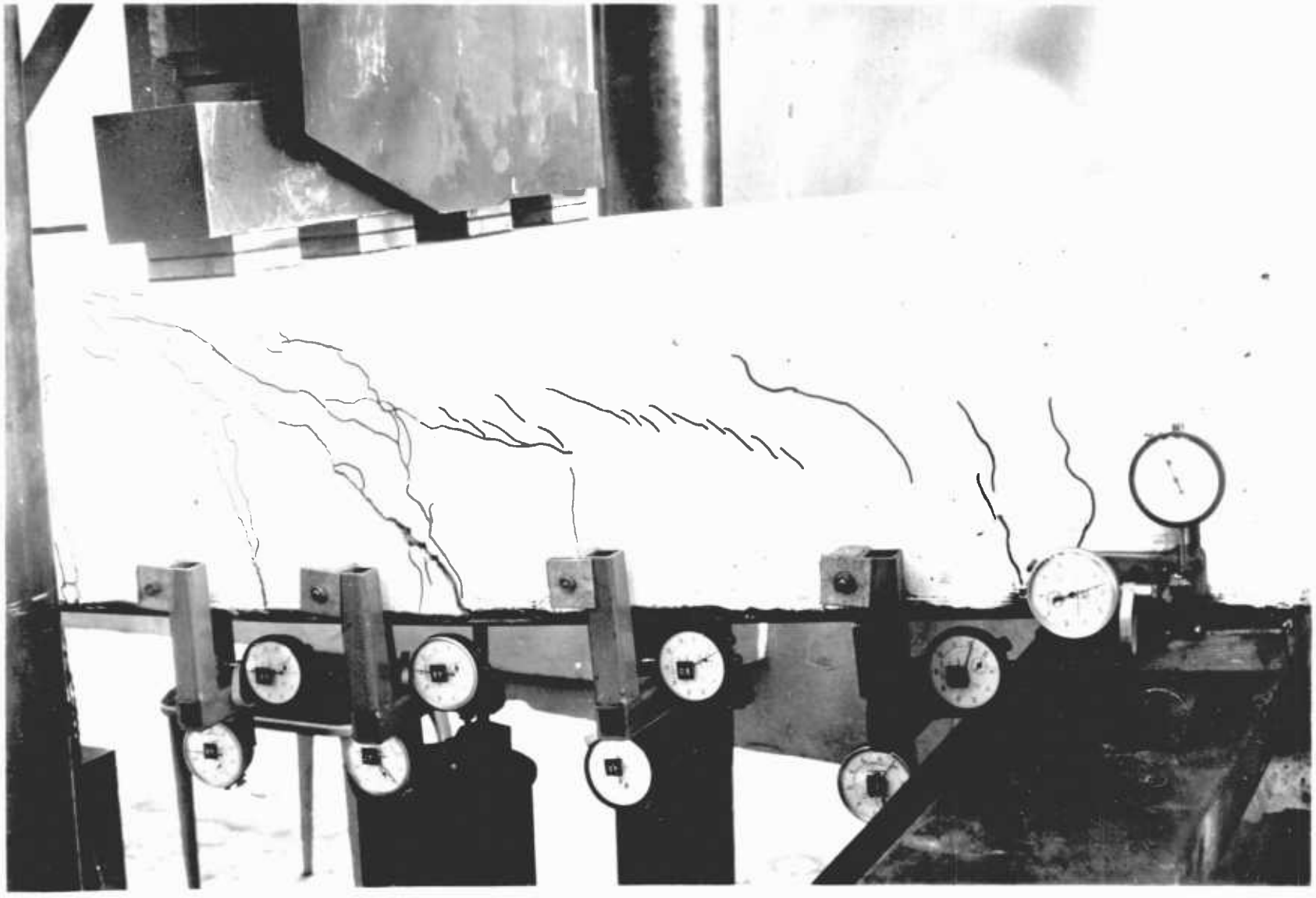


PLATE 11. TEST 4 - NORTH SHEAR SPAN, AFTER FAILURE

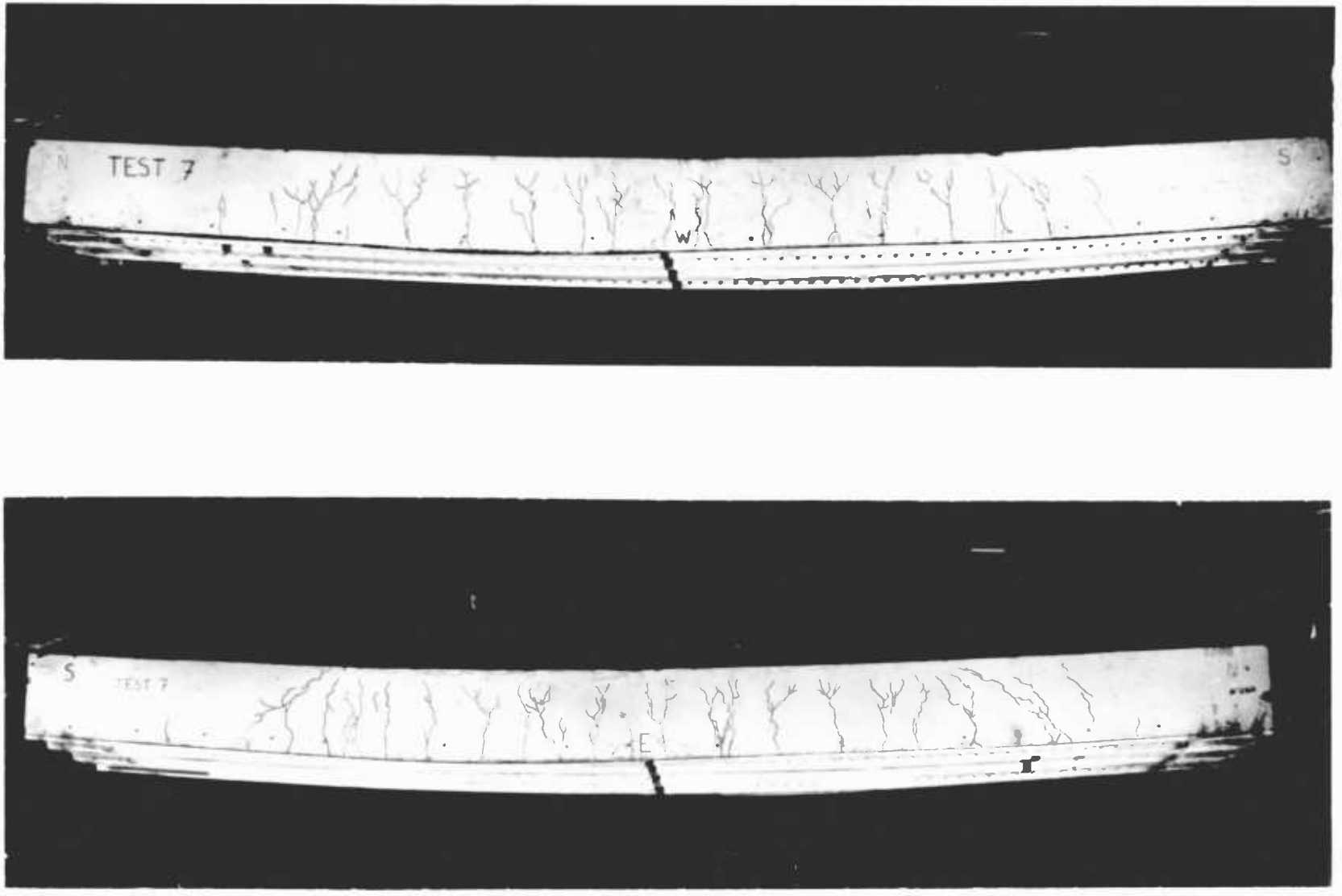


PLATE 12. TEST 7 - AFTER FAILURE

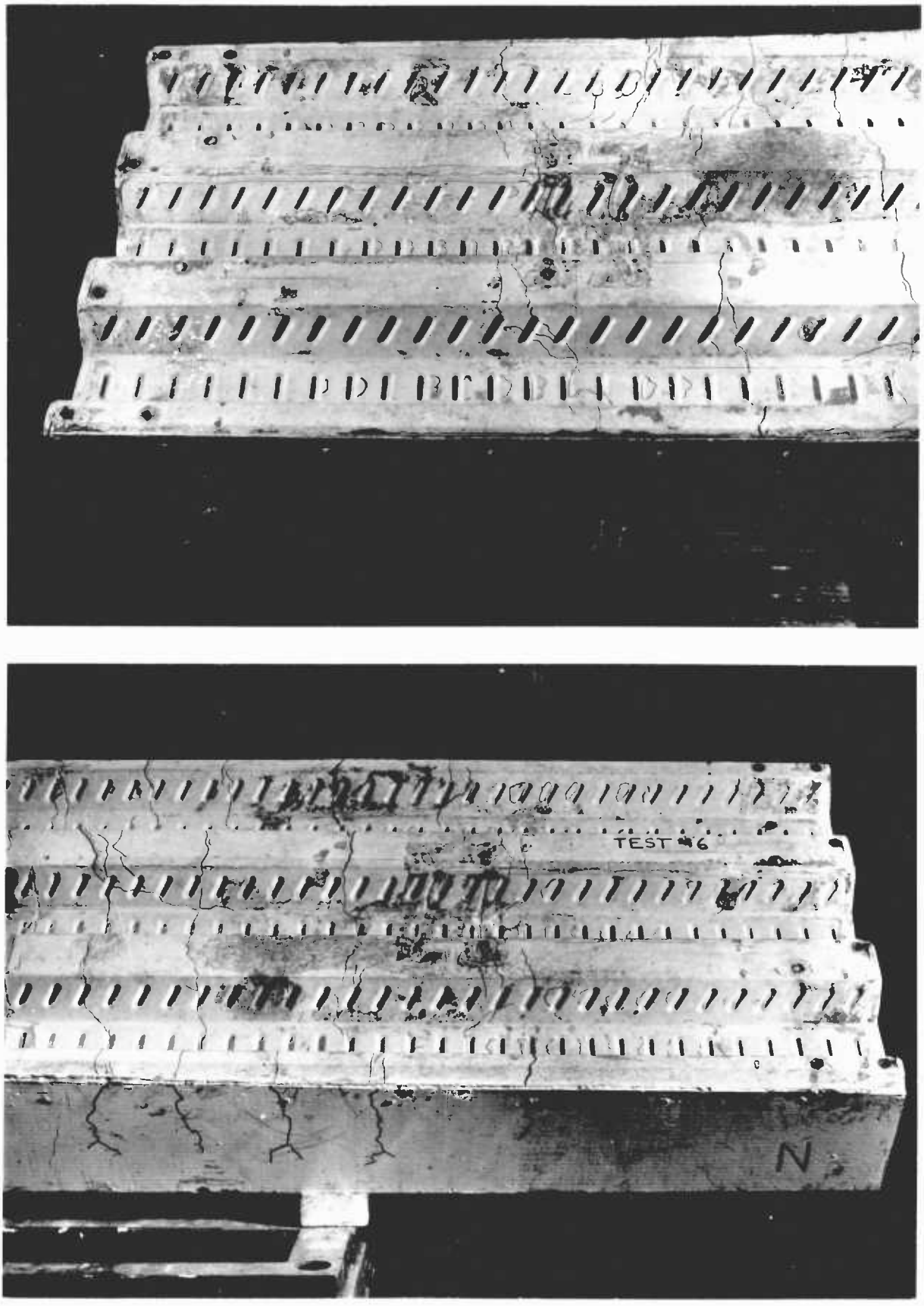
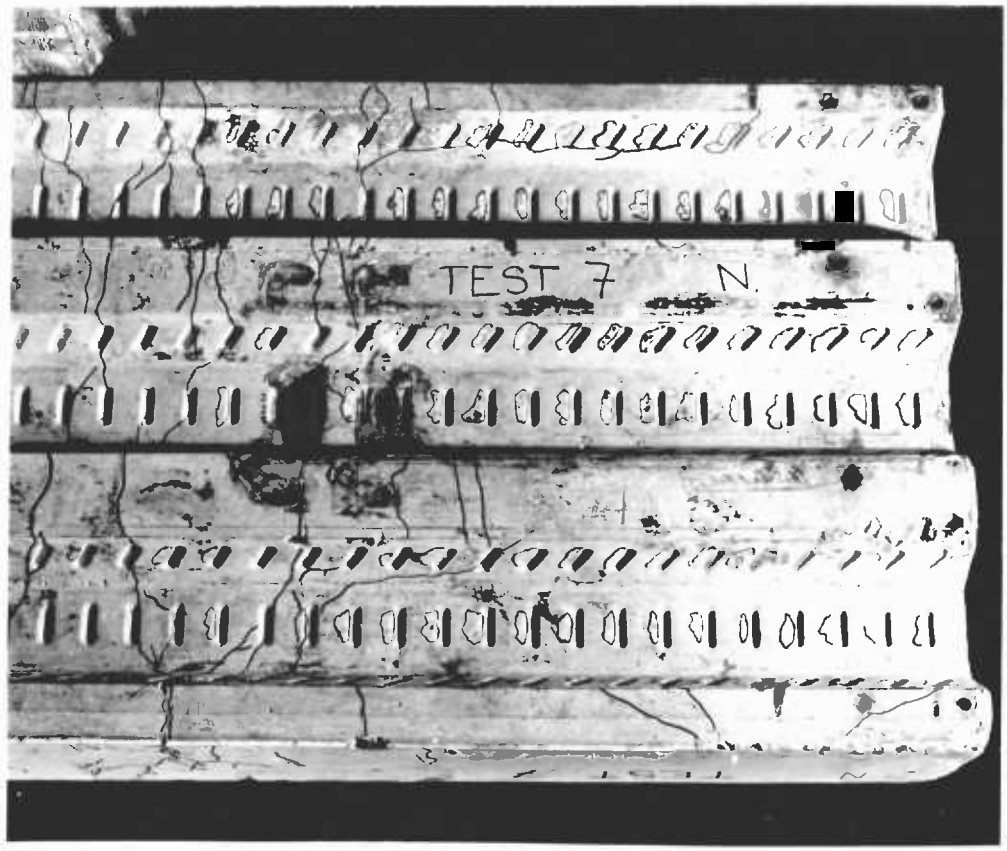


PLATE 13. TEST 6 - NORTH SHEAR SPAN
(FORMWORK REMOVED)



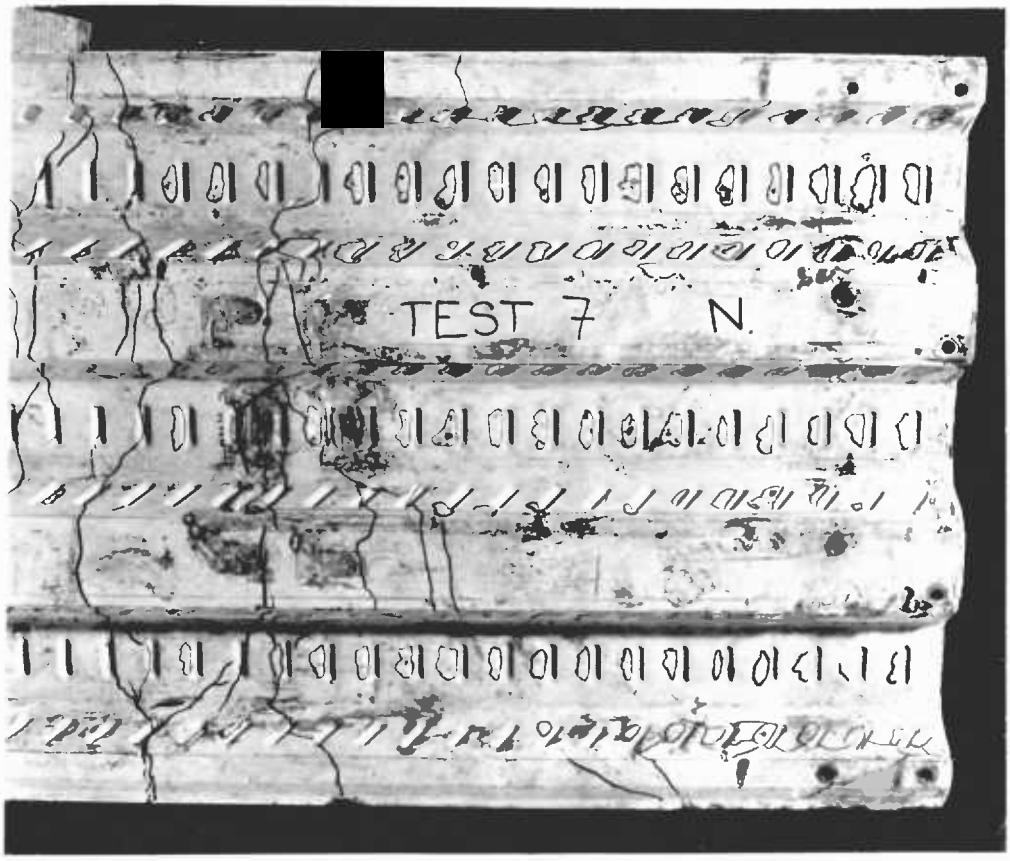


PLATE 14. TEST 7 - NORTH SHEAR SPAN
(FORMWORK REMOVED)



PLATE 15. VIBROPHORE SPECIMEN UNDER TEST

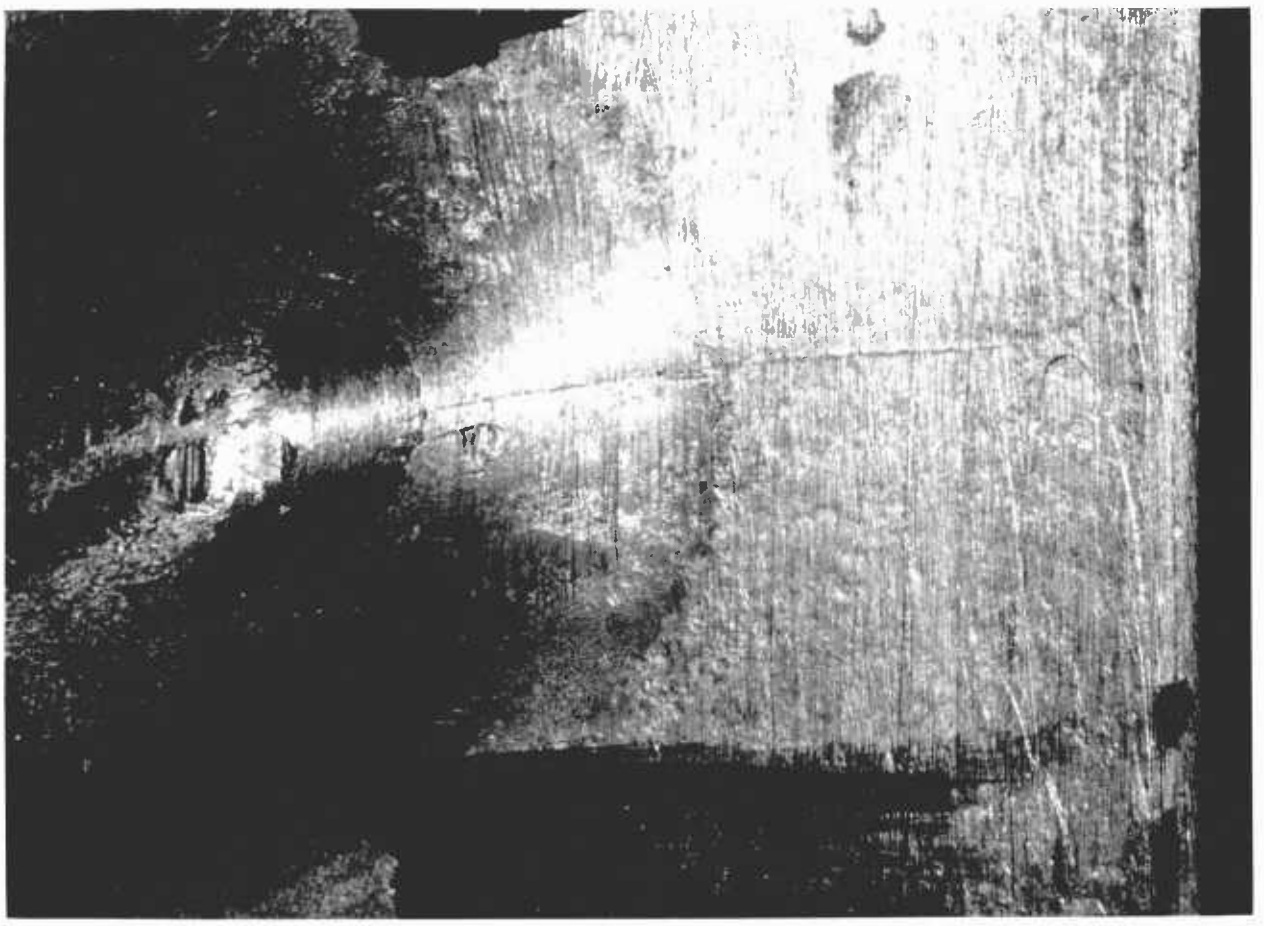


PLATE 16. TYPICAL FAILURE OF VIBROPHORE SPECIMEN